Theoretical Moment-Rotation Curve for Steel Piles Embedded in Concrete

by

Stephen Thomas Hammett

A thesis submitted to the Graduate Faculty of
Auburn University
in partial fulfillment of the
requirements for the Degree of
Master of Science

Auburn, Alabama
August 5, 2017

Keywords: Connection stiffness, Moment-rotation curve, Embedded steel pile, Bridge bent, Frame analysis, Second order effects

Approved by

Justin D. Marshall, Chair, Associate Professor of Civil Engineering
J. Brian Anderson, Associate Professor of Civil Engineering
Robert W. Barnes, Associate Professor of Civil Engineering

Abstract

The accurate modelling and analysis of connections formed by embedding steel piles in concrete is a difficult undertaking that has only recently begun to receive attention in the research community. These connections are inherently three-dimensional problems that involve the nonlinear behavior of the constituent materials. Despite these complexities, the author postulates that simpler, two-dimensional analysis methods can be used to model the flow of stresses from the face of the pile (where the resisting couple exists) into the encasing concrete. This paper examines four two-dimensional methods to evaluate their potential as connection models. One of these methods (Method 3) yielded results that closely matched the rotational stiffness results from full-scale tests, while another method (Method 4) yielded results that closely matched the currently accepted calculations for moment capacity. The shortcomings of the two-dimensional methods are discussed and recommendations for improvements are provided.

Acknowledgements

I would like to thank Dr. Marshall and Dr. Davidson for the outstanding graduate education I have received at Auburn University over the past two years. The engineering tools I have acquired over that time have already proven to be indispensable in my professional practice. As a husband, father and practicing engineer, I am grateful for the patience that I have been afforded while taking these courses and working through this thesis. I am looking forward to continuing my educational efforts as I begin doctoral coursework this fall.

I would also like to thank my wife, Bridget and my sons, Thomas, Joseph and Christopher for their patience over the past two years. Their interest in my work and the adventures we have had in spite of the time I have spent studying have made this journey especially fulfilling. The love, joy and innocence that exists in my family has been revealed during this time and it is something I will never take for granted.

Table of Contents

List of Tables

List of Figures

Chapter 1 Introduction

1.1 Overview

One of the most common bent types found on bridges in Alabama with individual spans not exceeding roughly 40 feet is a rigid (moment) frame consisting of a concrete cap supported on driven steel piles. The girders are placed directly above the piles so that no significant gravity loads are applied to the concrete cap between piles. The typical steel pile bridge bent shown in Figure 1-1 is representative of these structures and is foundational to the work investigated herein.

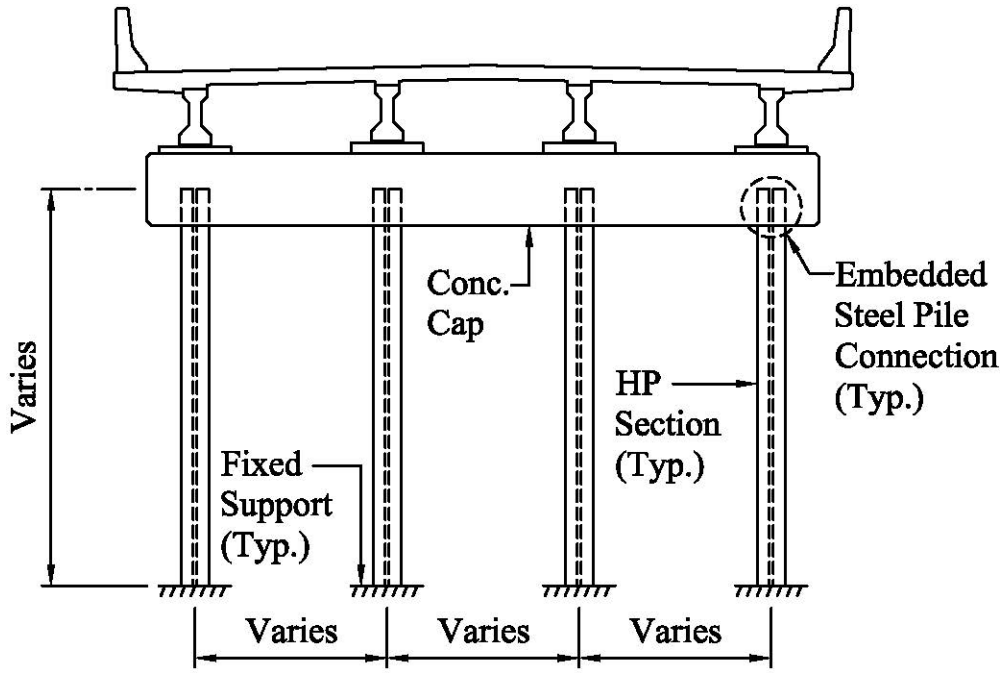

Figure 1-1 Typical Steel Pile Bridge Bent

Many of these bents use a cast-in-place reinforced concrete cap (bent cap, beam) in which the tops of the driven steel piles are embedded. Figure 1-2 shows the typical construction

of an embedded steel pile connection. The steel reinforcement in the cap has been omitted for clarity.

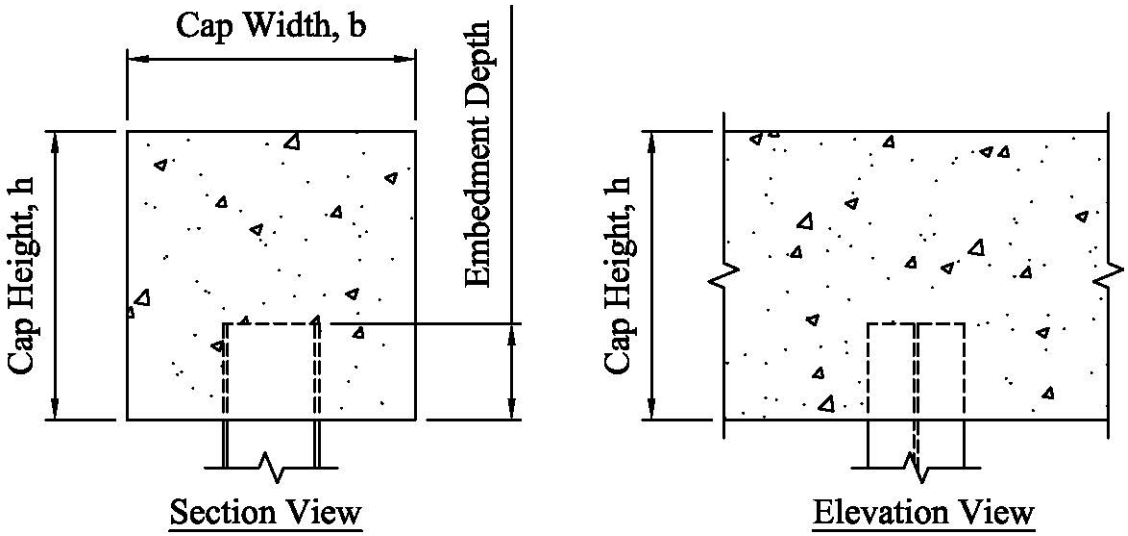

Figure 1-2 Illustration of Typical Embedded Steel Pile Connection

The pile-to-cap connections resulting from this embedment contribute significantly to the capacity, stability and serviceability of these rigid frames. This paper investigates the influence of embedment depth, concrete compressive strength, pile section properties, analysis methods and bending stresses in the concrete beam due to frame action on the in-plane performance of embedded steel pile connections.

1.2 Problem Statement

A thorough understanding of beam-to-column connection stiffness is essential to the accurate analysis of rigid frames; however, the moment-rotation relationship for steel piles embedded in concrete beams is poorly understood. Based on the experience of the author, the rotational stiffness of embedded steel pile-to-concrete cap connections is usually considered to be infinitely large. This assumption is problematic because it artificially stiffens the structural model by failing to capture connection rotation (the relative rotation between the pile and the cap at the shared node). Deflections determined by an analysis using this assumption are smaller

than the more analytically correct values for both first and second order analyses that include connection flexibility. This effect may be negligible for short and stiff structures, but as structures or individual components therein become increasingly slender the need to include appropriate connection stiffness values in the structural model increases as well.

1.3 Research Objectives

The primary objective of this research paper is to develop a generalized understanding of the relationship between an applied moment and the corresponding rotational deformation of connections created by embedding steel piles in concrete. The rotational deformation considered here occurs only within the embedded pile segment.

The secondary objective of this research paper is to develop a simple moment-rotation relationship that takes into account pile embedment length, concrete compressive strength, pile section properties and bending stresses in the concrete beam due to frame action.

1.4 Research Scope

The structural properties of connections consisting of steel piles embedded in concrete depend on pile embedment depth, concrete compressive strength and pile section properties. The connection behavior further depends on the bending stresses in the concrete beam due to frame action. It seems intuitive that an increase in any or all of these factors, with the exception of tensile bending stresses, would yield an increase in connection strength and stiffness. The veracity of this intuition is investigated using the analytical methods described in Chapter 3 to explore the influence of each of these factors on the behavior of steel piles embedded in concrete.

The moments acting at the pile-to-cap connections are assumed to be caused by lateral loads only. These loads originate in the superstructure and are transferred to the bent through

bearings located directly above the piles. The connection moments resulting from these lateral loads are discussed in detail in Section 3.4. Axial force effects in the concrete beam and the pile are not considered.

Two pile embedment depths are evaluated for each pile section included in this research paper. The smallest embedment depth considered is 12 inches. It is included because it is the minimum allowed by Article 10.7.1.2 in the AASHTO LRFD Bridge Design Specifications (AASHTO 2012) without special attachment requirements and it is commonly used by the Alabama Department of Transportation (ALDOT) in the construction of pile bents. Larger embedment depths are included because it is anticipated that the larger pile sections evaluated will require a deeper embedment to develop their yield moment. The HP10x42, HP12x53 and HP14x89 pile sections are each evaluated for 12 inch and 18 inch embedments. The HP18x204 pile section is evaluated for 18 inch and 24 inch embedments.

Three concrete compression strengths are evaluated in this paper. The 28 day compressive strengths considered are 3,000, 5,000 and 10,000 psi. The 3,000 psi strength is included because it is ubiquitous in ALDOT substructure components. The 10,000 psi strength is included because it is representative of contemporary higher-strength concrete. The 5,000 psi strength is included because it provides an intermediate data point between the two extremes.

Four pile sections, all bent about the weak axis, are evaluated in this paper. The four pile sections considered are the HP10x42, the HP12x53, the HP14x89 and the HP18x204. The HP10x42 was commonly used on many older ALDOT bridge bents. This relatively flexible section is included to evaluate the lower bound of embedment stiffness. The HP18x204 is the largest HP section currently in production. This section is included to evaluate the upper bound of embedment stiffness. The HP12x53 and the HP14x89 are included because they are

commonly used by ALDOT and because they provide intermediate data points between the two extremes.

Connection stiffness is also thought to be a function of the bending stresses that exist in the concrete beam in the vicinity of the connection. These bending stresses correspond to cap moments that develop when the bent cap undergoes displacements, especially those resulting from lateral loads. The four cases of cap bending moments evaluated in this paper are illustrated in Figure 1-3.

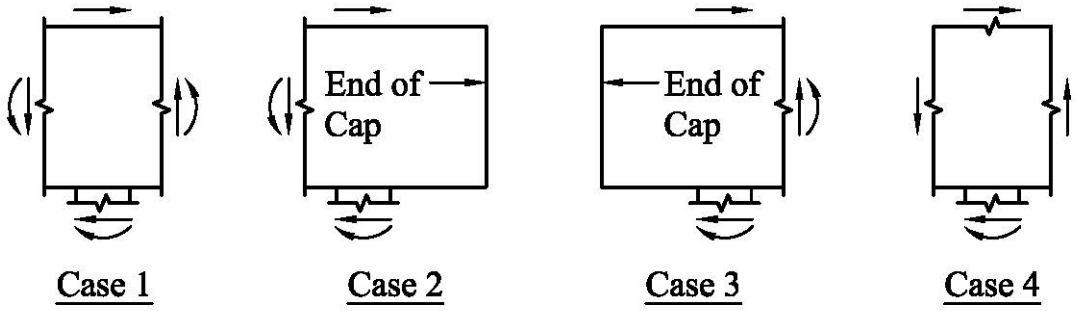

Figure 1-3 Illustration of Cap Bending Cases

Case 1 consists of equal cap bending moments acting at the near end of the beam on each side of the embedded pile. Case 2 consists of a bending moment acting at the right end of the left beam only. Case 3 consists of a bending moment at the left end of the right beam only. The bending moment at the right end of the left beam is set equal to zero. Case 4 consists of setting the beam moments on each side of the pile equal to zero.

Two general approaches to the analysis of this connection methodology are also investigated. The first approach provides for the inclusion of deformations of the pile along the embedded length. The second approach evaluates rigid body rotation of the embedded pile segment within the concrete cap.

1.5 Organization of Thesis

This thesis comprises five chapters. Chapter 1 provides an overview, problem statement and succinct introduction into this research on the rotational stiffness of connections formed by embedding steel piles in concrete. Chapter 2 provides the background information and literature review for prior work related to this problem. Chapter 3 covers the development of the analytical methods used to evaluate connection stiffness. The results of the multiple connection configurations and parameter variations are included in this section. Chapter 4 presents the results from the work in Chapter 3. Chapter 5 summarizes this thesis and offers final conclusions and recommendations based on the findings of the research presented herein.

Chapter 2 Background and Literature Review

2.1 Background

The motivation for this research into the rotational stiffness of connections formed by embedding steel piles into concrete beams originated with the ALDOT research project by Marshall et al. (2017) that sought to experimentally validate analysis and design methods for steel pile bridge bents. The typical steel pile bridge bent shown in Figure 1-1 is representative of these structures and is foundational to the work investigated herein.

The complexities of this structure type generally require the engineer to make many careful assumptions to transform the actual bent into a manageable assembly of simpler components and boundary conditions that can be modelled with reasonable effort and without losing the essential nature of the real structure. Over the years, engineers within the ALDOT Bridge Bureau as well as their structural engineering consultants have approached pile bent analysis and design using a variety of methods. While most these various methodologies appear to be founded on rational engineering judgment, the results between the different approaches can vary dramatically. Marshall et al. (2017) used the following research objectives to identify the actual behavior of steel pile bridge bents and to make corresponding recommendations for the design thereof:

- Identify the load path for dead, live and lateral loads from the point of application to the point of support (the external world).

- Develop accurate modelling assumptions for the soil-structure interaction of the supporting piles using data from load tests.
- Develop accurate modelling assumptions for boundary conditions (soil-structure interaction), composite sections (concrete encased steel piles) and connection springs (embedded steel pile-to-concrete cap connections) using calibrated analytical models.
- Evaluate the effect of inclined (battered) exterior piles on bent behavior.
- Develop analysis procedures for steel pile bridge bents that provide a balance between accuracy, required effort and design economy.
- Develop LRFD design procedures for steel pile bridge bents that are coupled with the analysis recommendations.

The author was assigned two tasks related to the Marshall et al. (2017) project. The first task, which is not the subject of this thesis, required the author to develop a flowchart for the analysis and design of steel pile bridge bents using data gleaned from the research efforts, knowledge from graduate coursework and his extensive experience as a structural engineer specializing in the design of highway bridges. This flowchart addresses a broad spectrum of considerations from the very simple (e.g., pile layout and pile section orientation) to the more complex (e.g., soil-structure interaction and bent drift limitations) and provides a method that allows for the reasonably accurate analysis and the more confident design of steel pile bridge bents. The completed flowchart is included in Appendix D of this thesis.

The second task, which is the subject of this thesis, required the author to investigate the moment-rotation relationship of connections formed by embedding steel piles in concrete. The embedded steel pile connection considered in this thesis is shown in Figure 1-2.

2.2 Literature Review

There has been extensive research into the flexural strength of connections formed by embedding steel components into concrete. Two of the most commonly used methods for calculating capacity are presented in this section. Figure 6.9.2 (B) in the PCI Design Handbook (PCI 1999) provides a method for calculating the flexural strength of an embedded component supporting a pure moment. The calculations are based on the development of a resisting couple between the stress blocks that form at each end of the embedded pile segment. This recommended model is shown in Figure 2-1, where f'c is the concrete compressive strength, L_e is the embedment depth and β_1 is the multiplier for the depth of the stress block. The stress block multiplier is taken as 0.85 for 3,000 psi concrete, 0.80 for 5,000 psi concrete and 0.65 for 10,000 psi concrete. This method for calculating the moment capacity of an embedded component should also provide a reasonable estimate for connections supporting a moment combined with a relatively small horizontal shear force acting in the plane of the bent.

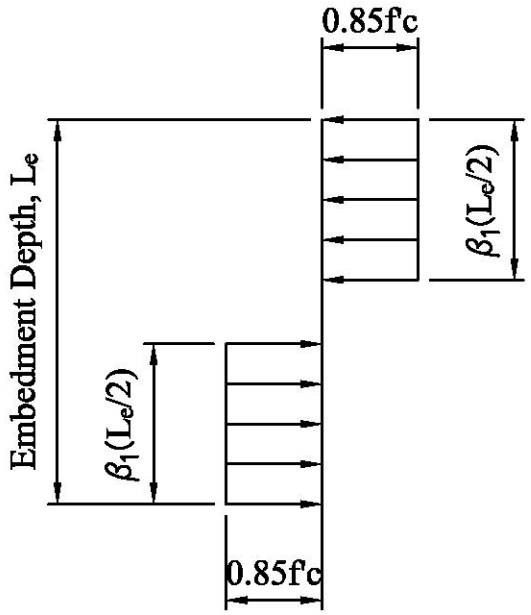

Figure 2-1 Illustration of Moment Capacity Calculation (PCI 1999)

The moment capacity of connections supporting a relatively large horizontal shear force acting in the plane of the bent may not be reasonably estimated by the above method. Xiao et al. (2006) improved on the calculations for this more complex loading condition by modifying the shear equation (Equation 6.9.1) in the PCI Design Handbook (PCI 1999) to accommodate an applied moment. The modified equation is:

$$M_{ue} := \left[\frac{0.85 \cdot (f_{co}) \cdot b \cdot L_e}{1 + 3.6 \cdot \left(\frac{e}{L_e} \right)} \right] \cdot a$$

In the above equation, the variable f_{co} is the concrete compressive strength, b is the effective pile width, L_e is the embedment depth, a is the shear span and e is the shear span plus one-half the embedment depth. These terms are shown in Figure 2-2 below.

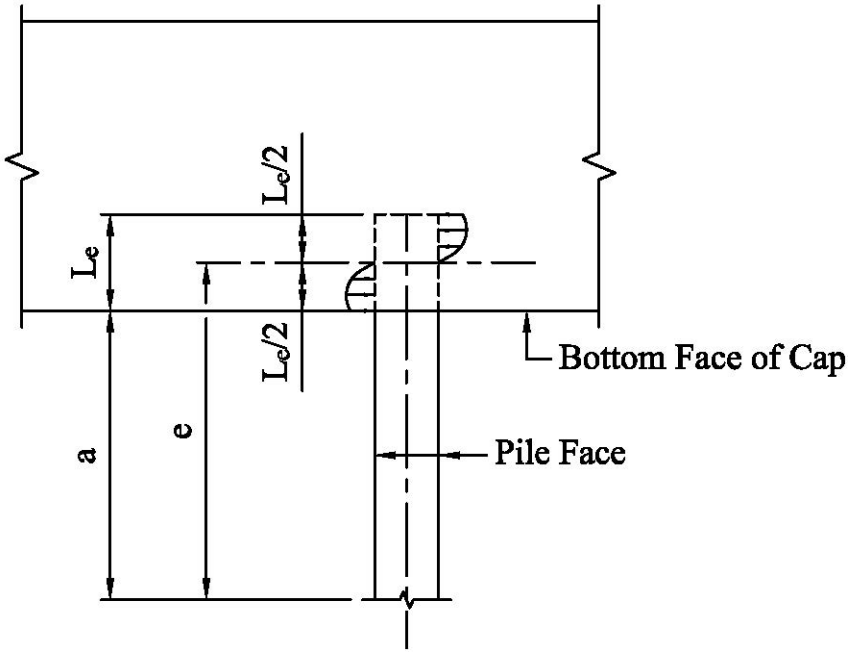

Figure 2-2 Illustration of Moment Capacity Calculation by Xiao et al. (2006)

It is important to note that the effective pile width used in their equation is 2.5 times the actual pile width. According to the PCI Design Handbook (PCI 1999), the foundational document for their equation, the use of the larger effective width is based on the presence of

closely spaced confining reinforcement. Reinforcement meeting these requirements is not typically provided in ALDOT bridge bents, so that effect has not been included here. The actual pile width is used in the evaluation of their equation for comparison to the methods used in this paper.

Additional research into the capacity and performance of embedded connections can be found in Shama et al. (2002a and 2002b).

In contrast to the mature state of research into the flexural capacity of embedded steel pile connections, Rodas et al. (2017) note that the experimental research into the rotational stiffness of these connections is relatively sparse. This void in the connection knowledge base undoubtedly contributes to the tendency of practicing engineers to model these connections as rotationally fixed. But this assumption is problematic, as noted in Section 1.2, because it artificially stiffens the structural model by failing to capture connection rotation. The significance of this omission is assessed by Zareian and Kanvinde (2013) wherein 2-, 4-, 8- and 12-story steel moment frames are investigated through push-over and nonlinear response history analyses. In general, they found that the rotational flexibility of a more realistic connection changes the member force distribution and the plastic mechanism causing a corresponding increase in member forces and a reduction in ductile capacity and collapse resilience. In an effort to advance the practice of engineering, Rodas et al. (2017) present a method to characterize the rotational stiffness of deeply embedded column base connections based on the test configuration shown in Figure 2-3 below.

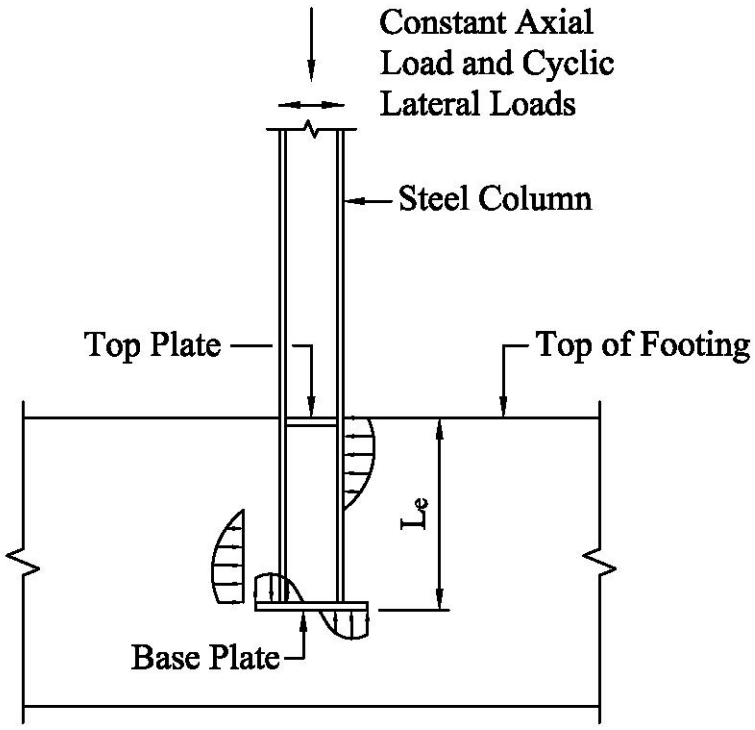

Figure 2-3 Illustration of Testing Configuration Used by Rodas et al. (2017)

Rodas et al. (2017) estimate the rotation of an embedded steel connection with the following equation:

$$\Theta_{base} := \Theta_{RBMbase} + \Theta_{CaseIbase} + \Theta_{CaseIIbase}$$

where θ_{base} is the net connection rotation at the top of the footing defined as the summation of $\theta_{RBMbase}$ (the rigid body rotation of the embedment), $\theta_{CaseIbase}$ (deformations due to concentrated loads acting on the embedment) and $\theta_{CaseIIbase}$ (deformations due to distributed loads acting on the embedment). The three terms on the right of this equation are simply the rotations attributed to the isolated rotation modes defined in the paper. They further estimate connection stiffness with the following equation:

$$\beta_{base} := \frac{M_{base}}{\Theta_{base}}$$

where β_{base} is the estimated rotational stiffness using their proposed method and M_{base} is 70 percent of the maximum moment taken as the value determined by connection tests or the flexural strength of the column.

The above literature review is believed to contain the most relevant work related to the focus of this thesis. The performance of connections evaluated by the methods in this paper are compared against the performance of connections evaluated using the methods suggested in the above works. The interested reader is referred to Grilli and Kanvinde (2015) and Grilli et al. (2017) for related work not requiring inclusion in this thesis.

Chapter 3 Analysis of Embedded Steel Pile Connections

3.1 General Comments on the Behavior of Embedded Steel Pile Connections

As stated above, the primary purpose of this research is to develop a generalized, theoretical understanding of the relationship between an applied moment and the corresponding rotational displacement for steel piles embedded in concrete. The behavior of these embedded steel pile connections depends on pile embedment depth, concrete compressive strength and pile section properties. The connection behavior further depends on the bending stresses in the concrete beam due to frame action. The influence of each of these factors on connection stiffness is investigated in this chapter. The moment capacity of these connections is also investigated because its magnitude is an important design consideration and because it can be calculated using methods similar to those used for the determination of connection stiffness.

3.2 Local Pile Bearing Stresses and Idealized Concrete Beam Bending Stresses

The embedded portion of a steel pile rotates when acted upon by an externally applied moment. This rotated pile segment bears against the encasing concrete on opposite faces to form a resisting couple that is equal in magnitude to the applied moment. The compression in the concrete caused by the formation of this couple is a localized response existing only in the concrete volume that is in close proximity to the connection. These localized pile bearing stresses dissipate as the distance (along the longitudinal axis of the beam) from the face of the pile increases. At some distance away from the bearing face of the pile, there exists a cross section in the concrete beam that exhibits internal stresses due to frame action only. These

stresses are referred to as idealized bending stresses since they correspond to the moments calculated from an idealized structural analysis.

3.3 Connection Scenarios

This research project investigates the influence of embedment depth, concrete compressive strength, pile section properties and cap bending stresses on connections stiffness. This is accomplished in part by exposing each pile section to every possible combination of the other three factors. For example, the evaluation of the HP10x42 with a 12 inch embedment into 3,000 psi concrete must be evaluated separately for all four cap bending cases. This scenario is repeated for the 5,000 psi concrete and then the 10,000 psi concrete. Extending this approach to include 18 inch embedment yields 24 unique combinations for each pile section. Considering all four pile sections, there are a total of 96 connection scenarios that are evaluated in this thesis.

3.4 Pile Moment and Corresponding Connection Forces

The pile yield moment for weak axis bending at the bottom face of the cap is taken to be the moment that must be resisted by the connection. This moment is defined by the initial yielding of the extreme fiber and is intended to be the limiting condition for each connection scenario evaluated is this research. The data for the moment-rotation curves for each connection scenario is obtained by evaluating the applied pile moment occurring at tenth points between zero and the yield moment for the pile section being investigated. The moment and corresponding connection rotation from each of these 11 data points is used to plot the moment-rotation curve for each connection scenario. Since the moment acting on the pile at the bottom face of the cap is a governing feature of this research, all relevant forces acting in the vicinity of the connection are derived from the pile moment and various assumptions regarding the construction of the bent. Referring to Figure 1-1, the geometry of the bent considered in this

thesis is assumed to be 20 feet tall with 4 vertical piles spaced at 8 feet center-to-center. The piles are fixed supported at the base and inflection points are assumed to exist at the midpoint of all beams and columns. A portal analysis, assuming equal shear in each pile (since all piles have the same section properties and similar boundary conditions), is used to back into the idealized forces resulting from frame action that correspond to each applied moment that is evaluated. The bent is assumed to be loaded by lateral forces acting through the idealized beam-to-column joints. The impact of axial forces in the beam or the column on connection stiffness is not considered in this research. Figure 3-1 shows the typical connection forces. The equal beam forces shown here are consistent with Case 1 in figure 1-3. The beam forces in Bending Cases 2, 3 and 4 will vary depending on the scenario being considered.

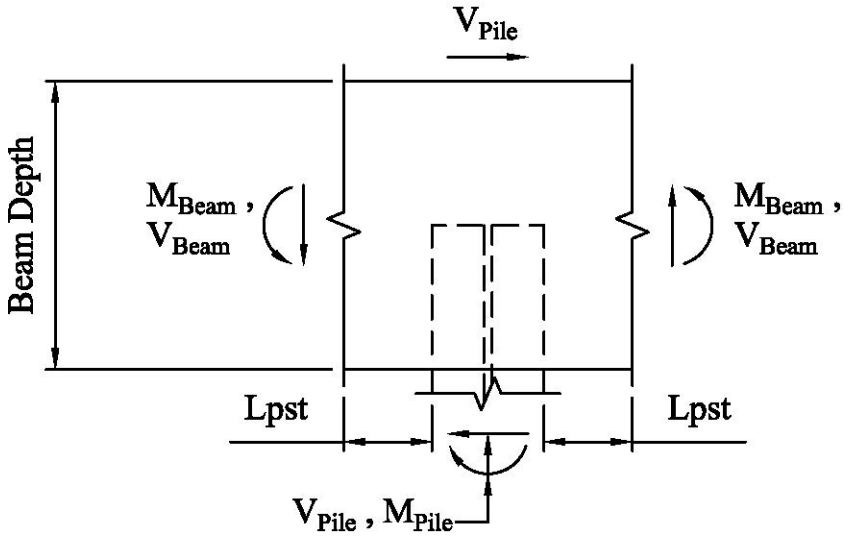

Figure 3-1 Illustration of Relevant Forces Acting in the Vicinity of the Connection

3.5 Pile Stress Transformation Length

The distance over which the localized pile bearing stresses are transformed into idealized bending stresses is referred to in this paper as the pile stress transformation length and is denoted by the abbreviation L_{pst}. Figure 3-2 shows this length at a typical interior pile on a bridge bent.

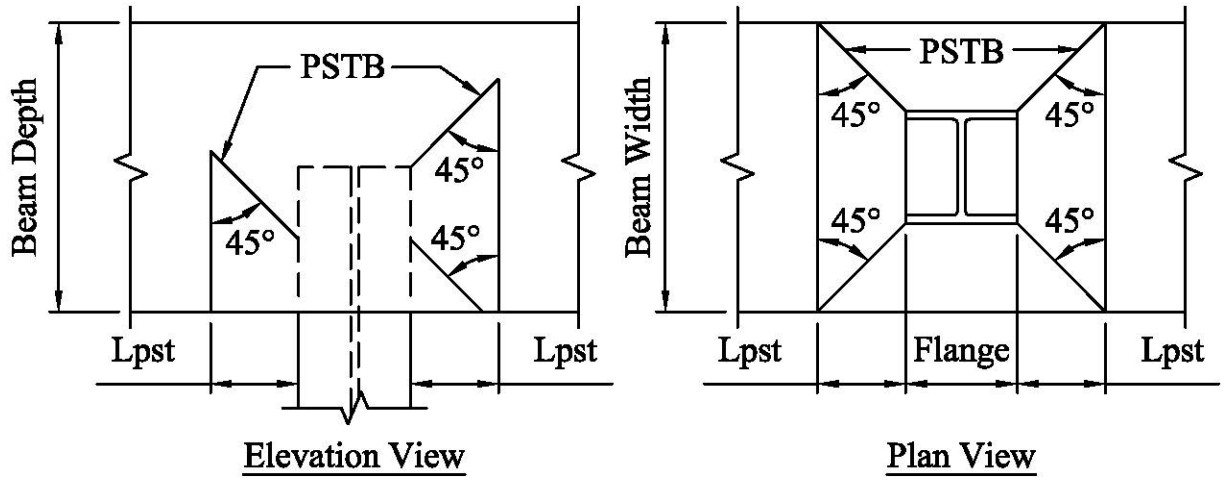

Figure 3-2 Illustration of PSTB and L_{pst} at Embedded Steel Pile Connection

3.6 Pile Stress Transfer Block

The volume through which the localized pile bearing stresses are reduced and become equal to the idealized bending stresses is referred to in this paper as the pile stress transfer block (PSTB). This volume is defined primarily by four planes (top, bottom and two sides) that originate at the compression area on the face of the pile and extend into the length of the beam at 45 degree angles measured from the face of the pile. The selection of the 45 degree angle is based on the work by Xiao et al. (2006) where it was used to calculate the concrete block rupture strength for embedded piles located near the edge of the supporting concrete component. This condition is often encountered at the exterior piles of bridge bents and is considered to be a reasonable approximation for both interior and exterior piles. Figure 3-2 shows the elevation and plan view of the PSTB volumes at a typical interior pile on a bridge bent.

The interior end of the PSTB volume is the vertical plane defined by the compression area at the face of the pile. The exterior end of the PSTB volume is the vertical plane at the end of the pile stress transformation length, L_{pst}. The length L_{pst} is defined as the distance parallel to the longitudinal axis of the beam between the face of the pile and the point at which the planes

on each side of the PSTB intersect the vertical sides of the concrete beam. Various configurations of PSTB geometry can occur depending on the embedment depth, pile size, beam dimensions and the location of the compression area of the resisting couple (top or bottom of embedded pile segment); however, the most important aspect of the PSTB volume is that it defines the length L_{pst} over which the localized pile bearing stresses are transformed into idealized bending stresses. This length is one of the primary factors influencing the flow of stresses through this volume and determining the stiffness characteristics of embedded steel pile connections.

3.7 Bending Stresses in the Concrete Beam Due to Frame Action

Connection stiffness is also thought to be a function of the bending stresses that exist in the concrete beam in the vicinity of the connection. In the pile bents being considered, these bending stresses correspond to moments that develop when the bent cap undergoes rotational displacements resulting from lateral loads. These bending stresses can exist in the cap on both sides of the pile, but the beam moments corresponding to these stresses always act in the positive (counterclockwise) sense on the connection under investigation. In an effort to fully capture the influence of cap bending stresses on connection behavior, four cap bending cases are evaluated. Figure 1-3 illustrates the four cap bending scenarios considered.

Case 1 consists of equal cap bending moments acting at the near end of the beam on each side of the embedded pile. This scenario is representative of the conditions at a typical interior pile of a bent. Case 2 consists of a bending moment acting at the right end of the left beam only. The bending moment at the left end of the right beam is set equal to zero. This scenario is representative of the conditions at an exterior pile of a bent where forces in the cantilevered cap segment are not influenced by frame action. Case 3 consists of a bending moment at the left end

of the right beam only. The bending moment at the right end of the left beam is set equal to zero. Like Case 2, this scenario is also representative of the conditions at an exterior pile of a bent where forces in the cantilevered cap segment are not influenced by frame action. The difference between Case 2 and Case 3 is the nature of the cap bending stresses (compression or tension) that act in the vicinity of the pile. Case 4 consists of setting the beam moments on each side of the pile equal to zero. This scenario is not representative of typical bent behavior at any pile location; however, piles embedded in large concrete components (such as basement walls or mat foundations) may experience support conditions approaching those idealized by this case. Evaluation of the cap bending stresses in Case 4 is intended to broaden the applicable range of this research. The routine M_{Beam} included in the Mathcad calculations in Appendix C calculates the idealized bending moments for each load condition evaluated.

Additionally, Harries and Petrou (2001) recommend that pile-to-cap connections be designed to avoid damage to the cap by maintaining elastic material behavior in the cap in the vicinity of the connection. This is accomplished in this thesis by limiting the tension bending stresses in the cap to the modulus of rupture. To ensure this condition is satisfied, the tension bending stresses in the cap are checked for all pile sizes and bending cases considering an unreinforced section. The typical ALDOT cap with a width of 36 inches and height of 36 inches is determined to be adequate for the HP10x42 and HP12x53. The HP14x89 requires a cap with a width of 36 inches and height of 42 inches. The HP18x204 requires a cap with a width of 48 inches and a height of 66 inches.

3.8 Modelling a Three-Dimensional Phenomenon in Two-Dimensions

A stress analysis of the PSTB volume is inherently a three-dimensional problem. This analysis is further complicated because the PSTB exists as a relatively small component within

the larger volume of beam concrete. Deformations within the PSTB will naturally interact with neighboring elements in the concrete beam that are outside this smaller volume. Despite these complexities, the author postulates that simpler, two-dimensional analysis methods can be used to model the flow of stresses from the localized pile bearing stress at the face of the pile to the idealized bending stresses assumed to exist at distance L_{pst}. Four two-dimensional methods are employed in this thesis to develop moment-rotation relationships for the connection conditions under investigation. The analytical methods and foundational assumptions used to model these various approaches are described below.

3.8.1 Stress-Strain Relationships for Concrete and Steel Components

The analyses performed as part of this research include the nonlinear behavior of the concrete. Tensile bending stresses in the concrete beam are limited to the modulus of rupture. Compressive stresses in the concrete beam are limited to the peak concrete stress (no post-peak behavior is allowed in the analysis procedures). The performance of the pile is also based on a nonlinear stress-strain curve; however, the limiting condition for most connection evaluations is the yield moment of the pile section where the strain in all interior fibers is below the elastic limit. As a result, the behavior of the steel pile will not reflect any significant nonlinear characteristics. The nonlinear stress-strain curves used for both the concrete in the beam and the steel in the pile are taken from the paper by Karthik and Mander (2011). The concrete within the PSTB volume is considered unconfined because of its proximity to the edges of the beam and because of the lack of confining reinforcement present in typical pile-to-cap connections in ALDOT bridge bents. Representative stress-strain curves for both the concrete and steel components are shown in Figure 3-3.

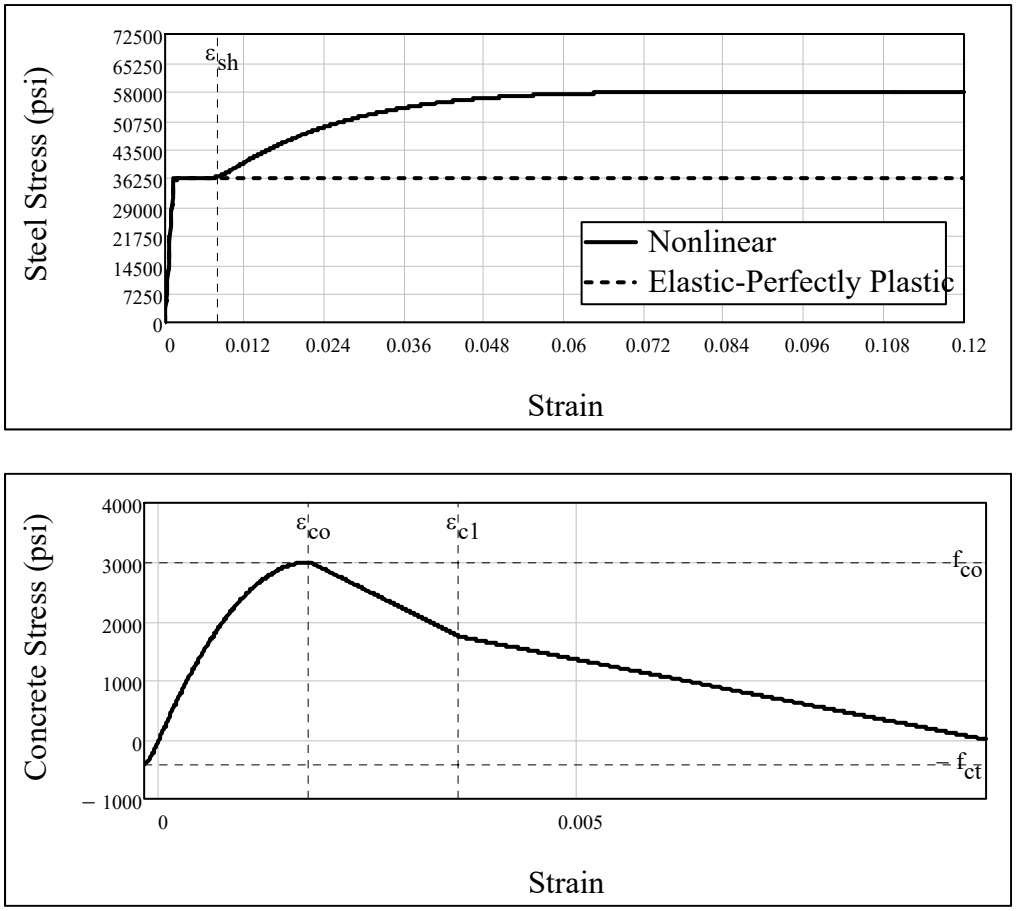

Figure 3-3 Representative Stress-Strain Curves for Steel and Concrete Components

A wide range of concrete compressive strengths are investigated in this thesis. The suitability of the Karthik and Mander (2011) stress-strain relationships for the 3,000 psi, 5,000 psi and 10,000 psi strengths was verified through personal communication with J. B. Mander in an email on April 14, 2017. Dr. Mander indicated that the concrete stress-strain relationships were valid for concrete strengths up to about 12,000 psi to 14,000 psi.

The preferred steel material for HP sections changed from ASTM A36 to ASTM A572 Grade 50 with the publication of the AISC Steel Construction Manual, 13th Edition (AISC 2005) published in 2005. Because of this, two steel materials are considered in this thesis. ASTM A36 is used for HP10x42 evaluations because of the common appearance of this section in older ALDOT bridges. ASTM A572 Grade 50 is used for HP12x53, HP14x89 and HP18x204

evaluations because the HP12x53 and the HP14x89 are frequently specified in contemporary structures and the HP18x204 was only recently added to the ASTM A6 document (Anderson and Carter 2012).

3.8.2 Four Approaches for Modelling the Flow of Stresses through the PSTB

The first three of the four methods used to model the flow of stresses through the PSTB are based largely on assumptions about the PSTB concrete and its interaction with the adjoining beam concrete. These methods use one-dimensional link elements to evaluate a wide range of potential connection behaviors. These link elements use traction forces acting along their length to model the load sharing between the PSTB and the surrounding cap concrete. Figure 3-4 shows the structural model used in Methods 1, 2 and 3. The fourth method assumes that the embedded pile segment rotates as a rigid body in response to the applied load. A thorough explanation of each method is provided below.

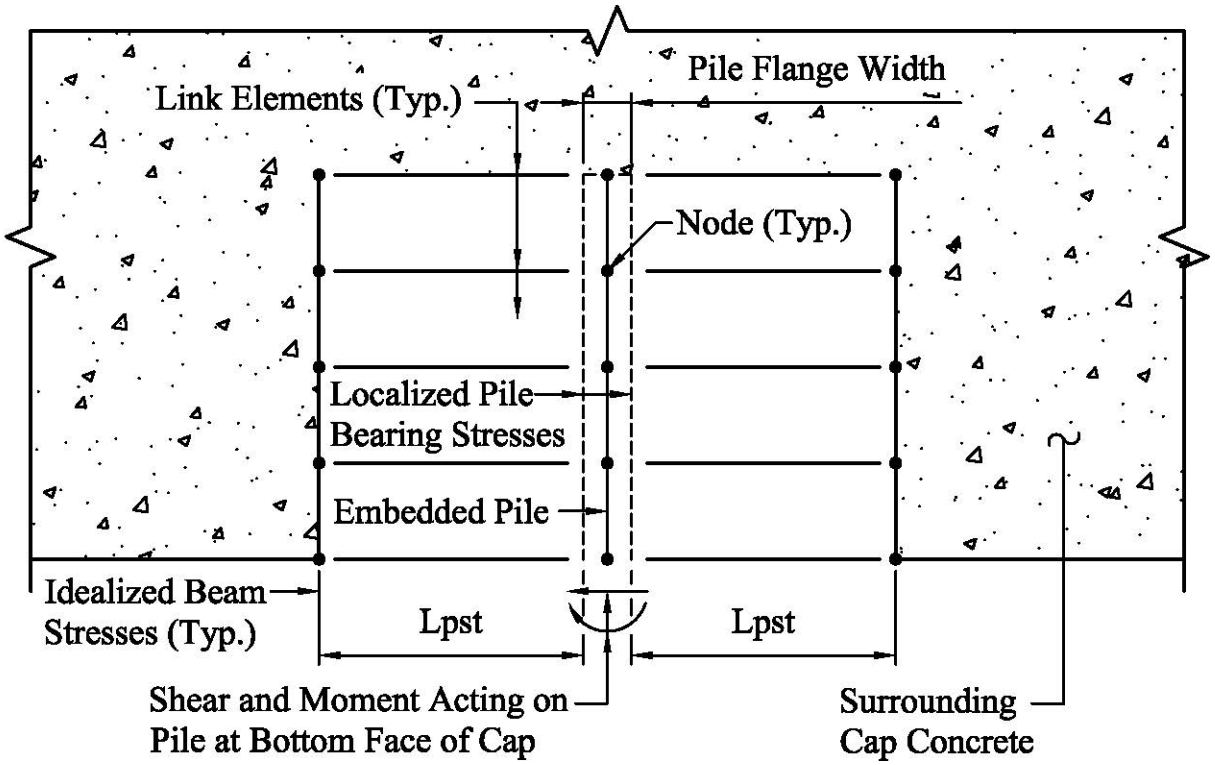

Figure 3-4 Illustration of Connection Model Used in Methods 1, 2 and 3

3.8.3 Method 1: Link Element with Linear Traction Force – Peak at Pile Face

The first method assumes a parabolic flow of axial stresses in the link element from the face of the pile to the idealized cross section (beam cross section at distance L_{pst} from face of pile with idealized bending stresses). This condition is modelled by a one-dimensional element with length L_{pst} that links the localized pile bearing stresses to those in the idealized cross section. The one-dimensional element employed in this method assumes the presence of a linear traction force along its length. The linear traction force is zero at the idealized cross section with its peak at the pile face at the opposite end of the element. Most of the load sharing between the PSTB and surrounding cap concrete occurs very close to the pile face. This characteristic minimizes deflections at the pile face and maximizes connection stiffness. Figure 3-5 shows this element and a graph illustrating the load sharing between the PSTB and surrounding cap concrete.

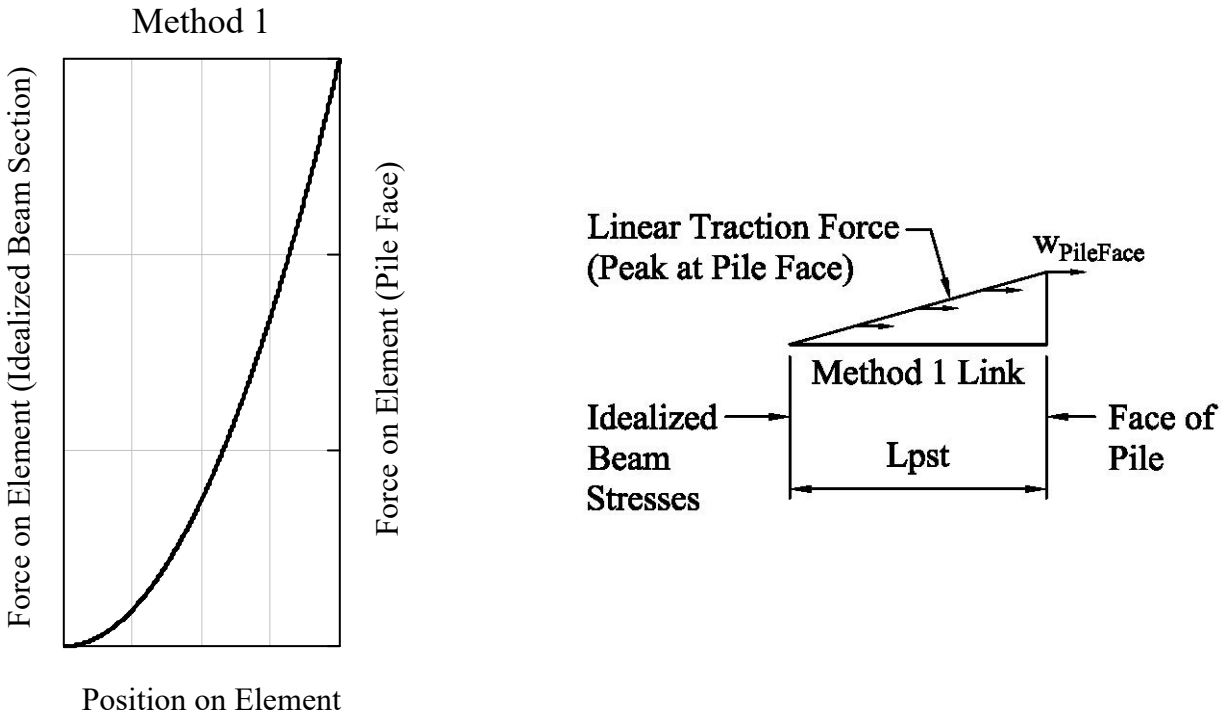

Figure 3-5 Illustration of Link Element Characteristics for Method 1

3.8.4 Method 2: Link Element with Uniform Traction Force

The second method assumes a linear flow of stresses from the face of the pile to the idealized cross section. This condition is modelled by a one-dimensional element with length L_{pst} that links the localized pile bearing stresses to those in the idealized cross section. The one-dimensional element employed in this method assumes the presence of a uniform traction force along its length. The load sharing between the PSTB and surrounding cap concrete occurs uniformly along the element. The deflections at the pile face and the connection stiffness determined through the use of this element are between the extremes captured by the first and third methods. Figure 3-6 shows this element and a graph illustrating the load sharing between the PSTB and surrounding cap concrete.

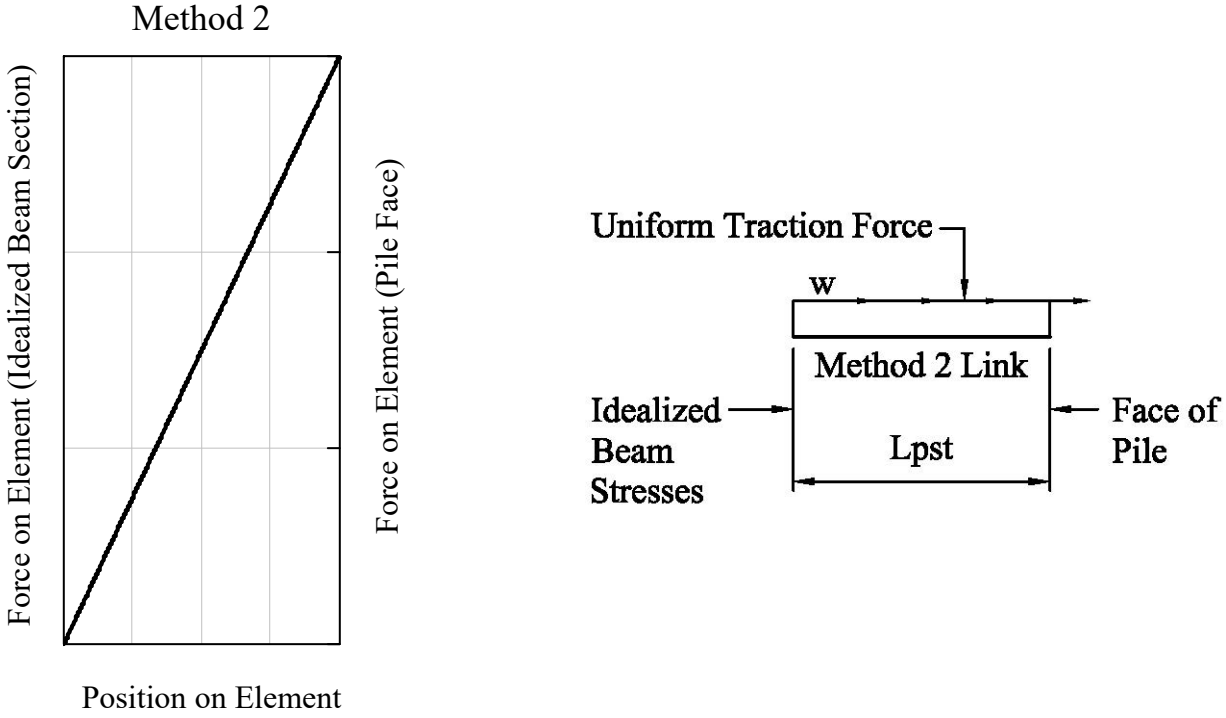

Figure 3-6 Illustration of Link Element Characteristics for Method 2

3.8.5 Method 3: Link Element with Linear Traction Force – Peak at Idealized Beam Section

The third method assumes a parabolic flow of axial stresses in the link element from the face of the pile to the idealized cross section. This condition is modelled by a one-dimensional element with length L_{pst} that links the localized pile bearing stresses to those in the idealized cross section. The one-dimensional element employed in this method assumes the presence of a linear traction force along its length. The linear traction force is zero at the pile face with its peak at the idealized cross section at the opposite end of the element. Most of the load sharing between the PSTB and surrounding cap concrete occurs very close to the idealized cross section. This characteristic maximizes deflections at the pile face and minimizes connection stiffness. Figure 3-7 shows this element and a graph illustrating the load sharing between the PSTB and surrounding cap concrete.

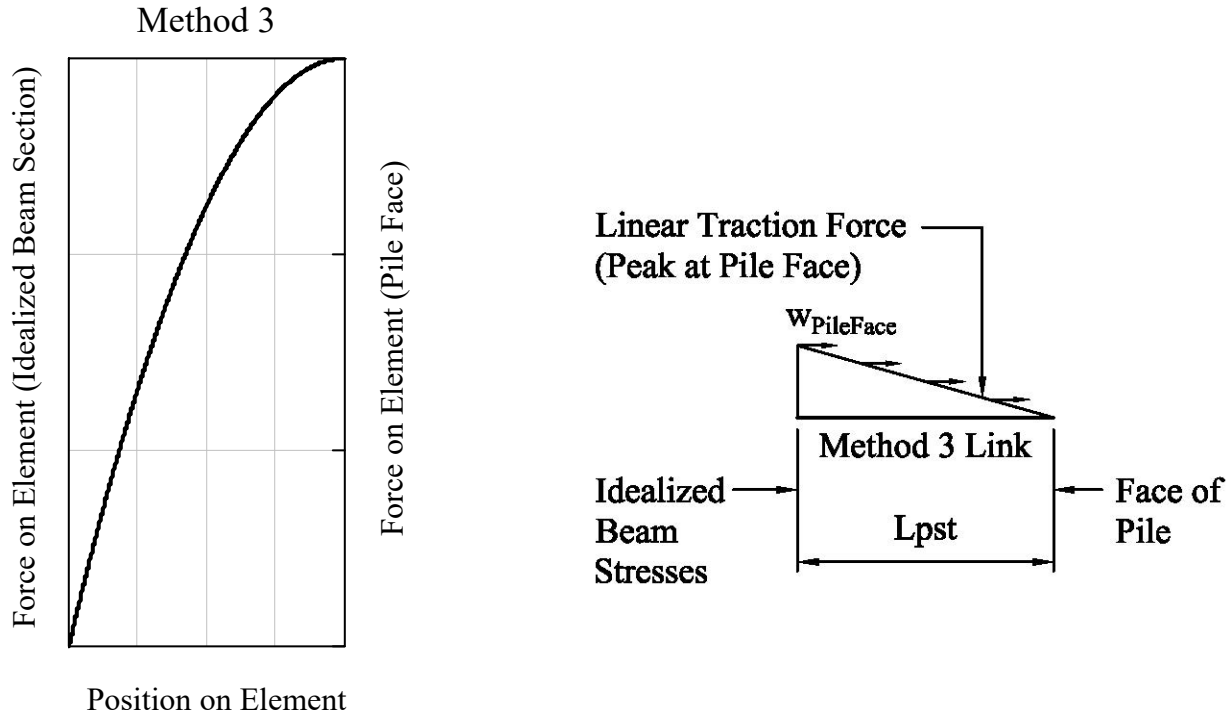

Figure 3-7 Illustration of Link Element Characteristics for Method 3

3.8.6 Structural Analysis Approach for Methods 1, 2 and 3

Methods 1, 2 and 3 employ an iterative, nonlinear structural analysis to find the equilibrium position of the pile under the influence of the applied load and the support of the encasing concrete. The embedded pile segment is discretized into a number of elements of sufficiently small size to capture the nonlinear behavior of the concrete with reasonable accuracy. The beam elements used in these analyses have two degrees-of-freedom (DOFs) at each node. Both shear and bending deformations are accounted for in the stiffness matrices used in these analyses. The node at the ends of each beam element is supported by a transverse compression only spring represented by one of the link elements described above. The encasing concrete is not considered to provide any rotational support at the nodes along the embedded pile segment. The link elements span between the node at the face of the pile and the corresponding node at the idealized beam section and have length L_{pst}. Figure 3-8 illustrates the structural analysis model used for Methods 1, 2 and 3.

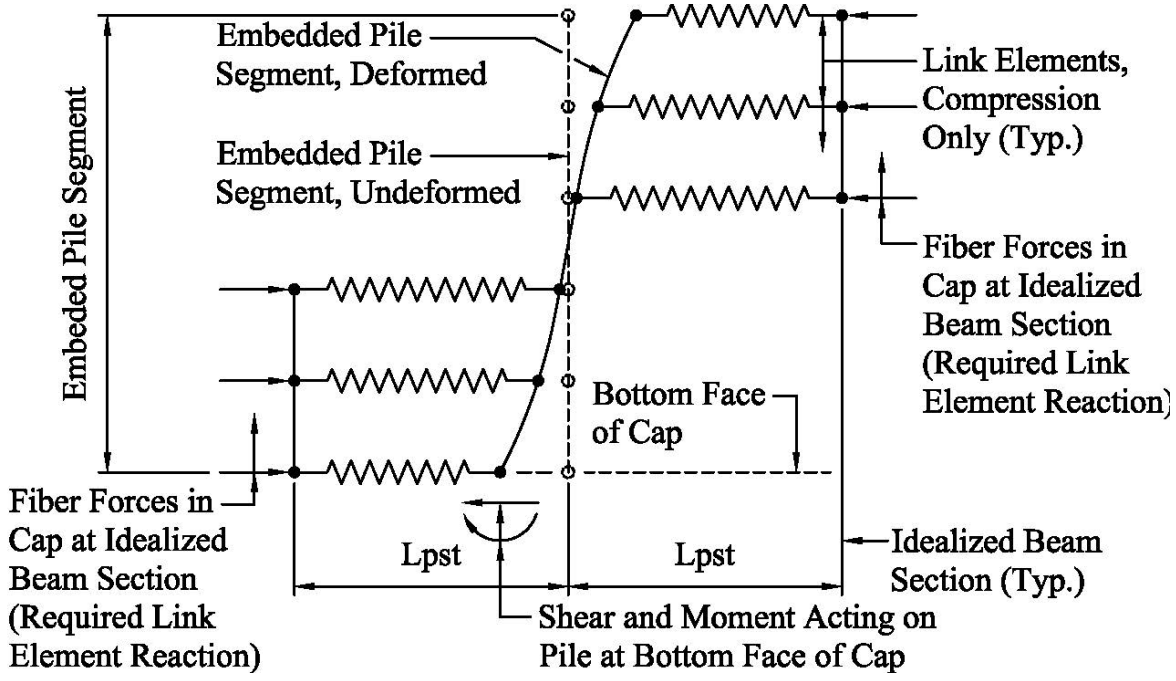

Figure 3-8 Structural Analysis Model for Methods 1, 2 and 3

As discussed in Section 3.5, bending stresses exist in the concrete beam when lateral loads applied to the bent are resisted by frame action. These idealized bending stresses are applied to the tributary area for each fiber in the analysis model to determine the required link element reaction at the idealized beam section. These reactions contribute to link element behavior and facilitate the inclusion of cap bending stresses into the structural evaluation of the embedded pile connection. These link element reactions (fiber forces due to cap bending at the idealized beam section) have a constant value during the analysis of each connection scenario evaluated.

For each of these three methods, the first iteration is performed using a stiffness analysis with simple transverse springs as supports at each node. These first iteration springs (link elements without traction forces) have length L_{pst}, concrete modulus E_c and a cross section area equal to the tributary area of the pile face for each fiber (node) in the structural analysis. The first iteration determines the force in each link element at both the pile face and at the idealized beam section. These forces are equal and opposite at this point since traction forces are not applied to the elements for the initial stiffness analysis (i.e., the load sharing between the PSTB and surrounding cap concrete is not yet being modelled). The link element force at the idealized beam section (the link element reaction) thus determined is compared against the corresponding required link element reaction. The difference between these two forces is referred to in this paper as the reaction error and is equal to the total traction force that needs to be added to the link element to satisfy equilibrium conditions for the element. The stress at the midpoint of this element is then used to calculate the midpoint strain by inverting the stress equation provided by Karthik and Mander (2011). The strain equation is:

$$\varepsilon_{Midpoint} := \varepsilon_{co} \cdot \left[1 - \left(\left| 1 - \frac{\sigma_{Midpoint}}{f_{co}} \right| \right)^{\left(\frac{1}{n_c} \right)} \right]$$

The concrete modulus of elasticity that will be used in the next iteration of the analysis is taken as the tangent to the concrete stress-strain curve at the midpoint strain just calculated. The equation of the tangent modulus is simply the first derivative of their concrete stress-strain equation. The equation of the midpoint tangent modulus is:

$$E_{MidpointTangent} := \frac{f_{co} \cdot n_c}{\varepsilon_{co}} \cdot \left(\left| 1 - \frac{\varepsilon_{Midpoint}}{\varepsilon_{co}} \right| \right)^{\left(n_c - 1 \right)}$$

The second and subsequent iterations of the analysis are performed using link elements with updated values for the modulus of elasticity and for the traction forces calculated in the previous iteration. A new global stiffness matrix is assembled to reflect the change in link element stiffness and a new force at the idealized beam section is calculated for comparison against the required link element reaction. Adjustments are again made to the traction force and the tangent modulus and the process is repeated until the maximum reaction error considering all link elements in a given iteration is less than 0.1 pounds. A check of the equilibrium condition of the embedded pile segment is performed by summing shear forces and moments for the converged condition.

3.8.7 Method 4: Rigid Body Behavior -- Deformations by Strain Density

As stated above, the fourth method assumes that the embedded pile segment rotates as a rigid body in response to the applied loads. The pile segment is rotated about multiple trial neutral axis locations until the stresses induced by one of these rotations reaches a condition of equilibrium with the applied load. The strains in the concrete at the face of the pile on both sides

are always in compression (due to resisting couple action) and are used in conjunction with the idealized beam strains over the pile stress transformation length, L_{pst} to perform a strain density calculation. The results of this calculation for the node at the top of the pile and the node at the bottom face of the cap are used to determine the rotation of the pile.

The analysis for rigid body behavior is somewhat difficult because the stress-strain curve is nonlinear and because the presence of an applied shear force moves the neutral axis off of the centroid of the embedded pile segment. Summing shear forces and moments for the embedded pile segment yields two equations in two unknowns (strain at the bottom face of the cap and neutral axis). Figure 3-9 shows the geometry of the embedded pile segment used in the rigid body analysis.

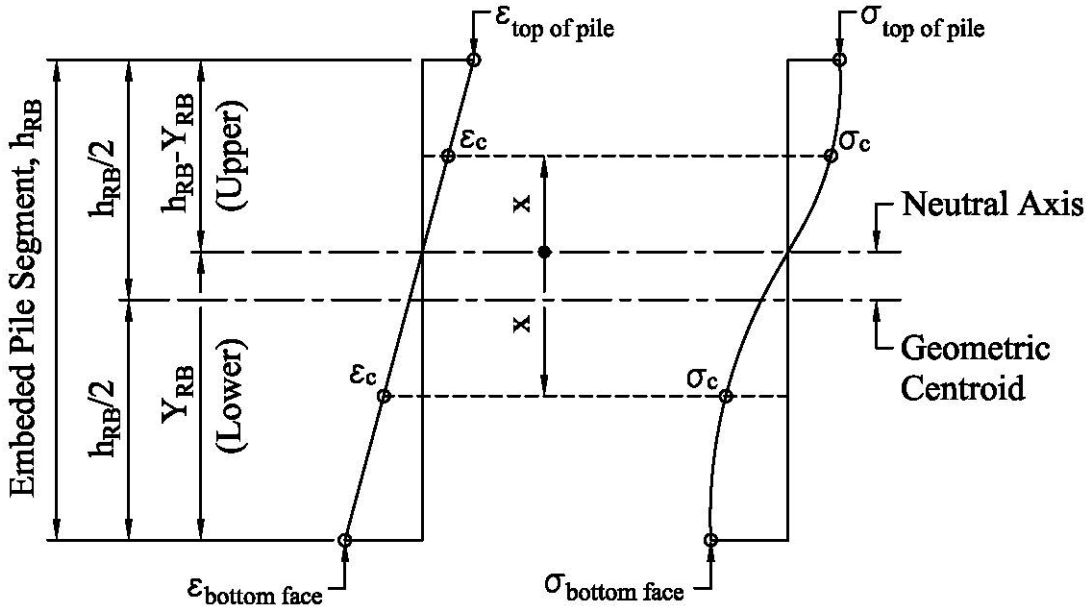

Figure 3-9 Geometry of Embedded Pile Segment

Several integrations are required to determine the internal concrete forces due to rigid body pile displacements. The calculations for the internal shear force are based on integrating the concrete stress equation from Karthik and Mander (2011) as shown below where σ_{co} is the design (peak) compressive strength, ε_{co} is the strain that corresponds to the compressive strength,

ε_{bf} is the strain at the bottom face of the cap, Y_{RB} is the location of the neutral axis measured from the bottom face of the cap, d_p is the pile depth and x is the distance from the neutral axis.

The general equation for the internal shear forces developed by a rotational displacement of the cross section is:

$$V_{GeneralEquation} := \int_0^{Y_{RB}} \sigma_{co} \cdot \left[1 - \left[\left| 1 - \frac{\varepsilon_{bf} \cdot (x)}{\varepsilon_{co} \cdot \left(Y_{RB} \right)} \right| \right]^{n_c} \right] \cdot \left(d_p \right) dx$$

Performing the integration for the lower portion of the embedded pile segment yields:

$$V_{Lower} := \sigma_{co} \cdot d \cdot \left[Y_{RB} + \frac{\varepsilon_{co} \cdot Y_{RB} \cdot \left(\left| 1 - \frac{\varepsilon_{bf}}{\varepsilon_{co}} \right| \right)^{n_c + 1}}{\varepsilon_{bf} \cdot \left(n_c + 1 \right)} - \frac{\varepsilon_{co} \cdot Y_{RB}}{\varepsilon_{bf} \cdot \left(n_c + 1 \right)} \right]$$

Performing the integration for the upper portion of the pile segment (the upper limit of integration must be changed from Y_{RB} to $h_{RB} - Y_{RB}$) yields:

$$V_{Upper} := \sigma_{co} \cdot d \cdot \left[h_{RB} - Y_{RB} + \frac{\varepsilon_{co} \cdot Y_{RB} \cdot \left[\left| 1 - \frac{\varepsilon_{bf} \cdot \left(h_{RB} - Y_{RB} \right)}{\varepsilon_{co} \cdot Y_{RB}} \right| \right]^{n_c + 1}}{\varepsilon_{bf} \cdot \left(n_c + 1 \right)} - \frac{\varepsilon_{co} \cdot Y_{RB}}{\varepsilon_{bf} \cdot \left(n_c + 1 \right)} \right]$$

The sum of these two equations yields the total internal shear force acting on the section due to the rotational displacement:

$$V_{Total} = V_{Lower} + V_{Upper}$$

The calculations for the internal moment are based on integrating the stress equation from Karthik and Mander (2011) multiplied by the moment arm from the neutral axis as shown below:

$$M_{GeneralEquation} := \int_0^{Y_{RB}} \sigma_{co} \cdot \left[1 - \left[\left| 1 - \frac{\varepsilon_{bf} \cdot (x)}{\varepsilon_{co} \cdot (Y_{RB})} \right| \right]^{n_c} \right] \cdot (x) \cdot (d_p) \, dx$$

Performing the integration for the lower portion of the embedded pile segment yields:

$$M_{Lower} := \sigma_{co} \cdot d \cdot \left[\frac{Y_{RB}^{\,2}}{2} + \frac{\varepsilon_{co} \cdot Y_{RB}^{\,2} \cdot \left(\left| 1 - \frac{\varepsilon_{bf}}{\varepsilon_{co}} \right| \right)^{n_c+1}}{\varepsilon_{bf} \cdot (n_c + 1)} + \right.$$

$$\left. + \frac{\varepsilon_{co}^{\,2} \cdot Y_{RB}^{\,2} \cdot \left(\left| 1 - \frac{\varepsilon_{bf}}{\varepsilon_{co}} \right| \right)^{n_c+2}}{\varepsilon_{bf}^{\,2} \cdot (n_c + 1) \cdot (n_c + 2)} - \frac{\varepsilon_{co}^{\,2} \cdot Y_{RB}^{\,2}}{\varepsilon_{bf}^{\,2} \cdot (n_c + 1) \cdot (n_c + 2)} \right]$$

Performing the integration for the upper portion of the pile segment (upper limit of integration must be changed from Y_{RB} to $h_{RB} - Y_{RB}$) yields:

$$M_{Upper} := \sigma_{co} \cdot d \cdot \left[\frac{(h_{RB} - Y_{RB})^2}{2} + \frac{(h_{RB} - Y_{RB}) \cdot \varepsilon_{co} \cdot Y_{RB} \cdot \left[\left| 1 - \frac{\varepsilon_{bf} \cdot (h_{RB} - Y_{RB})}{\varepsilon_{co} \cdot Y_{RB}} \right| \right]^{n_c+1}}{\varepsilon_{bf} \cdot (n_c + 1)} + \right.$$

$$\left. \frac{\varepsilon_{co}^{\,2} \cdot Y_{RB}^{\,2} \cdot \left[\left| 1 - \frac{\varepsilon_{bf} \cdot (h_{RB} - Y_{RB})}{\varepsilon_{co} \cdot Y_{RB}} \right| \right]^{n_c+2}}{\varepsilon_{bf}^{\,2} \cdot (n_c + 1) \cdot (n_c + 2)} - \frac{\varepsilon_{co}^{\,2} \cdot Y_{RB}^{\,2}}{\varepsilon_{bf}^{\,2} \cdot (n_c + 1) \cdot (n_c + 2)} \right]$$

The sum of these two equations yields the total moment acting on the section due to the rotational displacement:

$$M_{Total} = M_{Lower} + M_{Upper}$$

Because the simultaneous solution of these equations is difficult, if not impossible, the routine Analysis_{RB} was written in Mathcad (see attached Appendix C) to find the solution to these equations that satisfies the equilibrium condition for the loads applied to the pile at the base of the cap and the forces in the concrete due to the displaced pile. The routine operates by summing shear forces and moments (about the bottom face of the cap) for a range of potential neutral axis locations and for a range of potential strains at the bottom face of the cap. The routine evaluates 501 potential neutral axis locations and 1500 potential strain values to create a results matrix with 751,500 entries. For each neutral axis location considered, the potential strains from zero to the peak strain (ε_{co}) are evaluated and residual forces are calculated by summing internal and external forces. The maximum residual force for each scenario evaluated, representing one entry in the results matrix, is taken as the larger of the absolute value of the shear force summation and the absolute value of the moment summation. The entry in the entire results matrix with the smallest value (the smallest residual force) is taken as the equilibrium position. The refined graduation of potential neutral axis and strain values and the resulting large number of sample points yield very low residual forces for the approximate solution thus obtained. This indicates that the values determine by this approximate analysis are very close to the exact (correct) values.

The strain data from the Analysis_{RB} routine discussed above is used in conjunction with the idealized beam strains to determine the translational displacement of the node at the bottom of the cap and the node at the top of the pile. The strain due to localized pile bearing stresses at the face of the pile is considered to vary linearly until it terminates at the point where the idealized beam strain profile intersects a vertical line at L_{pst}. The area between the idealized beam strains and the localized strains due to rigid body displacements represents the strain

density for the point under consideration. This area is equal to the translational displacement at this point. These translations are calculated for the point on the pile at the bottom face of the cap and the point at the top of the pile. The rotation of the pile is calculated as the arctangent of the difference between the displacements at the ends of the embedded pile segment divided by the length of the embedded pile segment. An illustration of the geometry used for these strain density calculations is shown in Figure 3-10.

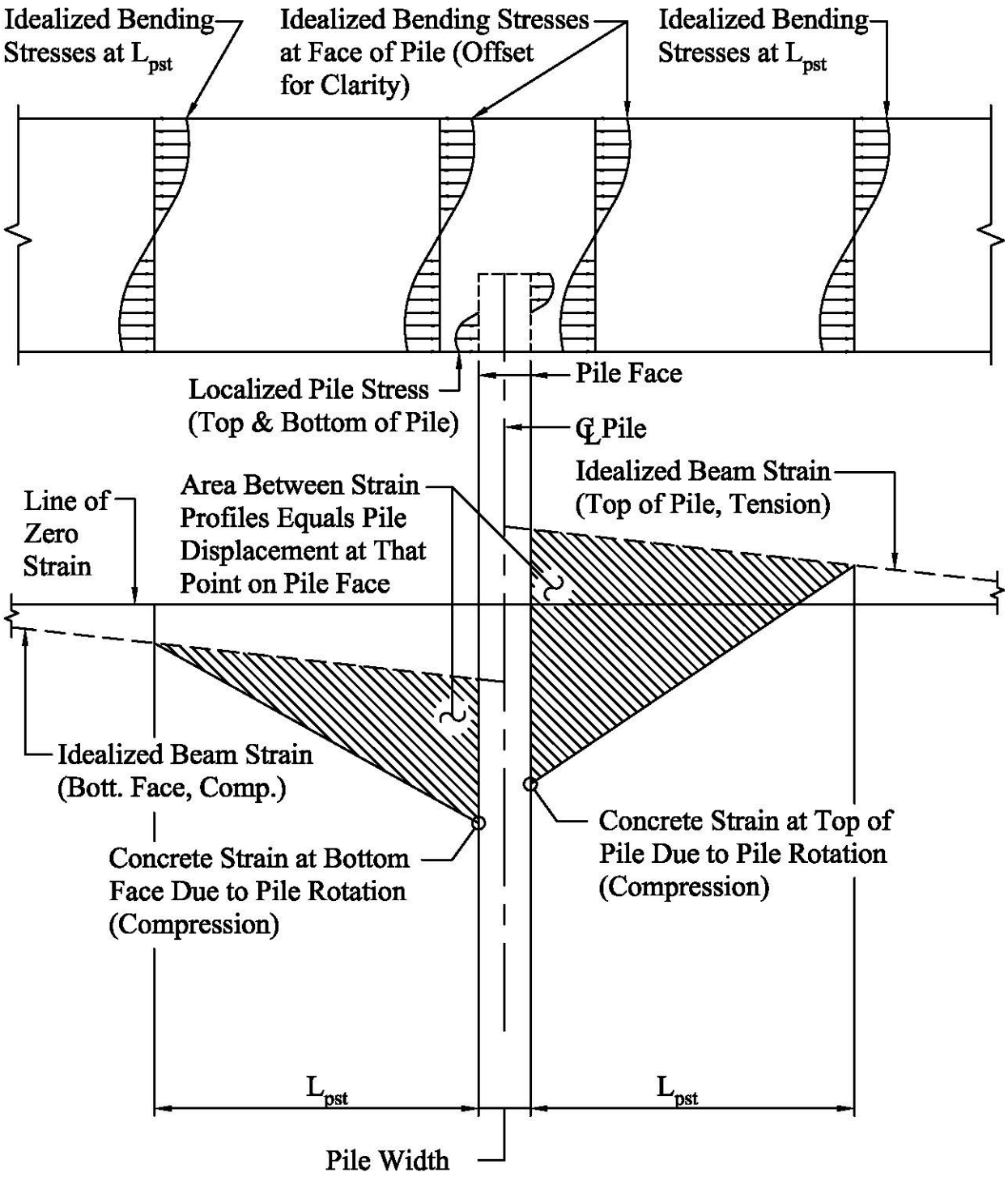

Figure 3-10 Illustration of Geometry Used for Strain Density Calculations in Method 4

3.9 Moment Capacity of Steel Piles Embedded in Concrete

The moment capacity of steel piles embedded in concrete has also been evaluated as part of this research. The capacity calculations are an abbreviated form of the rigid body calculations implemented in the Method 4 approach to connection stiffness. Instead of evaluating a range of potential strain values, the strain in the concrete at the bottom face of the cap is simply taken as the ultimate concrete strain, denoted as ε_{co} in the Mathcad calculations in Appendix C. The capacities for selected connection scenarios are compared to the capacities determined by the procedures outlined by Xiao et al. (2006) and those included in the PCI Design Handbook (PCI 1999). Refer to the literature review in Section 2.2 for a detailed description of these methods.

Chapter 4 Analysis Results

This thesis on the rotational stiffness of steel piles embedded in concrete considers the effects of pile embedment depth, concrete compressive strength and pile section properties. The effect of bending stresses in the concrete beam due to frame action is also considered. This research further includes the effects of four unique analysis approaches, referred to as Methods 1, 2, 3 and 4 in this paper, on the performance of these connections. Selected results intended to highlight the impact of each of these factors are included below. The trends apparent in this selected data are also apparent in the data not included in this chapter. The complete set of tabulated results is included in Appendix A and the complete set of graphical results is included in Appendix B.

4.1 Rotational Stiffness Results

Section 4.1 examines the effect of pile embedment depth, concrete compressive strength and pile section properties on the rotational stiffness of the connection. The effect of bending stresses in the concrete beam and analysis methods on rotational stiffness are considered as well. Observations based on these results are provided at the end of each section.

4.1.1 Impact of Pile Embedment Depth on Rotational Stiffness

Tables 4-1, 4-2, 4-3 and 4-4 provide selected rotational stiffness results for pile embedment depths for the HP10x42, HP12x53, HP14x89 and HP18x204, respectively. Figures 4-1 and 4-2 are also included to provide a graphical illustration of the rotational stiffness results of the HP10x42 for 12 inch and 18 inch embedments, respectively.

Table 4-1 Embedment Depth and Rotational Stiffness for HP10x42

HP10x42 Connection Performance Data Rotational Stiffness						
ASTM A36 Material (Fy = 36,000 psi, Fu = 58,000 psi)						
			Connection Stiffness (in-lbs/rad)			
Bend. Case	Depth (in)	f'c (psi)	Link Elements with Traction Forces			Rigid Body
			Method 1	Method 2	Method 3	Method 4
1	12	3,000	6.51E+08	4.23E+08	2.75E+08	5.95E+08
1	18	3,000	1.47E+09	1.05E+09	8.06E+08	2.34E+09

Table 4-2 Embedment Depth and Rotational Stiffness for HP12x53

HP12x53 Connection Performance Data Rotational Stiffness						
ASTM A572 Grade 50 Material (Fy = 50,000 psi, Fu = 65,000 psi)						
			Connection Stiffness (in-lbs/rad)			
Bend. Case	Depth (in)	f'c (psi)	Link Elements with Traction Forces			Rigid Body
			Method 1	Method 2	Method 3	Method 4
1	12	3,000	8.78E+08	5.62E+08	3.67E+08	6.68E+08
1	18	3,000	2.05E+09	1.43E+09	1.01E+09	2.95E+09

Table 4-3 Embedment Depth and Rotational Stiffness for HP14x89

HP14x89 Connection Performance Data Rotational Stiffness						
ASTM A572 Grade 50 Material (Fy = 50,000 psi, Fu = 65,000 psi)						
			Connection Stiffness (in-lbs/rad)			
Bend. Case	Depth (in)	f'c (psi)	Link Elements with Traction Forces			Rigid Body
			Method 1	Method 2	Method 3	Method 4
1	12	3,000	1.21E+09	7.46E+08	5.09E+08	8.46E+08
1	18	3,000	3.08E+09	2.09E+09	1.38E+09	3.19E+09

Table 4-4 Embedment Depth and Rotational Stiffness for HP18x204

HP18x204 Connection Performance Data Rotational Stiffness						
ASTM A572 Grade 50 Material (Fy = 50,000 psi, Fu = 65,000 psi)						
			Connection Stiffness (in-lbs/rad)			
Bend. Case	Depth (in)	f'c (psi)	Link Elements with Traction Forces			Rigid Body
			Method 1	Method 2	Method 3	Method 4
1	18	3,000	3.69E+09	2.27E+09	1.55E+09	3.03E+09
1	24	3,000	7.00E+09	4.59E+09	3.05E+09	6.97E+09

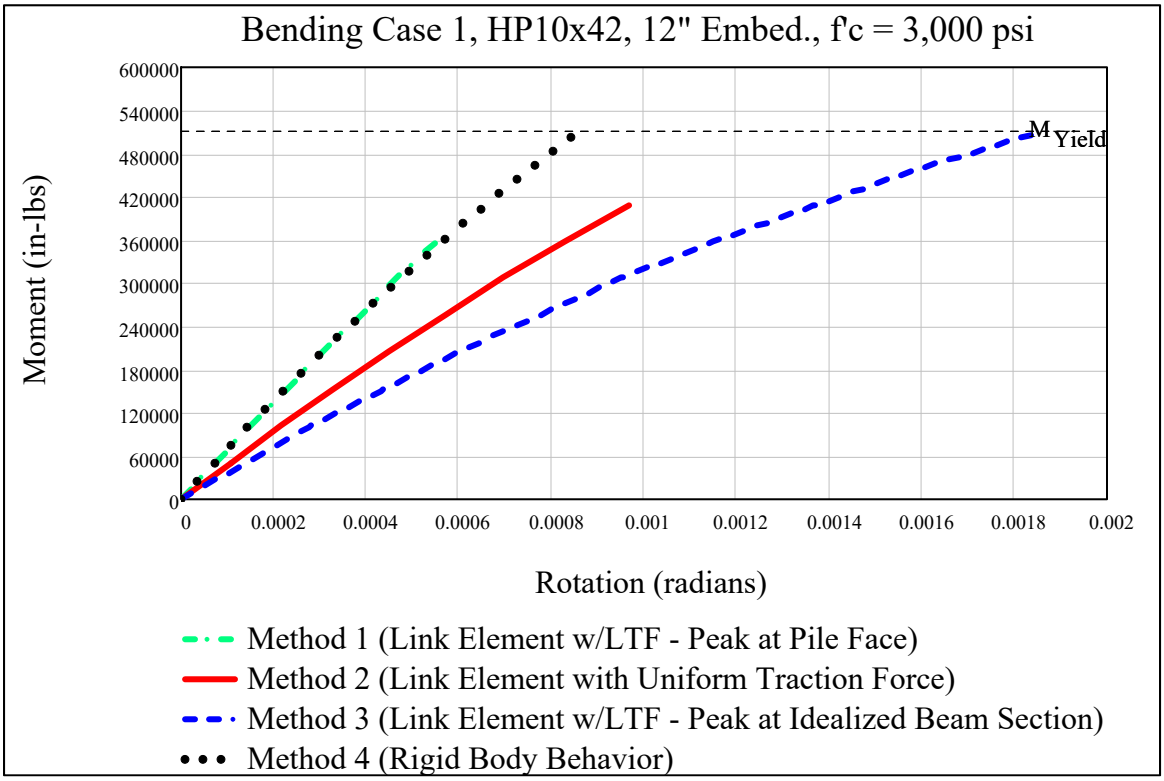

Figure 4-1 Illustration of Rotational Stiffness of HP10x42 with 12 Inch Embedment

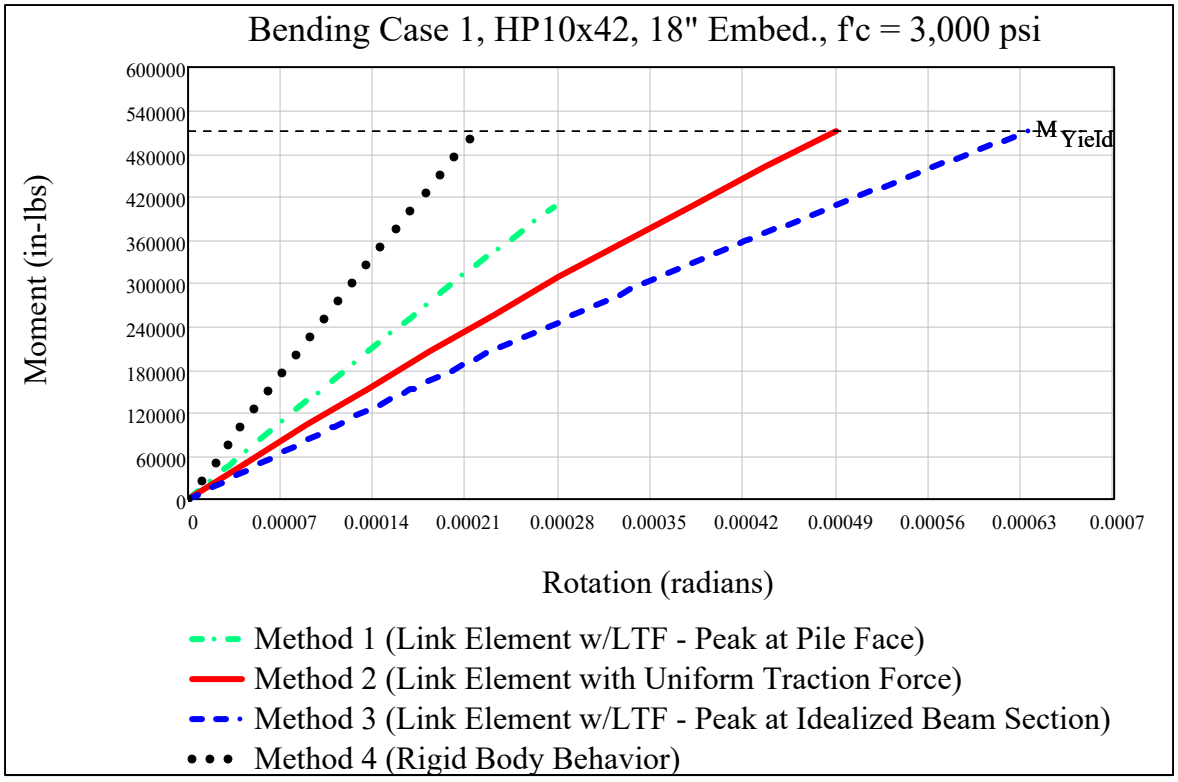

Figure 4-2 Illustration of Rotational Stiffness of HP10x42 with 18 Inch Embedment

These results clearly indicate that embedment depth has a very significant impact on the rotational stiffness of steel piles embedded in concrete. The data provided in Tables 4-1, 4-2 and 4-3 for Methods 1, 2 and 3 reveals a rotational stiffness increase between 124 and 193 percent when the embedment depth of the three smallest piles is increased from 12 inches to 18 inches. Similarly, the data provided in Table 4-4 for Methods 1, 2 and 3 reveals a rotational stiffness increase between 88 and 103 percent when the embedment depth of the HP18x204 is increased from 18 inches to 24 inches. The embedment depth increase is 150 percent for the three smallest piles, but only 133 percent for the HP18x204. This difference in the percentage increase of embedment depth causes the three smallest piles to have a larger percentage increase in stiffness than the HP18x204.

The data provided in Tables 4-1, 4-2 and 4-3 for Method 4 reveals a rotational stiffness increase between 270 and 352 percent when the embedment depth of the three smallest piles is

increased from 12 inches to 18 inches. Similarly, the data provided in Table 4-4 for Method 4 reveals a rotational stiffness increase between 127 and 133 percent when the embedment depth of the HP18x204 is increased from 18 inches to 24 inches. The rotational stiffness increase due to a larger embedment depth is greater for all piles analyzed by Method 4 because the rigid body behavior maximizes the resisting potential of the concrete. Methods 1, 2 and 3 include pile flexibility and are subsequently unable to fully utilize this potential.

Figures 4-1 and 4-2 graphically supplement the data included in Tables 4-1, 4-2, 4-3 and 4-4 and the conclusions based thereon.

4.1.2 Impact of Concrete Compressive Strength on Rotational Stiffness

Tables 4-5, 4-6, 4-7 and 4-8 provide selected rotational stiffness results for the concrete compressive strengths investigated for the HP10x42, HP12x53, HP14x89 and HP18x204, respectively. Figures 4-3, 4-4, and 4-5 are also included to provide a graphical illustration of the rotational stiffness results for the HP12x53 embedded 12 inches into 3,000, 5,000 and 10,000 psi concrete, respectively.

Table 4-5 Concrete Strength and Rotational Stiffness for HP10x42

HP10x42 Connection Performance Data Rotational Stiffness						
ASTM A36 Material (Fy = 36,000 psi, Fu = 58,000 psi)						
			Connection Stiffness (in-lbs/rad)			
Bend. Case	Depth (in)	f'c (psi)	Link Elements with Traction Forces			Rigid Body
			Method 1	Method 2	Method 3	Method 4
1	12	3,000	6.51E+08	4.23E+08	2.75E+08	5.95E+08
1	12	5,000	8.04E+08	5.53E+08	4.10E+08	8.48E+08
1	12	10,000	1.06E+09	7.66E+08	5.97E+08	1.26E+09

Table 4-6 Concrete Strength and Rotational Stiffness for HP12x53

HP12x53 Connection Performance Data Rotational Stiffness						
ASTM A572 Grade 50 Material (Fy = 50,000 psi, Fu = 65,000 psi)						
	Embed.		Connection Stiffness (in-lbs/rad)			
Bend.	Depth	f'c	Link Elements with Traction Forces			Rigid Body
Case	(in)	(psi)	Method 1	Method 2	Method 3	Method 4
1	12	3,000	8.78E+08	5.62E+08	3.67E+08	6.68E+08
1	12	5,000	1.08E+09	7.15E+08	4.80E+08	1.05E+09
1	12	10,000	1.41E+09	1.00E+09	7.64E+08	1.63E+09

Table 4-7 Concrete Strength and Rotational Stiffness for HP14x89

HP14x89 Connection Performance Data Rotational Stiffness						
ASTM A572 Grade 50 Material (Fy = 50,000 psi, Fu = 65,000 psi)						
	Embed.		Connection Stiffness (in-lbs/rad)			
Bend.	Depth	f'c	Link Elements with Traction Forces			Rigid Body
Case	(in)	(psi)	Method 1	Method 2	Method 3	Method 4
1	12	3,000	1.21E+09	7.46E+08	5.09E+08	8.46E+08
1	12	5,000	1.50E+09	9.57E+08	6.24E+08	1.18E+09
1	12	10,000	1.99E+09	1.33E+09	9.42E+08	1.97E+09

Table 4-8 Concrete Strength and Rotational Stiffness for HP18x204

HP18x204 Connection Performance Data Rotational Stiffness						
ASTM A572 Grade 50 Material (Fy = 50,000 psi, Fu = 65,000 psi)						
	Embed.		Connection Stiffness (in-lbs/rad)			
Bend.	Depth	f'c	Link Elements with Traction Forces			Rigid Body
Case	(in)	(psi)	Method 1	Method 2	Method 3	Method 4
1	18	3,000	3.69E+09	2.27E+09	1.55E+09	3.03E+09
1	18	5,000	4.54E+09	3.01E+09	2.03E+09	3.94E+09
1	18	10,000	6.03E+09	4.09E+09	2.85E+09	6.78E+09

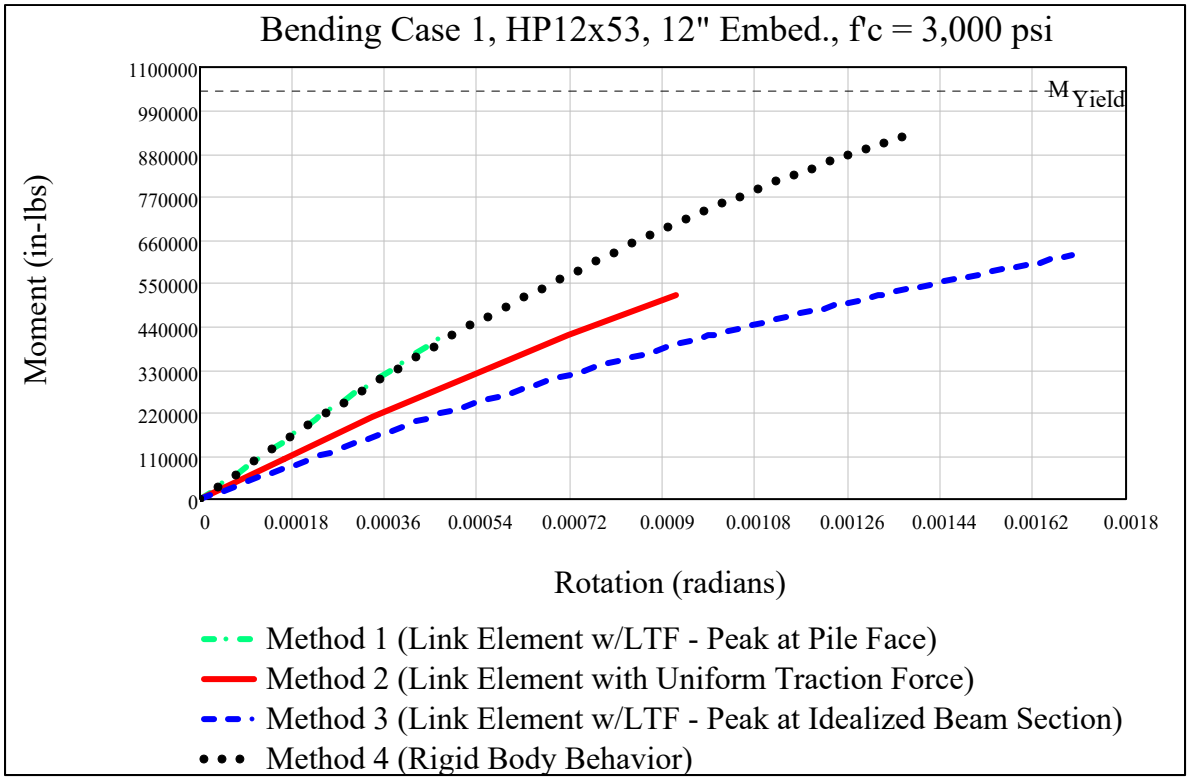

Figure 4-3 Illustration of Rotational Stiffness of HP12x53 with 3,000 psi Concrete

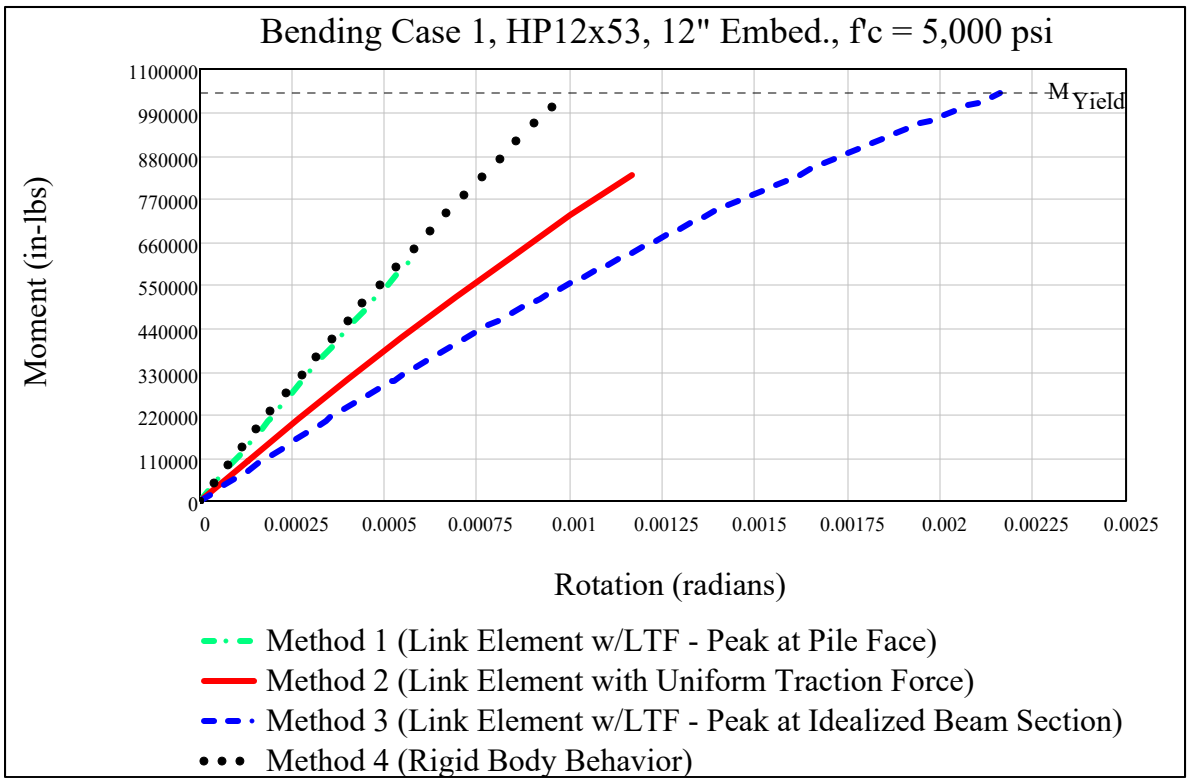

Figure 4-4 Illustration of Rotational Stiffness of HP12x53 with 5,000 psi Concrete

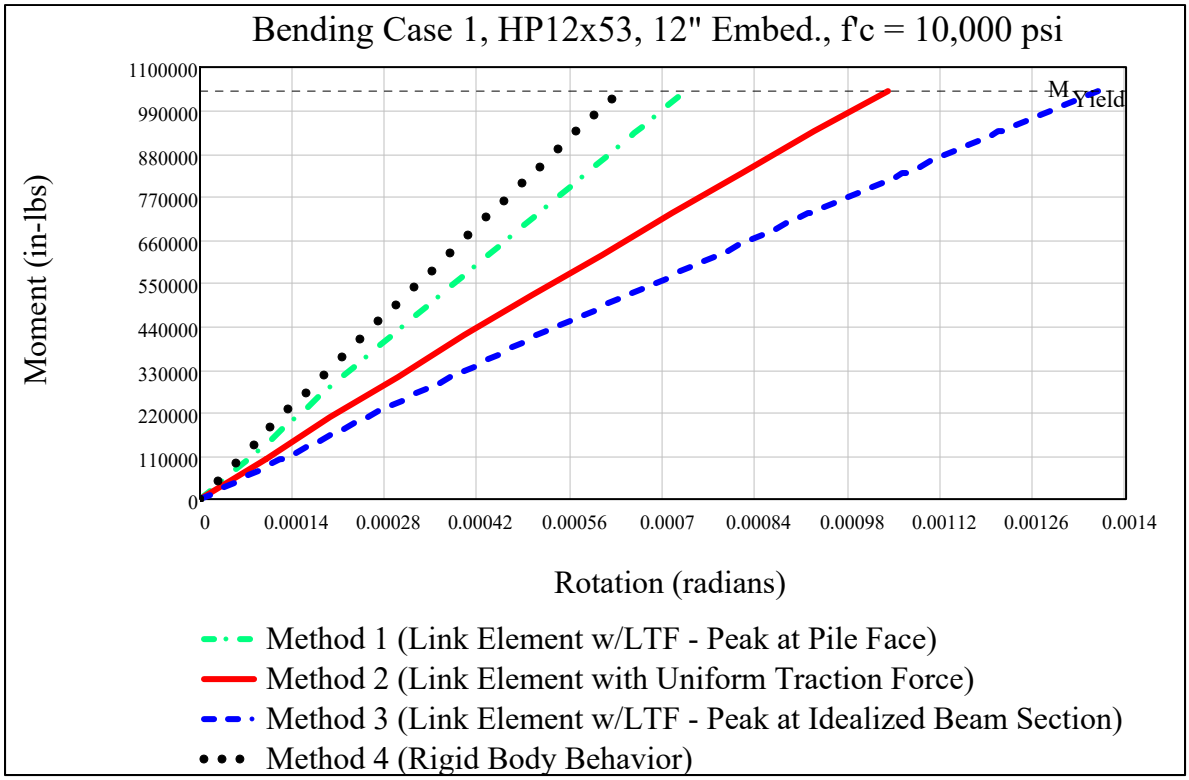

Figure 4-5 Illustration of Rotational Stiffness of HP12x53 with 10,000 psi Concrete

These results clearly indicate that concrete compressive strength has a significant impact on the rotational stiffness of steel piles embedded in concrete. The data provided in Tables 4-5, 4-6, 4-7 and 4-8 for all four analysis methods reveals a rotational stiffness increase between 23 and 57 percent when the compressive strength of the concrete is increased from 3,000 psi to 5,000 psi. These tables indicated a rotational stiffness increase between 31 and 72 percent when the compressive strength of the concrete is increased from 5,000 psi to 10,000 psi.

Figures 4-3, 4-4 and 4-5 graphically supplement the data included in Tables 4-5, 4-6, 4-7 and 4-8 and the conclusions based thereon.

4.1.3 Impact of Pile Section Properties on Rotational Stiffness

Table 4-9 provides selected rotational stiffness results for all four pile sections, each of which is embedded 18 inches into 5,000 psi compressive strength concrete. Figures 4-6, 4-7, 4-8 and 4-9 are also included to provide a graphical illustration of the effects of pile section

properties on the rotational stiffness results for the HP10x42, HP12x53, HP14x89 and HP18x204, respectively.

Table 4-9 Pile Section Properties and Rotational Stiffness

Effect of Pile Section Properties on Rotational Stiffness (Bending Case 1, 18 Inch Embedment and 5,000 psi Concrete)						
	Embed.		Connection Stiffness (in-lbs/rad)			
Pile	Depth	f'c	Link Elements with Traction Forces			Rigid Body
Section	(in)	(psi)	Method 1	Method 2	Method 3	Method 4
HP10x42	18	5,000	1.75E+09	1.31E+09	1.04E+09	3.13E+09
HP12x53	18	5,000	2.43E+09	1.74E+09	1.36E+09	4.07E+09
HP14x89	18	5,000	3.68E+09	2.54E+09	1.81E+09	4.86E+09
HP18x204	18	5,000	4.54E+09	3.01E+09	2.03E+09	3.94E+09

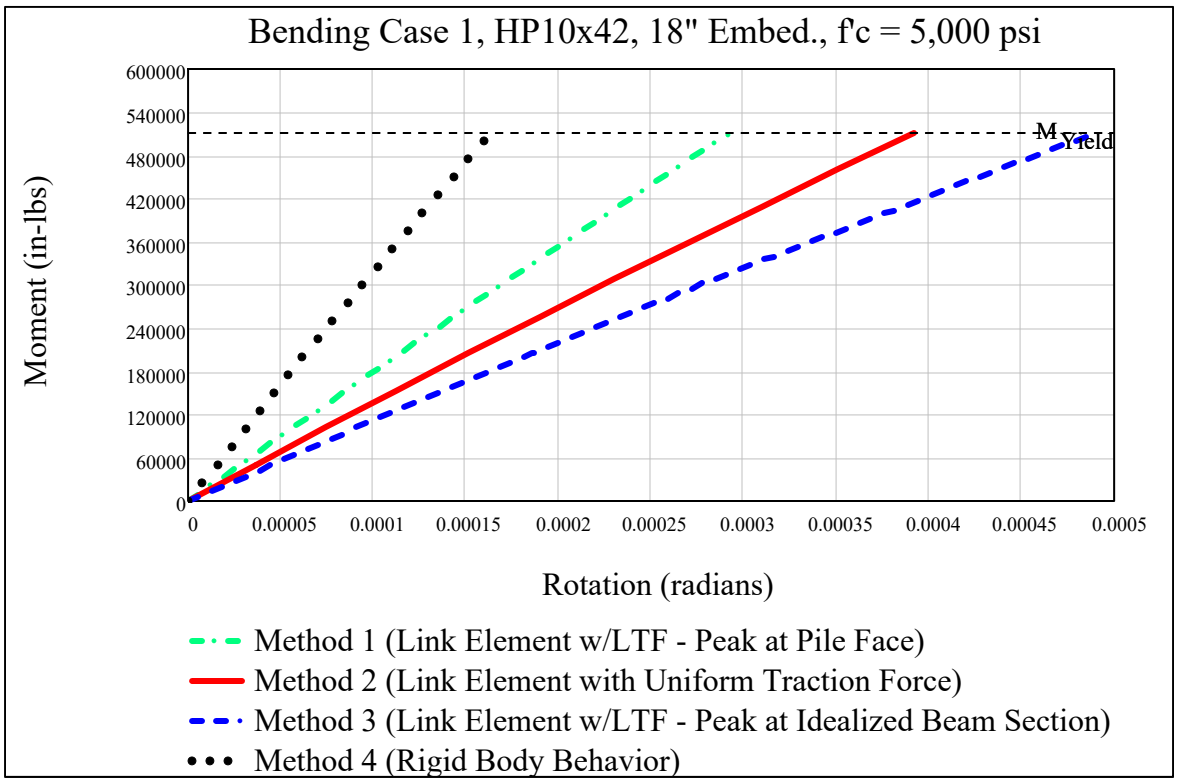

Figure 4-6 Illustration of Pile Section Properties and Rotational Stiffness of HP10x42

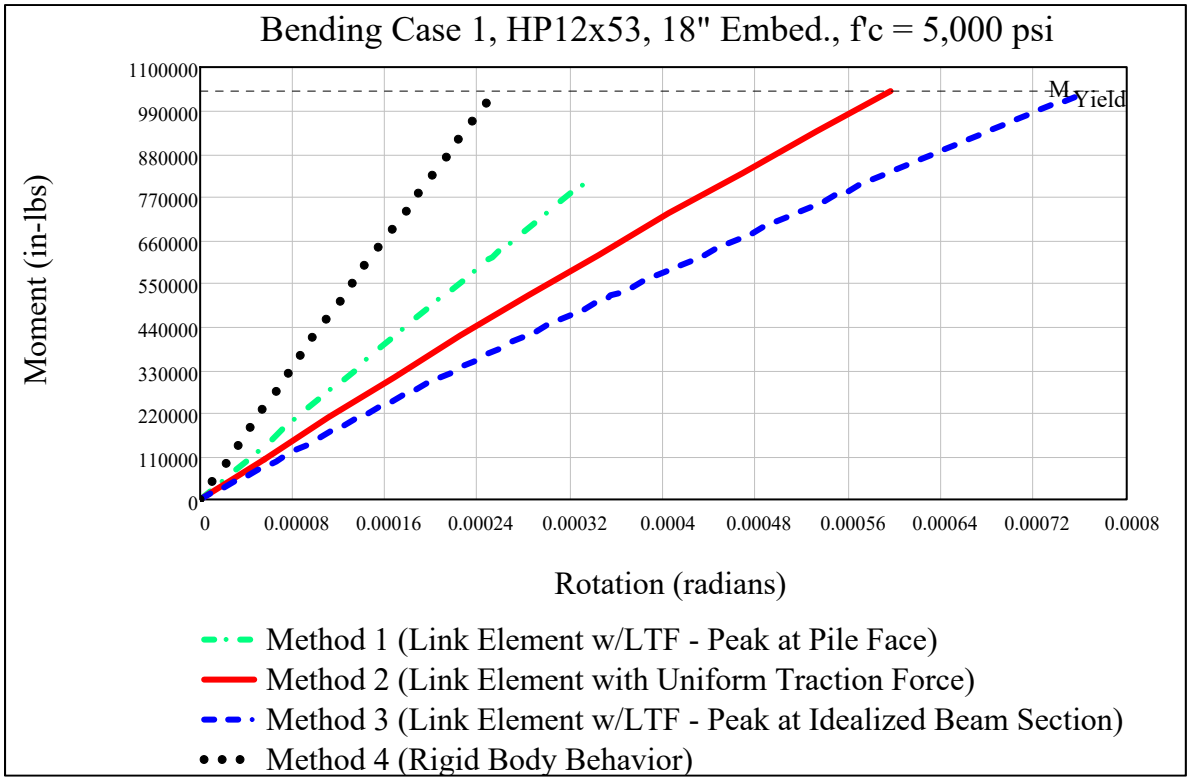

Figure 4-7 Illustration of Pile Section Properties and Rotational Stiffness of HP12x53

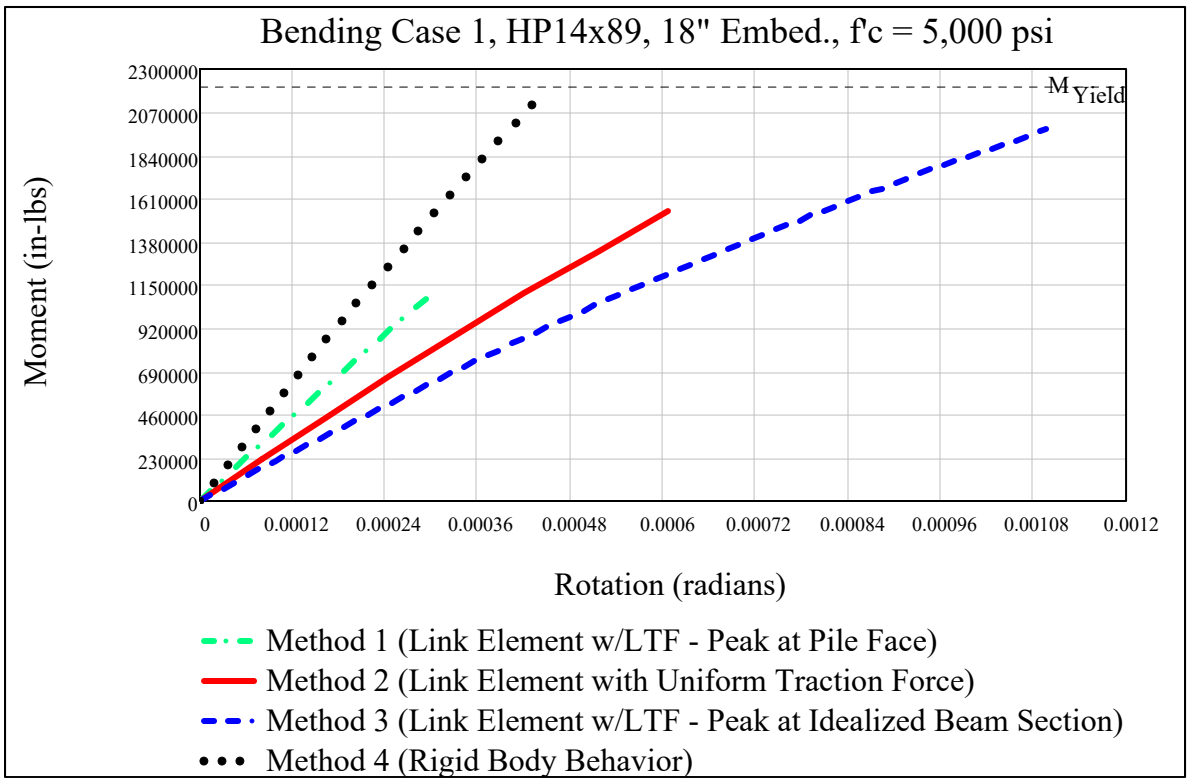

Figure 4-8 Illustration of Pile Section Properties and Rotational Stiffness of HP14x89

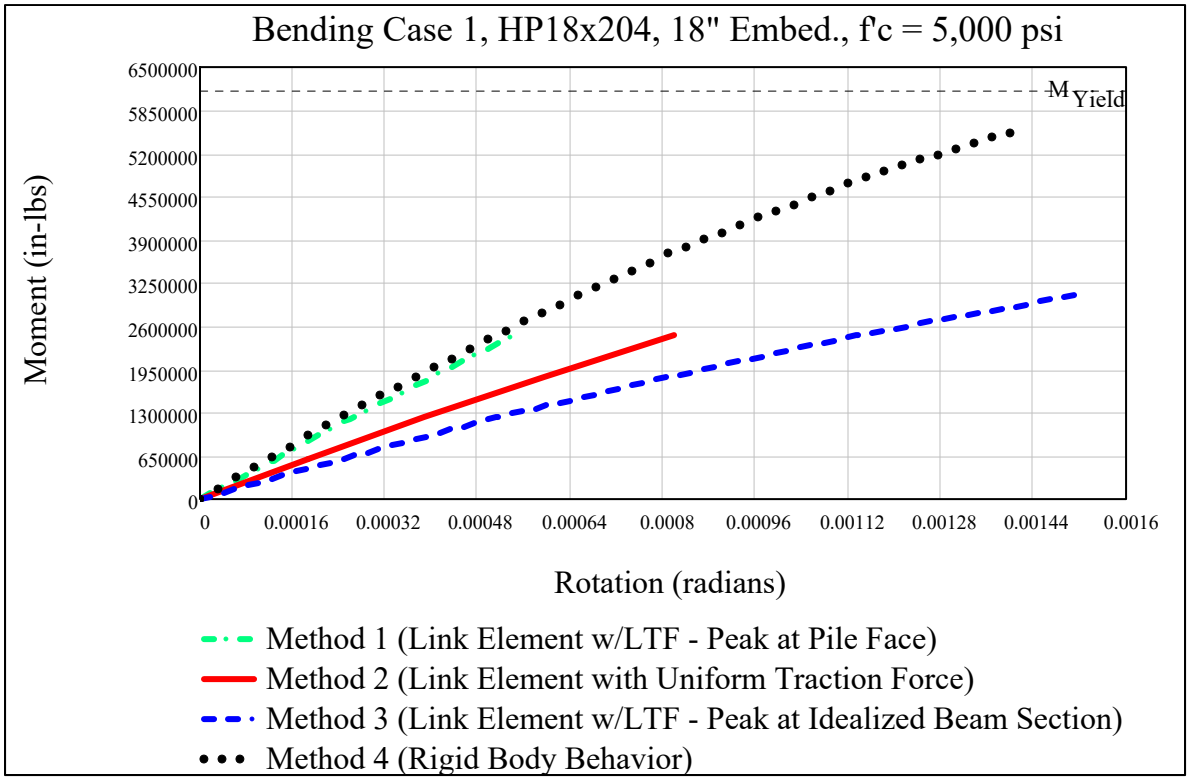

Figure 4-9 Illustration of Pile Section Properties and Rotational Stiffness of HP18x204

These results indicate that the rotational stiffness of steel piles embedded in concrete is affected by pile section properties. The data provided in Table 4-9 for all four analysis methods reveals an average rotational stiffness increase of 33 percent when the pile section is increased from an HP10x42 to an HP12x53. This table indicates an average rotational stiffness increase for all four analysis methods of 38 percent when the pile section is increased from an HP12x53 to an HP14x89. Increasing the pile section from an HP14x89 to an HP18x204 indicates an average increase in rotational stiffness of 9 percent for all four methods.

It is interesting to note the decrease in rotational stiffness under Method 4 corresponding to the change from an HP14x89 to an HP18x204. The maximum moment resisted by the HP14x89 is 2,206,172 in-lbs compared to 5,539,523 in-lbs for the HP18x204. The HP18x204 provides a much larger moment capacity than the HP14x89 as expected. Additionally, the HP18x204 section is 4.5 inches (1.33 times) deeper than the HP14x89. This larger section depth

allows the HP18x204 to engage more encasing concrete as it is rotated to form the resisting couple; a characteristic that would appear to yield a stiffer connection. But, the moment of inertia of the HP18x204 is 3.44 times larger than the moment of inertia of the HP14x89. Because the increase in cross section stiffness from the HP14x89 to the HP18x204 is so much larger than the increase in section depth (an important component in resisting couple capacity), the HP18x204 will have to rotate much more than the HP14x89 to develop its yield moment. Calculating the rotational stiffness as a straight line between the origin and the terminal point on the moment-rotation curve, it is a straightforward observation that the rotational stiffness of this HP14x89 connection is larger than the rotational stiffness of this HP18x204 connection.

Figures 4-6, 4-7, 4-8 and 4-9 graphically supplement the data included in Table 4-9 and the conclusions based thereon.

4.1.4 Impact of Cap Bending Stresses on Rotational Stiffness

Table 4-10 provides selected rotational stiffness results for an HP12x53 pile section embedded 18 inches into 5,000 psi compressive strength concrete for all four bending cases. Figures 4-10, 4-11, 4-12 and 4-13 are also included to provide a graphical illustration of the effects of cap bending stresses on the rotational stiffness of this connection.

Table 4-10 Cap Bending Stresses and Rotational Stiffness

HP12x53 Connection Performance Data Effect of Cap Bending Stresses on Rotational Stiffness						
ASTM A572 Grade 50 Material (Fy = 50,000 psi, Fu = 65,000 psi)						
			Connection Stiffness (in-lbs/rad)			
Bend. Case	Depth (in)	f'c (psi)	Link Elements with Traction Forces			Rigid Body
			Method 1	Method 2	Method 3	Method 4
1	18	5,000	2.43E+09	1.74E+09	1.36E+09	4.07E+09
2	18	5,000	2.49E+09	1.77E+09	1.37E+09	4.25E+09
3	18	5,000	2.36E+09	1.71E+09	1.34E+09	3.91E+09
4	18	5,000	2.35E+09	1.71E+09	1.34E+09	3.91E+09

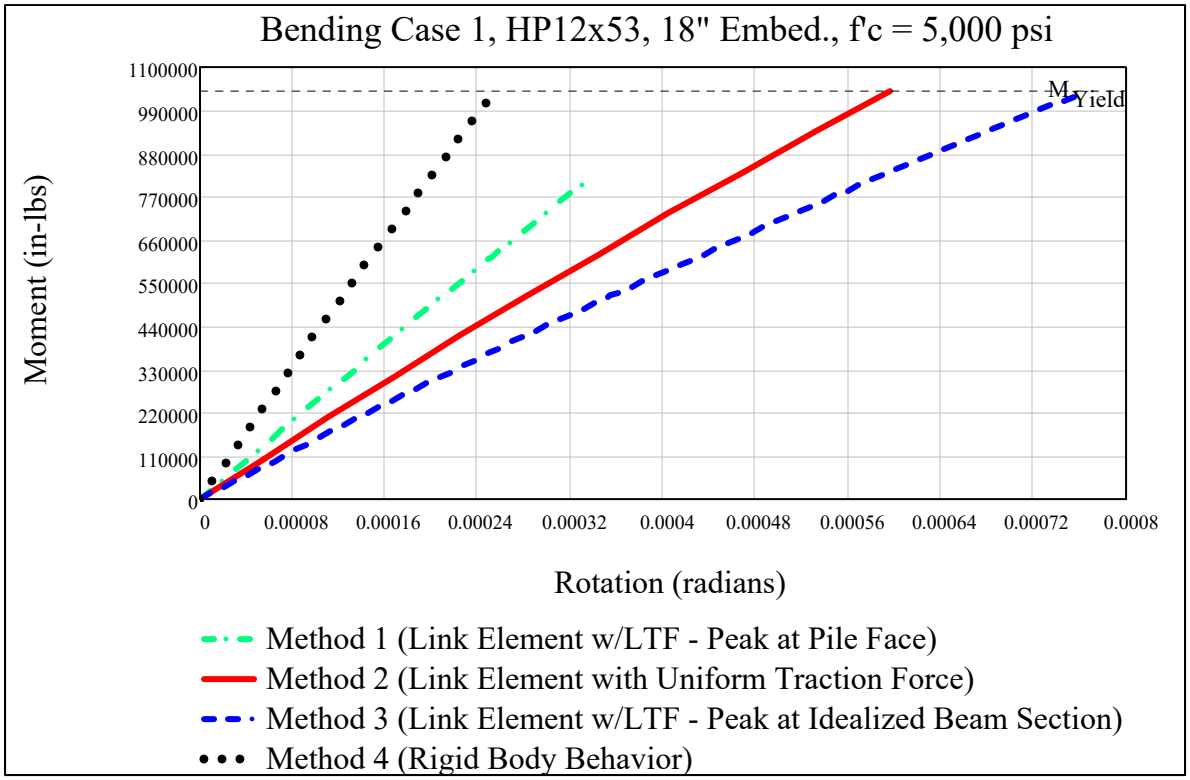

Figure 4-10 Illustration of Bending Case 1 and Rotational Stiffness of HP12x53

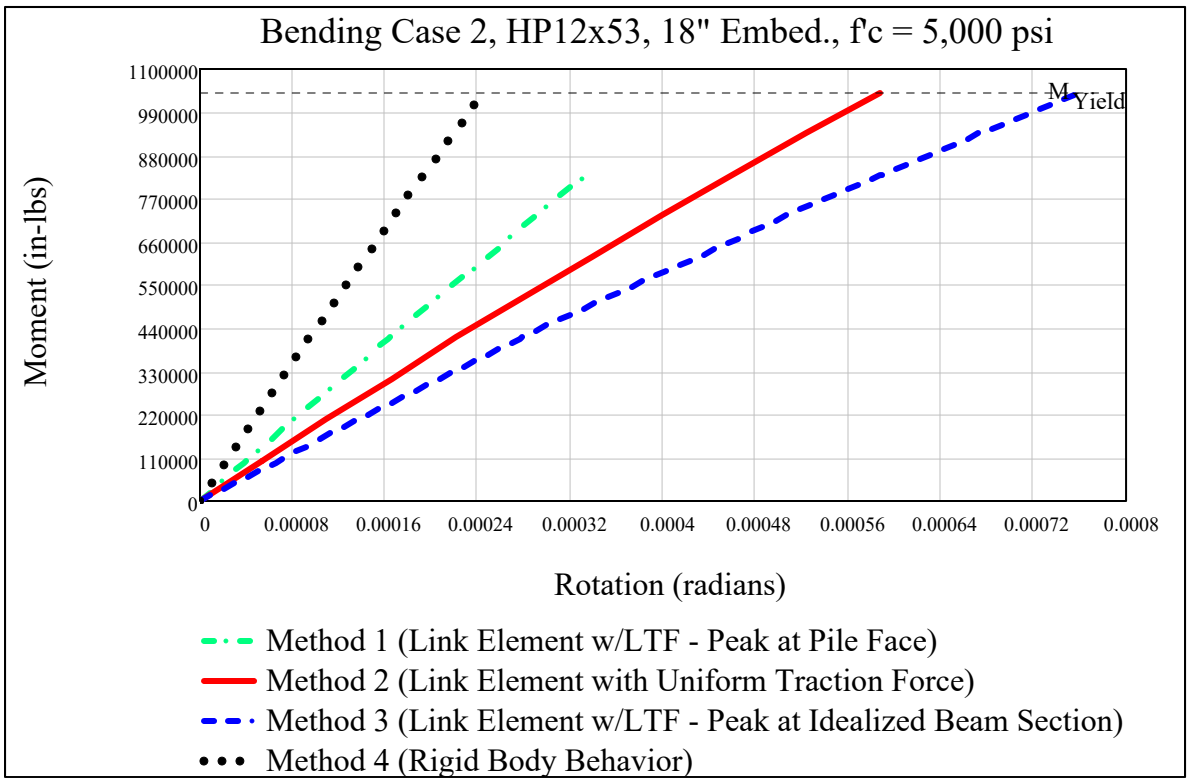

Figure 4-11 Illustration of Bending Case 2 and Rotational Stiffness of HP12x53

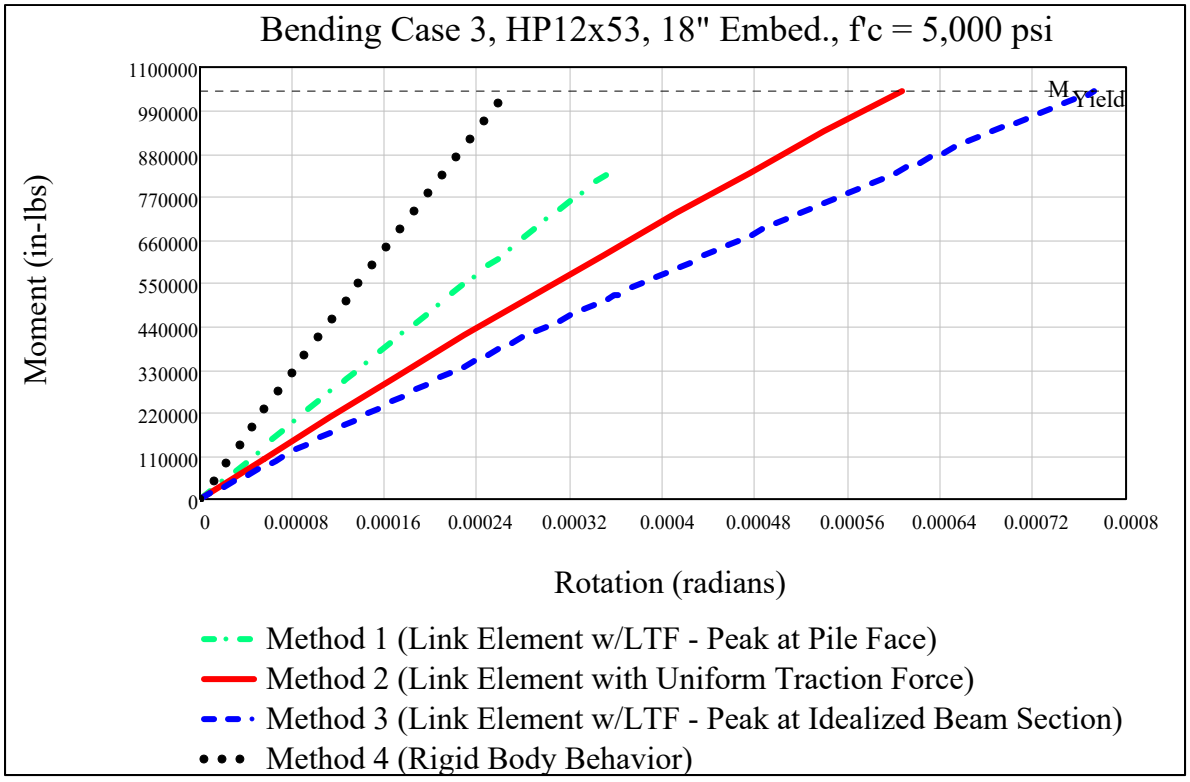

Figure 4-12 Illustration of Bending Case 3 and Rotational Stiffness of HP12x53

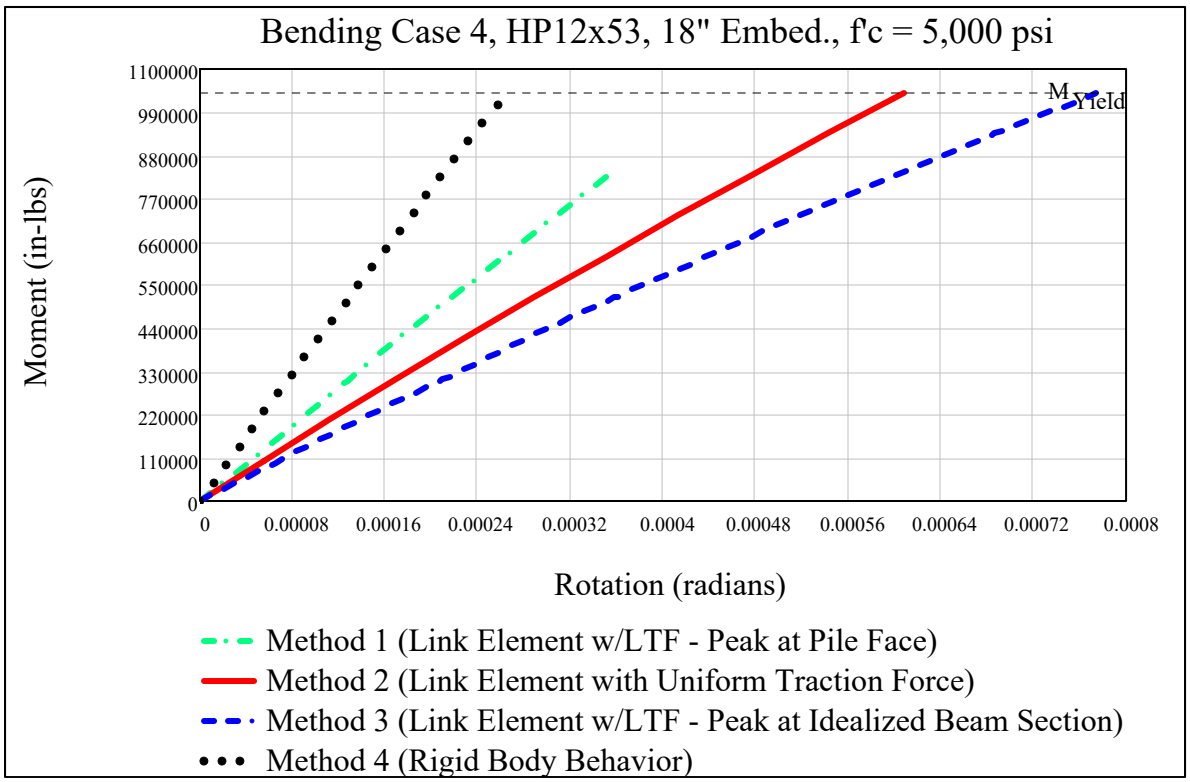

Figure 4-13 Illustration of Bending Case 4 and Rotational Stiffness of HP12x53

These results indicate that the rotational stiffness of steel piles embedded in concrete is not significantly impacted by bending stresses in the cap resulting from frame action. The data provided in Table 4-10 reveals that the rotational stiffness for each bending case is within about 3 percent of the average rotational stiffness for the analysis method being considered.

Figures 4-10, 4-11, 4-12 and 4-13 graphically supplement the data included in Table 4-10 and the conclusions based thereon.

4.1.5 Impact of Analysis Methods on Rotational Stiffness

Table 4-11 provides the rotational stiffness results for all four analysis methods for an HP14x89 embedded 18 inches into 3,000 psi compressive strength concrete. Figure 4-14 is also included to provide a graphical illustration of the effect of analysis methods on rotational stiffness.

Table 4-11 Analysis Methods and Rotational Stiffness

HP14x89 Connection Performance Data Effect of Analysis Methods on Rotational Stiffness						
ASTM A572 Grade 50 Material (Fy = 50,000 psi, Fu = 65,000 psi)						
	Embed.		Connection Stiffness (in-lbs/rad)			
Bend.	Depth	f'c	Link Elements with Traction Forces			Rigid Body
Case	(in)	(psi)	Method 1	Method 2	Method 3	Method 4
1	18	3,000	3.08E+09	2.09E+09	1.38E+09	3.19E+09

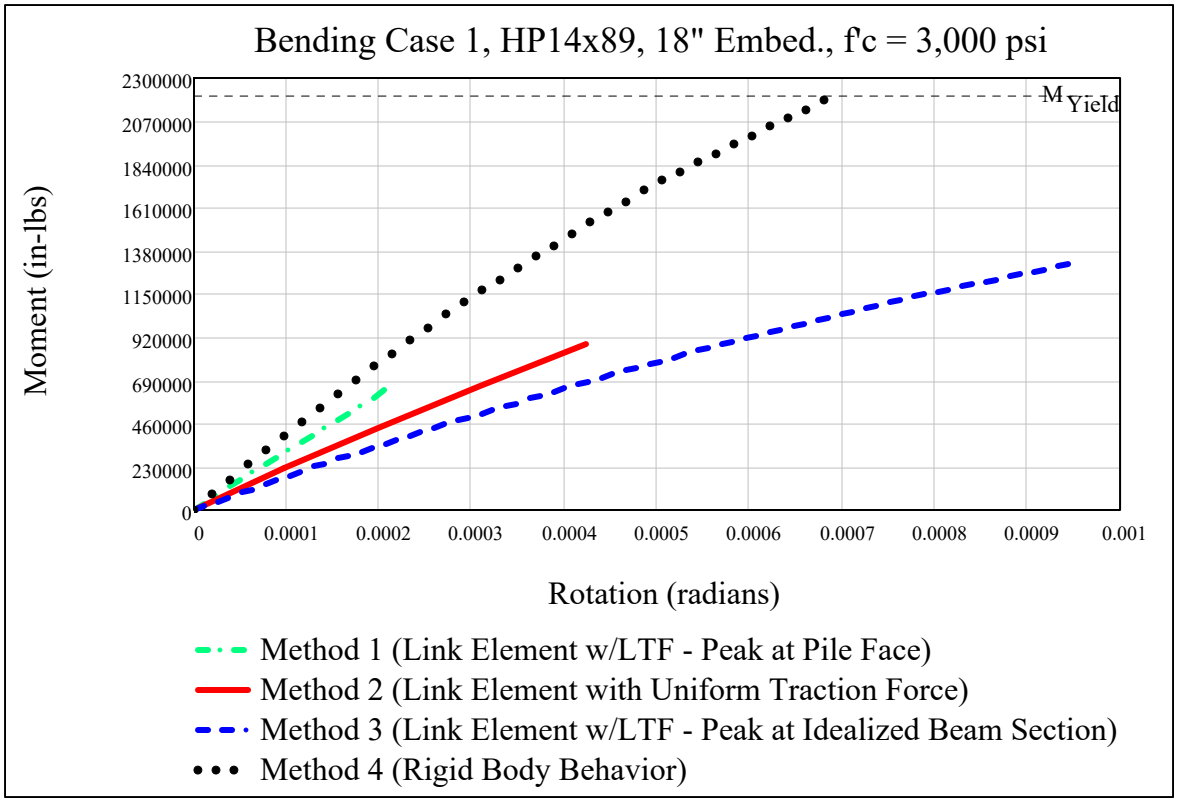

Figure 4-14 Illustration of Analysis Methods and Rotational Stiffness

These results indicate that analysis methods and assumptions have a very significant impact on the calculated rotational stiffness of embedded steel pile connections. All four of these analysis methods consider the nonlinear behavior of the concrete and can be generalized into two primary categories, each of which is intended to represent one surface of the envelope that bounds potential connection behavior. The distinguishing characteristic of the first category is the inclusion of pile deformations. The distinguishing characteristic of the second category is the exclusion of pile deformations (i.e., rigid body rotation of the embedded pile segment within the concrete cap).

The first analysis category includes pile deformations and is divided into the three approaches referred to in this paper as Methods 1, 2 and 3 that use link elements to connect the embedded pile segment to the encasing cap concrete. Recall that the link elements in these

methods are simply the tools used to model the load sharing between the pile stress transfer block (PSTB) and the surrounding concrete in the cap. The link element employed in Method 1 sheds its load quickly to the surrounding concrete. This behavior causes the stresses in the PSTB concrete to become very sensitive to the translational displacement of the pile under the applied loads. Method 1 provides very stiff connection values that are similar to the rotational stiffness values determined using Method 4 (rigid body approach, discussed below); however, the flexibility of the pile in Method 1 exacerbates the effects of pile deformations. This exacerbation causes high stresses to develop in the PSTB concrete at much smaller connection rotations than the other three methods.

The link element employed in Method 2 sheds its load uniformly to the surrounding concrete. This behavior is between the extremes modelled by Methods 1 and 3 (discussed below). The rotational stiffness values for Method 2 are generally found to be near the midpoint between the corresponding values calculated for Methods 1 and 3.

The link element employed in Method 3 sheds its load rather slowly to the surrounding concrete. This behavior causes the stresses in the PSTB concrete to be less sensitive to the translational displacements of the pile under the applied loads than Methods 1, 2 or 4. This reduced sensitivity allows larger connection rotations and translational displacements of the embedded pile segment without exceeding the compressive strength of the concrete at the bottom face of the cap. Method 3 provides the lowest rotational stiffness values of all the methods evaluated in this research.

The second analysis category does not include pile deformations. This approach is referred to in this thesis as Method 4. The rigid body rotation of the embedded pile segment considered in this method causes a linear increase in concrete strains as the distance from the

neutral axis increases. This assumed behavior maximizes the moment capacity of the embedded pile connection since the detrimental effects of pile deformations on PSTB concrete stresses are not included. This strain density approach to connection rotation yields the stiffest connection model among all for methods considered.

Rodas et al. (2017) provides results for multiple full-scale tests using the test configuration described in Section 2.2. The rotational stiffness for the test referred to in their paper as UCS Test Number 3 consisted of a W14x370 embedded 30 inches into 4,000 psi concrete is 3,062,357 in-kips/rad. The rotational stiffness for this scenario using Method 3 is 3,406,881 in-kips/rad, which is 11 percent stiffer than the test value. The rotational stiffness for the test referred to in their paper as BYU Test Number B2 consisted of a W8x48 embedded 16 inches into 4,000 psi concrete is 187,636 in-kips/rad. The rotational stiffness for this scenario using Method 3 is 254,993 in-kips/rad, which is 36 percent stiffer than the test value.

4.2 Maximum Moment Results

Section 4.2 examines the effect of pile embedment depth, concrete compressive strength and pile section properties on the maximum moment supported by the connection when the structural evaluation is terminated. This termination occurs when the moment acting on the pile is equal to the yield moment or when the concrete stresses in the PSTB exceeds the compressive strength of the concrete. The effect of bending stresses in the concrete beam and analysis methods on the maximum moment are considered as well. Observations based on these results are provided at the end of each section.

4.2.1 Impact of Pile Embedment Depth on Maximum Moment

Tables 4-12, 4-13 and 4-14 provide maximum moment results for the three smallest pile sections embedded 12 inches and 18 inches into 3,000 psi concrete. Table 4-15 provides

maximum moment results for an HP18x204 embedded 18 inches and 24 inches into 3,000 psi concrete. Figures 4-15 and 4-16 are also included to provide a graphical illustration of the effect of embedment depth on the maximum moment of an HP12x53 embedded 12 and 18 inches into 3,000 psi concrete, respectively.

Table 4-12 Embedment Depth and Maximum Moment for HP10x42

HP10x42 Connection Performance Data Maximum Moment						
ASTM A36 Material (Fy = 36,000 psi, Fu = 58,000 psi)						
			Maximum Moment Resisted by Embedded Pile (in-lbs)			
Bend. Case	Depth (in)	f'c (psi)	Link Elements with Traction Forces			Rigid Body
			Method 1	Method 2	Method 3	Method 4
1	12	3,000	3.58E+05	4.10E+05	5.12E+05	5.12E+05
1	18	3,000	4.10E+05	5.12E+05	5.12E+05	5.12E+05

Table 4-13 Embedment Depth and Maximum Moment for HP12x53

HP12x53 Connection Performance Data Maximum Concrete Compressive Stress						
ASTM A572 Grade 50 Material (Fy = 50,000 psi, Fu = 65,000 psi)						
			Maximum Moment Resisted by Embedded Pile (in-lbs)			
Bend. Case	Depth (in)	f'c (psi)	Link Elements with Traction Forces			Rigid Body
			Method 1	Method 2	Method 3	Method 4
1	12	3,000	4.16E+05	5.20E+05	6.24E+05	9.36E+05
1	18	3,000	5.20E+05	7.28E+05	9.36E+05	1.04E+06

Table 4-14 Embedment Depth and Maximum Moment for HP14x89

HP14x89 Connection Performance Data Maximum Moment						
ASTM A572 Grade 50 Material (Fy = 50,000 psi, Fu = 65,000 psi)						
			Maximum Moment Resisted by Embedded Pile (in-lbs)			
Bend. Case	Depth (in)	f'c (psi)	Link Elements with Traction Forces			Rigid Body
			Method 1	Method 2	Method 3	Method 4
1	12	3,000	4.41E+05	6.62E+05	6.62E+05	1.10E+06
1	18	3,000	6.62E+05	8.82E+05	1.32E+06	2.21E+06

Table 4-15 Embedment Depth and Maximum Moment for HP18x204

HP18x204 Connection Performance Data Maximum Moment						
ASTM A572 Grade 50 Material (Fy = 50,000 psi, Fu = 65,000 psi)						
			Maximum Moment Resisted by Embedded Pile (in-lbs)			
Bend. Case	Depth (in)	f'c (psi)	Link Elements with Traction Forces			Rigid Body
			Method 1	Method 2	Method 3	Method 4
1	18	3,000	1.23E+06	1.85E+06	1.85E+06	3.08E+06
1	24	3,000	1.85E+06	2.46E+06	3.08E+06	6.16E+06

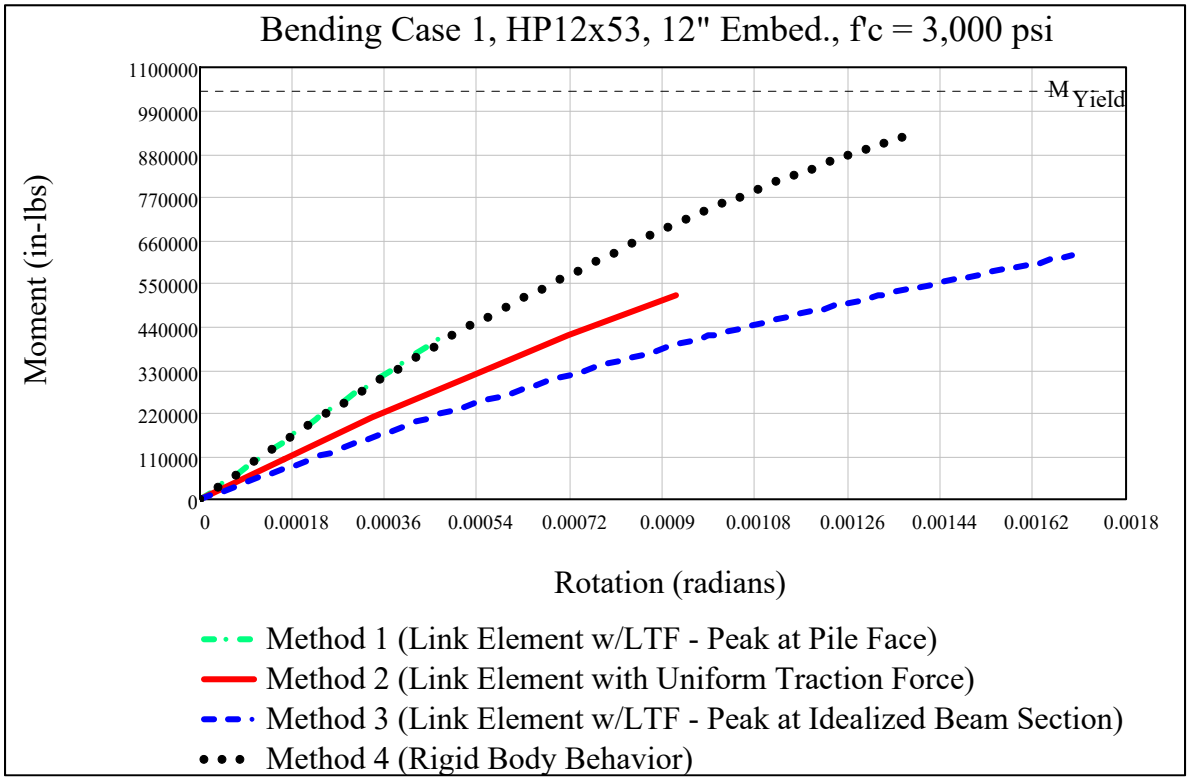

Figure 4-15 Illustration of 12 Inch Embedment Depth and Maximum Moment

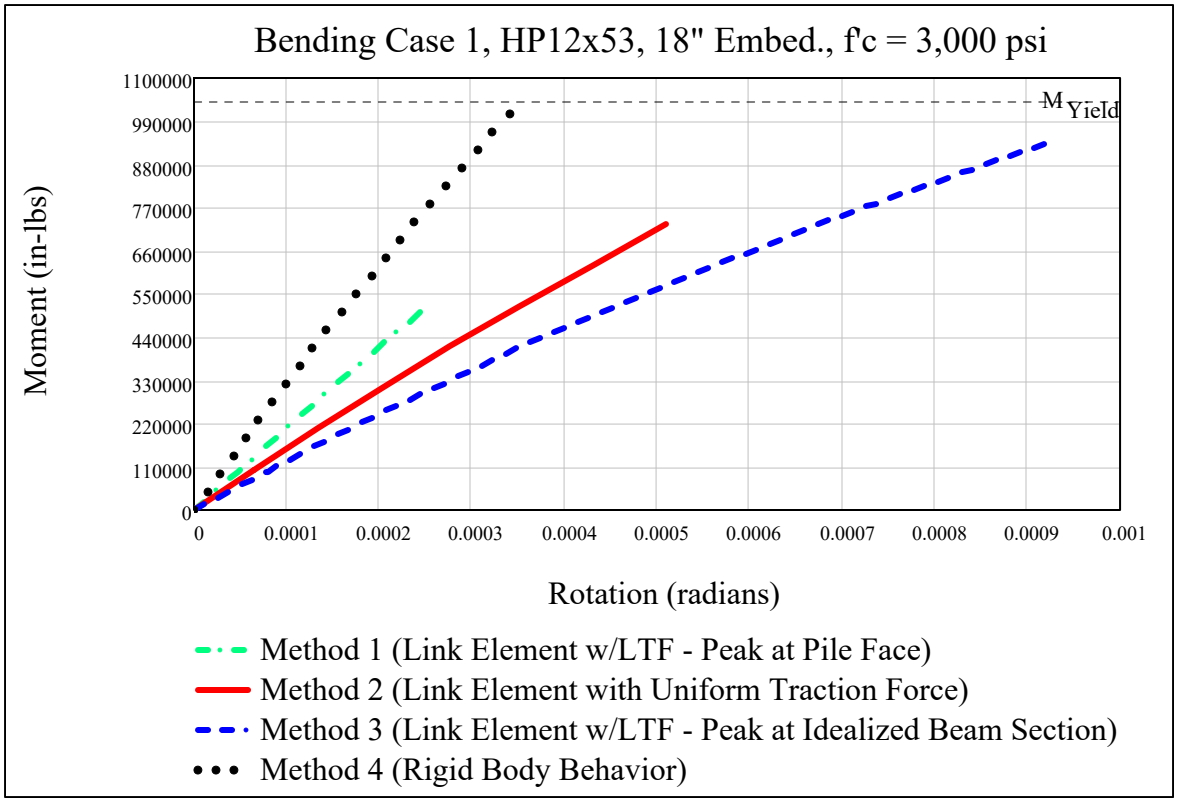

Figure 4-16 Illustration of 18 Inch Embedment Depth and Maximum Moment

These results indicate that embedment depth has a significant impact on the maximum moment of steel piles embedded in concrete. The maximum moment for all piles considered increases between 14 and 100 percent with the increase in embedment depth. The exception to this tendency to increase occurs under Methods 3 and 4 in Table 4-12. The HP10x42 is able to develop its yield moment with a 12 inch embedment in these two cases, so there is no increase in the maximum moment for the HP10x42 for these methods. An increase in the maximum moment for the HP10x42 might have occurred if the plastic moment was considered to be a limiting condition instead of the yield moment.

Figures 4-15 and 4-16 graphically supplement the tabulated data and the conclusions based thereon.

4.2.2 Impact of Concrete Compressive Strength on Maximum Moment

Tables 4-16, 4-17, 4-18 and 4-19 provide selected maximum moment results for the concrete compressive strengths investigated for the HP10x42, HP12x53, HP14x89 and HP18x204, respectively. Figures 4-17, 4-18, and 4-19 are also included to provide a graphical illustration of the maximum moment results for the HP14x89 embedded 12 inches into 3,000, 5,000 and 10,000 psi concrete, respectively.

Table 4-16 Concrete Strength and Maximum Moment for HP10x42

HP10x42 Connection Performance Data Maximum Moment						
ASTM A36 Material (Fy = 36,000 psi, Fu = 58,000 psi)						
	Embed.		Maximum Moment Resisted by Embedded Pile (in-lbs)			
Bend.	Depth	f'c	Link Elements with Traction Forces			Rigid Body
Case	(in)	(psi)	Method 1	Method 2	Method 3	Method 4
1	12	3,000	3.58E+05	4.10E+05	5.12E+05	5.12E+05
1	12	5,000	5.12E+05	5.12E+05	5.12E+05	5.12E+05
1	12	10,000	5.12E+05	5.12E+05	5.12E+05	5.12E+05

Table 4-17 Concrete Strength and Maximum Moment for HP12x53

HP12x53 Connection Performance Data Maximum Moment						
ASTM A572 Grade 50 Material (Fy = 50,000 psi, Fu = 65,000 psi)						
	Embed.		Maximum Moment Resisted by Embedded Pile (in-lbs)			
Bend.	Depth	f'c	Link Elements with Traction Forces			Rigid Body
Case	(in)	(psi)	Method 1	Method 2	Method 3	Method 4
1	12	3,000	4.16E+05	5.20E+05	6.24E+05	9.36E+05
1	12	5,000	6.24E+05	8.32E+05	1.04E+06	1.04E+06
1	12	10,000	1.04E+06	1.04E+06	1.04E+06	1.04E+06

Table 4-18 Concrete Strength and Maximum Moment for HP14x89

HP14x89 Connection Performance Data Maximum Moment						
ASTM A572 Grade 50 Material (Fy = 50,000 psi, Fu = 65,000 psi)						
	Embed.		Maximum Moment Resisted by Embedded Pile (in-lbs)			
Bend.	Depth	f'c	Link Elements with Traction Forces			Rigid Body
Case	(in)	(psi)	Method 1	Method 2	Method 3	Method 4
1	12	3,000	4.41E+05	6.62E+05	6.62E+05	1.10E+06
1	12	5,000	8.82E+05	1.10E+06	1.32E+06	1.76E+06
1	12	10,000	1.54E+06	1.99E+06	2.21E+06	2.21E+06

Table 4-19 Concrete Strength and Maximum Moment for HP18x204

HP18x204 Connection Performance Data Maximum Moment						
ASTM A572 Grade 50 Material (Fy = 50,000 psi, Fu = 65,000 psi)						
	Embed.		Maximum Moment Resisted by Embedded Pile (in-lbs)			
Bend.	Depth	f'c	Link Elements with Traction Forces			Rigid Body
Case	(in)	(psi)	Method 1	Method 2	Method 3	Method 4
1	18	3,000	1.23E+06	1.85E+06	1.85E+06	3.08E+06
1	18	5,000	2.46E+06	2.46E+06	3.08E+06	5.54E+06
1	18	10,000	4.31E+06	4.92E+06	6.16E+06	6.16E+06

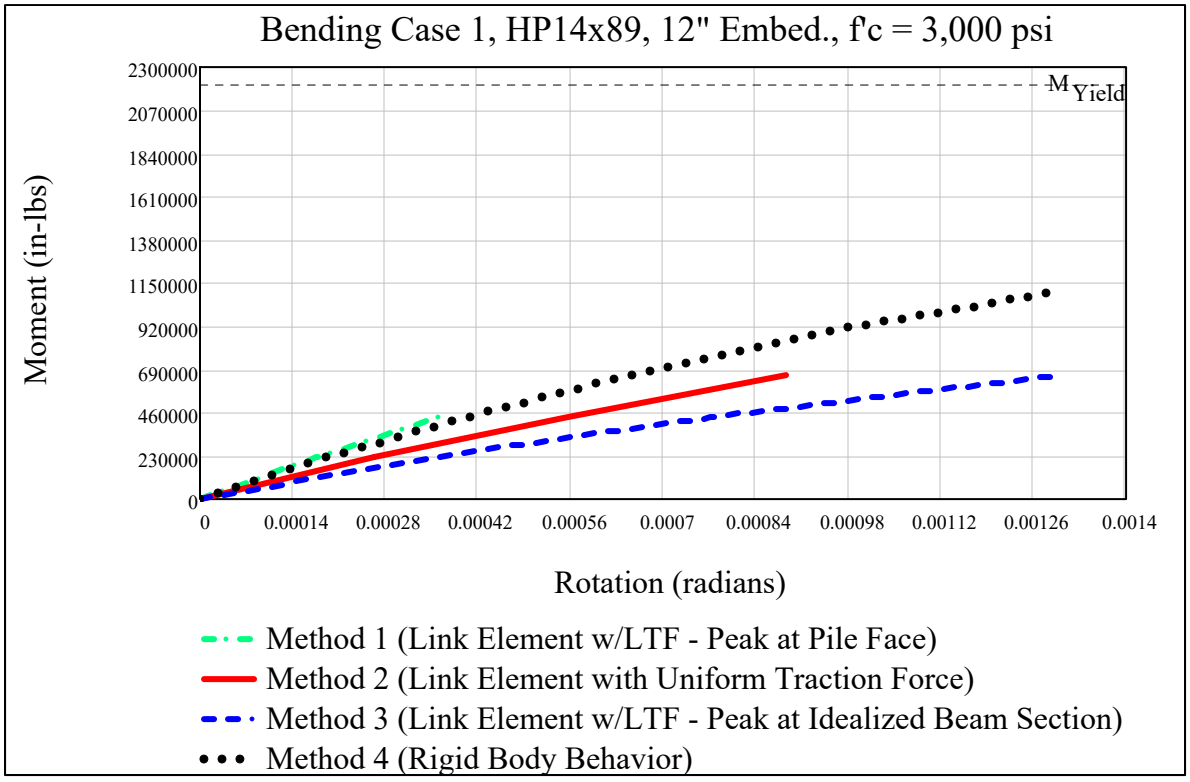

Figure 4-17 Illustration of Concrete Strength (3,000 psi) and Maximum Moment

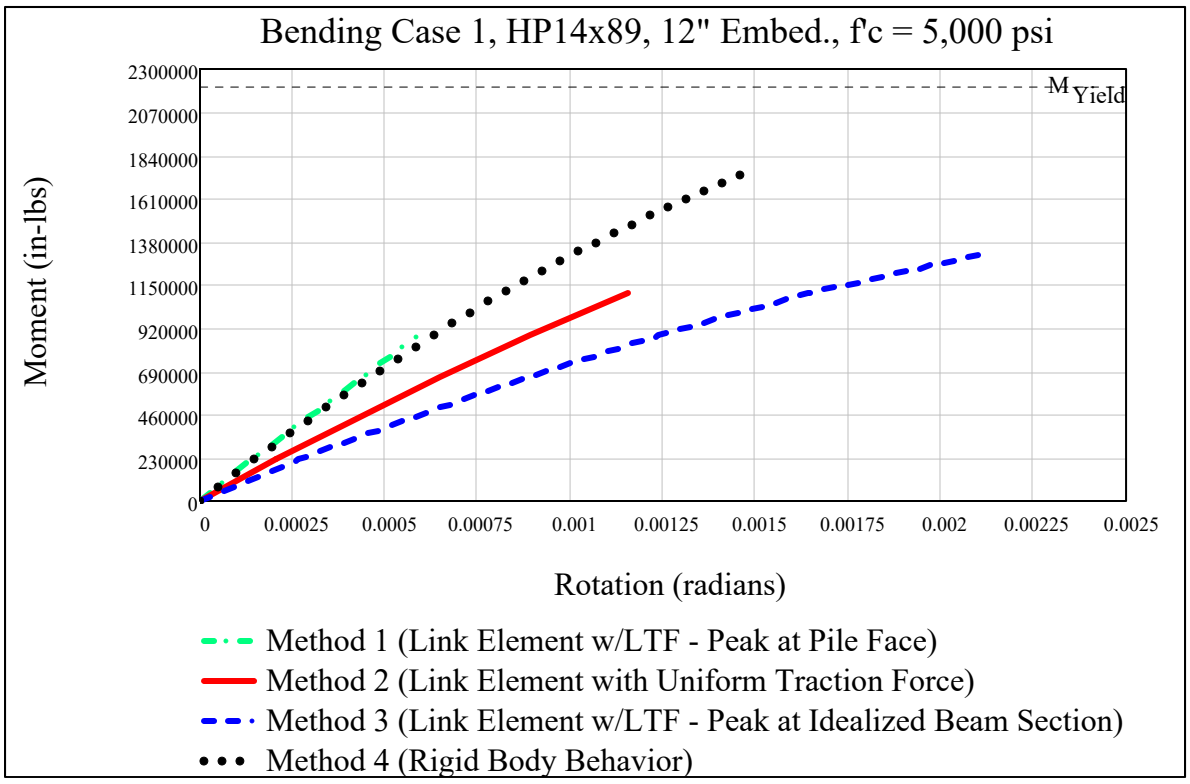

Figure 4-18 Illustration of Concrete Strength (5,000 psi) and Maximum Moment

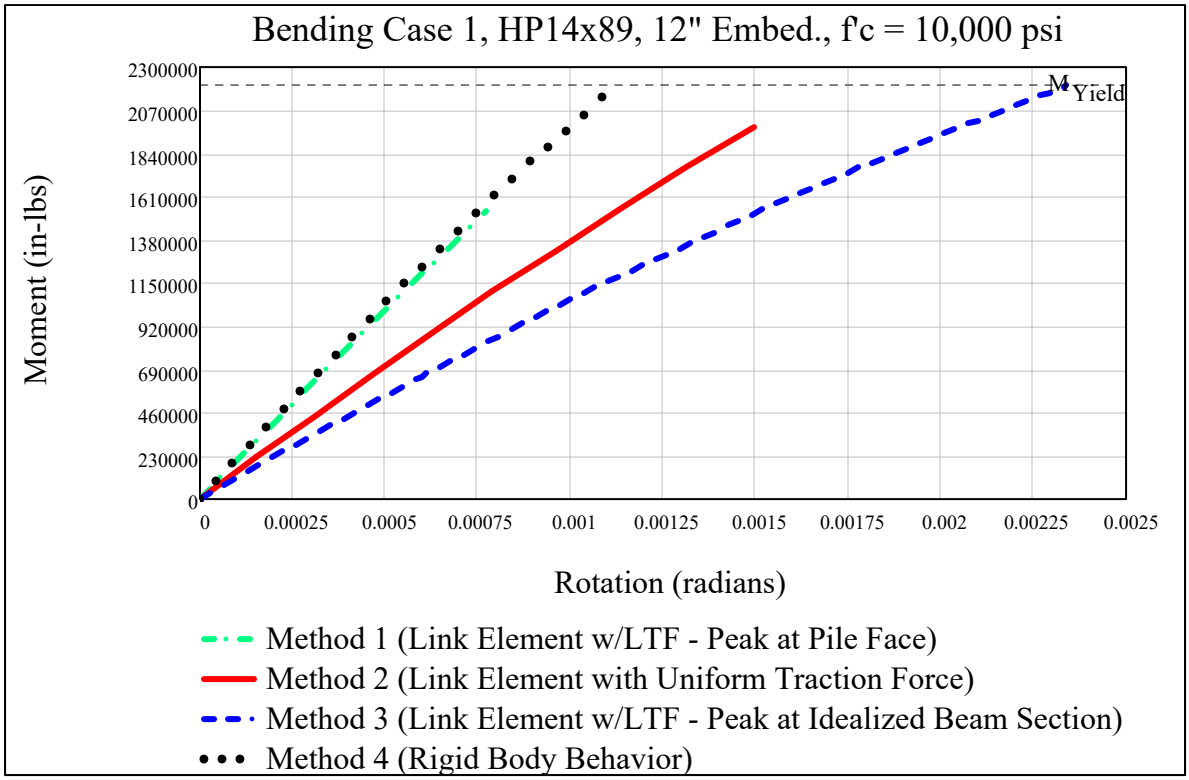

Figure 4-19 Illustration of Concrete Strength (10,000 psi) and Maximum Moment

These results indicate that concrete compressive strength has a significant impact on the maximum moment of steel piles embedded in concrete. The maximum moment for all piles considered increases between 0 and 100 percent with the increase in embedment depth. The exception to this tendency to increase occurs when a pile section is able to develop its yield moment with one of the lower two concrete compressive strengths. In these situations, there is no increase in the maximum moment corresponding to an increase in concrete compressive strength since the yield moment is taken as a limiting condition in this paper.

Figures 4-17, 4-18 and 4-19 graphically supplement the tabulated data and the conclusions based thereon.

4.2.3 Impact of Pile Section Properties on Maximum Moment

Table 4-20 provides selected rotational stiffness results for all four pile sections, each of which is embedded 18 inches into 5,000 psi compressive strength concrete.

Table 4-20 Pile Section Properties and Maximum Moment

Effect of Pile Section Properties on Moment Moment (Bending Case 1, 18 Inch Embedment and 5,000 psi Concrete)						
	Embed.		Maximum Moment Resisted by Embedded Pile (in-lbs)			
Pile	Depth	f'c	Link Elements with Traction Forces			Rigid Body
Section	(in)	(psi)	Method 1	Method 2	Method 3	Method 4
HP10x42	18	5,000	5.12E+05	5.12E+05	5.12E+05	5.12E+05
HP12x53	18	5,000	8.32E+05	1.04E+06	1.04E+06	1.04E+06
HP14x89	18	5,000	1.10E+06	1.54E+06	1.99E+06	2.21E+06
HP18x204	18	5,000	2.46E+06	2.46E+06	3.08E+06	5.54E+06

These results indicate that the maximum moment of steel piles embedded in concrete is significantly affected by pile section properties. The data provided in Table 4-20 for all four analysis methods reveals an average maximum moment increase of 93 percent when the pile section is increased from an HP10x42 to an HP12x53. This table indicates an average maximum moment increase for all four analysis methods of 71 percent when the pile section is increased from an HP12x53 to an HP14x89. Increasing the pile section from an HP14x89 to an HP18x204 indicates an average increase in the maximum moment of 97 percent for all four methods.

4.2.4 Impact of Cap Bending Stresses on Maximum Moment

Table 4-21 provides selected maximum moment results for an HP14x89 pile section embedded 18 inches into 5,000 psi compressive strength concrete for all four bending cases.

Table 4-21 Cap Bending Stresses and Maximum Moment

HP14x89 Connection Performance Data Effect of Cap Bending Stresses on Moment Capacity ASTM A572 Grade 50 Material (Fy = 50,000 psi, Fu = 65,000 psi)						
			Maximum Moment Resisted by Embedded Pile (in-lbs)			
Bend.	Depth	f'c	Link Elements with Traction Forces			Rigid Body
Case	(in)	(psi)	Method 1	Method 2	Method 3	Method 4
1	18	5,000	1.10E+06	1.54E+06	1.99E+06	2.21E+06
2	18	5,000	1.10E+06	1.54E+06	1.99E+06	2.21E+06
3	18	5,000	1.10E+06	1.54E+06	1.99E+06	2.21E+06
4	18	5,000	1.10E+06	1.54E+06	1.99E+06	2.21E+06

These results indicate that the maximum moment of steel piles embedded in concrete is not significantly impacted by bending stresses in the cap resulting from frame action. The data provided in Table 4-21 reveals that the maximum moment for each connection scenario does not vary between bending cases for the analysis method being considered. The reason for this is the disparity between the relatively small cap bending stresses and the relatively large compressive stresses in the resisting couple. For example, the peak cap bending stress at the bottom face of the cap is about 314 psi for the HP14x89 embedded 18 inches into 5,000 psi concrete for Bending Case 2. These stresses are much smaller than any of the peak stresses in the PSTB concrete shown in Table 4-22 and thus do not significantly influence the maximum moment supported by the connection.

Table 4-22 Maximum Concrete Compressive Stresses at the Pile Face

HP14x89 Connection Performance Data Maximum Concrete Compressive Stress						
ASTM A572 Grade 50 Material (Fy = 50,000 psi, Fu = 65,000 psi)						
			Maximum Concrete Compressive Stress (psi)			
Bend. Case	Depth (in)	f'c (psi)	Link Elements with Traction Forces			Rigid Body
			Method 1	Method 2	Method 3	Method 4
2	18	5,000	4,417	4,804	4,831	3,010

4.2.5 Impact of Analysis Methods on Maximum Moment

Table 4-23 provides the maximum moment results for all four analysis methods for an HP14x89 embedded 18 inches into 3,000 psi compressive strength concrete. Figure 4-20 is also included to provide a graphical illustration of the effect of analysis methods on the maximum moment.

Table 4-23 Analysis Methods and Maximum Moment

HP14x89 Connection Performance Data Effect of Analysis Methods on Moment Capacity						
ASTM A572 Grade 50 Material (Fy = 50,000 psi, Fu = 65,000 psi)						
	Embed.		Maximum Moment Resisted by Embedded Pile (in-lbs)			
Bend.	Depth	f'c	Link Elements with Traction Forces			Rigid Body
Case	(in)	(psi)	Method 1	Method 2	Method 3	Method 4
1	18	3,000	6.62E+05	8.82E+05	1.32E+06	2.21E+06

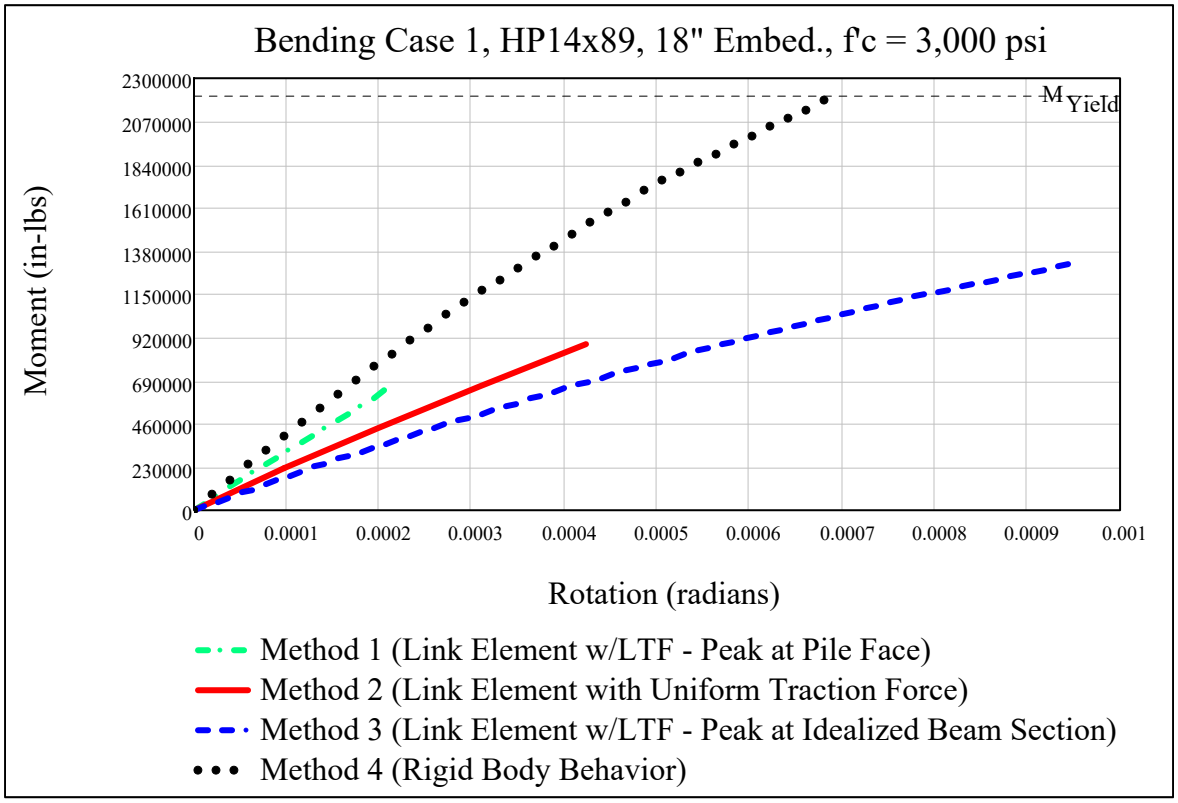

Figure 4-20 Illustration of Analysis Methods and Maximum Moment

These results indicate that analysis methods and assumptions have a very significant impact on the calculated maximum moment of embedded steel pile connections. As discussed in Section 4.1.5, analysis Methods 1, 2 and 3 include pile flexibility and are differentiated by the link element employed to model load sharing between the PSTB and the surrounding cap concrete. The link element in Method 1 sheds its load quickly to the surrounding concrete. This

behavior causes the stresses in the PSTB concrete to become very sensitive to the translational displacement of the pile under the applied loads. Method 1 provides very stiff connection values, but the flexibility of the pile exacerbates the effects of pile deformations. Large concrete stresses develop in the PSTB for relatively small applied moments, yielding the lowest maximum moment among all four analysis methods.

The link element employed in Method 2 sheds its load uniformly to the surrounding concrete. This behavior is between the extremes modelled by Methods 1 and 3. The maximum moment values for Method 2 are generally found to be near the midpoint between the corresponding values calculated for Methods 1 and 3.

The link element employed in Method 3 sheds its load rather slowly to the surrounding concrete. This behavior causes the stresses in the PSTB concrete to be less sensitive to the translational displacements of the pile under the applied loads than Methods 1 or 2. This reduced sensitivity allows larger connection rotations and translational displacements of the embedded pile segment without exceeding the compressive strength of the concrete at the bottom face of the cap. Method 3 provides the highest maximum moment values among analysis methods that include pile flexibility (Methods 1, 2 and 3).

Analysis Method 4 assumes rigid body rotation of the embedded pile segment and the subsequent linear increase in concrete strains as the distance from the neutral axis increases. These assumptions maximize the moment supported by the embedded pile connection since the detrimental effects of pile deformations on PSTB concrete stresses are not included. This strain density approach to connection rotation yields the largest maximum moment among all four analysis methods.

4.2.6 Moment Capacity of the Connection

The moment capacity of connections formed by embedding steel piles in concrete is investigated in Section 4.2.6. Methods 1, 2, 3 and 4 are designed primarily to investigate connection stiffness and are limited by either the pile yield moment or the concrete compressive strength. Since the shape factor for HP shapes bent about the weak axis is approximately 1.5, these methods provide very poor approximations of connection strength. Because of this, the $Capacity_{RB}$ routine (see Mathcad calculations in Appendix C) was written to evaluate the rigid body rotation of the embedded pile segment. This routine rotates the connection about its centroid and calculates the resisting moment of the embedded segment by evaluating the moment integrals used in the Method 4 approach discussed above. Shear forces at the connection are not considered in this routine.

The values calculated by the $Capacity_{RB}$ routine compare favorably to those values determined by Equation 3 in Xiao et al (2006) discussed in detail in Section 2.2. The ratio of the moment capacity values determined in this thesis divided by the values determined using their equation varied somewhat, but the average for all pile sections was about 1.07. The reason the values determined by the method used in this paper are slightly larger is likely due to the lack of shear force considerations in the calculations.

The values calculated by the $Capacity_{RB}$ routine also compare favorably to those values determined by the method shown in Figure 6.9.2 (B) in the PCI Design Handbook (PCI 1999) discussed in detail in Section 2.2. The ratio of the values determined in this paper divided by the values determined using their approach varied somewhat, but the average for all pile sections was about 1.04.

4.3 Neutral Axis Location

The determination of the neutral axis location for embedded steel pile connections is included in the routines for all four analysis methods. For Methods 1, 2 and 3, the neutral axis location is calculated by drawing a straight line between the displacement at the top of the pile and the displacement at the bottom face of the cap. The elevation above the bottom face of the cap where this line crosses the zero displacement line is taken to be the location of the neutral axis. Figure 4-21 graphically illustrates this calculation.

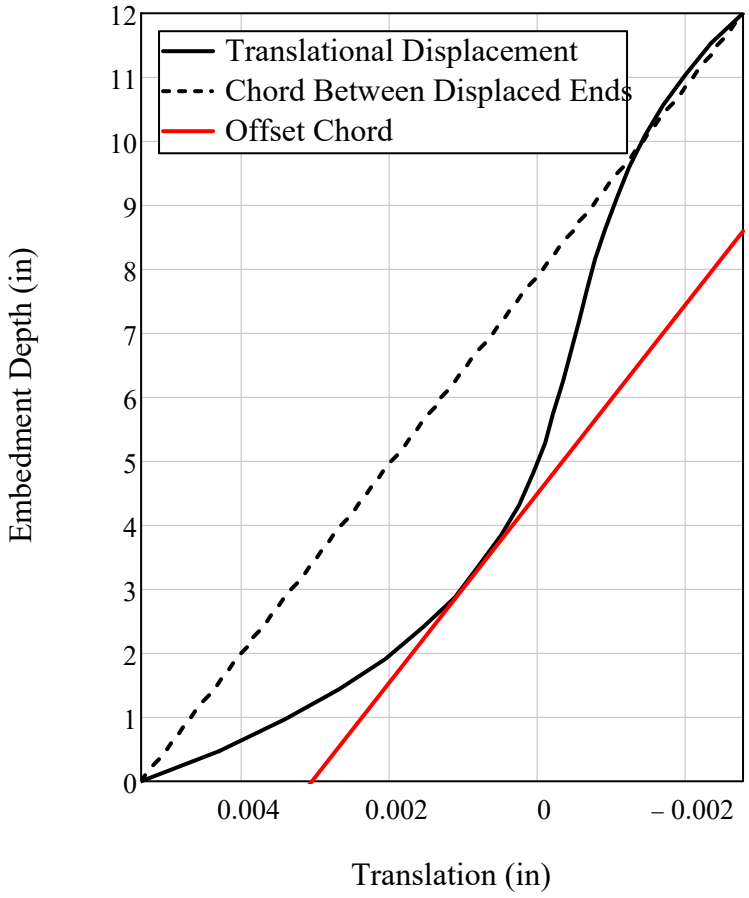

Figure 4-21 Illustration of Neutral Axis Location Calculation for Methods 1, 2 and 3

Figure 4-21 shows the translational displacement curve for an HP12x53 embedded 12 inches into a 5,000 psi concrete and subjected to bending case 1 (See table in Appendix A). The

neutral axis from the graph appears to be just below 8 inches, which is consistent with the value of 7.92 inches determined numerically.

The neutral axis location determined by Method 4 is simply the neutral axis location of the displaced rigid body at the equilibrium position. Rigid body motion is the fundamental mechanism that allows the precise calculation of the neutral axis location; however, this assumption ignores member flexibility and the shift in neutral axis location toward the face of the encasing concrete that will likely accompany the actual behavior. The neutral axis location determined by Method 4 for the scenario shown in Figure 4-21 is 6.42 inches above the bottom face of the cap. This is considerably lower than the location predicted by Methods 1, 2 or 3. This is true for all connection scenarios investigated in this research paper.

The connection rotations in this thesis are considered to occur about a neutral axis located somewhere along the embedded portion of the pile. The neutral axis locations determined by all of the methods in this thesis appear to be too deep within the embedment. A much better approximation of the neutral axis appears to be the point where the red line in Figure 4-21 is tangent to the displacement curve. This point is located at a distance from the face of concrete equal to roughly one-quarter to one-third the embedment depth. This red line is parallel to the one calculated by Methods 1, 2 and 3, but is shifted toward the face of the encasing concrete. This shift is an intuitive consequence of pile flexibility and likely provides a much better estimation of the actual neutral axis location.

Chapter 5 Summary, Recommendations and Conclusions

5.1 Summary

The results in Chapter 4 clearly indicate that embedment depth, concrete compressive strength and pile section properties each have a significant effect on the rotational stiffness and flexural capacity of embedded steel pile connections. Similarly, the analysis assumptions used to model these connections has a significant impact on the calculated rotational stiffness and flexural capacity. The bending stresses in the cap due to frame action did not noticeably impact connection behavior.

The rotational stiffness determined by analysis Method 3 was somewhat higher than the connection test result in Rodas et al. (2017), but it did provide a reasonable comparison to their data. This rotational stiffness values determined by analysis Methods 1, 2 and 4 were much higher than that determined by Method 3, thus providing a poor comparison to the test value.

The flexural capacities determined by analysis Method 4 compared well against the method in Xiao et al. (2006) and the method in the PCI Design Handbook (PCI 1999). Analysis Methods 1, 2 and 3 consistently underestimated flexural capacity with Method 3 providing the best estimate among the three methods that included pile flexibility.

All four analysis methods appeared to provide a neutral axis location that is too deep within the embedment.

5.2 Recommendations and Conclusions

Method 3 appears to have the most potential for modelling the behavior of connections formed by embedding steel piles in concrete because it provides the best estimate of rotational stiffness and flexural capacity among Methods 1, 2 and 3. It is believed that adjustments to the pile stress transformation length L_{pst} and the traction force used to derive the Method 3 link element can yield a single method capable of providing reasonable estimates of the rotational stiffness and flexural capacity of embedded connections. While Method 4 did provide the best estimates of flexural capacity, the author believes that Method 3 will provide comparable results with the proper adjustments to L_{pst} and the link element traction force.

All four analysis methods appeared to overestimate the depth to the neutral axis from the face of the encasing concrete; however, the author believes that the offset (red) line shown in Figure 4-21 likely provides a very good estimate of the theoretical location. The author further believes that a simple multiplier, a fraction in the vicinity of one-quarter to one-third, multiplied times the embedment length will likely provide a reasonable estimate of the neutral axis location for most embedded connections. The performance of additional full scale testing is recommended to facilitate the necessary adjustments to Method 3 and to verify the proposed multiplier for neutral axis location.

Additional work on this topic is currently underway with the goal of developing a relationship between embedment depth, pile section properties and concrete strength that provides accurate values for the rotational stiffness and moment capacity of these connections. While the complexity of this relationship will not significantly impact its implementation into computer programs, every effort is being made to keep this relationship simple enough to encourage its use in hand calculations.

References

AISC. (2005). *Steel Construction Manual* (13th ed.). United States: American Institute of Steel Construction.

American Association of State Highway and Transportation Officials (AASHTO). (2012). *AASHTO LRFD Bridge Design Specifications, 6th Edition*, Washington, D.C.

Anderson, M., Carter, C. J. (2012). Are You Properly Specifying Materials?, AISC, *Modern Steel Construction*, Vol. 52, No. 2

Grilli, D., Jones, R. and Kanvinde, A. (2015). Embedded Column Base Connections Subjected to Flexure and Axial Loads, *Rep. 3-11,* Charles Pankow Foundation, Vancouver, WA.

Grilli, D., Jones, R. and Kanvinde, A. (2017). Seismic Performance of Embedded Column Base Connections Subjected to Axial and Lateral Loads, ASCE, *Journal of Structural Engineering*, Vol. 143, No. 5

Harries, K. A., Petrou, M. F. (2001). Behavior of Precast, Prestressed Concrete Pile to Cast-in-Place Pile Cap Connections, *PCI Journal*, Vol. 46, No. 4

Karthik, M. M. and Mander, J. B. (2011). Stress-Block Parameters for Unconfined and Confined Concrete Based on a Unified Stress-Strain Model, ASCE, *Journal of Structural Engineering*, Vol. 137, No. 2

Marshall, J. D., Anderson, J. B., Campbell, J., Skinner, Z. and Hammett, S.T. (2017), *Experimental Validation of Analysis Methods and Design Procedures for Steel Pile Bridge Bents*, Auburn, AL: Auburn University

Precast/Prestressed Concrete Institute (PCI). (1999). Precast and Prestressed Concrete, *PCI Design Handbook*, 5th Ed., PCI, Chicago

Rodas, P. T., Kanvinde, A., Zareian, F. (2017). Rotational Stiffness of Deeply Embedded Column-Base Connections, ASCE, *Journal of Structural Engineering*, Vol. 143, No. 8

Shama, A. A., Mander, J. B., Blabac, B. A., Chen, S. S. (2002a). Seismic Investigation of Steel Pile Bents: I. Evaluation of Performance, EERI, *Earthquake Spectra*, Vol. 18, No. 1

Shama, A. A., Mander, J. B., Chen, S. S. (2002b). Seismic Investigation of Steel Pile Bents: II. Retrofit and Vulnerability Analysis, EERI, *Earthquake Spectra*, Vol. 18, No. 1

Xiao, Y., Wu, H., Yaprak, T. T., Martin, G. R. and Mander, J. B. (2006). Experimental Studies on Seismic Behavior of Steel Pile-to-Pile Cap Behavior, ASCE, *Journal of Bridge Engineering*, Vol. 11, No. 2

Zareian, F. and Kanvinde, A. (2013). Effect of Column-Base Flexibility on the Seismic Response and Safety of Steel Moment-Resisting Frames, EERI, *Earthquake Spectra*, Vol. 29, No. 4

HP10x42 Connection Performance Data Rotational Stiffness						
ASTM A36 Material (Fy = 36,000 psi, Fu = 58,000 psi)						
			Connection Stiffness (in-lbs/rad)			
Bend. Case	Depth (in)	f'c (psi)	Link Elements with Traction Forces			Rigid Body
			Method 1	Method 2	Method 3	Method 4
1	12	3,000	650,718,435	423,223,181	275,220,295	594,720,884
1	12	5,000	804,247,694	552,501,852	410,314,584	848,254,592
1	12	10,000	1,061,409,798	765,800,539	596,555,859	1,259,515,750
1	18	3,000	1,473,593,235	1,045,825,302	805,519,465	2,342,791,633
1	18	5,000	1,748,884,337	1,305,345,413	1,043,083,323	3,131,791,455
1	18	10,000	2,186,205,309	1,679,401,636	1,378,589,137	4,517,355,540
2	12	3,000	657,866,125	426,030,634	276,348,255	605,090,403
2	12	5,000	812,303,188	555,679,667	411,583,105	864,541,186
2	12	10,000	1,070,267,962	769,398,261	598,048,820	1,284,884,958
2	18	3,000	1,508,120,589	1,060,920,209	811,871,220	2,425,019,101
2	18	5,000	1,784,638,844	1,321,025,051	1,049,938,054	3,244,992,408
2	18	10,000	2,223,014,853	1,695,973,793	1,386,091,009	4,683,659,025
3	12	3,000	643,685,847	420,444,284	274,102,388	584,712,491
3	12	5,000	796,398,159	549,387,974	409,070,186	832,541,586
3	12	10,000	1,052,661,716	762,223,902	595,067,365	1,235,073,912
3	18	3,000	1,440,588,552	1,031,156,960	799,294,254	2,266,676,652
3	18	5,000	1,714,764,955	1,290,160,619	1,036,388,510	3,026,609,323
3	18	10,000	2,150,706,773	1,663,206,799	1,371,197,339	4,362,869,873
4	12	3,000	632,956,408	416,217,966	272,454,824	589,780,960
4	12	5,000	784,294,167	544,443,777	407,072,131	840,487,118
4	12	10,000	1,039,331,559	756,426,361	592,605,270	1,247,422,488
4	18	3,000	1,435,080,880	1,028,138,533	797,697,494	2,267,699,948
4	18	5,000	1,710,915,231	1,287,587,572	1,034,832,428	3,028,079,247
4	18	10,000	2,148,737,061	1,661,307,287	1,369,813,173	4,365,004,780

HP10x42 Connection Performance Data Maximum Concrete Compressive Stress						
ASTM A36 Material (Fy = 36,000 psi, Fu = 58,000 psi)						
	Embed.		Maximum Concrete Compressive Stress (psi)			
Bend.	Depth	f'c	Link Elements with Traction Forces			Rigid Body
Case	(in)	(psi)	Method 1	Method 2	Method 3	Method 4
1	12	3,000	2,974	2,775	2,832	2,147
1	12	5,000	4,702	3,912	3,443	2,254
1	12	10,000	5,536	4,660	4,156	2,303
1	18	3,000	2,910	2,755	2,282	1,017
1	18	5,000	4,175	3,334	2,833	1,033
1	18	10,000	5,036	4,106	3,551	1,042
2	12	3,000	2,984	2,785	2,841	2,147
2	12	5,000	4,714	3,920	3,448	2,254
2	12	10,000	5,542	4,664	4,158	2,303
2	18	3,000	2,922	2,767	2,288	1,017
2	18	5,000	4,186	3,341	2,837	1,033
2	18	10,000	5,041	4,110	3,553	1,042
3	12	3,000	2,963	2,765	2,824	2,147
3	12	5,000	4,689	3,903	3,438	2,254
3	12	10,000	5,531	4,656	4,153	2,303
3	18	3,000	2,898	2,742	2,275	1,017
3	18	5,000	4,165	3,326	2,829	1,033
3	18	10,000	5,031	4,103	3,549	1,042
4	12	3,000	2,969	2,769	2,827	2,147
4	12	5,000	4,698	3,908	3,440	2,254
4	12	10,000	5,537	4,660	4,155	2,303
4	18	3,000	2,896	2,741	2,275	1,017
4	18	5,000	4,160	3,324	2,829	1,033
4	18	10,000	5,025	4,100	3,548	1,042

HP10x42 Connection Performance Data Maximum Moment						
ASTM A36 Material (Fy = 36,000 psi, Fu = 58,000 psi)						
	Embed.		Maximum Moment Resisted by Embedded Pile (in-lbs)			
Bend.	Depth	f'c	Link Elements with Traction Forces			Rigid Body
Case	(in)	(psi)	Method 1	Method 2	Method 3	Method 4
1	12	3,000	358,486	409,698	512,122	512,122
1	12	5,000	512,122	512,122	512,122	512,122
1	12	10,000	512,122	512,122	512,122	512,122
1	18	3,000	409,698	512,122	512,122	512,122
1	18	5,000	512,122	512,122	512,122	512,122
1	18	10,000	512,122	512,122	512,122	512,122
2	12	3,000	358,486	409,698	512,122	512,122
2	12	5,000	512,122	512,122	512,122	512,122
2	12	10,000	512,122	512,122	512,122	512,122
2	18	3,000	409,698	512,122	512,122	512,122
2	18	5,000	512,122	512,122	512,122	512,122
2	18	10,000	512,122	512,122	512,122	512,122
3	12	3,000	358,486	409,698	512,122	512,122
3	12	5,000	512,122	512,122	512,122	512,122
3	12	10,000	512,122	512,122	512,122	512,122
3	18	3,000	409,698	512,122	512,122	512,122
3	18	5,000	512,122	512,122	512,122	512,122
3	18	10,000	512,122	512,122	512,122	512,122
4	12	3,000	358,486	409,698	512,122	512,122
4	12	5,000	512,122	512,122	512,122	512,122
4	12	10,000	512,122	512,122	512,122	512,122
4	18	3,000	409,698	512,122	512,122	512,122
4	18	5,000	512,122	512,122	512,122	512,122
4	18	10,000	512,122	512,122	512,122	512,122

HP10x42 Connection Performance Data Ratio of Applied Moment to Yield Moment						
ASTM A36 Material (Fy = 36,000 psi, Fu = 58,000 psi)						
	Embed.		Ratio of Applied Moment to Yield Moment			
Bend.	Depth	f'c	Link Elements with Traction Forces			Rigid Body
Case	(in)	(psi)	Method 1	Method 2	Method 3	Method 4
1	12	3,000	0.70	0.80	1.00	1.00
1	12	5,000	1.00	1.00	1.00	1.00
1	12	10,000	1.00	1.00	1.00	1.00
1	18	3,000	0.80	1.00	1.00	1.00
1	18	5,000	1.00	1.00	1.00	1.00
1	18	10,000	1.00	1.00	1.00	1.00
2	12	3,000	0.70	0.80	1.00	1.00
2	12	5,000	1.00	1.00	1.00	1.00
2	12	10,000	1.00	1.00	1.00	1.00
2	18	3,000	0.80	1.00	1.00	1.00
2	18	5,000	1.00	1.00	1.00	1.00
2	18	10,000	1.00	1.00	1.00	1.00
3	12	3,000	0.70	0.80	1.00	1.00
3	12	5,000	1.00	1.00	1.00	1.00
3	12	10,000	1.00	1.00	1.00	1.00
3	18	3,000	0.80	1.00	1.00	1.00
3	18	5,000	1.00	1.00	1.00	1.00
3	18	10,000	1.00	1.00	1.00	1.00
4	12	3,000	0.70	0.80	1.00	1.00
4	12	5,000	1.00	1.00	1.00	1.00
4	12	10,000	1.00	1.00	1.00	1.00
4	18	3,000	0.80	1.00	1.00	1.00
4	18	5,000	1.00	1.00	1.00	1.00
4	18	10,000	1.00	1.00	1.00	1.00

HP10x42 Connection Performance Data Neutral Axis Location for Rotation of Embedded Pile						
ASTM A36 Material (Fy = 36,000 psi, Fu = 58,000 psi)						
	Embed.		NA Location Measured from Bottom Face of Cap (in)			
Bend.	Depth	f'c	Link Elements with Traction Forces			Rigid Body
Case	(in)	(psi)	Method 1	Method 2	Method 3	Method 4
1	12	3,000	8.07	7.65	7.34	6.43
1	12	5,000	8.32	7.90	7.62	6.42
1	12	10,000	8.65	8.25	7.96	6.41
1	18	3,000	15.52	14.89	14.32	9.93
1	18	5,000	15.81	15.30	14.82	9.91
1	18	10,000	16.11	15.74	15.38	9.91
2	12	3,000	7.97	7.59	7.32	6.43
2	12	5,000	8.24	7.85	7.59	6.42
2	12	10,000	8.58	8.21	7.94	6.41
2	18	3,000	15.47	14.85	14.29	9.93
2	18	5,000	15.77	15.27	14.81	9.91
2	18	10,000	16.08	15.72	15.36	9.91
3	12	3,000	8.16	7.70	7.37	6.43
3	12	5,000	8.41	7.95	7.64	6.42
3	12	10,000	8.73	8.30	7.99	6.41
3	18	3,000	15.57	14.92	14.34	9.93
3	18	5,000	15.86	15.33	14.84	9.91
3	18	10,000	16.14	15.76	15.39	9.91
4	12	3,000	8.04	7.64	7.34	6.43
4	12	5,000	8.30	7.89	7.61	6.42
4	12	10,000	8.63	8.24	7.96	6.41
4	18	3,000	15.50	14.87	14.31	9.93
4	18	5,000	15.80	15.29	14.82	9.91
4	18	10,000	16.11	15.73	15.37	9.91

HP12x53 Connection Performance Data Rotational Stiffness						
ASTM A572 Grade 50 Material (Fy = 50,000 psi, Fu = 65,000 psi)						
	Embed.		Connection Stiffness (in-lbs/rad)			
Bend.	Depth	f'c	Link Elements with Traction Forces			Rigid Body
Case	(in)	(psi)	Method 1	Method 2	Method 3	Method 4
1	12	3,000	877,597,775	562,272,798	367,089,619	668,497,285
1	12	5,000	1,082,884,827	714,683,359	479,652,623	1,047,564,102
1	12	10,000	1,413,669,760	1,000,580,809	764,487,746	1,632,202,160
1	18	3,000	2,052,731,737	1,425,284,723	1,012,972,008	2,950,995,823
1	18	5,000	2,425,867,131	1,742,204,461	1,355,127,997	4,069,717,282
1	18	10,000	3,042,492,466	2,299,379,361	1,860,869,094	5,965,483,570
2	12	3,000	889,285,408	566,856,076	368,914,783	680,557,131
2	12	5,000	1,095,712,893	720,140,262	481,931,095	1,070,491,684
2	12	10,000	1,429,230,459	1,006,878,510	767,075,209	1,671,359,834
2	18	3,000	2,114,256,417	1,452,109,634	1,024,409,563	3,073,095,660
2	18	5,000	2,491,641,354	1,771,239,022	1,367,519,073	4,247,788,958
2	18	10,000	3,111,303,109	2,329,800,325	1,874,375,749	6,233,917,789
3	12	3,000	866,124,203	557,737,201	365,294,568	656,879,062
3	12	5,000	1,069,944,097	709,376,635	477,450,226	1,025,549,460
3	12	10,000	1,398,821,904	994,529,346	761,995,457	1,594,658,246
3	18	3,000	1,994,581,692	1,399,530,898	967,810,997	2,840,429,714
3	18	5,000	2,364,143,894	1,714,585,946	1,343,223,959	3,907,906,243
3	18	10,000	2,978,003,965	2,270,394,780	1,847,874,157	5,720,613,831
4	12	3,000	847,859,181	550,648,016	362,570,571	662,878,491
4	12	5,000	1,049,305,292	701,163,356	474,140,228	1,036,935,932
4	12	10,000	1,375,593,382	984,649,990	757,846,061	1,613,997,891
4	18	3,000	1,984,631,218	1,392,831,892	964,725,694	2,843,747,318
4	18	5,000	2,352,878,599	1,708,342,351	1,339,939,911	3,912,733,003
4	18	10,000	2,968,791,290	2,264,741,276	1,845,393,198	5,727,598,374

HP12x53 Connection Performance Data Maximum Concrete Compressive Stress						
ASTM A572 Grade 50 Material (Fy = 50,000 psi, Fu = 65,000 psi)						
	Embed.		Maximum Concrete Compressive Stress (psi)			
Bend.	Depth	f'c	Link Elements with Traction Forces			Rigid Body
Case	(in)	(psi)	Method 1	Method 2	Method 3	Method 4
1	12	3,000	2,712	2,786	2,789	2,917
1	12	5,000	4,456	4,820	4,910	3,623
1	12	10,000	8,494	7,110	6,291	3,799
1	18	3,000	2,764	2,902	2,835	1,655
1	18	5,000	4,966	4,758	3,959	1,707
1	18	10,000	7,445	6,022	5,170	1,737
2	12	3,000	2,723	2,798	2,799	2,917
2	12	5,000	4,473	4,839	4,927	3,623
2	12	10,000	8,512	7,123	6,298	3,799
2	18	3,000	2,778	2,921	2,851	1,655
2	18	5,000	4,987	4,782	3,972	1,707
2	18	10,000	7,461	6,033	5,177	1,737
3	12	3,000	2,702	2,773	2,780	2,917
3	12	5,000	4,442	4,802	4,894	3,623
3	12	10,000	8,475	7,096	6,283	3,799
3	18	3,000	2,749	2,882	2,994	1,655
3	18	5,000	4,944	4,734	3,946	1,707
3	18	10,000	7,429	6,010	5,164	1,737
4	12	3,000	2,711	2,780	2,783	2,917
4	12	5,000	4,456	4,810	4,899	3,623
4	12	10,000	8,494	7,107	6,288	3,799
4	18	3,000	2,745	2,882	2,994	1,655
4	18	5,000	4,942	4,732	3,946	1,707
4	18	10,000	7,424	6,008	5,161	1,737

HP12x53 Connection Performance Data Maximum Moment						
ASTM A572 Grade 50 Material (Fy = 50,000 psi, Fu = 65,000 psi)						
	Embed.		Maximum Moment Resisted by Embedded Pile (in-lbs)			
Bend.	Depth	f'c	Link Elements with Traction Forces			Rigid Body
Case	(in)	(psi)	Method 1	Method 2	Method 3	Method 4
1	12	3,000	415,852	519,815	623,778	935,667
1	12	5,000	623,778	831,704	1,039,630	1,039,630
1	12	10,000	1,039,630	1,039,630	1,039,630	1,039,630
1	18	3,000	519,815	727,741	935,667	1,039,630
1	18	5,000	831,704	1,039,630	1,039,630	1,039,630
1	18	10,000	1,039,630	1,039,630	1,039,630	1,039,630
2	12	3,000	415,852	519,815	623,778	935,667
2	12	5,000	623,778	831,704	1,039,630	1,039,630
2	12	10,000	1,039,630	1,039,630	1,039,630	1,039,630
2	18	3,000	519,815	727,741	935,667	1,039,630
2	18	5,000	831,704	1,039,630	1,039,630	1,039,630
2	18	10,000	1,039,630	1,039,630	1,039,630	1,039,630
3	12	3,000	415,852	519,815	623,778	935,667
3	12	5,000	623,778	831,704	1,039,630	1,039,630
3	12	10,000	1,039,630	1,039,630	1,039,630	1,039,630
3	18	3,000	519,815	727,741	1,039,630	1,039,630
3	18	5,000	831,704	1,039,630	1,039,630	1,039,630
3	18	10,000	1,039,630	1,039,630	1,039,630	1,039,630
4	12	3,000	415,852	519,815	623,778	935,667
4	12	5,000	623,778	831,704	1,039,630	1,039,630
4	12	10,000	1,039,630	1,039,630	1,039,630	1,039,630
4	18	3,000	519,815	727,741	1,039,630	1,039,630
4	18	5,000	831,704	1,039,630	1,039,630	1,039,630
4	18	10,000	1,039,630	1,039,630	1,039,630	1,039,630

HP12x53 Connection Performance Data Ratio of Applied Moment to Yield Moment						
ASTM A572 Grade 50 Material (Fy = 50,000 psi, Fu = 65,000 psi)						
	Embed.		Ratio of Applied Moment to Yield Moment			
Bend.	Depth	f'c	Link Elements with Traction Forces			Rigid Body
Case	(in)	(psi)	Method 1	Method 2	Method 3	Method 4
1	12	3,000	0.40	0.50	0.60	0.90
1	12	5,000	0.60	0.80	1.00	1.00
1	12	10,000	1.00	1.00	1.00	1.00
1	18	3,000	0.50	0.70	0.90	1.00
1	18	5,000	0.80	1.00	1.00	1.00
1	18	10,000	1.00	1.00	1.00	1.00
2	12	3,000	0.40	0.50	0.60	0.90
2	12	5,000	0.60	0.80	1.00	1.00
2	12	10,000	1.00	1.00	1.00	1.00
2	18	3,000	0.50	0.70	0.90	1.00
2	18	5,000	0.80	1.00	1.00	1.00
2	18	10,000	1.00	1.00	1.00	1.00
3	12	3,000	0.40	0.50	0.60	0.90
3	12	5,000	0.60	0.80	1.00	1.00
3	12	10,000	1.00	1.00	1.00	1.00
3	18	3,000	0.50	0.70	1.00	1.00
3	18	5,000	0.80	1.00	1.00	1.00
3	18	10,000	1.00	1.00	1.00	1.00
4	12	3,000	0.40	0.50	0.60	0.90
4	12	5,000	0.60	0.80	1.00	1.00
4	12	10,000	1.00	1.00	1.00	1.00
4	18	3,000	0.50	0.70	1.00	1.00
4	18	5,000	0.80	1.00	1.00	1.00
4	18	10,000	1.00	1.00	1.00	1.00

HP12x53 Connection Performance Data						
Neutral Axis Location for Rotation of Embedded Pile						
ASTM A572 Grade 50 Material (Fy = 50,000 psi, Fu = 65,000 psi)						
	Embed.		NA Location Measured from Bottom Face of Cap (in)			
Bend.	Depth	f'c	Link Elements with Traction Forces			Rigid Body
Case	(in)	(psi)	Method 1	Method 2	Method 3	Method 4
1	12	3,000	7.71	7.37	7.14	6.46
1	12	5,000	7.92	7.58	7.33	6.42
1	12	10,000	8.20	7.87	7.63	6.41
1	18	3,000	14.63	14.03	13.48	9.96
1	18	5,000	14.93	14.43	13.98	9.93
1	18	10,000	15.26	14.87	14.50	9.95
2	12	3,000	7.59	7.30	7.10	6.46
2	12	5,000	7.81	7.51	7.29	6.42
2	12	10,000	8.10	7.81	7.60	6.41
2	18	3,000	14.53	13.96	13.44	9.96
2	18	5,000	14.85	14.38	13.94	9.93
2	18	10,000	15.19	14.83	14.48	9.95
3	12	3,000	7.83	7.44	7.17	6.46
3	12	5,000	8.03	7.64	7.36	6.42
3	12	10,000	8.30	7.92	7.66	6.41
3	18	3,000	14.72	14.09	13.51	9.96
3	18	5,000	15.01	14.49	14.01	9.93
3	18	10,000	15.32	14.91	14.53	9.95
4	12	3,000	7.70	7.37	7.14	6.46
4	12	5,000	7.90	7.57	7.33	6.42
4	12	10,000	8.18	7.86	7.62	6.41
4	18	3,000	14.62	14.02	13.46	9.96
4	18	5,000	14.93	14.43	13.97	9.93
4	18	10,000	15.26	14.87	14.50	9.95

HP14x89 Connection Performance Data Rotational Stiffness						
ASTM A572 Grade 50 Material (Fy = 50,000 psi, Fu = 65,000 psi)						
	Embed.		Connection Stiffness (in-lbs/rad)			
Bend.	Depth	f'c	Link Elements with Traction Forces			Rigid Body
Case	(in)	(psi)	Method 1	Method 2	Method 3	Method 4
1	12	3,000	1,212,409,843	745,832,496	508,652,169	845,804,757
1	12	5,000	1,495,011,696	956,693,503	623,992,975	1,182,429,503
1	12	10,000	1,990,507,307	1,329,025,805	942,446,688	1,966,736,435
1	18	3,000	3,080,511,732	2,087,780,876	1,384,783,124	3,191,578,559
1	18	5,000	3,682,780,343	2,544,292,083	1,805,378,707	4,858,499,917
1	18	10,000	4,646,143,377	3,379,288,227	2,644,704,376	7,389,211,901
2	12	3,000	1,225,827,862	751,035,290	510,616,902	860,420,054
2	12	5,000	1,511,169,852	963,081,843	626,606,921	1,204,944,199
2	12	10,000	2,010,219,174	1,337,170,465	945,824,308	2,011,055,599
2	18	3,000	3,165,925,372	2,122,822,002	1,399,688,050	3,313,166,416
2	18	5,000	3,776,918,664	2,584,731,664	1,822,804,362	5,072,017,941
2	18	10,000	4,750,820,962	3,422,153,692	2,664,053,031	7,733,323,965
3	12	3,000	1,199,152,646	740,640,582	506,700,769	831,657,469
3	12	5,000	1,479,105,009	950,448,487	621,454,416	1,160,572,047
3	12	10,000	1,971,474,599	1,321,304,816	939,273,411	1,923,806,513
3	18	3,000	2,999,367,813	1,990,380,756	1,370,451,329	3,080,622,757
3	18	5,000	3,594,484,385	2,506,035,841	1,788,954,632	4,663,629,884
3	18	10,000	4,550,048,340	3,337,355,733	2,626,661,071	7,074,961,573
4	12	3,000	1,168,623,731	729,399,614	502,505,809	840,323,109
4	12	5,000	1,443,367,656	936,895,701	616,255,615	1,174,191,796
4	12	10,000	1,929,071,739	1,304,326,027	932,475,061	1,950,734,242
4	18	3,000	2,944,794,144	1,965,550,286	1,360,130,758	3,113,912,416
4	18	5,000	3,539,337,523	2,479,016,013	1,777,159,529	4,720,618,527
4	18	10,000	4,493,561,834	3,307,783,671	2,613,662,948	7,165,071,451

HP14x89 Connection Performance Data Maximum Concrete Compressive Stress						
ASTM A572 Grade 50 Material (Fy = 50,000 psi, Fu = 65,000 psi)						
	Embed.		Maximum Concrete Compressive Stress (psi)			
Bend.	Depth	f'c	Link Elements with Traction Forces			Rigid Body
Case	(in)	(psi)	Method 1	Method 2	Method 3	Method 4
1	12	3,000	2,173	2,759	2,479	2,929
1	12	5,000	4,602	4,856	4,928	4,851
1	12	10,000	8,985	9,639	9,232	6,713
1	18	3,000	2,377	2,504	2,856	2,742
1	18	5,000	4,398	4,776	4,806	3,010
1	18	10,000	9,215	8,195	7,011	3,122
2	12	3,000	2,180	2,771	2,486	2,929
2	12	5,000	4,617	4,875	4,945	4,851
2	12	10,000	9,008	9,669	9,255	6,713
2	18	3,000	2,389	2,518	2,874	2,742
2	18	5,000	4,417	4,804	4,831	3,010
2	18	10,000	9,246	8,228	7,027	3,122
3	12	3,000	2,166	2,747	2,472	2,929
3	12	5,000	4,587	4,837	4,911	4,851
3	12	10,000	8,963	9,609	9,209	6,713
3	18	3,000	2,365	2,980	2,839	2,742
3	18	5,000	4,379	4,748	4,780	3,010
3	18	10,000	9,183	8,166	6,995	3,122
4	12	3,000	2,179	2,756	2,476	2,929
4	12	5,000	4,610	4,851	4,918	4,851
4	12	10,000	8,996	9,633	9,221	6,713
4	18	3,000	2,367	2,984	2,841	2,742
4	18	5,000	4,379	4,753	4,783	3,010
4	18	10,000	9,181	8,171	6,996	3,122

HP14x89 Connection Performance Data Maximum Moment						
ASTM A572 Grade 50 Material (Fy = 50,000 psi, Fu = 65,000 psi)						
	Embed.		Maximum Moment Resisted by Embedded Pile (in-lbs)			
Bend.	Depth	f'c	Link Elements with Traction Forces			Rigid Body
Case	(in)	(psi)	Method 1	Method 2	Method 3	Method 4
1	12	3,000	441,234	661,852	661,852	1,103,086
1	12	5,000	882,469	1,103,086	1,323,703	1,764,937
1	12	10,000	1,544,320	1,985,555	2,206,172	2,206,172
1	18	3,000	661,852	882,469	1,323,703	2,206,172
1	18	5,000	1,103,086	1,544,320	1,985,555	2,206,172
1	18	10,000	1,985,555	2,206,172	2,206,172	2,206,172
2	12	3,000	441,234	661,852	661,852	1,103,086
2	12	5,000	882,469	1,103,086	1,323,703	1,764,937
2	12	10,000	1,544,320	1,985,555	2,206,172	2,206,172
2	18	3,000	661,852	882,469	1,323,703	2,206,172
2	18	5,000	1,103,086	1,544,320	1,985,555	2,206,172
2	18	10,000	1,985,555	2,206,172	2,206,172	2,206,172
3	12	3,000	441,234	661,852	661,852	1,103,086
3	12	5,000	882,469	1,103,086	1,323,703	1,764,937
3	12	10,000	1,544,320	1,985,555	2,206,172	2,206,172
3	18	3,000	661,852	1,103,086	1,323,703	2,206,172
3	18	5,000	1,103,086	1,544,320	1,985,555	2,206,172
3	18	10,000	1,985,555	2,206,172	2,206,172	2,206,172
4	12	3,000	441,234	661,852	661,852	1,103,086
4	12	5,000	882,469	1,103,086	1,323,703	1,764,937
4	12	10,000	1,544,320	1,985,555	2,206,172	2,206,172
4	18	3,000	661,852	1,103,086	1,323,703	2,206,172
4	18	5,000	1,103,086	1,544,320	1,985,555	2,206,172
4	18	10,000	1,985,555	2,206,172	2,206,172	2,206,172

HP14x89 Connection Performance Data Ratio of Applied Moment to Yield Moment						
ASTM A572 Grade 50 Material (Fy = 50,000 psi, Fu = 65,000 psi)						
	Embed.		Ratio of Applied Moment to Yield Moment			
Bend.	Depth	f'c	Link Elements with Traction Forces			Rigid Body
Case	(in)	(psi)	Method 1	Method 2	Method 3	Method 4
1	12	3,000	0.20	0.30	0.30	0.50
1	12	5,000	0.40	0.50	0.60	0.80
1	12	10,000	0.70	0.90	1.00	1.00
1	18	3,000	0.30	0.40	0.60	1.00
1	18	5,000	0.50	0.70	0.90	1.00
1	18	10,000	0.90	1.00	1.00	1.00
2	12	3,000	0.20	0.30	0.30	0.50
2	12	5,000	0.40	0.50	0.60	0.80
2	12	10,000	0.70	0.90	1.00	1.00
2	18	3,000	0.30	0.40	0.60	1.00
2	18	5,000	0.50	0.70	0.90	1.00
2	18	10,000	0.90	1.00	1.00	1.00
3	12	3,000	0.20	0.30	0.30	0.50
3	12	5,000	0.40	0.50	0.60	0.80
3	12	10,000	0.70	0.90	1.00	1.00
3	18	3,000	0.30	0.50	0.60	1.00
3	18	5,000	0.50	0.70	0.90	1.00
3	18	10,000	0.90	1.00	1.00	1.00
4	12	3,000	0.20	0.30	0.30	0.50
4	12	5,000	0.40	0.50	0.60	0.80
4	12	10,000	0.70	0.90	1.00	1.00
4	18	3,000	0.30	0.50	0.60	1.00
4	18	5,000	0.50	0.70	0.90	1.00
4	18	10,000	0.90	1.00	1.00	1.00

HP14x89 Connection Performance Data Neutral Axis Location for Rotation of Embedded Pile						
ASTM A572 Grade 50 Material (Fy = 50,000 psi, Fu = 65,000 psi)						
	Embed.		NA Location Measured from Bottom Face of Cap (in)			
Bend.	Depth	f'c	Link Elements with Traction Forces			Rigid Body
Case	(in)	(psi)	Method 1	Method 2	Method 3	Method 4
1	12	3,000	7.17	6.94	6.81	6.47
1	12	5,000	7.33	7.08	6.92	6.45
1	12	10,000	7.56	7.29	7.11	6.42
1	18	3,000	13.25	12.62	12.11	10.04
1	18	5,000	13.60	13.02	12.56	9.95
1	18	10,000	14.01	13.52	13.11	9.95
2	12	3,000	7.04	6.87	6.77	6.47
2	12	5,000	7.20	7.01	6.88	6.45
2	12	10,000	7.44	7.22	7.08	6.42
2	18	3,000	13.05	12.50	12.04	10.04
2	18	5,000	13.42	12.92	12.50	9.95
2	18	10,000	13.86	13.43	13.06	9.95
3	12	3,000	7.31	7.02	6.85	6.47
3	12	5,000	7.46	7.15	6.96	6.45
3	12	10,000	7.68	7.36	7.15	6.42
3	18	3,000	13.45	12.74	12.17	10.04
3	18	5,000	13.77	13.13	12.62	9.95
3	18	10,000	14.16	13.61	13.16	9.95
4	12	3,000	7.17	6.95	6.81	6.47
4	12	5,000	7.32	7.08	6.92	6.45
4	12	10,000	7.54	7.29	7.11	6.42
4	18	3,000	13.21	12.60	12.10	10.04
4	18	5,000	13.56	13.01	12.55	9.95
4	18	10,000	13.98	13.50	13.10	9.95

HP18x204 Connection Performance Data Rotational Stiffness						
ASTM A572 Grade 50 Material (Fy = 50,000 psi, Fu = 65,000 psi)						
	Embed.		Connection Stiffness (in-lbs/rad)			
Bend.	Depth	f'c	Link Elements with Traction Forces			Rigid Body
Case	(in)	(psi)	Method 1	Method 2	Method 3	Method 4
1	18	3,000	3,689,272,370	2,270,217,610	1,546,330,791	3,030,529,260
1	18	5,000	4,538,437,174	3,007,228,364	2,031,514,616	3,942,691,341
1	18	10,000	6,026,697,484	4,087,481,478	2,853,768,527	6,782,550,092
1	24	3,000	6,998,565,212	4,589,511,708	3,050,109,531	6,966,375,783
1	24	5,000	8,523,360,691	5,771,093,003	4,120,348,796	11,391,657,110
1	24	10,000	10,816,595,629	7,677,457,122	5,900,735,215	17,589,937,857
2	18	3,000	3,725,346,620	2,284,785,061	1,551,914,656	3,097,176,728
2	18	5,000	4,640,668,167	3,024,011,605	2,038,540,420	4,032,530,890
2	18	10,000	6,079,327,096	4,109,084,517	2,863,272,076	6,970,160,081
2	24	3,000	7,129,888,486	4,644,461,009	3,073,017,898	7,218,790,080
2	24	5,000	8,666,368,428	5,833,574,447	4,146,810,520	11,902,971,070
2	24	10,000	10,979,943,949	7,749,749,827	5,931,406,891	18,438,594,962
3	18	3,000	3,653,496,423	2,255,618,077	1,540,761,354	2,966,542,843
3	18	5,000	4,495,504,043	2,990,642,071	2,024,623,728	3,855,731,833
3	18	10,000	5,975,828,023	4,066,566,421	2,844,720,626	6,602,095,325
3	24	3,000	6,870,949,739	4,535,847,491	3,027,711,922	6,731,986,610
3	24	5,000	8,385,806,812	5,711,044,108	4,094,858,963	10,921,140,295
3	24	10,000	10,662,538,290	7,609,610,257	5,871,832,123	16,811,006,218
4	18	3,000	3,566,903,644	2,223,971,240	1,528,997,848	3,007,345,480
4	18	5,000	4,394,734,173	2,952,575,906	2,010,068,321	3,912,583,161
4	18	10,000	5,856,941,637	4,019,166,863	2,825,899,530	6,719,944,993
4	24	3,000	6,722,517,233	4,475,784,810	3,004,020,647	6,843,897,191
4	24	5,000	8,228,575,158	5,644,381,358	4,067,083,917	11,140,982,558
4	24	10,000	10,495,229,992	7,534,670,936	5,838,364,749	17,169,745,629

HP18x204 Connection Performance Data Maximum Concrete Compressive Stress						
ASTM A572 Grade 50 Material (Fy = 50,000 psi, Fu = 65,000 psi)						
	Embed.		Maximum Concrete Compressive Stress (psi)			
Bend.	Depth	f'c	Link Elements with Traction Forces			Rigid Body
Case	(in)	(psi)	Method 1	Method 2	Method 3	Method 4
1	18	3,000	2,339	2,906	2,576	2,832
1	18	5,000	4,981	4,256	4,510	4,977
1	18	10,000	9,821	9,331	9,687	6,369
1	24	3,000	2,844	2,957	2,915	2,988
1	24	5,000	4,260	4,952	4,671	3,522
1	24	10,000	9,822	9,672	8,199	3,697
2	18	3,000	2,346	2,918	2,583	2,832
2	18	5,000	3,807	4,268	4,521	4,977
2	18	10,000	9,844	9,354	9,710	6,369
2	24	3,000	2,857	2,974	2,929	2,988
2	24	5,000	4,273	4,975	4,688	3,522
2	24	10,000	9,849	9,704	8,218	3,697
3	18	3,000	2,333	2,894	2,570	2,832
3	18	5,000	4,965	4,244	4,499	4,977
3	18	10,000	9,798	9,308	9,664	6,369
3	24	3,000	2,831	2,941	2,902	2,988
3	24	5,000	4,246	4,929	4,654	3,522
3	24	10,000	9,794	9,640	8,181	3,697
4	18	3,000	2,344	2,902	2,574	2,832
4	18	5,000	4,988	4,255	4,505	4,977
4	18	10,000	9,830	9,328	9,674	6,369
4	24	3,000	2,838	2,945	2,905	2,988
4	24	5,000	4,253	4,935	4,658	3,522
4	24	10,000	9,805	9,647	8,186	3,697

HP18x204 Connection Performance Data Maximum Moment						
ASTM A572 Grade 50 Material (Fy = 50,000 psi, Fu = 65,000 psi)						
	Embed.		Maximum Moment Resisted by Embedded Pile (in-lbs)			
Bend.	Depth	f'c	Link Elements with Traction Forces			Rigid Body
Case	(in)	(psi)	Method 1	Method 2	Method 3	Method 4
1	18	3,000	1,231,027	1,846,541	1,846,541	3,077,568
1	18	5,000	2,462,055	2,462,055	3,077,568	5,539,623
1	18	10,000	4,308,596	4,924,109	6,155,137	6,155,137
1	24	3,000	1,846,541	2,462,055	3,077,568	6,155,137
1	24	5,000	2,462,055	3,693,082	4,308,596	6,155,137
1	24	10,000	4,924,109	6,155,137	6,155,137	6,155,137
2	18	3,000	1,231,027	1,846,541	1,846,541	3,077,568
2	18	5,000	1,846,541	2,462,055	3,077,568	5,539,623
2	18	10,000	4,308,596	4,924,109	6,155,137	6,155,137
2	24	3,000	1,846,541	2,462,055	3,077,568	6,155,137
2	24	5,000	2,462,055	3,693,082	4,308,596	6,155,137
2	24	10,000	4,924,109	6,155,137	6,155,137	6,155,137
3	18	3,000	1,231,027	1,846,541	1,846,541	3,077,568
3	18	5,000	2,462,055	2,462,055	3,077,568	5,539,623
3	18	10,000	4,308,596	4,924,109	6,155,137	6,155,137
3	24	3,000	1,846,541	2,462,055	3,077,568	6,155,137
3	24	5,000	2,462,055	3,693,082	4,308,596	6,155,137
3	24	10,000	4,924,109	6,155,137	6,155,137	6,155,137
4	18	3,000	1,231,027	1,846,541	1,846,541	3,077,568
4	18	5,000	2,462,055	2,462,055	3,077,568	5,539,623
4	18	10,000	4,308,596	4,924,109	6,155,137	6,155,137
4	24	3,000	1,846,541	2,462,055	3,077,568	6,155,137
4	24	5,000	2,462,055	3,693,082	4,308,596	6,155,137
4	24	10,000	4,924,109	6,155,137	6,155,137	6,155,137

HP18x204 Connection Performance Data Ratio of Applied Moment to Yield Moment						
ASTM A572 Grade 50 Material (Fy = 50,000 psi, Fu = 65,000 psi)						
	Embed.		Ratio of Applied Moment to Yield Moment			
Bend.	Depth	f'c	Link Elements with Traction Forces			Rigid Body
Case	(in)	(psi)	Method 1	Method 2	Method 3	Method 4
1	18	3,000	0.20	0.30	0.30	0.50
1	18	5,000	0.40	0.40	0.50	0.90
1	18	10,000	0.70	0.80	1.00	1.00
1	24	3,000	0.30	0.40	0.50	1.00
1	24	5,000	0.40	0.60	0.70	1.00
1	24	10,000	0.80	1.00	1.00	1.00
2	18	3,000	0.20	0.30	0.30	0.50
2	18	5,000	0.30	0.40	0.50	0.90
2	18	10,000	0.70	0.80	1.00	1.00
2	24	3,000	0.30	0.40	0.50	1.00
2	24	5,000	0.40	0.60	0.70	1.00
2	24	10,000	0.80	1.00	1.00	1.00
3	18	3,000	0.20	0.30	0.30	0.50
3	18	5,000	0.40	0.40	0.50	0.90
3	18	10,000	0.70	0.80	1.00	1.00
3	24	3,000	0.30	0.40	0.50	1.00
3	24	5,000	0.40	0.60	0.70	1.00
3	24	10,000	0.80	1.00	1.00	1.00
4	18	3,000	0.20	0.30	0.30	0.50
4	18	5,000	0.40	0.40	0.50	0.90
4	18	10,000	0.70	0.80	1.00	1.00
4	24	3,000	0.30	0.40	0.50	1.00
4	24	5,000	0.40	0.60	0.70	1.00
4	24	10,000	0.80	1.00	1.00	1.00

HP18x204 Connection Performance Data Neutral Axis Location for Rotation of Embedded Pile						
ASTM A572 Grade 50 Material (Fy = 50,000 psi, Fu = 65,000 psi)						
	Embed.		NA Location Measured from Bottom Face of Cap (in)			
Bend.	Depth	f'c	Link Elements with Traction Forces			Rigid Body
Case	(in)	(psi)	Method 1	Method 2	Method 3	Method 4
1	18	3,000	11.42	10.95	10.67	10.04
1	18	5,000	11.72	11.23	10.91	10.05
1	18	10,000	12.15	11.63	11.28	9.95
1	24	3,000	17.87	16.92	16.19	13.96
1	24	5,000	18.40	17.50	16.81	13.77
1	24	10,000	19.02	18.25	17.62	13.71
2	18	3,000	11.23	10.85	10.62	10.04
2	18	5,000	11.55	11.13	10.86	10.05
2	18	10,000	12.00	11.54	11.24	9.95
2	24	3,000	17.62	16.77	16.11	13.96
2	24	5,000	18.17	17.37	16.74	13.77
2	24	10,000	18.83	18.14	17.56	13.71
3	18	3,000	11.60	11.05	10.72	10.04
3	18	5,000	11.89	11.32	10.96	10.05
3	18	10,000	12.31	11.72	11.33	9.95
3	24	3,000	18.12	17.06	16.26	13.96
3	24	5,000	18.61	17.63	16.88	13.77
3	24	10,000	19.21	18.36	17.68	13.71
4	18	3,000	11.39	10.94	10.67	10.04
4	18	5,000	11.69	11.21	10.90	10.05
4	18	10,000	12.11	11.62	11.28	9.95
4	24	3,000	17.77	16.87	16.17	13.96
4	24	5,000	18.30	17.45	16.79	13.77
4	24	10,000	18.93	18.20	17.59	13.71

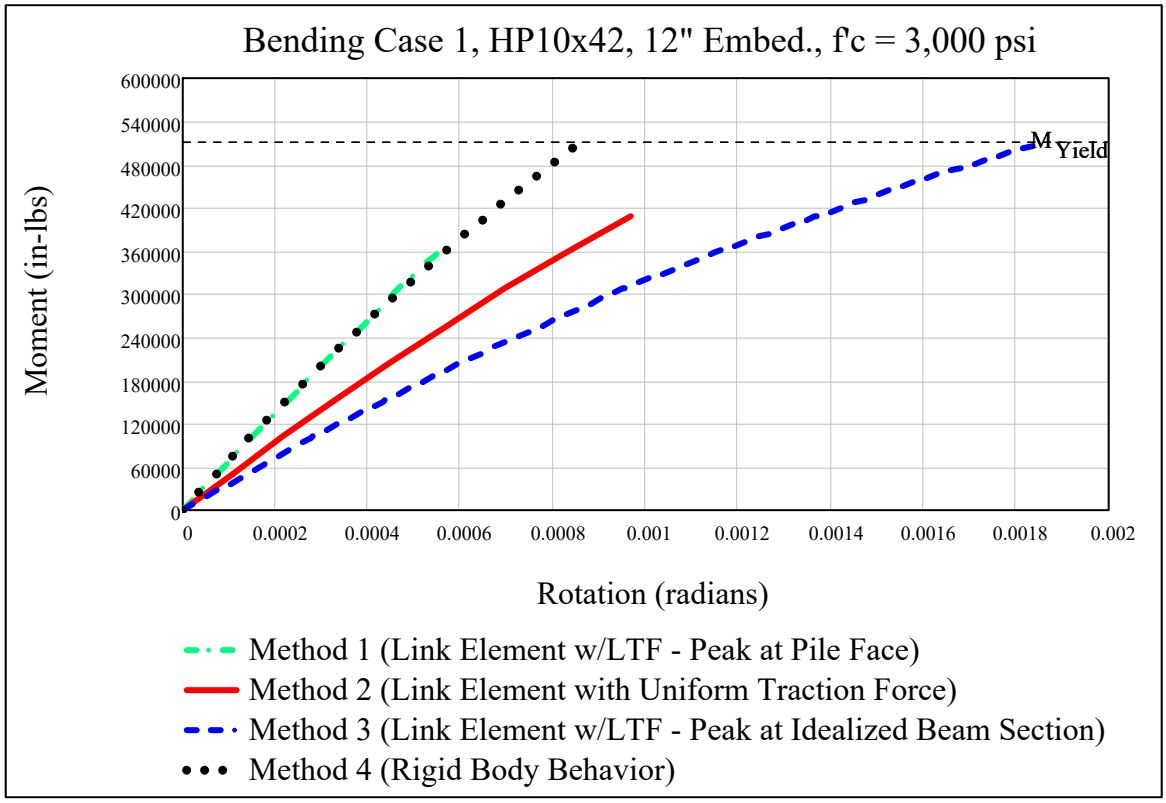
Bending Case 1, HP10x42, 12" Embed., f'c = 3,000 psi
Moment (in-lbs)
600000
540000
480000
420000
360000
300000
240000
180000
120000
60000
0
M Yield
0
0.0002
0.0004
0.0006
0.0008
0.001
0.0012
0.0014
0.0016
0.0018
0.002
Rotation (radians)
Method 1 (Link Element w/LTF - Peak at Pile Face)
Method 2 (Link Element with Uniform Traction Force)
Method 3 (Link Element w/LTF - Peak at Idealized Beam Section)
Method 4 (Rigid Body Behavior)

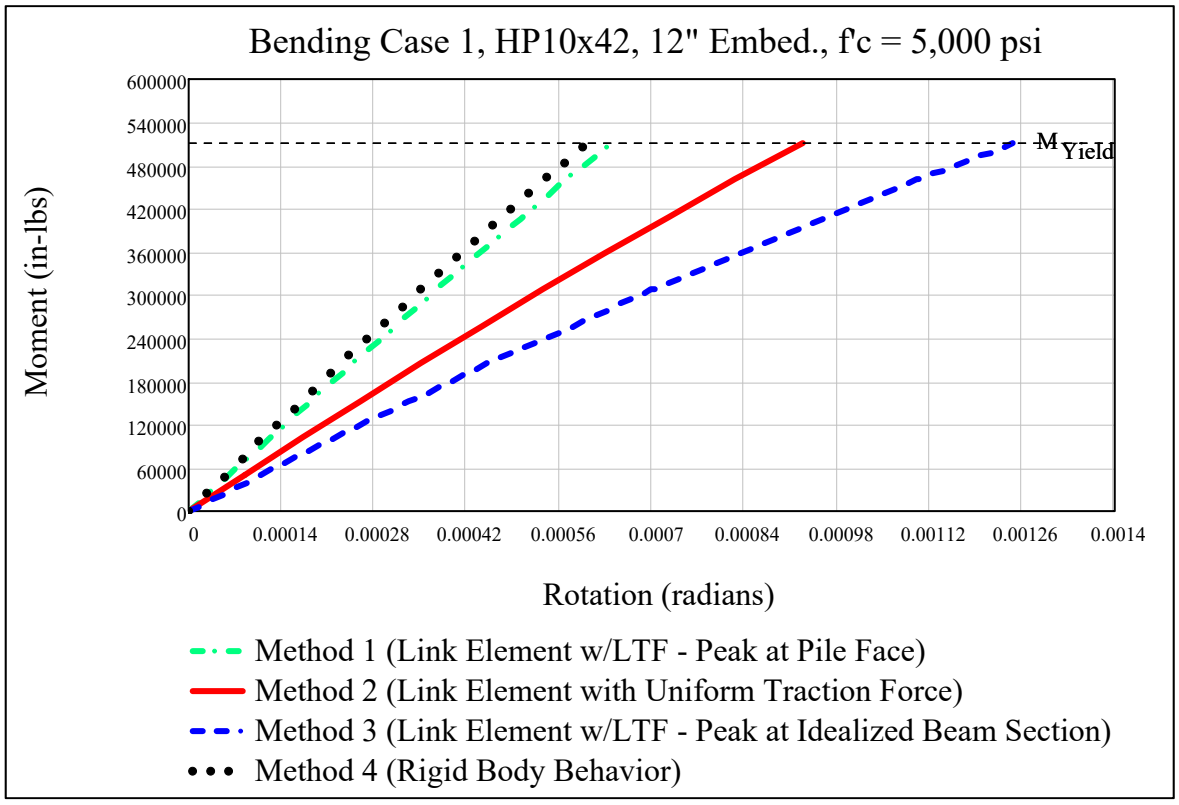
Bending Case 1, HP10x42, 12" Embed., f'c = 5,000 psi
Moment (in-lbs)
600000
540000
480000
420000
360000
300000
240000
180000
120000
60000
0
M Yield
0
0.00014
0.00028
0.00042
0.00056
0.0007
0.00084
0.00098
0.00112
0.00126
0.0014
Rotation (radians)
Method 1 (Link Element w/LTF - Peak at Pile Face)
Method 2 (Link Element with Uniform Traction Force)
Method 3 (Link Element w/LTF - Peak at Idealized Beam Section)
Method 4 (Rigid Body Behavior)

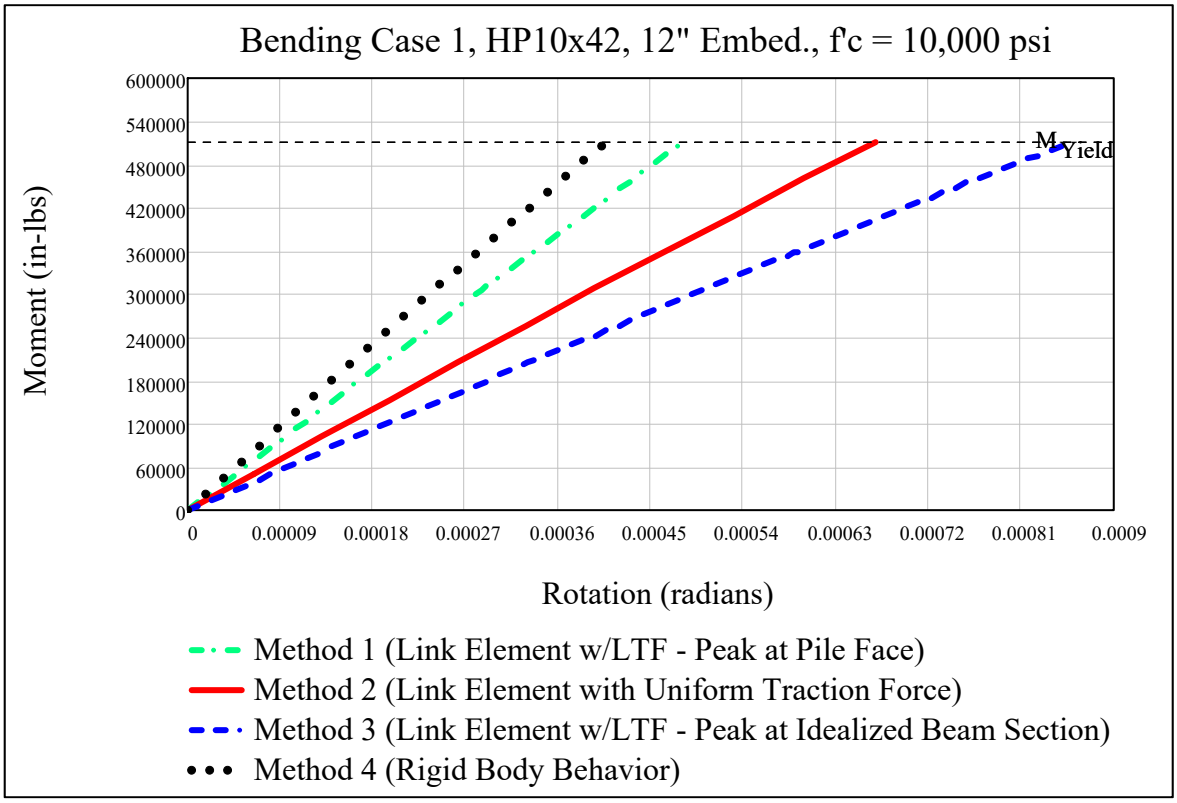
Bending Case 1, HP10x42, 12" Embed., f'c = 10,000 psi
Moment (in-lbs)
600000
540000
480000
420000
360000
300000
240000
180000
120000
60000
0
M Yield
0
0.00009
0.00018
0.00027
0.00036
0.00045
0.00054
0.00063
0.00072
0.00081
0.0009
Rotation (radians)
Method 1 (Link Element w/LTF - Peak at Pile Face)
Method 2 (Link Element with Uniform Traction Force)
Method 3 (Link Element w/LTF - Peak at Idealized Beam Section)
Method 4 (Rigid Body Behavior)

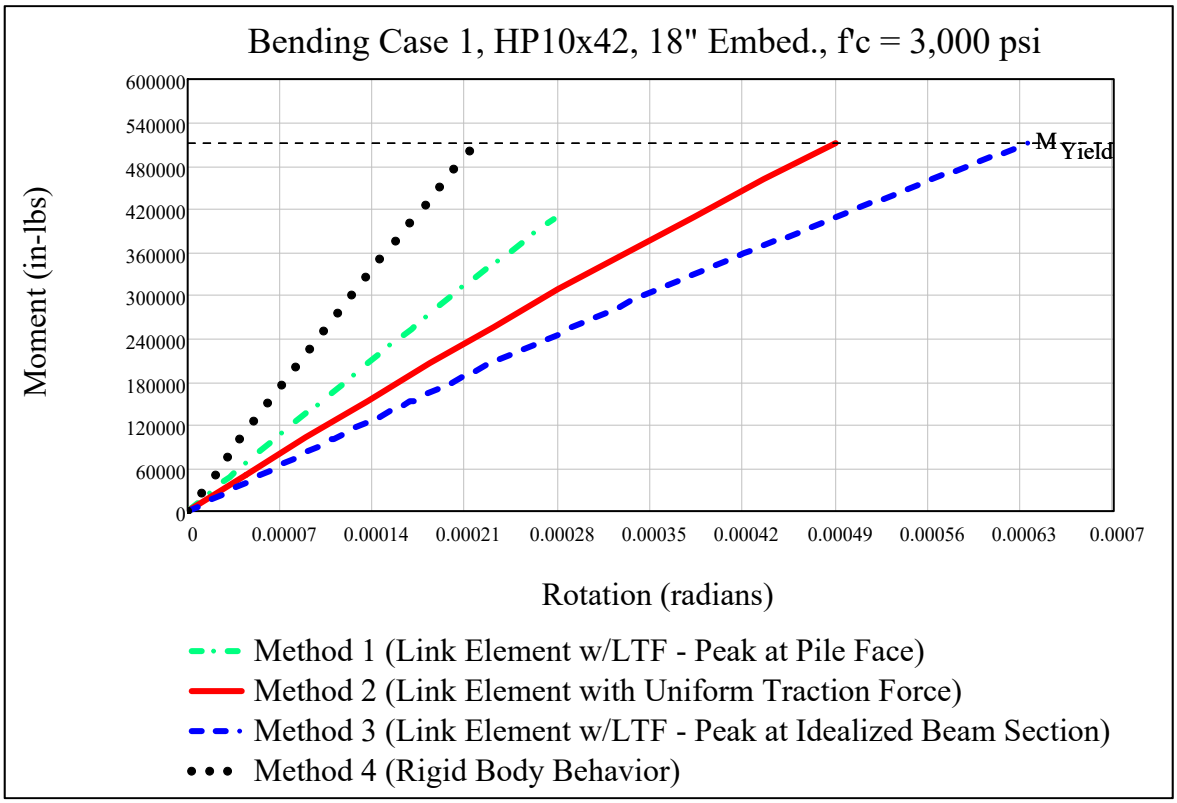
Bending Case 1, HP10x42, 18" Embed., f'c = 3,000 psi
Moment (in-lbs)
600000
540000
480000
420000
360000
300000
240000
180000
120000
60000
0
M Yield
0
0.00007
0.00014
0.00021
0.00028
0.00035
0.00042
0.00049
0.00056
0.00063
0.0007
Rotation (radians)
Method 1 (Link Element w/LTF - Peak at Pile Face)
Method 2 (Link Element with Uniform Traction Force)
Method 3 (Link Element w/LTF - Peak at Idealized Beam Section)
Method 4 (Rigid Body Behavior)

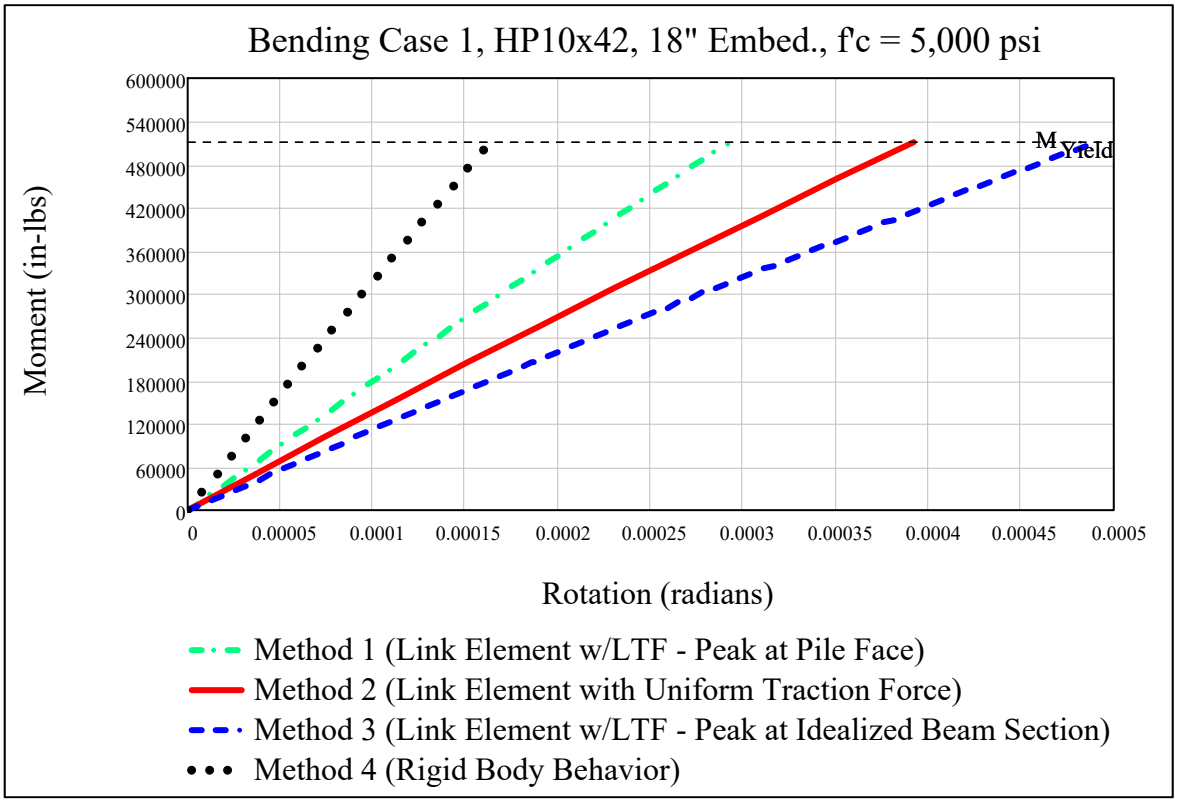
Bending Case 1, HP10x42, 18" Embed., f'c = 5,000 psi
Moment (in-lbs)
600000
540000
480000
420000
360000
300000
240000
180000
120000
60000
0
M Yield
0
0.00005
0.0001
0.00015
0.0002
0.00025
0.0003
0.00035
0.0004
0.00045
0.0005
Rotation (radians)
Method 1 (Link Element w/LTF - Peak at Pile Face)
Method 2 (Link Element with Uniform Traction Force)
Method 3 (Link Element w/LTF - Peak at Idealized Beam Section)
Method 4 (Rigid Body Behavior)

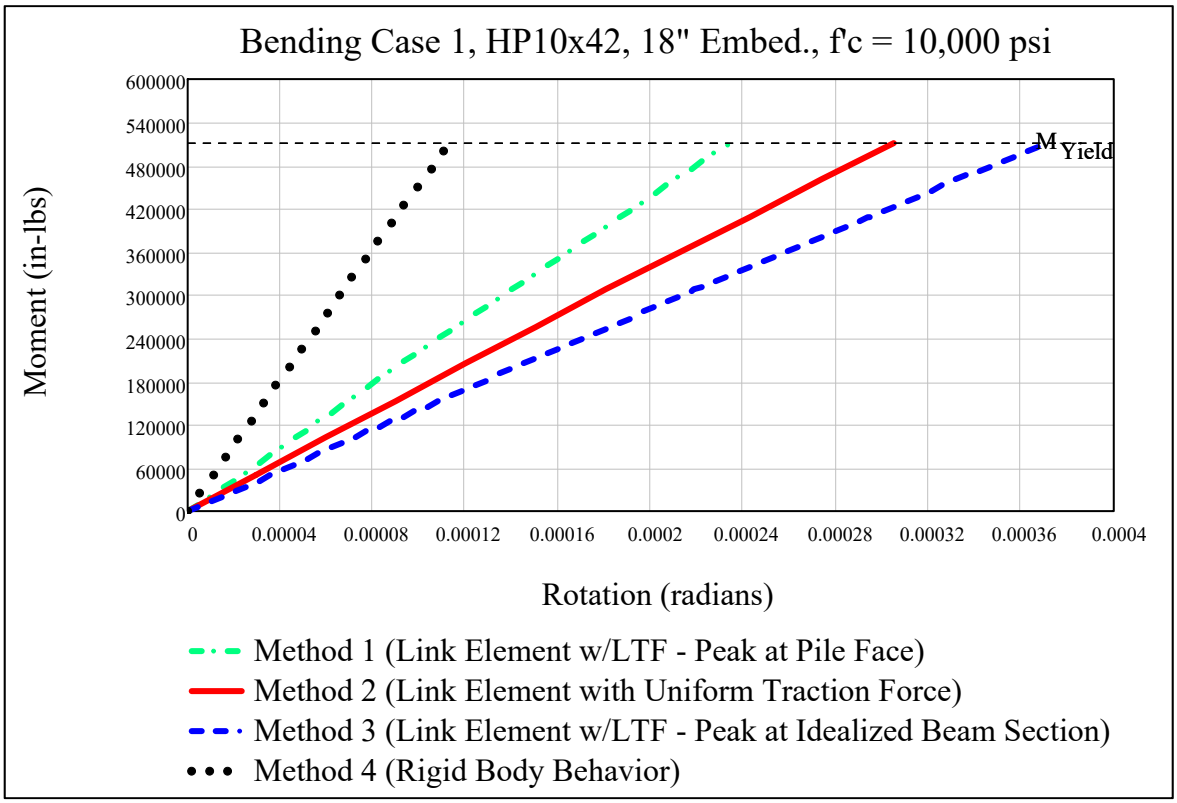
Bending Case 1, HP10x42, 18" Embed., f'c = 10,000 psi
Moment (in-lbs)
600000
540000
480000
420000
360000
300000
240000
180000
120000
60000
0
M Yield
0
0.00004
0.00008
0.00012
0.00016
0.0002
0.00024
0.00028
0.00032
0.00036
0.0004
Rotation (radians)
Method 1 (Link Element w/LTF - Peak at Pile Face)
Method 2 (Link Element with Uniform Traction Force)
Method 3 (Link Element w/LTF - Peak at Idealized Beam Section)
Method 4 (Rigid Body Behavior)

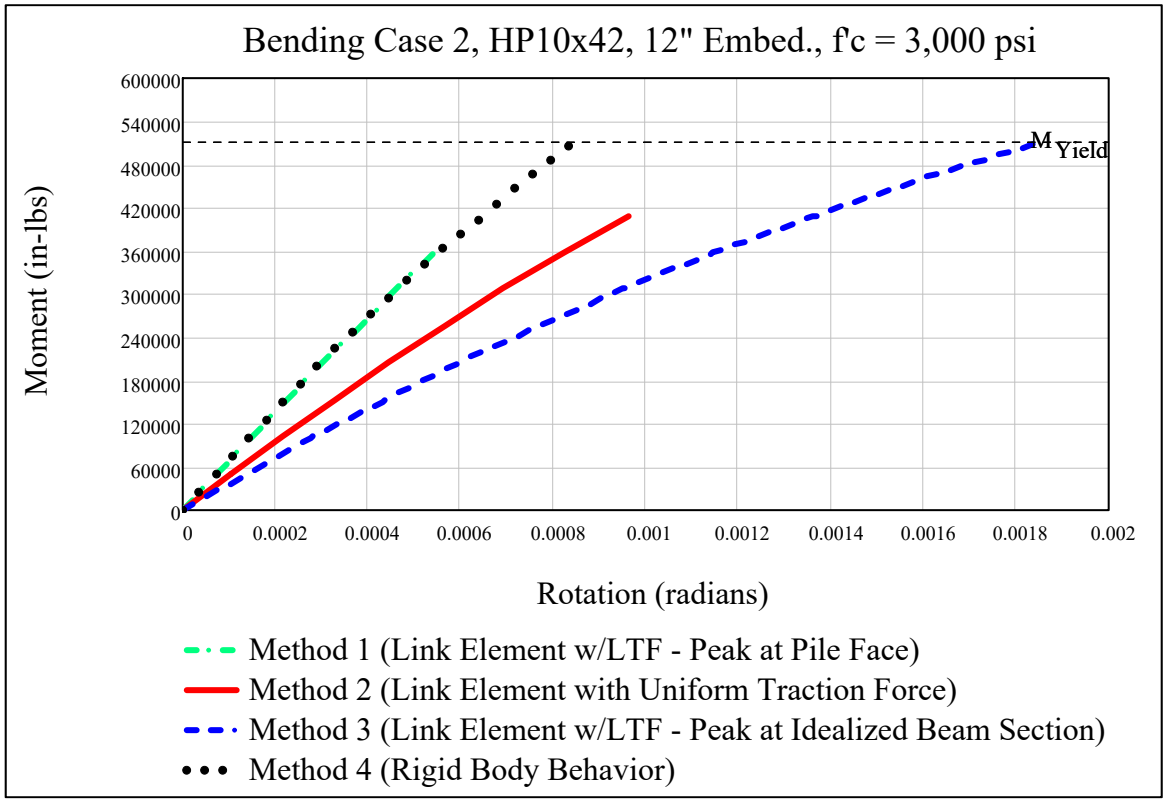
Bending Case 2, HP10x42, 12" Embed., f'c = 3,000 psi
Moment (in-lbs)
600000
540000
480000
420000
360000
300000
240000
180000
120000
60000
0
M Yield
0
0.0002
0.0004
0.0006
0.0008
0.001
0.0012
0.0014
0.0016
0.0018
0.002
Rotation (radians)
Method 1 (Link Element w/LTF - Peak at Pile Face)
Method 2 (Link Element with Uniform Traction Force)
Method 3 (Link Element w/LTF - Peak at Idealized Beam Section)
Method 4 (Rigid Body Behavior)

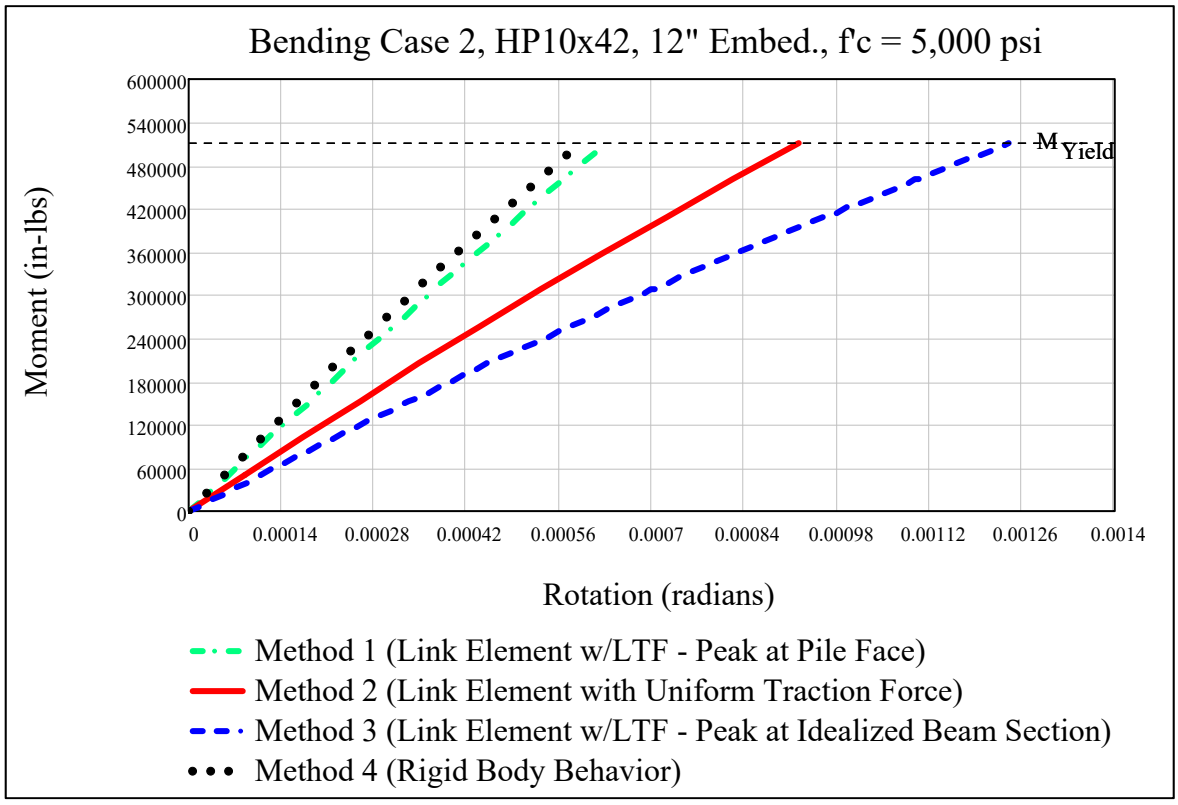
Bending Case 2, HP10x42, 12" Embed., f'c = 5,000 psi
Moment (in-lbs)
600000
540000
480000
420000
360000
300000
240000
180000
120000
60000
0
M Yield
0
0.00014
0.00028
0.00042
0.00056
0.0007
0.00084
0.00098
0.00112
0.00126
0.0014
Rotation (radians)
Method 1 (Link Element w/LTF - Peak at Pile Face)
Method 2 (Link Element with Uniform Traction Force)
Method 3 (Link Element w/LTF - Peak at Idealized Beam Section)
Method 4 (Rigid Body Behavior)

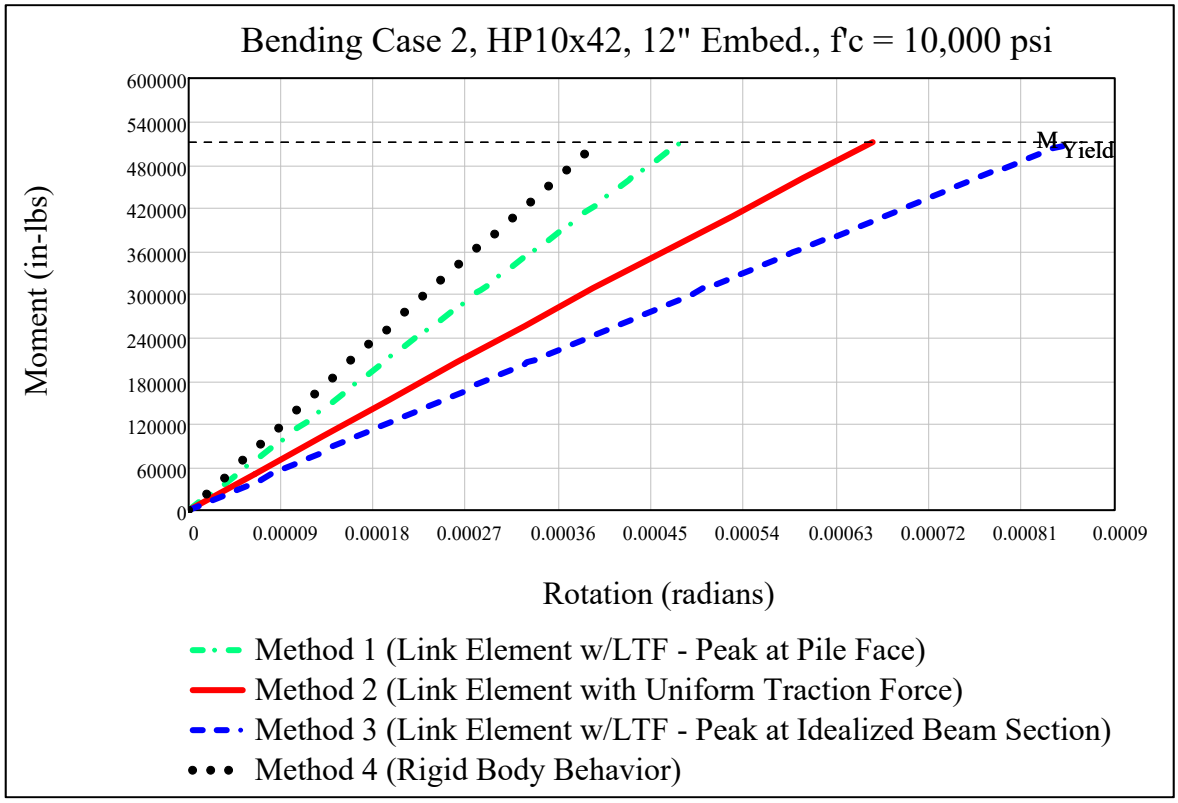
Bending Case 2, HP10x42, 12" Embed., f'c = 10,000 psi
Moment (in-lbs)
600000
540000
480000
420000
360000
300000
240000
180000
120000
60000
0
M Yield
0
0.00009
0.00018
0.00027
0.00036
0.00045
0.00054
0.00063
0.00072
0.00081
0.0009
Rotation (radians)
Method 1 (Link Element w/LTF - Peak at Pile Face)
Method 2 (Link Element with Uniform Traction Force)
Method 3 (Link Element w/LTF - Peak at Idealized Beam Section)
Method 4 (Rigid Body Behavior)

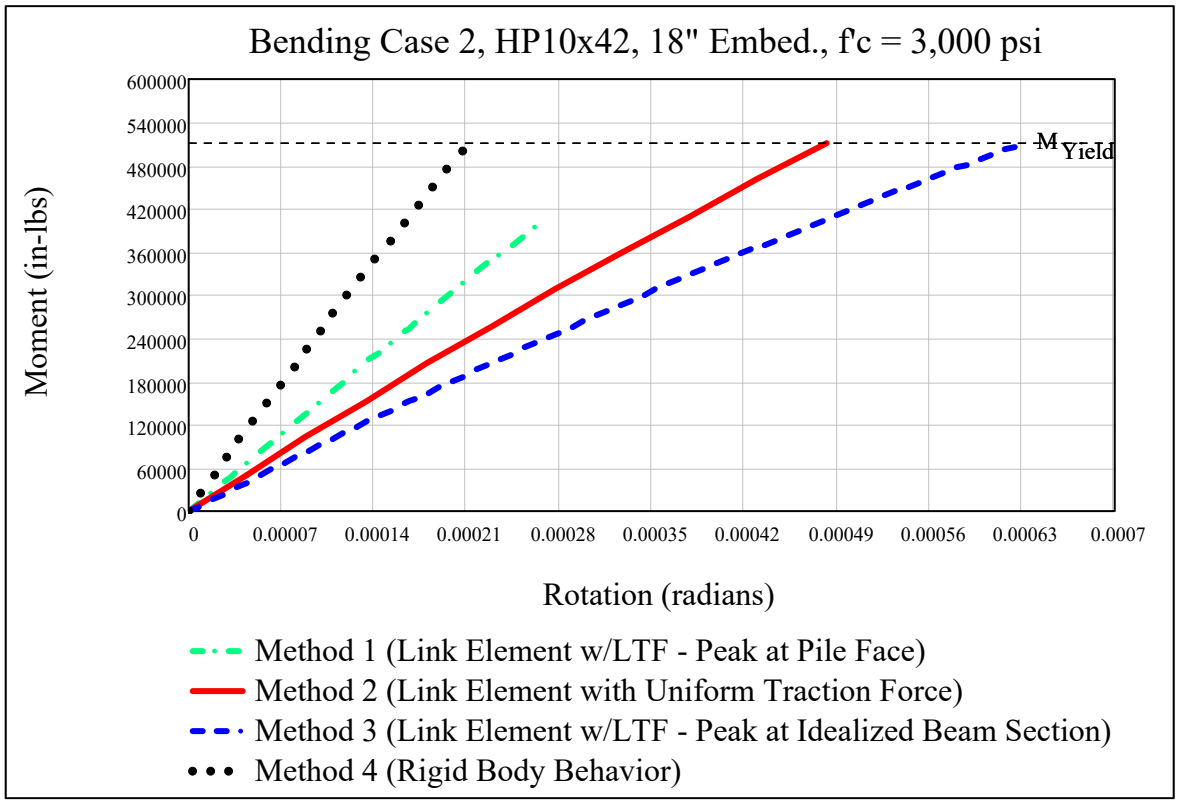
Bending Case 2, HP10x42, 18" Embed., f'c = 3,000 psi
Moment (in-lbs)
600000
540000
480000
420000
360000
300000
240000
180000
120000
60000
0
M Yield
0
0.00007
0.00014
0.00021
0.00028
0.00035
0.00042
0.00049
0.00056
0.00063
0.0007
Rotation (radians)
Method 1 (Link Element w/LTF - Peak at Pile Face)
Method 2 (Link Element with Uniform Traction Force)
Method 3 (Link Element w/LTF - Peak at Idealized Beam Section)
Method 4 (Rigid Body Behavior)

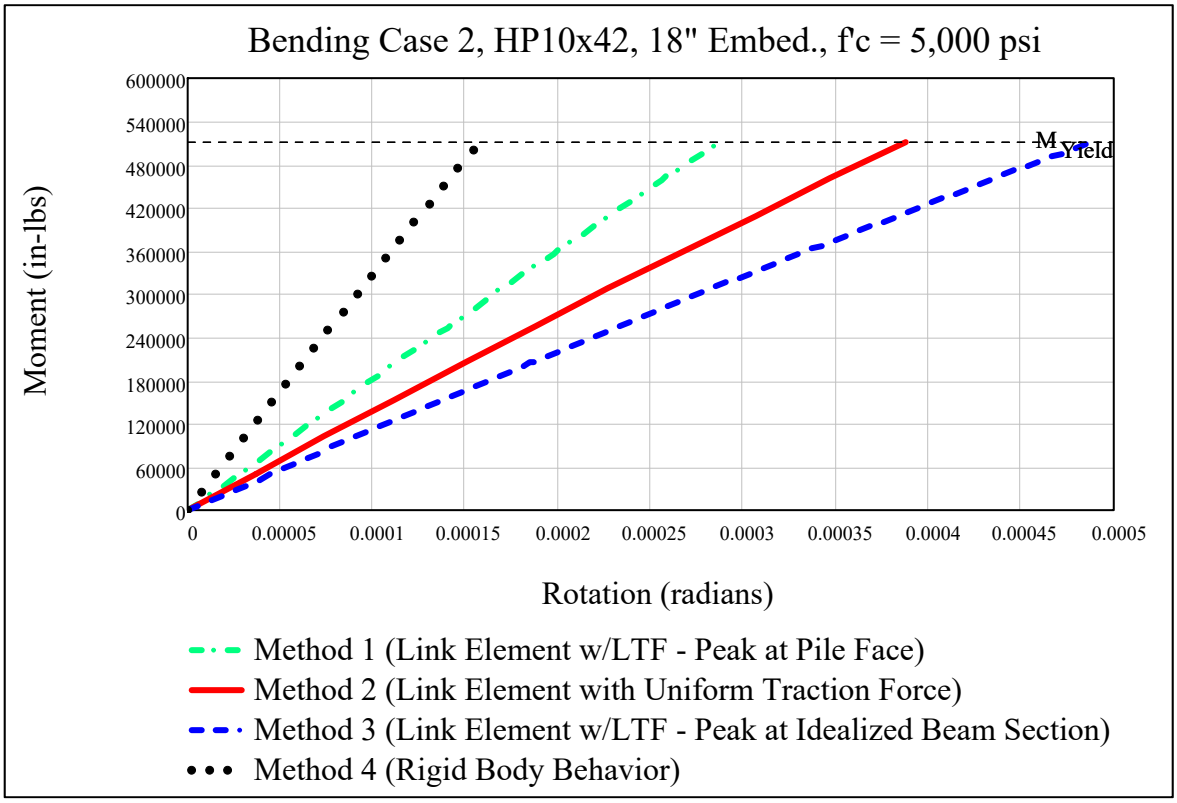
Bending Case 2, HP10x42, 18" Embed., f'c = 5,000 psi
Moment (in-lbs)
600000
540000
480000
420000
360000
300000
240000
180000
120000
60000
0
M Yield
0
0.00005
0.0001
0.00015
0.0002
0.00025
0.0003
0.00035
0.0004
0.00045
0.0005
Rotation (radians)
Method 1 (Link Element w/LTF - Peak at Pile Face)
Method 2 (Link Element with Uniform Traction Force)
Method 3 (Link Element w/LTF - Peak at Idealized Beam Section)
Method 4 (Rigid Body Behavior)

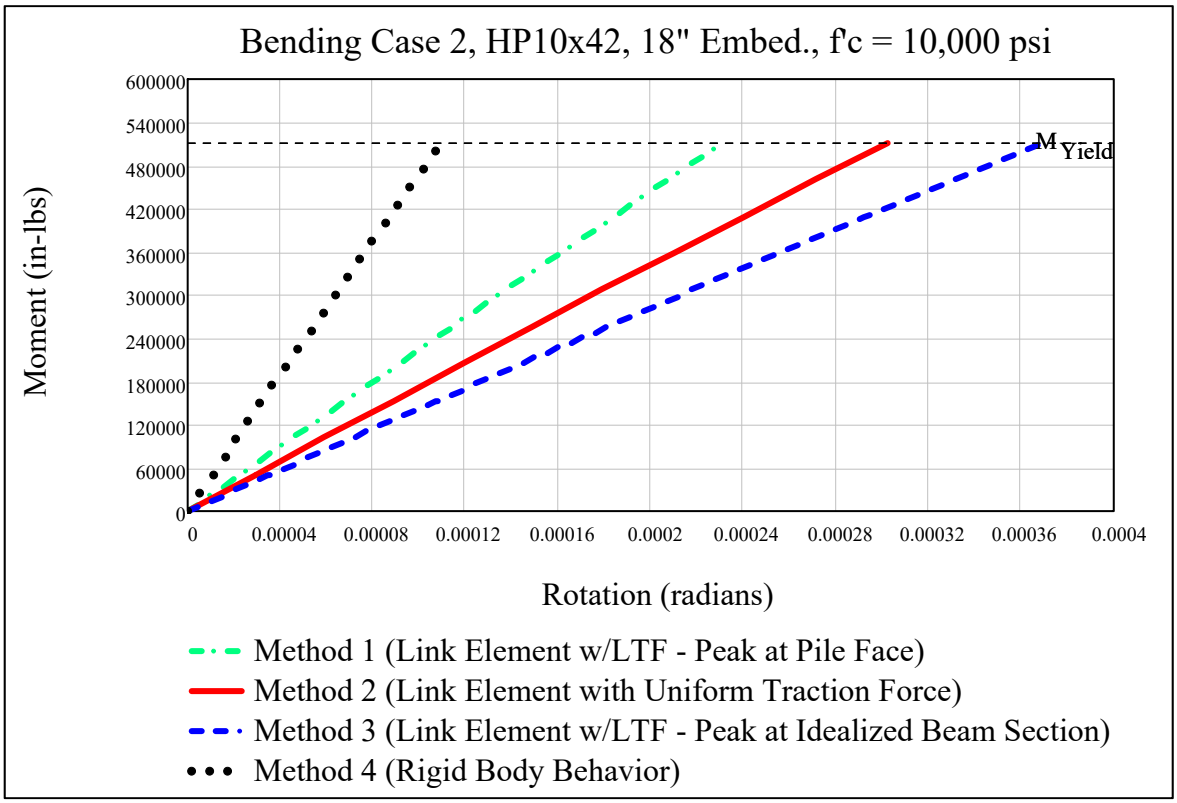
Bending Case 2, HP10x42, 18" Embed., f'c = 10,000 psi
Moment (in-lbs)
600000
540000
480000
420000
360000
300000
240000
180000
120000
60000
0
M Yield
0
0.00004
0.00008
0.00012
0.00016
0.0002
0.00024
0.00028
0.00032
0.00036
0.0004
Rotation (radians)
Method 1 (Link Element w/LTF - Peak at Pile Face)
Method 2 (Link Element with Uniform Traction Force)
Method 3 (Link Element w/LTF - Peak at Idealized Beam Section)
Method 4 (Rigid Body Behavior)

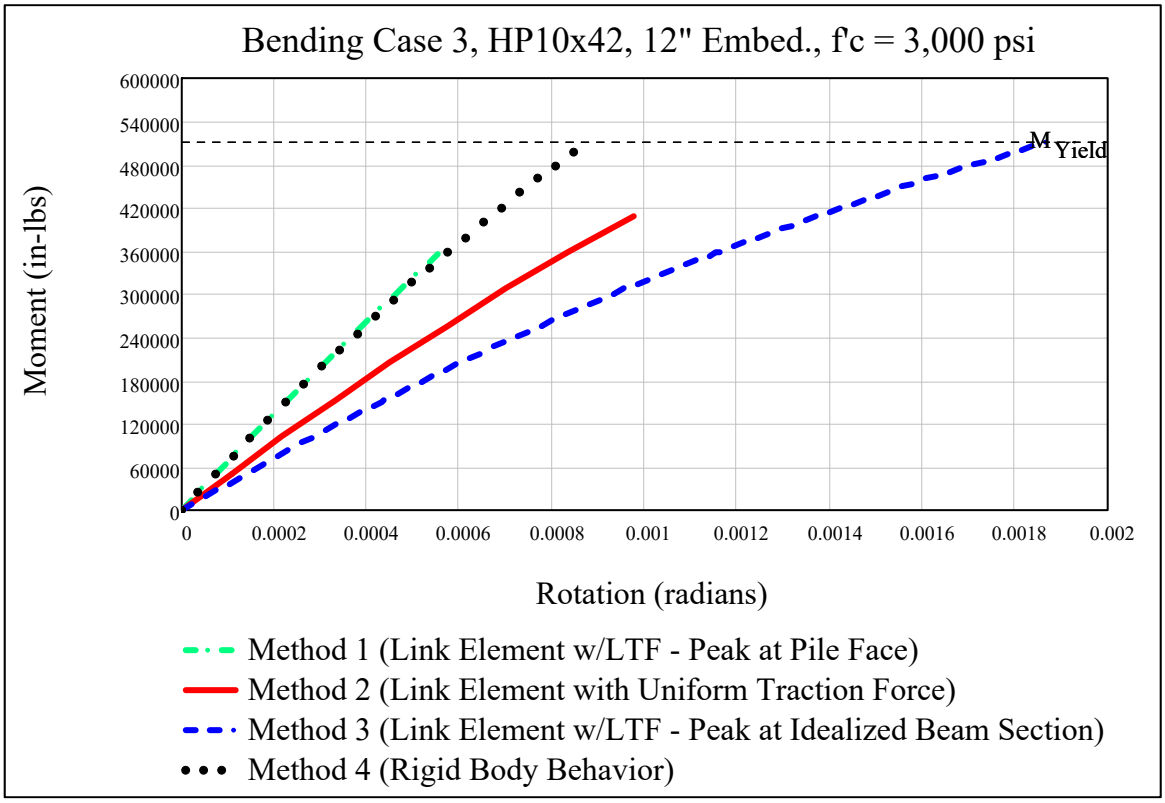
Bending Case 3, HP10x42, 12" Embed., f'c = 3,000 psi
Moment (in-lbs)
600000
540000
480000
420000
360000
300000
240000
180000
120000
60000
0
M Yield
0
0.0002
0.0004
0.0006
0.0008
0.001
0.0012
0.0014
0.0016
0.0018
0.002
Rotation (radians)
Method 1 (Link Element w/LTF - Peak at Pile Face)
Method 2 (Link Element with Uniform Traction Force)
Method 3 (Link Element w/LTF - Peak at Idealized Beam Section)
Method 4 (Rigid Body Behavior)

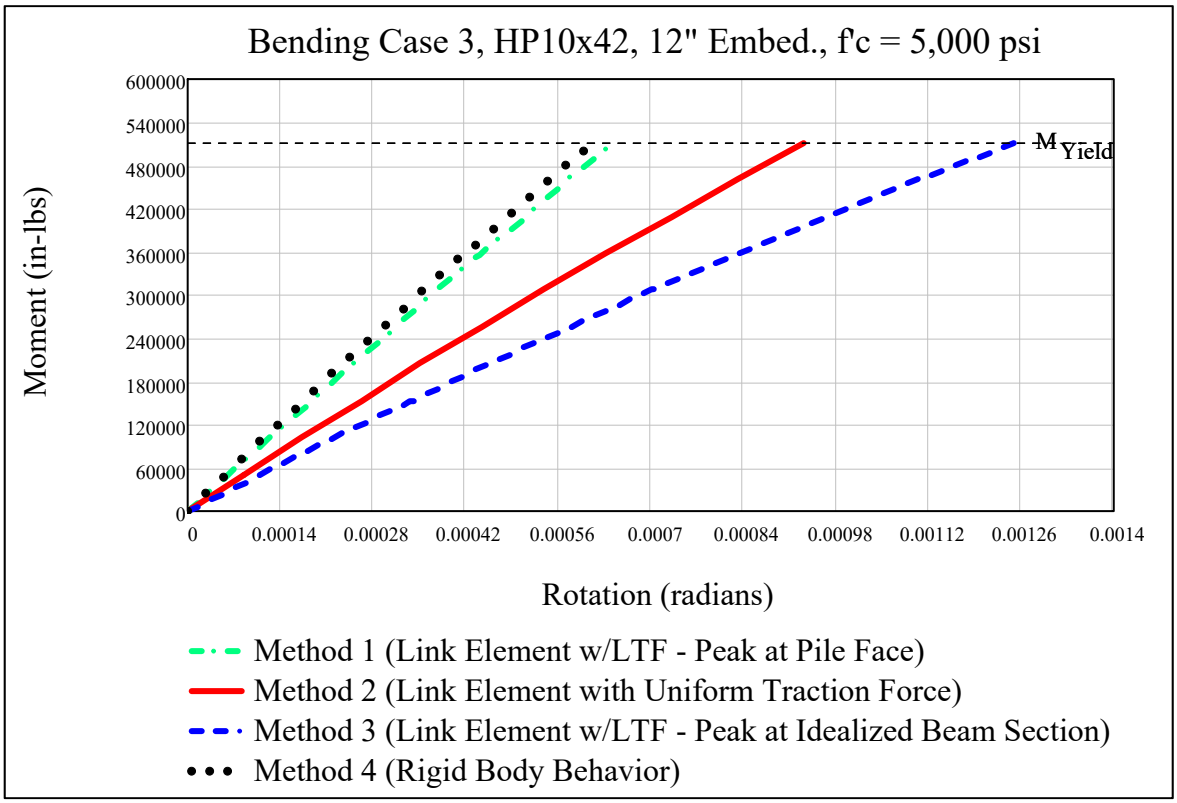
Bending Case 3, HP10x42, 12" Embed., f'c = 5,000 psi
Moment (in-lbs)
600000
540000
480000
420000
360000
300000
240000
180000
120000
60000
0
M Yield
0
0.00014
0.00028
0.00042
0.00056
0.0007
0.00084
0.00098
0.00112
0.00126
0.0014
Rotation (radians)
Method 1 (Link Element w/LTF - Peak at Pile Face)
Method 2 (Link Element with Uniform Traction Force)
Method 3 (Link Element w/LTF - Peak at Idealized Beam Section)
Method 4 (Rigid Body Behavior)

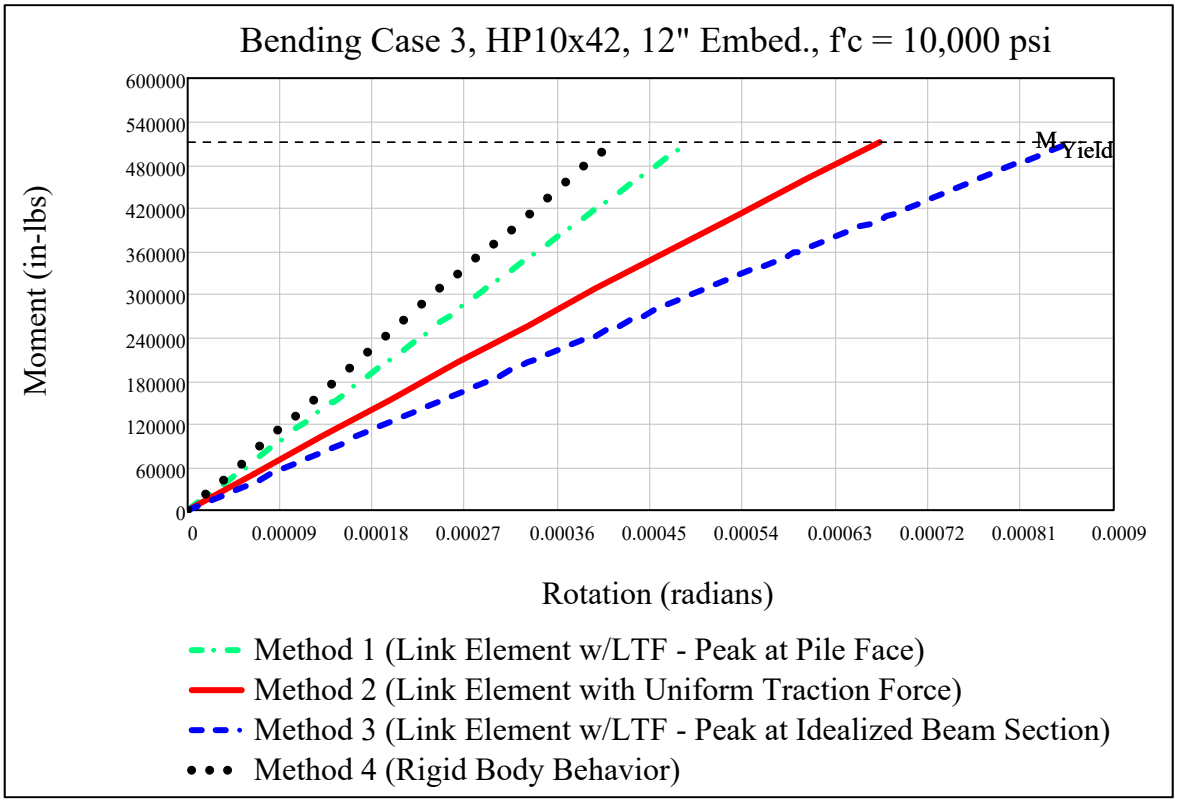
Bending Case 3, HP10x42, 12" Embed., f'c = 10,000 psi
Moment (in-lbs)
600000
540000
480000
420000
360000
300000
240000
180000
120000
60000
0
M Yield
0
0.00009
0.00018
0.00027
0.00036
0.00045
0.00054
0.00063
0.00072
0.00081
0.0009
Rotation (radians)
Method 1 (Link Element w/LTF - Peak at Pile Face)
Method 2 (Link Element with Uniform Traction Force)
Method 3 (Link Element w/LTF - Peak at Idealized Beam Section)
Method 4 (Rigid Body Behavior)

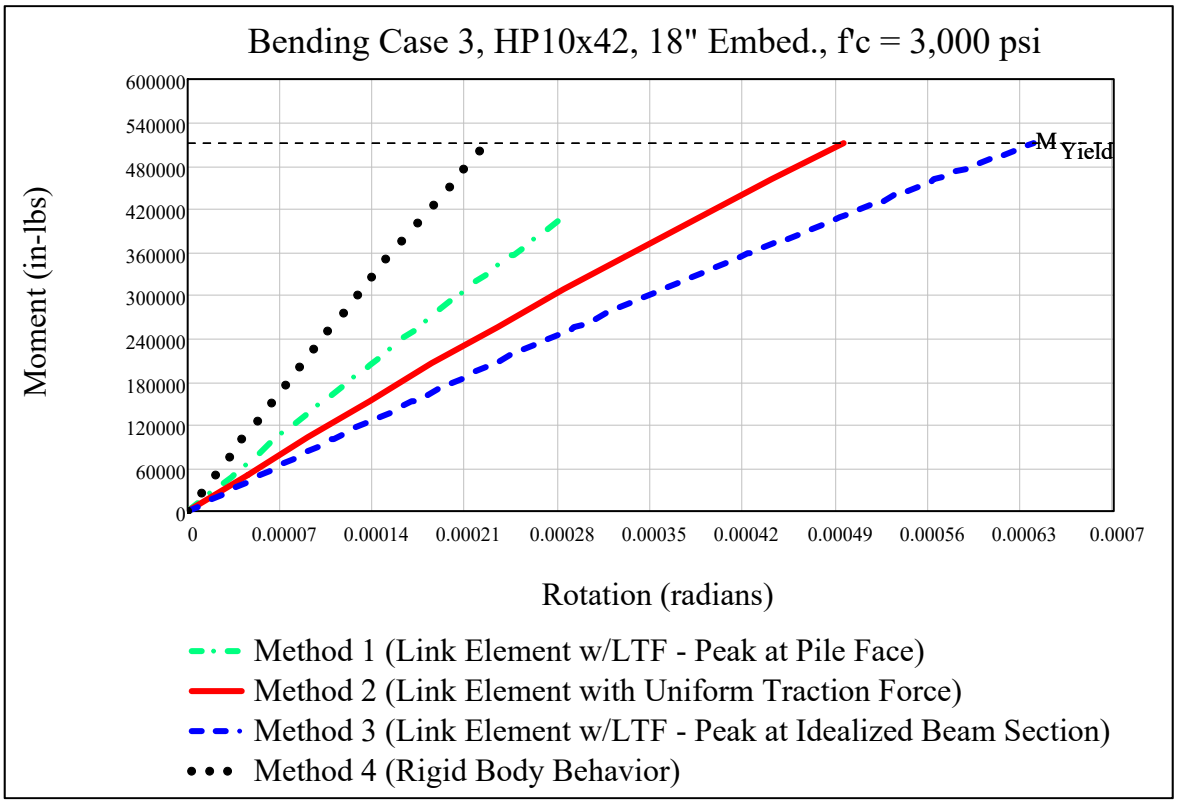
Bending Case 3, HP10x42, 18" Embed., f'c = 3,000 psi
Moment (in-lbs)
600000
540000
480000
420000
360000
300000
240000
180000
120000
60000
0
M Yield
0
0.00007
0.00014
0.00021
0.00028
0.00035
0.00042
0.00049
0.00056
0.00063
0.0007
Rotation (radians)
Method 1 (Link Element w/LTF - Peak at Pile Face)
Method 2 (Link Element with Uniform Traction Force)
Method 3 (Link Element w/LTF - Peak at Idealized Beam Section)
Method 4 (Rigid Body Behavior)

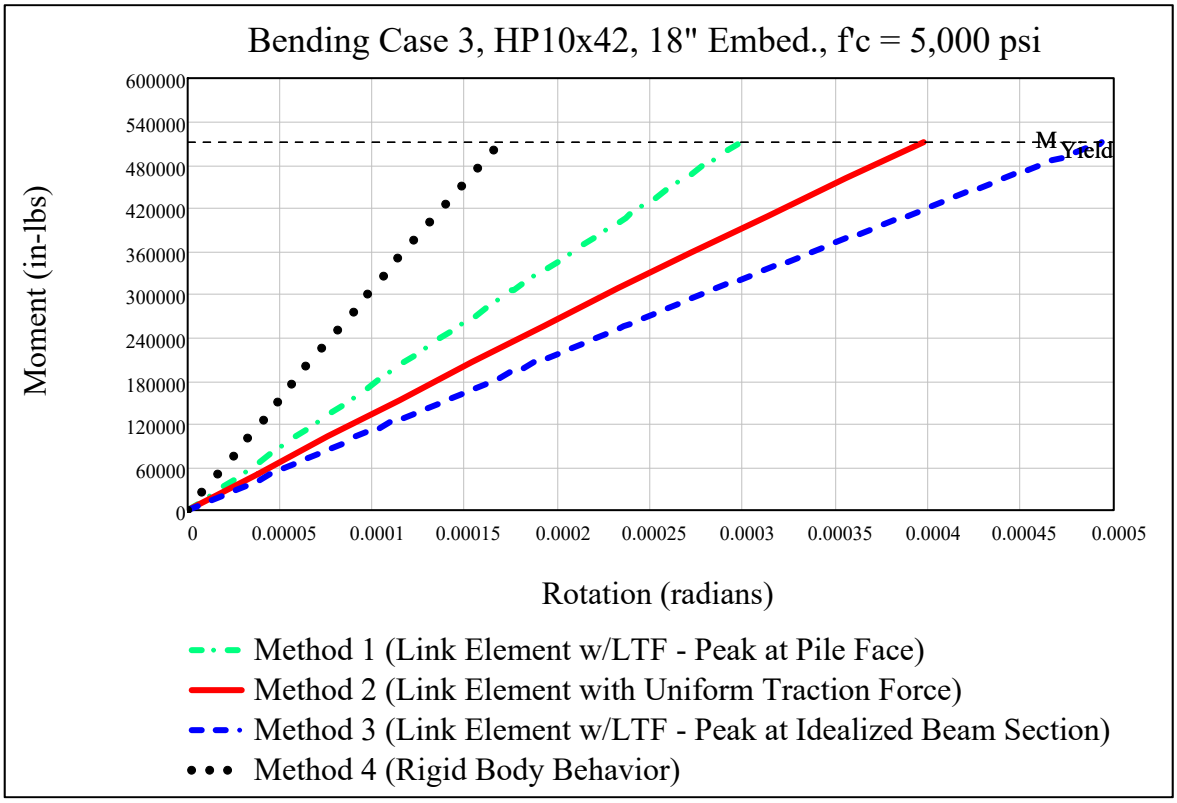
Bending Case 3, HP10x42, 18" Embed., f'c = 5,000 psi
Moment (in-lbs)
600000
540000
480000
420000
360000
300000
240000
180000
120000
60000
0
M Yield
0
0.00005
0.0001
0.00015
0.0002
0.00025
0.0003
0.00035
0.0004
0.00045
0.0005
Rotation (radians)
Method 1 (Link Element w/LTF - Peak at Pile Face)
Method 2 (Link Element with Uniform Traction Force)
Method 3 (Link Element w/LTF - Peak at Idealized Beam Section)
Method 4 (Rigid Body Behavior)

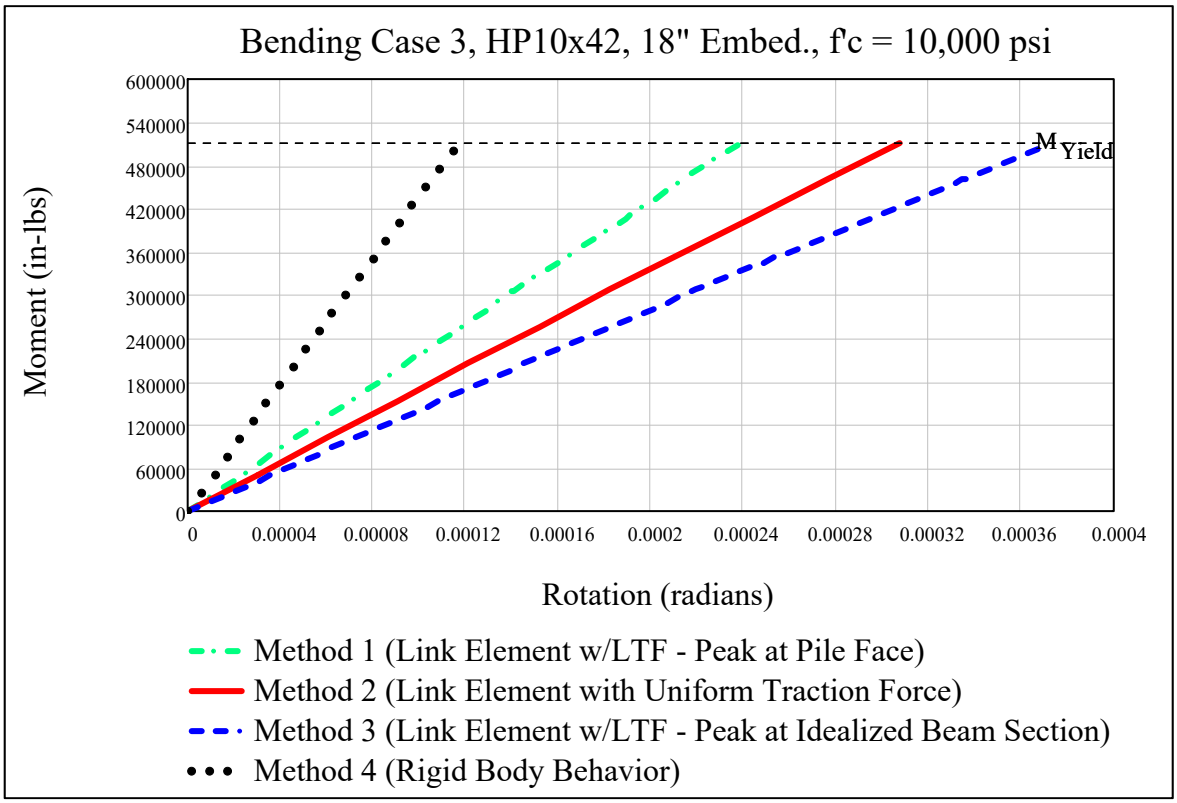
Bending Case 3, HP10x42, 18" Embed., f'c = 10,000 psi
Moment (in-lbs)
600000
540000
480000
420000
360000
300000
240000
180000
120000
60000
0
M Yield
0
0.00004
0.00008
0.00012
0.00016
0.0002
0.00024
0.00028
0.00032
0.00036
0.0004
Rotation (radians)
Method 1 (Link Element w/LTF - Peak at Pile Face)
Method 2 (Link Element with Uniform Traction Force)
Method 3 (Link Element w/LTF - Peak at Idealized Beam Section)
Method 4 (Rigid Body Behavior)

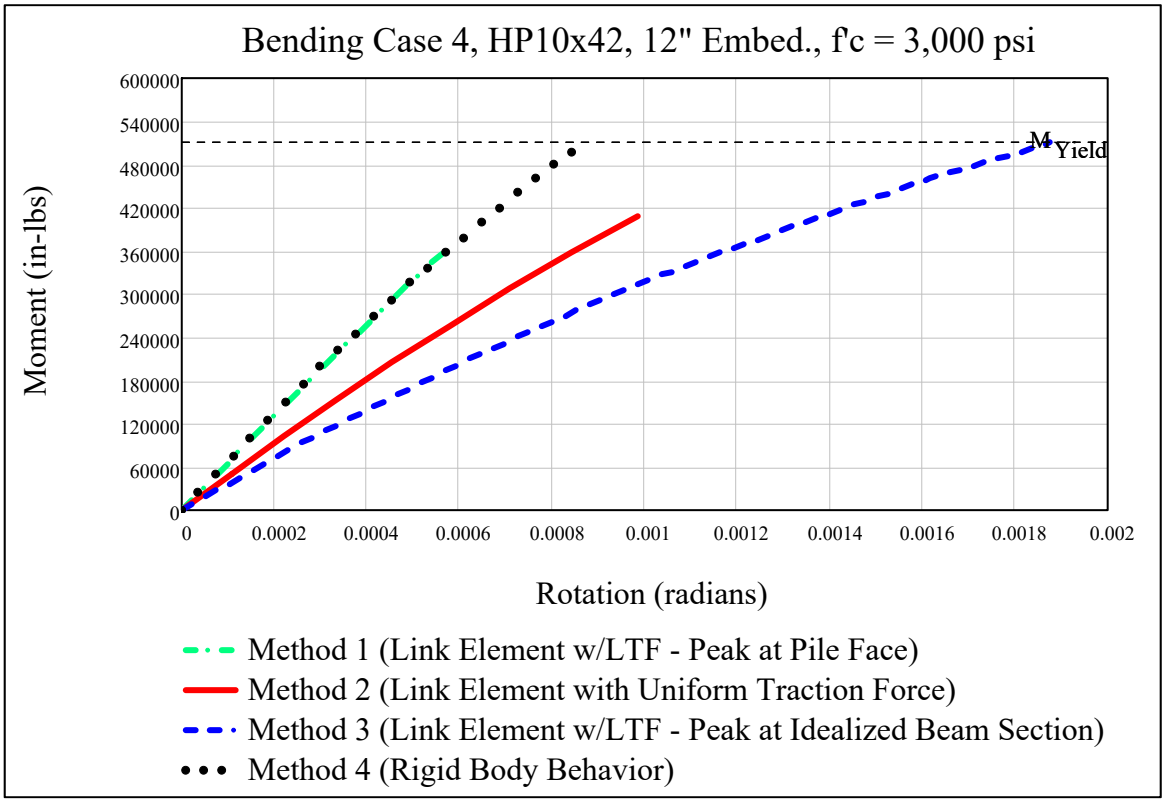
Bending Case 4, HP10x42, 12" Embed., f'c = 3,000 psi
Moment (in-lbs)
600000
540000
480000
420000
360000
300000
240000
180000
120000
60000
0
M Yield
0
0.0002
0.0004
0.0006
0.0008
0.001
0.0012
0.0014
0.0016
0.0018
0.002
Rotation (radians)
Method 1 (Link Element w/LTF - Peak at Pile Face)
Method 2 (Link Element with Uniform Traction Force)
Method 3 (Link Element w/LTF - Peak at Idealized Beam Section)
Method 4 (Rigid Body Behavior)

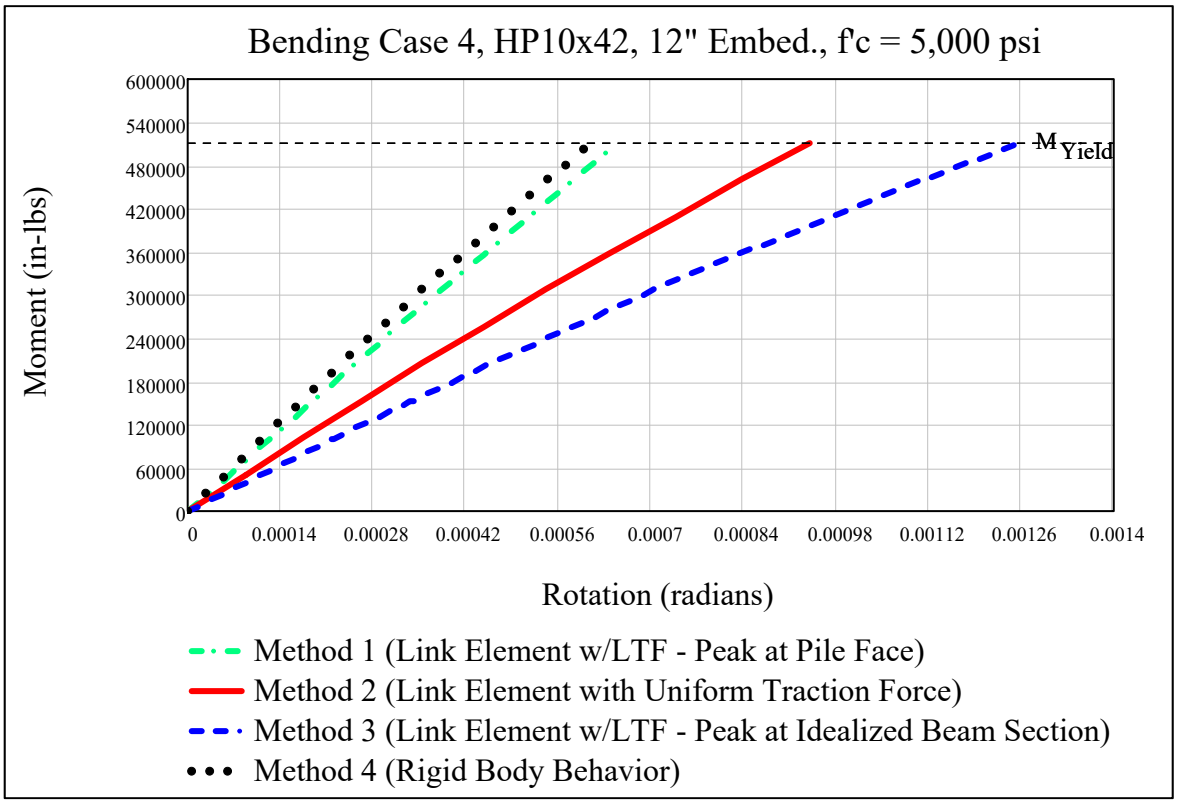
Bending Case 4, HP10x42, 12" Embed., f'c = 5,000 psi
Moment (in-lbs)
600000
540000
480000
420000
360000
300000
240000
180000
120000
60000
0
M Yield
0
0.00014
0.00028
0.00042
0.00056
0.0007
0.00084
0.00098
0.00112
0.00126
0.0014
Rotation (radians)
Method 1 (Link Element w/LTF - Peak at Pile Face)
Method 2 (Link Element with Uniform Traction Force)
Method 3 (Link Element w/LTF - Peak at Idealized Beam Section)
Method 4 (Rigid Body Behavior)

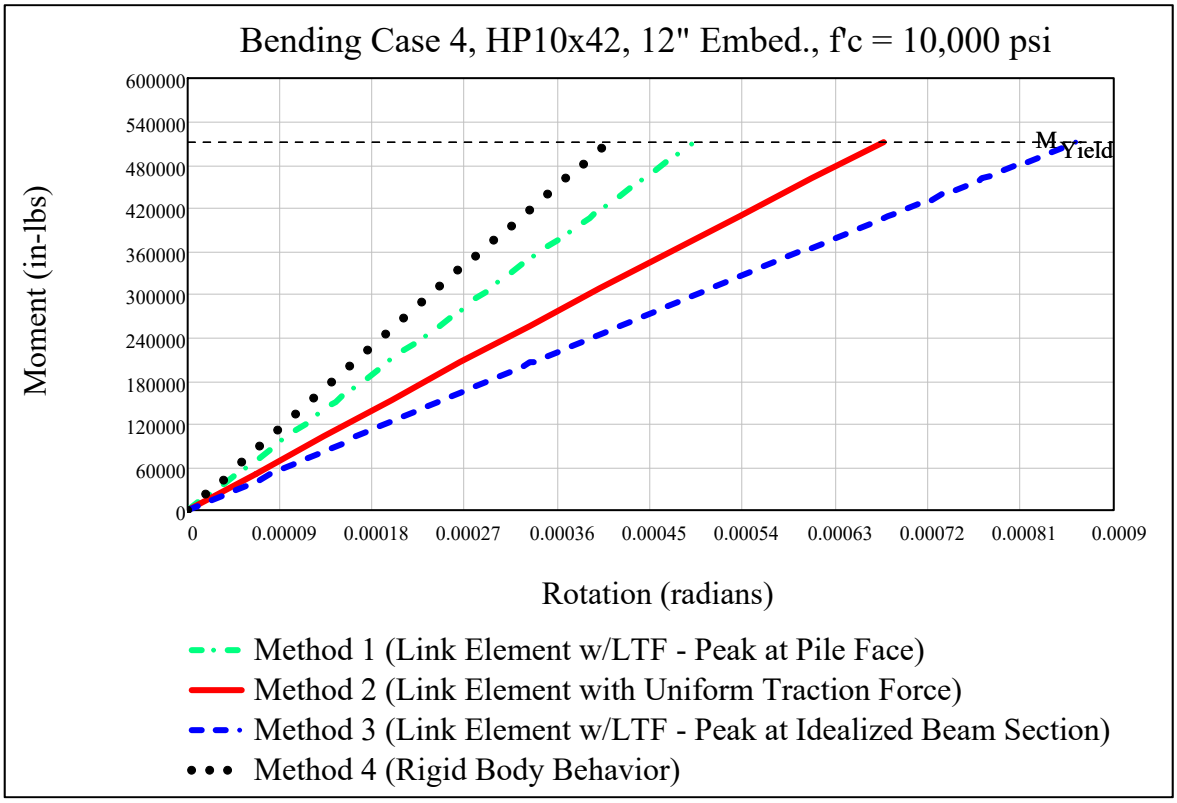
Bending Case 4, HP10x42, 12" Embed., f'c = 10,000 psi
Moment (in-lbs)
600000
540000
480000
420000
360000
300000
240000
180000
120000
60000
0
M Yield
0
0.00009
0.00018
0.00027
0.00036
0.00045
0.00054
0.00063
0.00072
0.00081
0.0009
Rotation (radians)
Method 1 (Link Element w/LTF - Peak at Pile Face)
Method 2 (Link Element with Uniform Traction Force)
Method 3 (Link Element w/LTF - Peak at Idealized Beam Section)
Method 4 (Rigid Body Behavior)

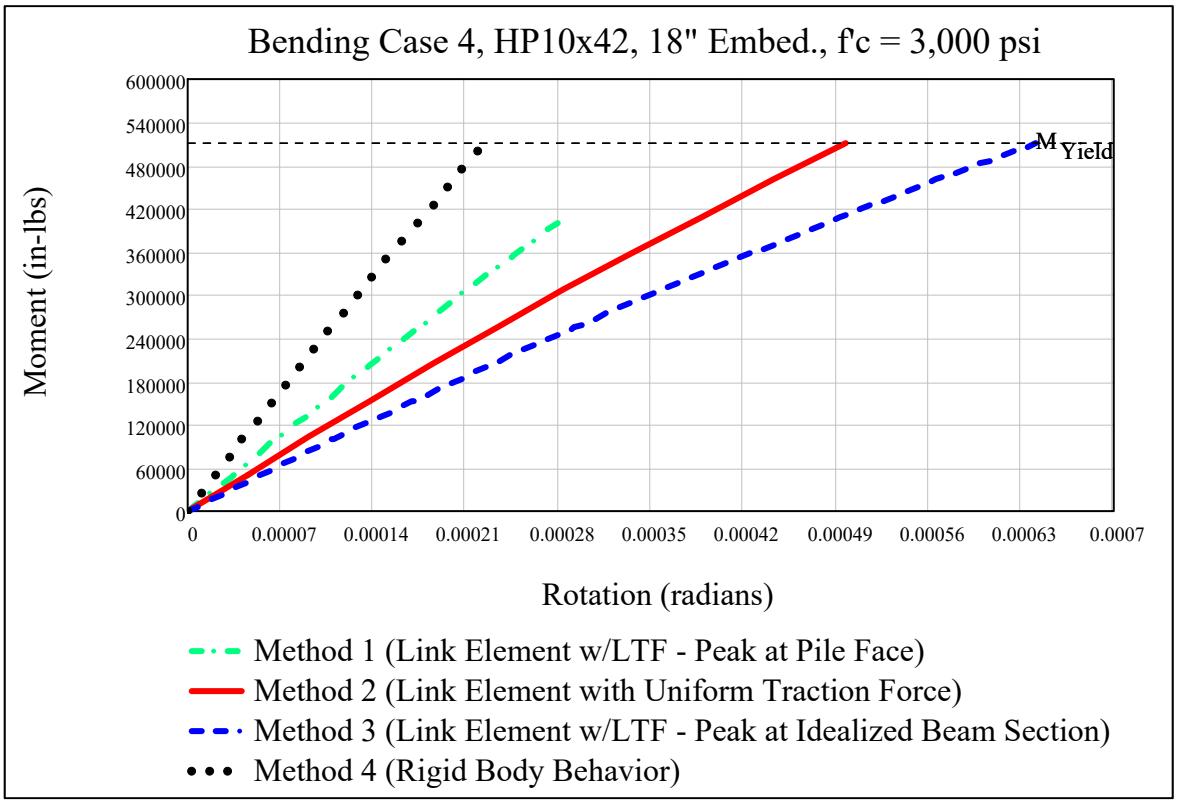
Bending Case 4, HP10x42, 18" Embed., f'c = 3,000 psi
Moment (in-lbs)
600000
540000
480000
420000
360000
300000
240000
180000
120000
60000
0
M Yield
0
0.00007
0.00014
0.00021
0.00028
0.00035
0.00042
0.00049
0.00056
0.00063
0.0007
Rotation (radians)
Method 1 (Link Element w/LTF - Peak at Pile Face)
Method 2 (Link Element with Uniform Traction Force)
Method 3 (Link Element w/LTF - Peak at Idealized Beam Section)
Method 4 (Rigid Body Behavior)

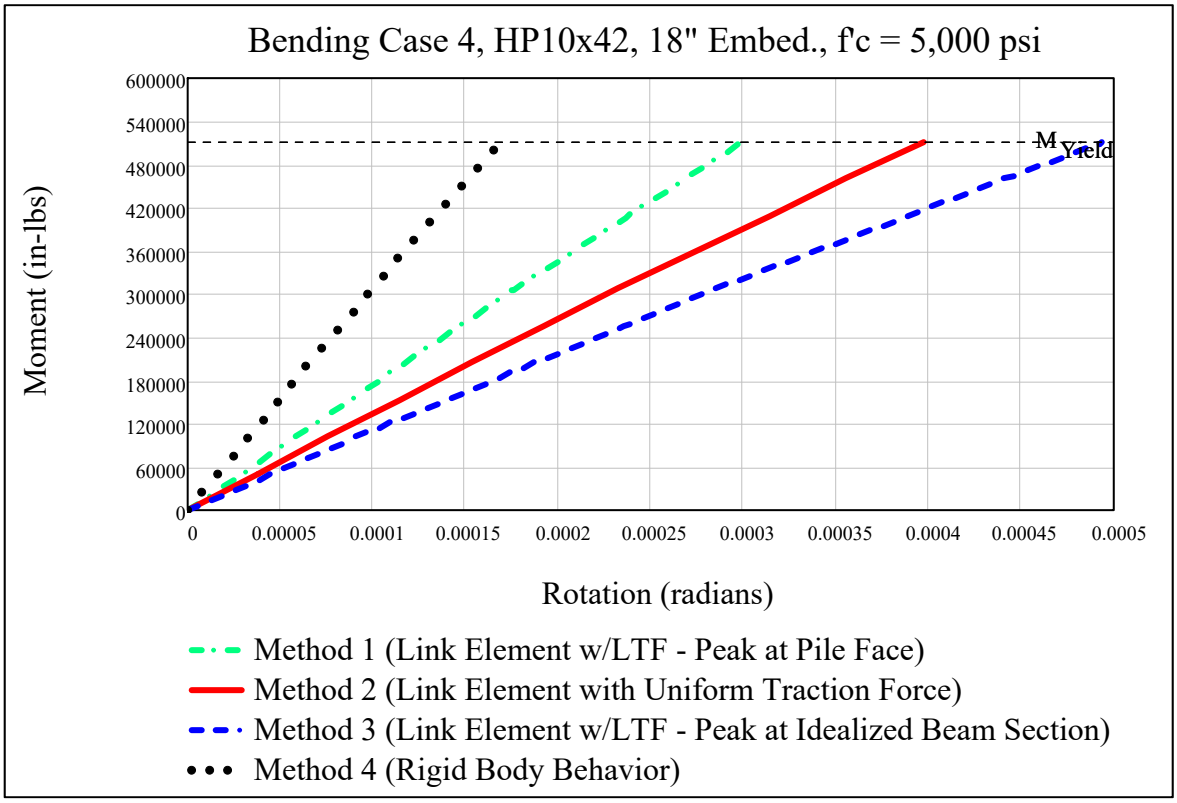
Bending Case 4, HP10x42, 18" Embed., f'c = 5,000 psi
Moment (in-lbs)
600000
540000
480000
420000
360000
300000
240000
180000
120000
60000
0
M Yield
0
0.00005
0.0001
0.00015
0.0002
0.00025
0.0003
0.00035
0.0004
0.00045
0.0005
Rotation (radians)
Method 1 (Link Element w/LTF - Peak at Pile Face)
Method 2 (Link Element with Uniform Traction Force)
Method 3 (Link Element w/LTF - Peak at Idealized Beam Section)
Method 4 (Rigid Body Behavior)

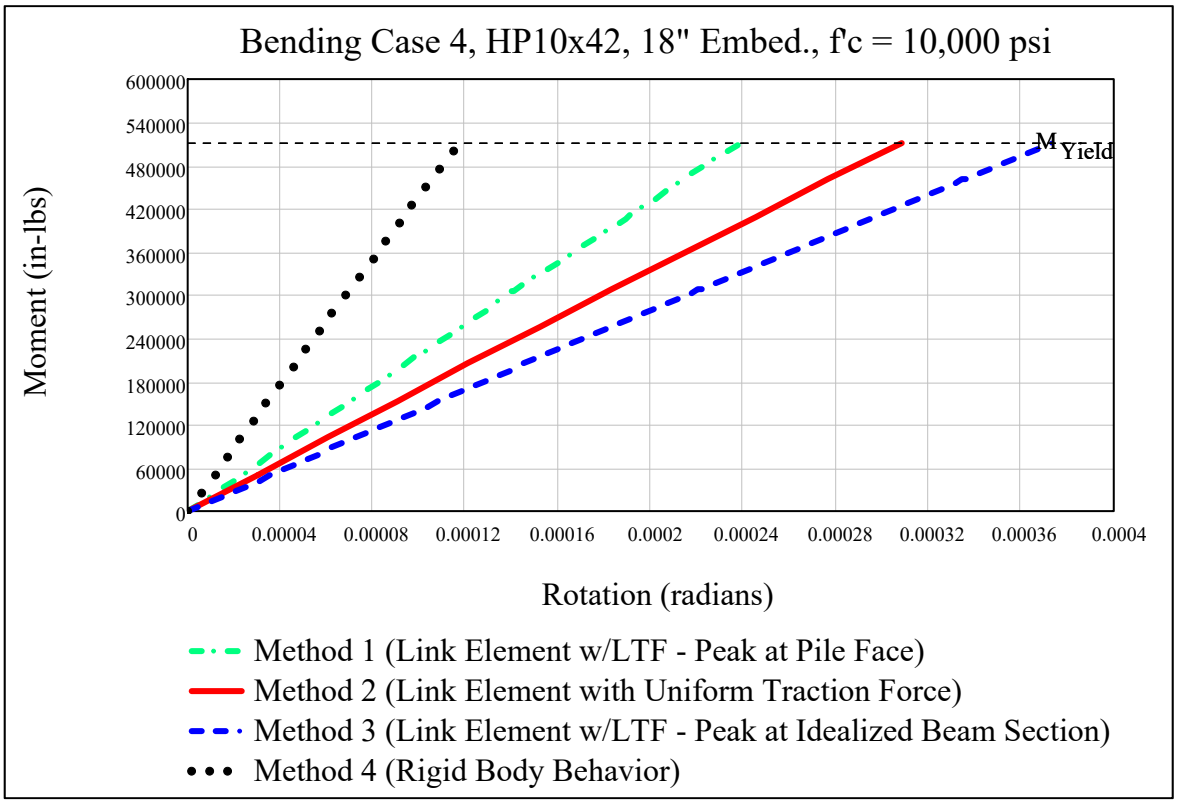
Bending Case 4, HP10x42, 18" Embed., f'c = 10,000 psi
Moment (in-lbs)
600000
540000
480000
420000
360000
300000
240000
180000
120000
60000
0
M Yield
0
0.00004
0.00008
0.00012
0.00016
0.0002
0.00024
0.00028
0.00032
0.00036
0.0004
Rotation (radians)
Method 1 (Link Element w/LTF - Peak at Pile Face)
Method 2 (Link Element with Uniform Traction Force)
Method 3 (Link Element w/LTF - Peak at Idealized Beam Section)
Method 4 (Rigid Body Behavior)

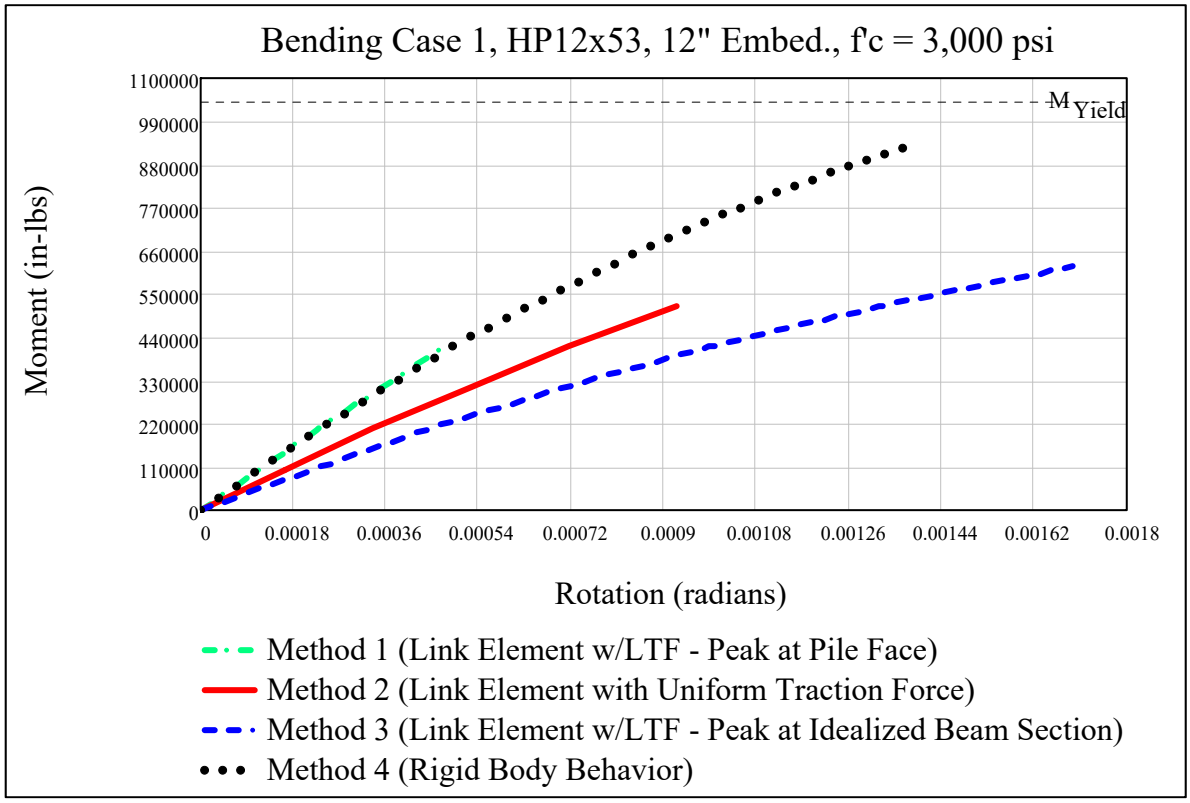
Bending Case 1, HP12x53, 12" Embed., f'c = 3,000 psi
Moment (in-lbs)
1100000
990000
880000
770000
660000
550000
440000
330000
220000
110000
0
M Yield
0
0.00018
0.00036
0.00054
0.00072
0.0009
0.00108
0.00126
0.00144
0.00162
0.0018
Rotation (radians)
Method 1 (Link Element w/LTF - Peak at Pile Face)
Method 2 (Link Element with Uniform Traction Force)
Method 3 (Link Element w/LTF - Peak at Idealized Beam Section)
Method 4 (Rigid Body Behavior)

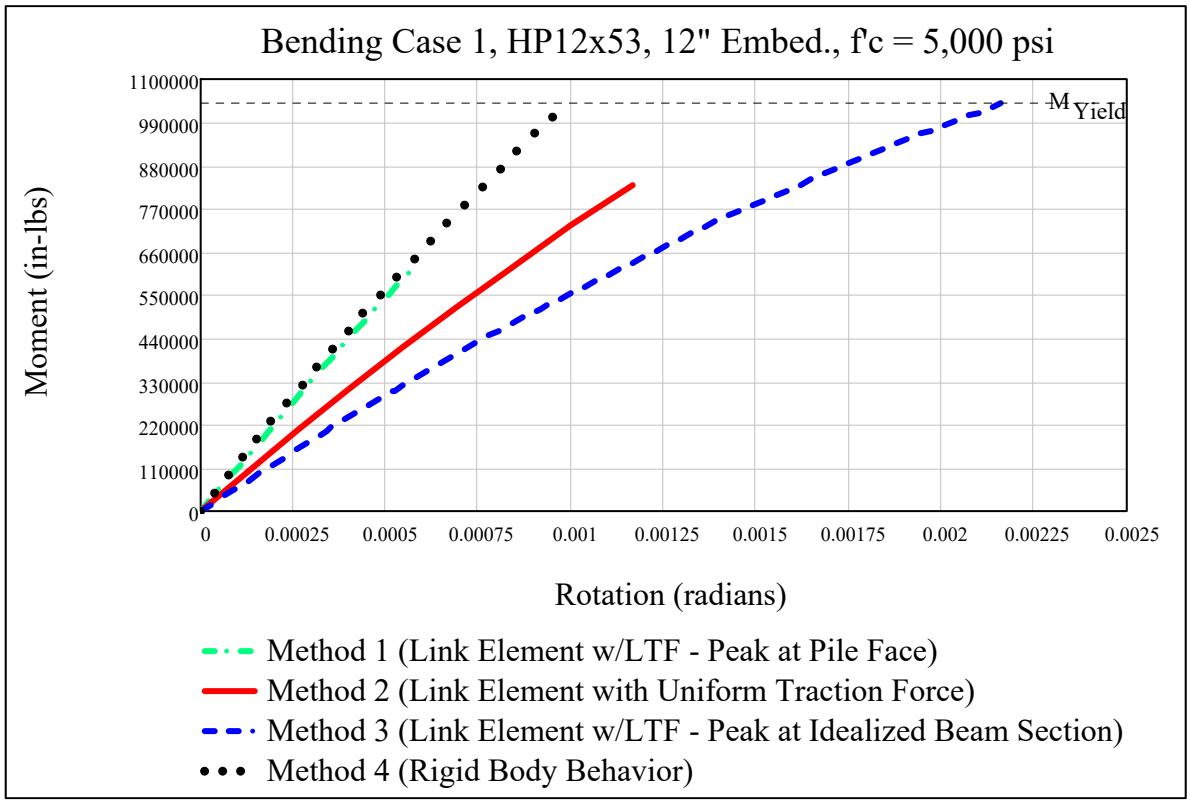
Bending Case 1, HP12x53, 12" Embed., f'c = 5,000 psi
Moment (in-lbs)
1100000
990000
880000
770000
660000
550000
440000
330000
220000
110000
0
M Yield
0
0.00025
0.0005
0.00075
0.001
0.00125
0.0015
0.00175
0.002
0.00225
0.0025
Rotation (radians)
Method 1 (Link Element w/LTF - Peak at Pile Face)
Method 2 (Link Element with Uniform Traction Force)
Method 3 (Link Element w/LTF - Peak at Idealized Beam Section)
Method 4 (Rigid Body Behavior)

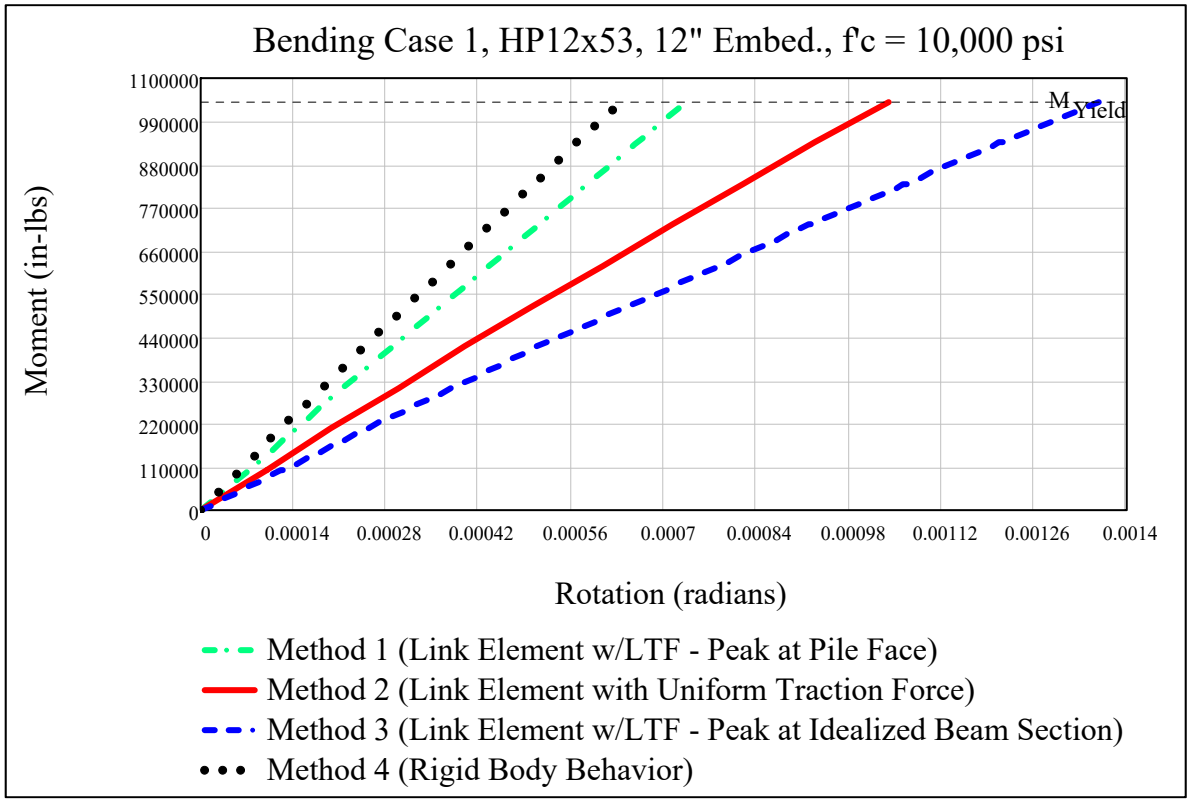
Bending Case 1, HP12x53, 12" Embed., f'c = 10,000 psi
Moment (in-lbs)
1100000
990000
880000
770000
660000
550000
440000
330000
220000
110000
0
M Yield
0
0.00014
0.00028
0.00042
0.00056
0.0007
0.00084
0.00098
0.00112
0.00126
0.0014
Rotation (radians)
Method 1 (Link Element w/LTF - Peak at Pile Face)
Method 2 (Link Element with Uniform Traction Force)
Method 3 (Link Element w/LTF - Peak at Idealized Beam Section)
Method 4 (Rigid Body Behavior)

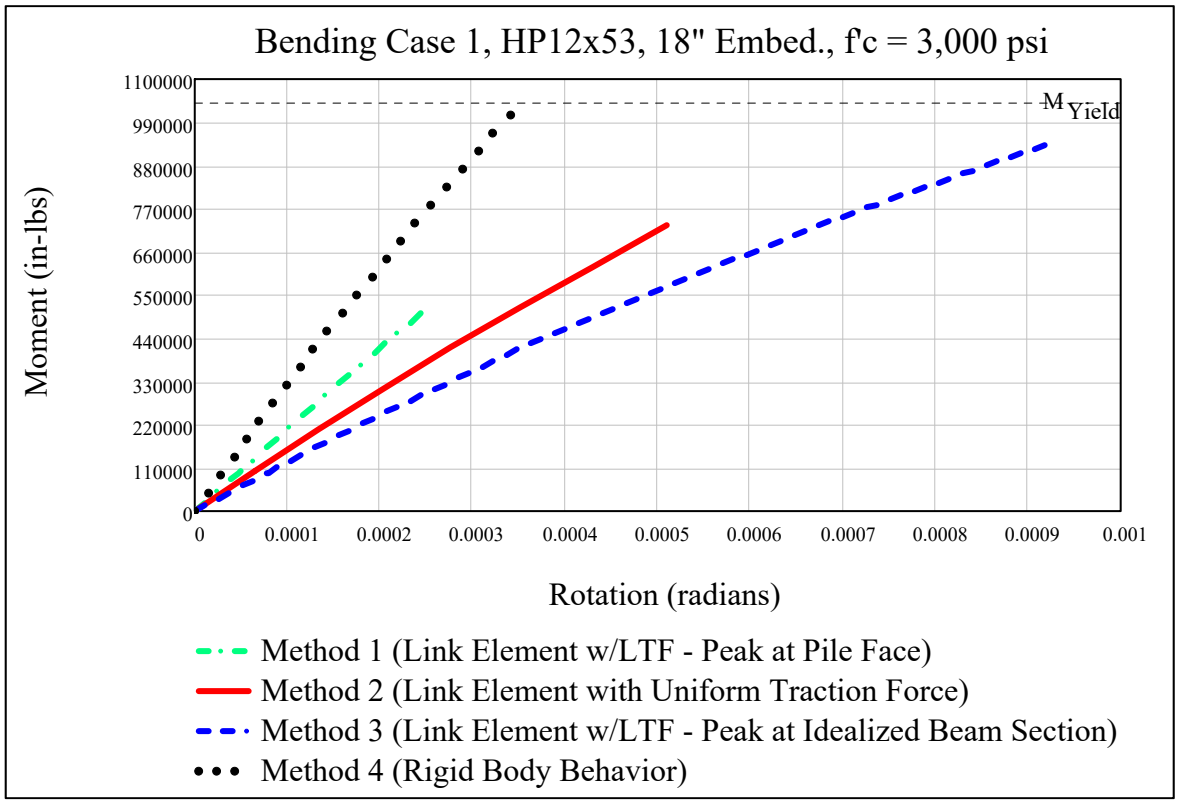
Bending Case 1, HP12x53, 18" Embed., f'c = 3,000 psi
Moment (in-lbs)
1100000
990000
880000
770000
660000
550000
440000
330000
220000
110000
0
M Yield
0
0.0001
0.0002
0.0003
0.0004
0.0005
0.0006
0.0007
0.0008
0.0009
0.001
Rotation (radians)
Method 1 (Link Element w/LTF - Peak at Pile Face)
Method 2 (Link Element with Uniform Traction Force)
Method 3 (Link Element w/LTF - Peak at Idealized Beam Section)
Method 4 (Rigid Body Behavior)

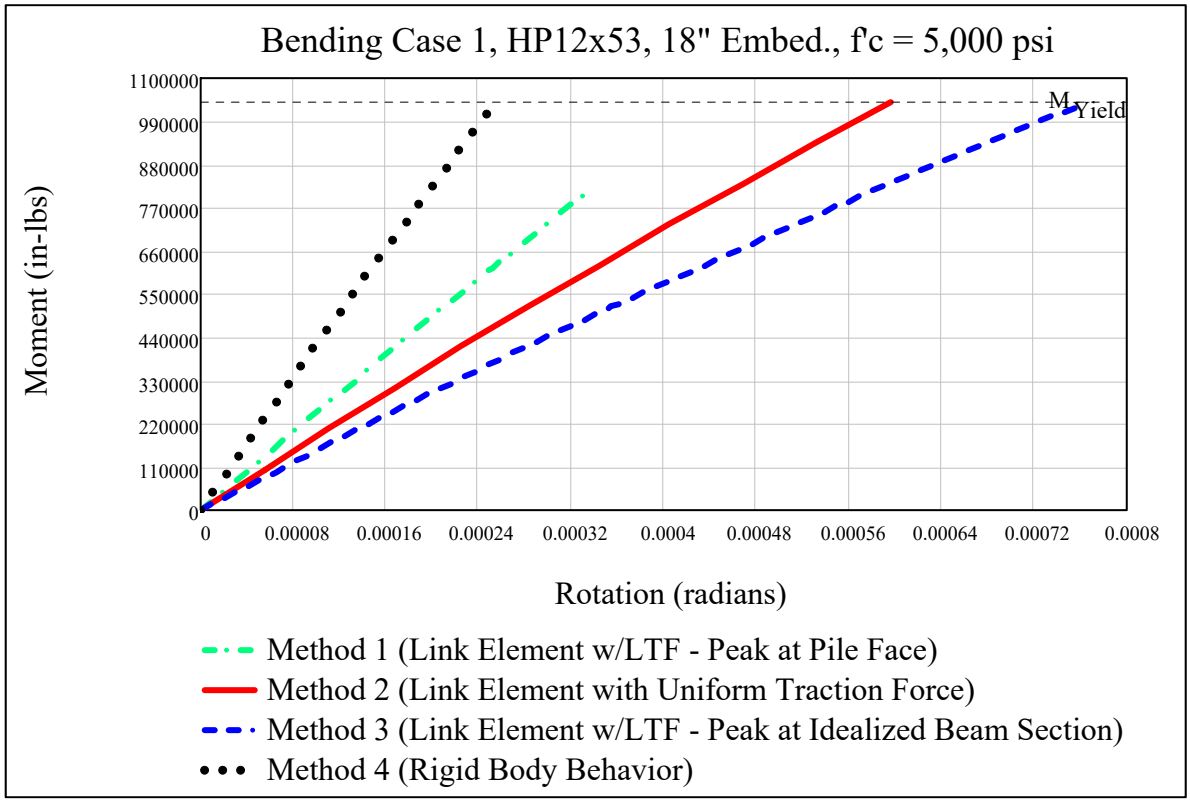
Bending Case 1, HP12x53, 18" Embed., f'c = 5,000 psi
Moment (in-lbs)
1100000
990000
880000
770000
660000
550000
440000
330000
220000
110000
0
M Yield
0
0.00008
0.00016
0.00024
0.00032
0.0004
0.00048
0.00056
0.00064
0.00072
0.0008
Rotation (radians)
Method 1 (Link Element w/LTF - Peak at Pile Face)
Method 2 (Link Element with Uniform Traction Force)
Method 3 (Link Element w/LTF - Peak at Idealized Beam Section)
Method 4 (Rigid Body Behavior)

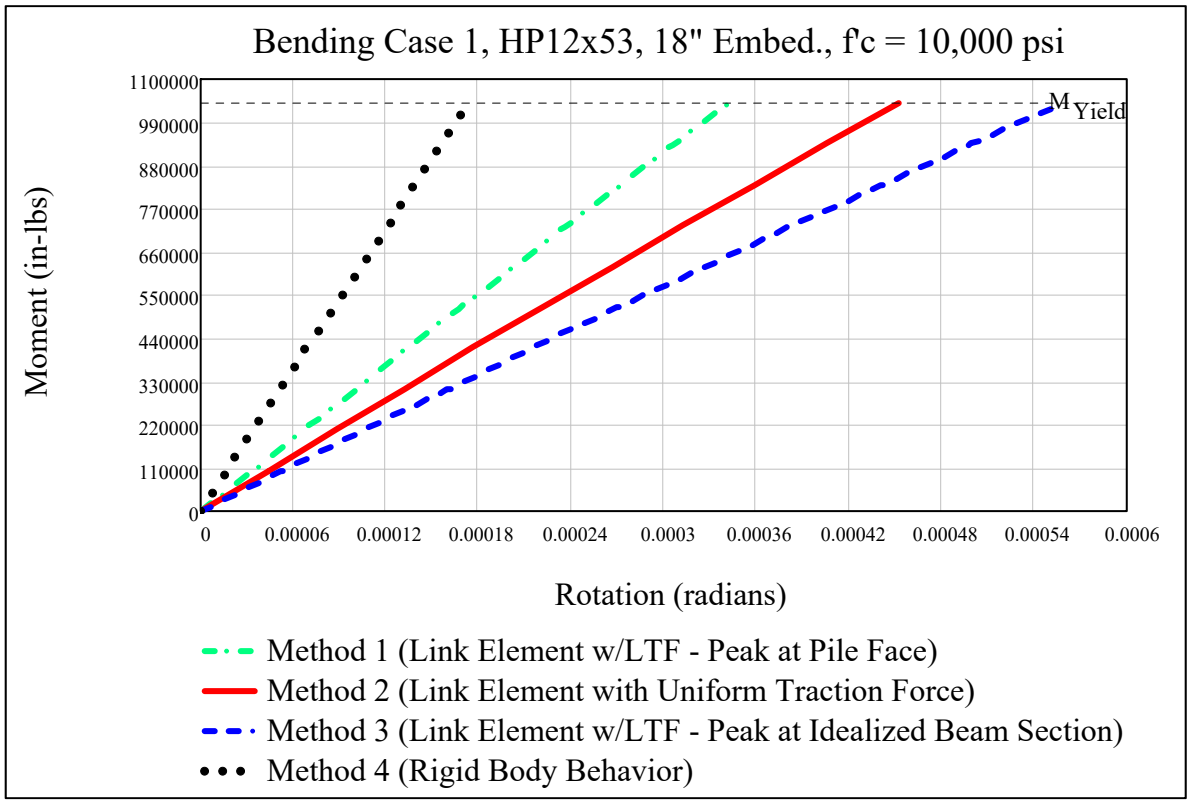
Bending Case 1, HP12x53, 18" Embed., f'c = 10,000 psi
Moment (in-lbs)
1100000
990000
880000
770000
660000
550000
440000
330000
220000
110000
0
M Yield
0
0.00006
0.00012
0.00018
0.00024
0.0003
0.00036
0.00042
0.00048
0.00054
0.0006
Rotation (radians)
Method 1 (Link Element w/LTF - Peak at Pile Face)
Method 2 (Link Element with Uniform Traction Force)
Method 3 (Link Element w/LTF - Peak at Idealized Beam Section)
Method 4 (Rigid Body Behavior)

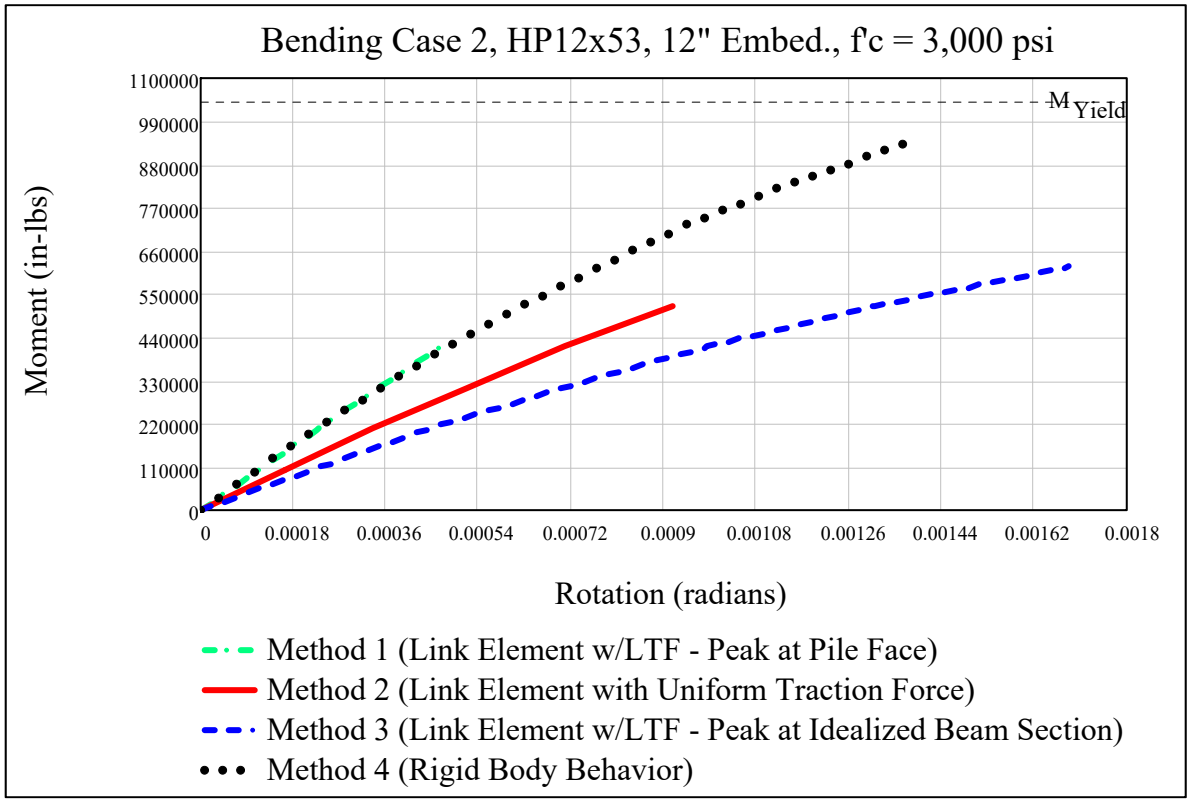
Bending Case 2, HP12x53, 12" Embed., f'c = 3,000 psi
Moment (in-lbs)
1100000
990000
880000
770000
660000
550000
440000
330000
220000
110000
0
M Yield
0
0.00018
0.00036
0.00054
0.00072
0.0009
0.00108
0.00126
0.00144
0.00162
0.0018
Rotation (radians)
Method 1 (Link Element w/LTF - Peak at Pile Face)
Method 2 (Link Element with Uniform Traction Force)
Method 3 (Link Element w/LTF - Peak at Idealized Beam Section)
Method 4 (Rigid Body Behavior)

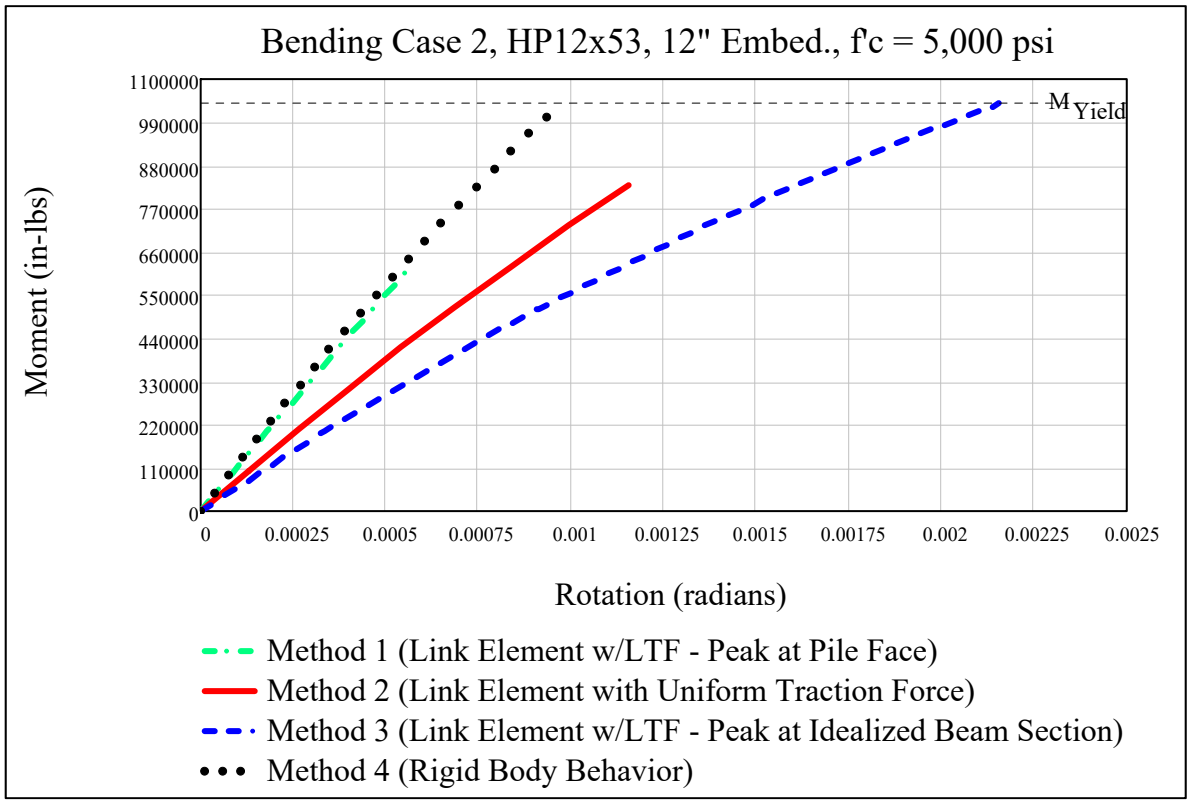
Bending Case 2, HP12x53, 12" Embed., f'c = 5,000 psi
Moment (in-lbs)
1100000
990000
880000
770000
660000
550000
440000
330000
220000
110000
0
M Yield
0
0.00025
0.0005
0.00075
0.001
0.00125
0.0015
0.00175
0.002
0.00225
0.0025
Rotation (radians)
Method 1 (Link Element w/LTF - Peak at Pile Face)
Method 2 (Link Element with Uniform Traction Force)
Method 3 (Link Element w/LTF - Peak at Idealized Beam Section)
Method 4 (Rigid Body Behavior)

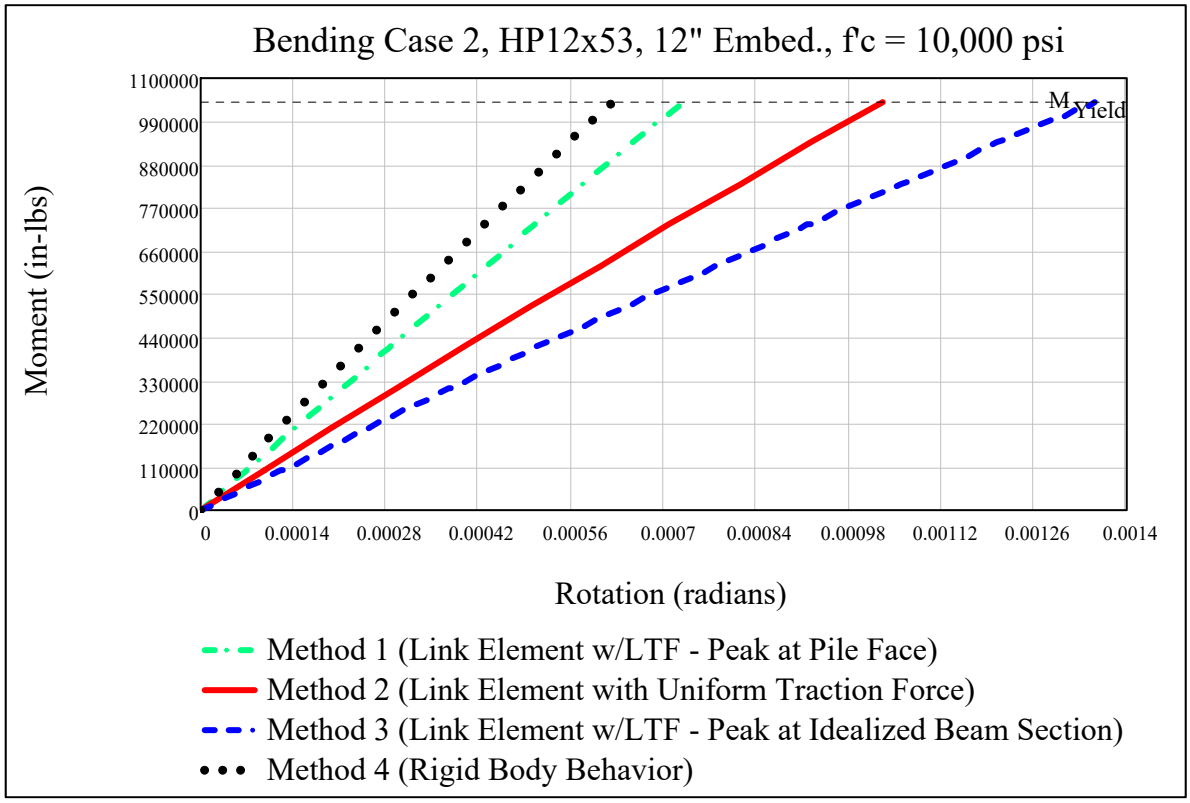
Bending Case 2, HP12x53, 12" Embed., f'c = 10,000 psi
Moment (in-lbs)
1100000
990000
880000
770000
660000
550000
440000
330000
220000
110000
0
M Yield
0
0.00014
0.00028
0.00042
0.00056
0.0007
0.00084
0.00098
0.00112
0.00126
0.0014
Rotation (radians)
Method 1 (Link Element w/LTF - Peak at Pile Face)
Method 2 (Link Element with Uniform Traction Force)
Method 3 (Link Element w/LTF - Peak at Idealized Beam Section)
Method 4 (Rigid Body Behavior)

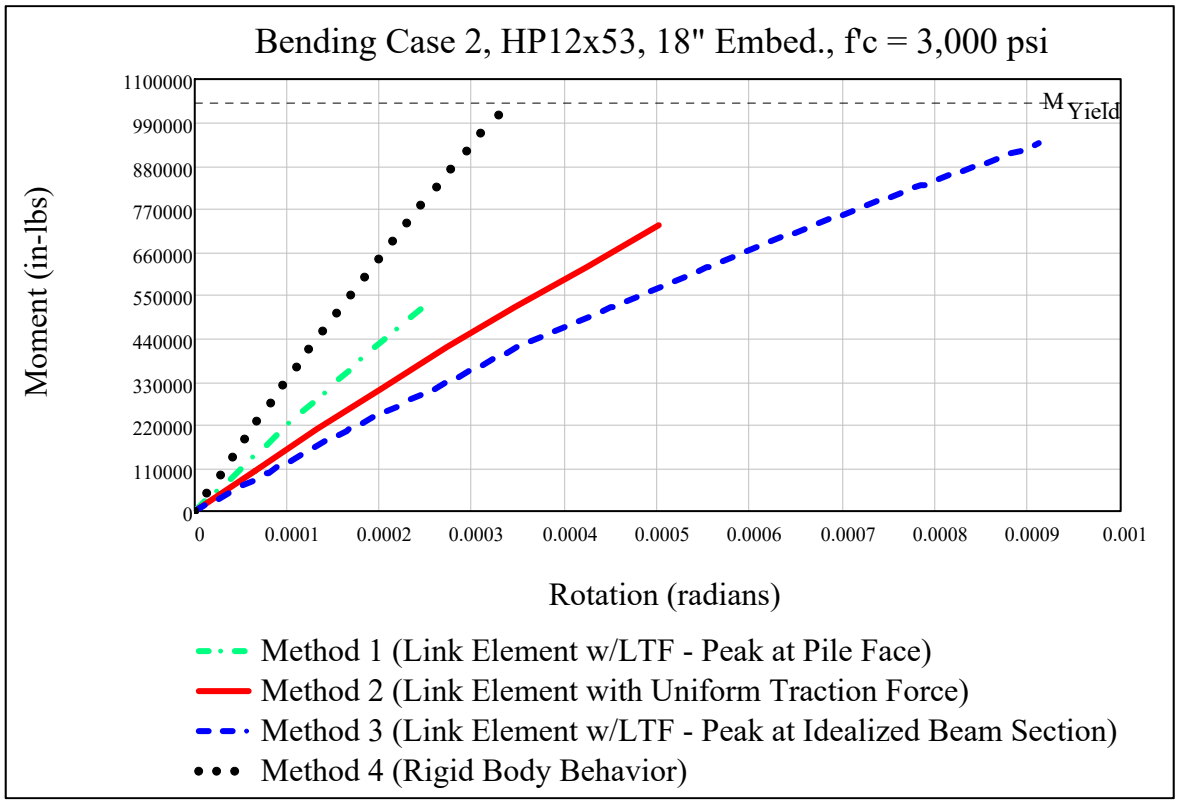
Bending Case 2, HP12x53, 18" Embed., f'c = 3,000 psi
Moment (in-lbs)
1100000
990000
880000
770000
660000
550000
440000
330000
220000
110000
0
M Yield
0
0.0001
0.0002
0.0003
0.0004
0.0005
0.0006
0.0007
0.0008
0.0009
0.001
Rotation (radians)
Method 1 (Link Element w/LTF - Peak at Pile Face)
Method 2 (Link Element with Uniform Traction Force)
Method 3 (Link Element w/LTF - Peak at Idealized Beam Section)
Method 4 (Rigid Body Behavior)

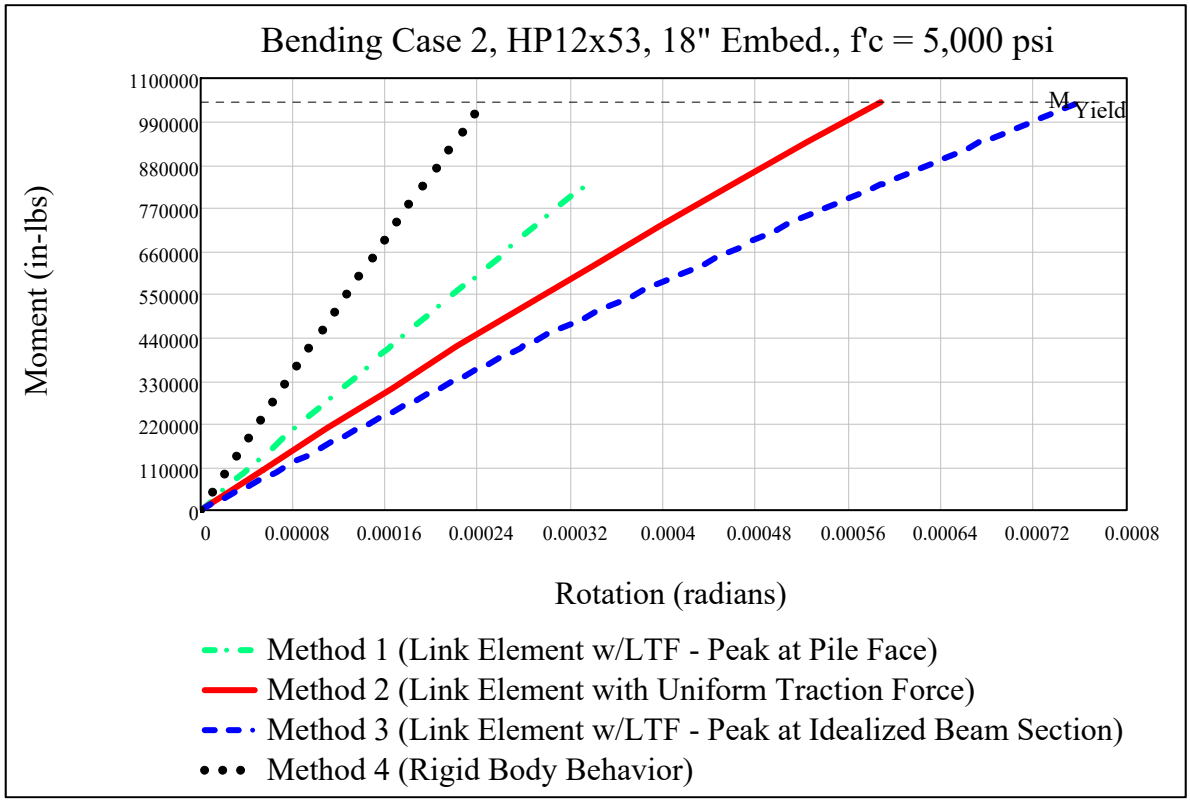
Bending Case 2, HP12x53, 18" Embed., f'c = 5,000 psi
Moment (in-lbs)
1100000
990000
880000
770000
660000
550000
440000
330000
220000
110000
0
M Yield
0
0.00008
0.00016
0.00024
0.00032
0.0004
0.00048
0.00056
0.00064
0.00072
0.0008
Rotation (radians)
Method 1 (Link Element w/LTF - Peak at Pile Face)
Method 2 (Link Element with Uniform Traction Force)
Method 3 (Link Element w/LTF - Peak at Idealized Beam Section)
Method 4 (Rigid Body Behavior)

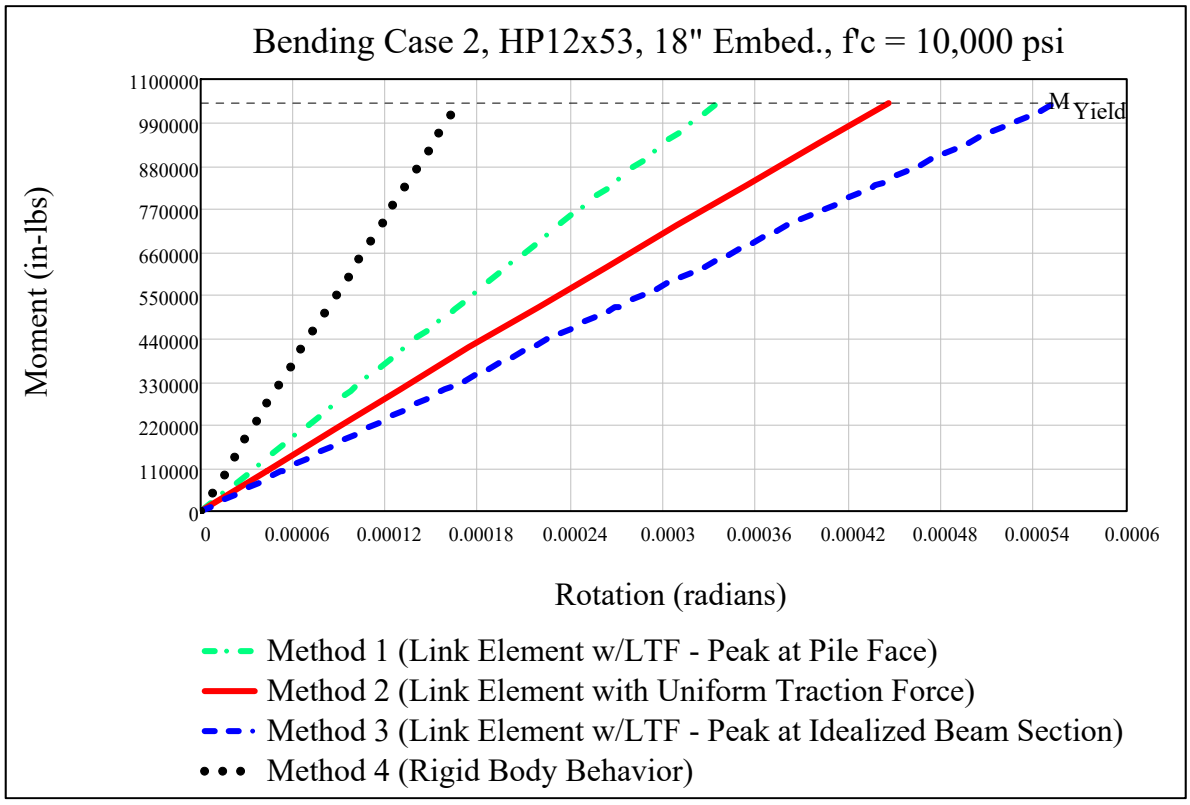
Bending Case 2, HP12x53, 18" Embed., f'c = 10,000 psi
Moment (in-lbs)
1100000
990000
880000
770000
660000
550000
440000
330000
220000
110000
0
M Yield
0
0.00006
0.00012
0.00018
0.00024
0.0003
0.00036
0.00042
0.00048
0.00054
0.0006
Rotation (radians)
Method 1 (Link Element w/LTF - Peak at Pile Face)
Method 2 (Link Element with Uniform Traction Force)
Method 3 (Link Element w/LTF - Peak at Idealized Beam Section)
Method 4 (Rigid Body Behavior)

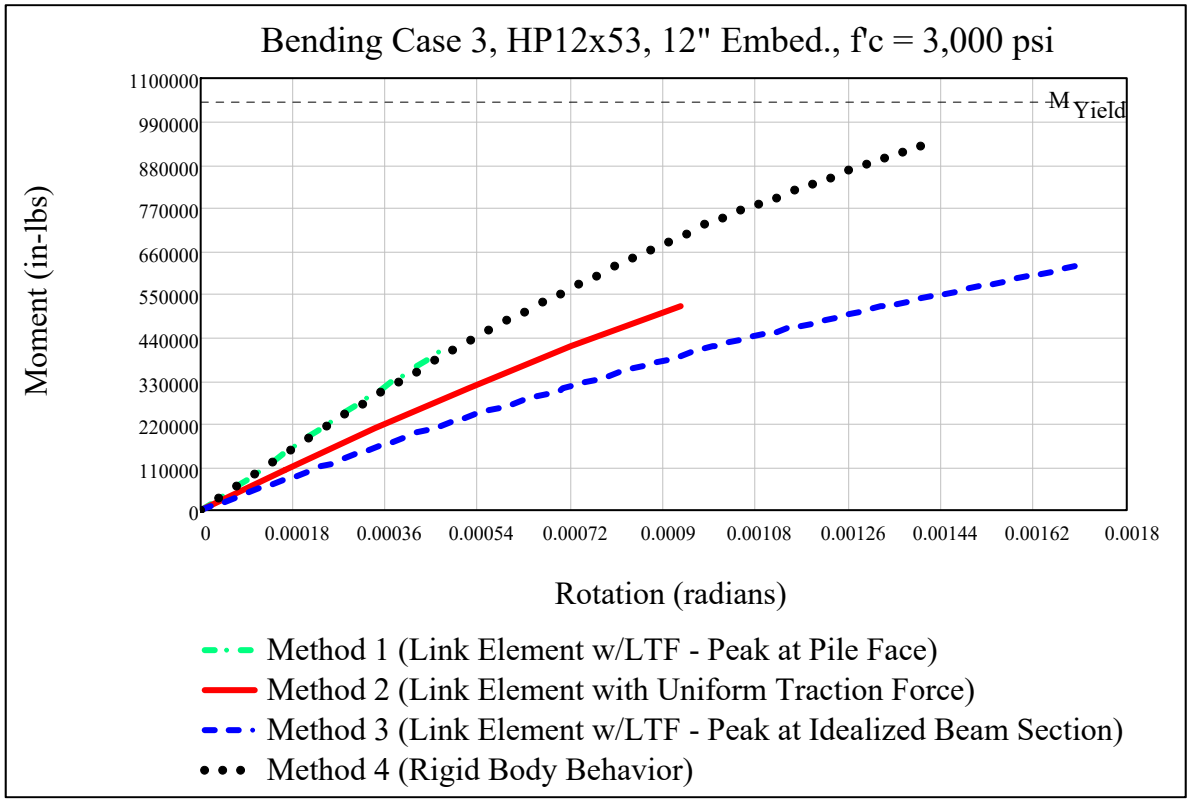
Bending Case 3, HP12x53, 12" Embed., f'c = 3,000 psi
Moment (in-lbs)
1100000
990000
880000
770000
660000
550000
440000
330000
220000
110000
0
M Yield
0
0.00018
0.00036
0.00054
0.00072
0.0009
0.00108
0.00126
0.00144
0.00162
0.0018
Rotation (radians)
Method 1 (Link Element w/LTF - Peak at Pile Face)
Method 2 (Link Element with Uniform Traction Force)
Method 3 (Link Element w/LTF - Peak at Idealized Beam Section)
Method 4 (Rigid Body Behavior)

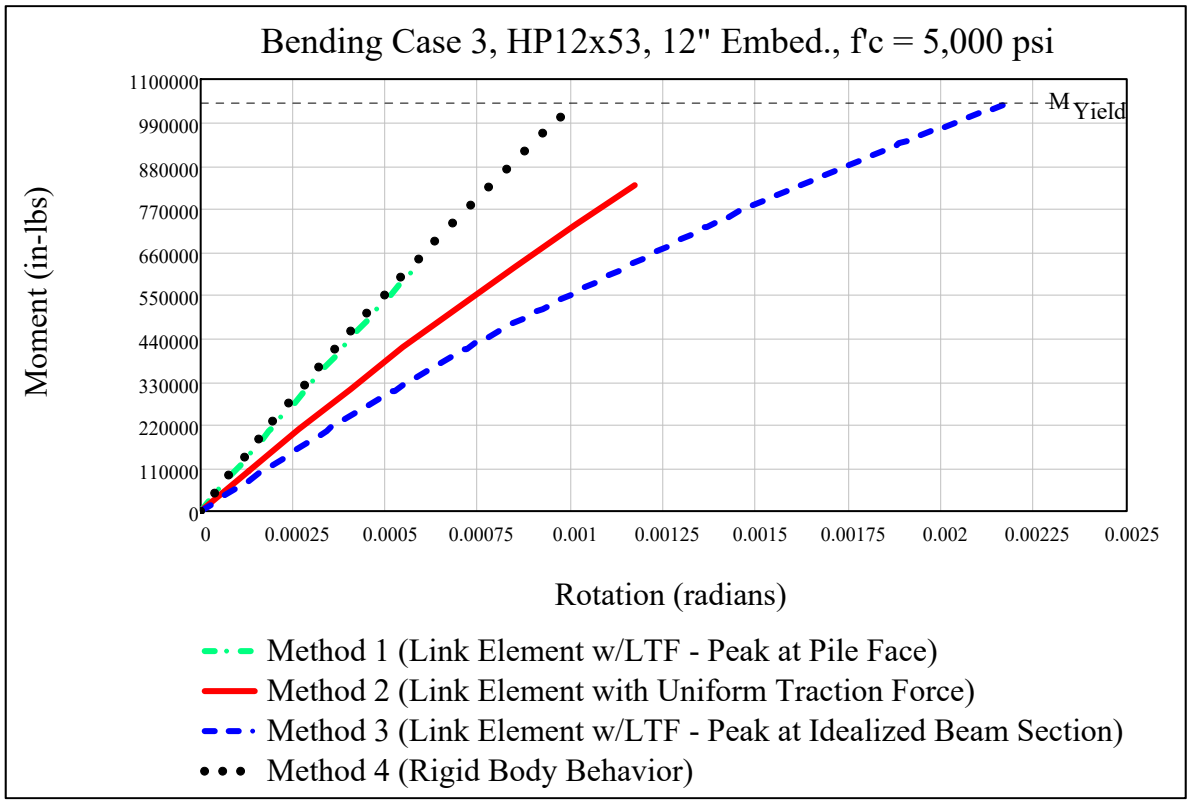
Bending Case 3, HP12x53, 12" Embed., f'c = 5,000 psi
Moment (in-lbs)
1100000
990000
880000
770000
660000
550000
440000
330000
220000
110000
0
M Yield
0
0.00025
0.0005
0.00075
0.001
0.00125
0.0015
0.00175
0.002
0.00225
0.0025
Rotation (radians)
Method 1 (Link Element w/LTF - Peak at Pile Face)
Method 2 (Link Element with Uniform Traction Force)
Method 3 (Link Element w/LTF - Peak at Idealized Beam Section)
Method 4 (Rigid Body Behavior)

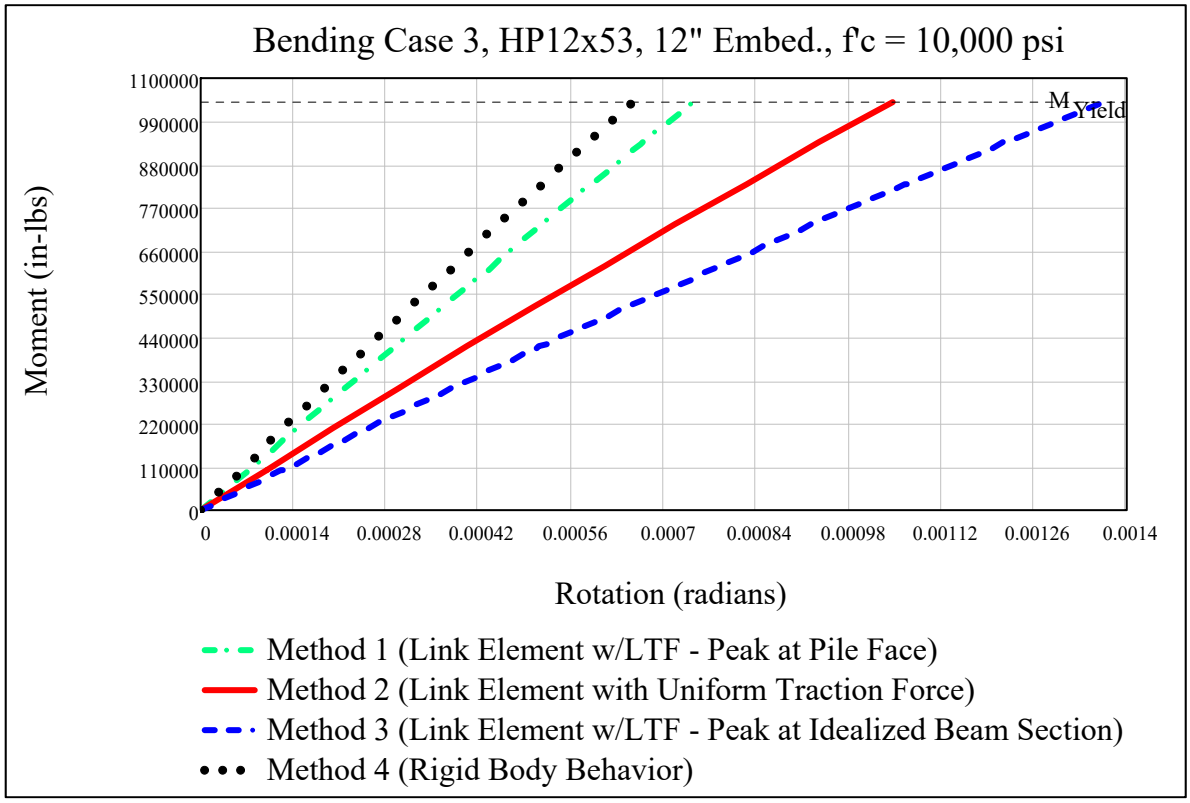
Bending Case 3, HP12x53, 12" Embed., f'c = 10,000 psi
Moment (in-lbs)
1100000
990000
880000
770000
660000
550000
440000
330000
220000
110000
0
M Yield
0
0.00014
0.00028
0.00042
0.00056
0.0007
0.00084
0.00098
0.00112
0.00126
0.0014
Rotation (radians)
Method 1 (Link Element w/LTF - Peak at Pile Face)
Method 2 (Link Element with Uniform Traction Force)
Method 3 (Link Element w/LTF - Peak at Idealized Beam Section)
Method 4 (Rigid Body Behavior)

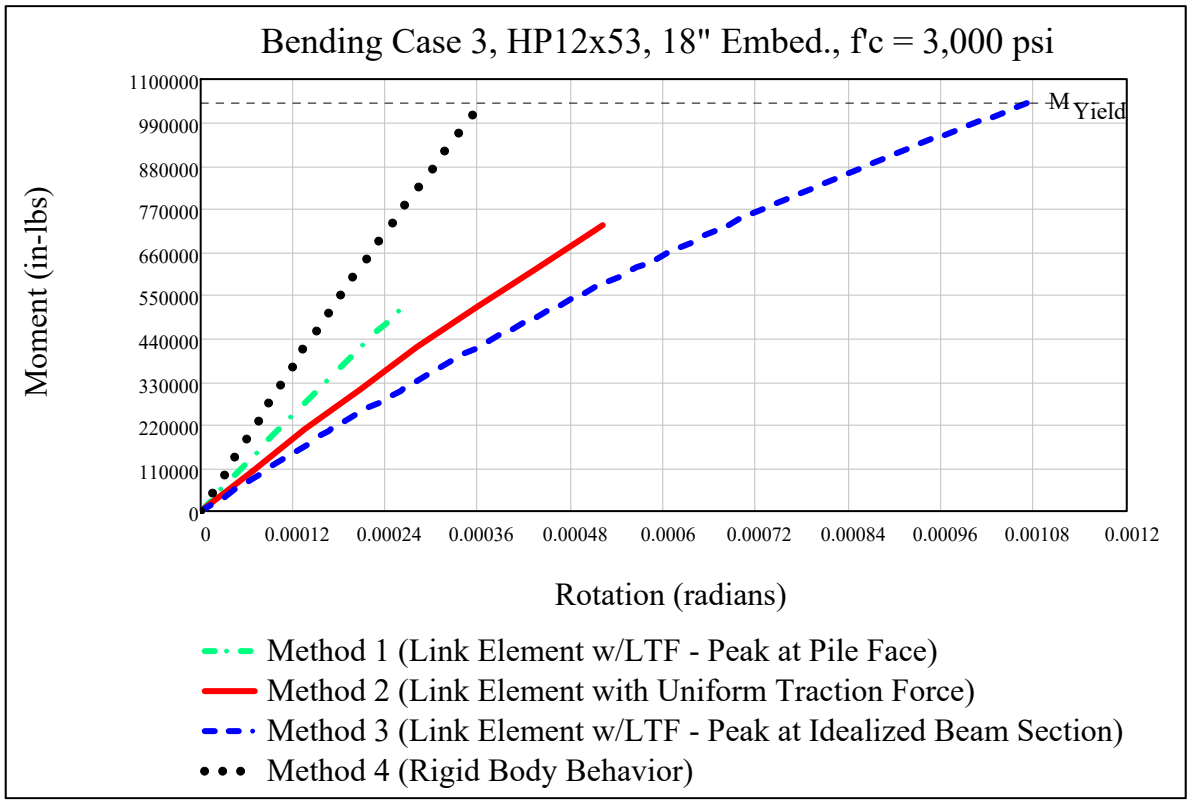
Bending Case 3, HP12x53, 18" Embed., f'c = 3,000 psi
Moment (in-lbs)
1100000
990000
880000
770000
660000
550000
440000
330000
220000
110000
0
M Yield
0
0.00012
0.00024
0.00036
0.00048
0.0006
0.00072
0.00084
0.00096
0.00108
0.0012
Rotation (radians)
Method 1 (Link Element w/LTF - Peak at Pile Face)
Method 2 (Link Element with Uniform Traction Force)
Method 3 (Link Element w/LTF - Peak at Idealized Beam Section)
Method 4 (Rigid Body Behavior)

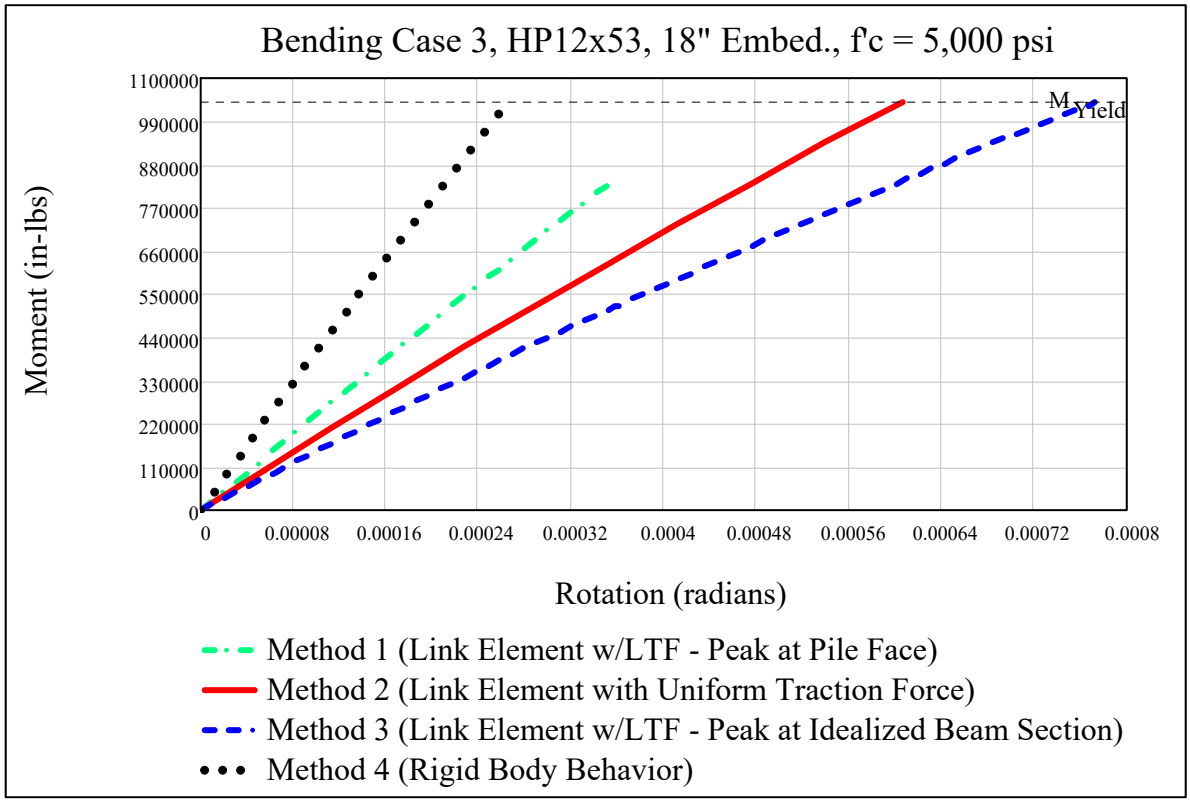
Bending Case 3, HP12x53, 18" Embed., f'c = 5,000 psi
Moment (in-lbs)
1100000
990000
880000
770000
660000
550000
440000
330000
220000
110000
0
M Yield
0
0.00008
0.00016
0.00024
0.00032
0.0004
0.00048
0.00056
0.00064
0.00072
0.0008
Rotation (radians)
Method 1 (Link Element w/LTF - Peak at Pile Face)
Method 2 (Link Element with Uniform Traction Force)
Method 3 (Link Element w/LTF - Peak at Idealized Beam Section)
Method 4 (Rigid Body Behavior)

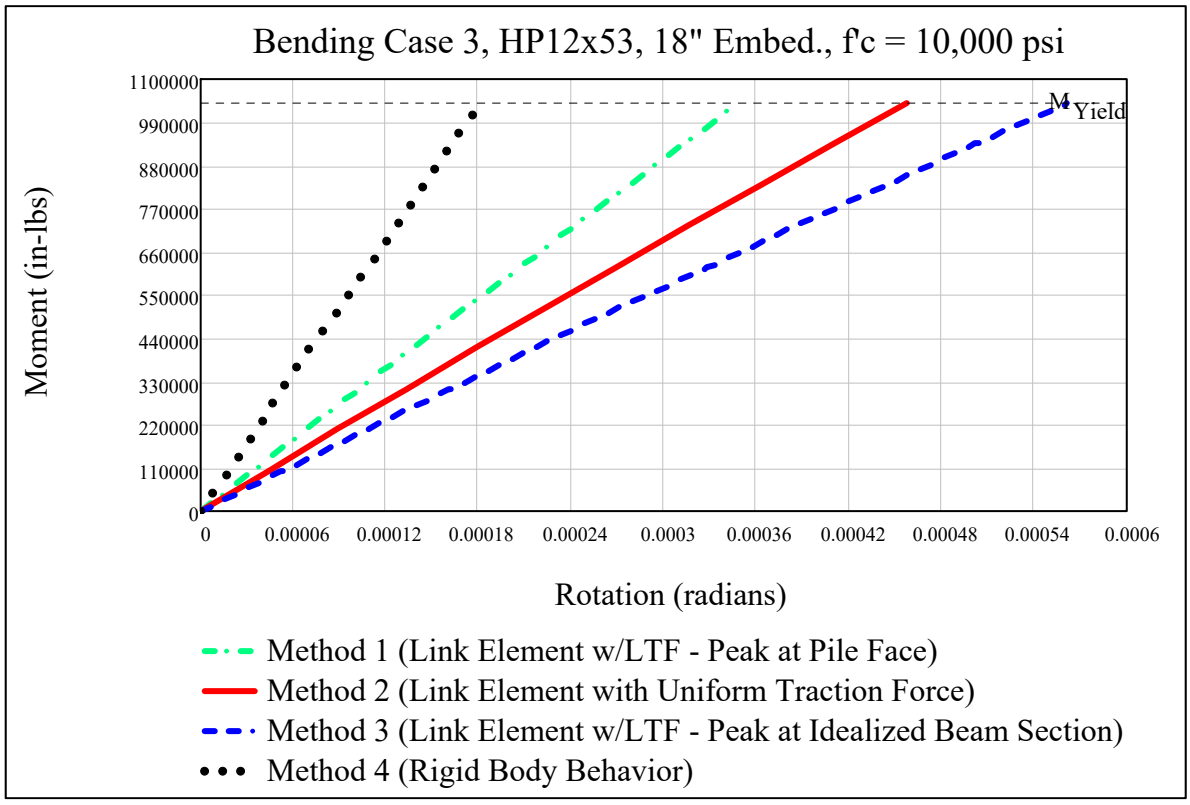
Bending Case 3, HP12x53, 18" Embed., f'c = 10,000 psi
Moment (in-lbs)
1100000
990000
880000
770000
660000
550000
440000
330000
220000
110000
0
M Yield
0
0.00006
0.00012
0.00018
0.00024
0.0003
0.00036
0.00042
0.00048
0.00054
0.0006
Rotation (radians)
Method 1 (Link Element w/LTF - Peak at Pile Face)
Method 2 (Link Element with Uniform Traction Force)
Method 3 (Link Element w/LTF - Peak at Idealized Beam Section)
Method 4 (Rigid Body Behavior)

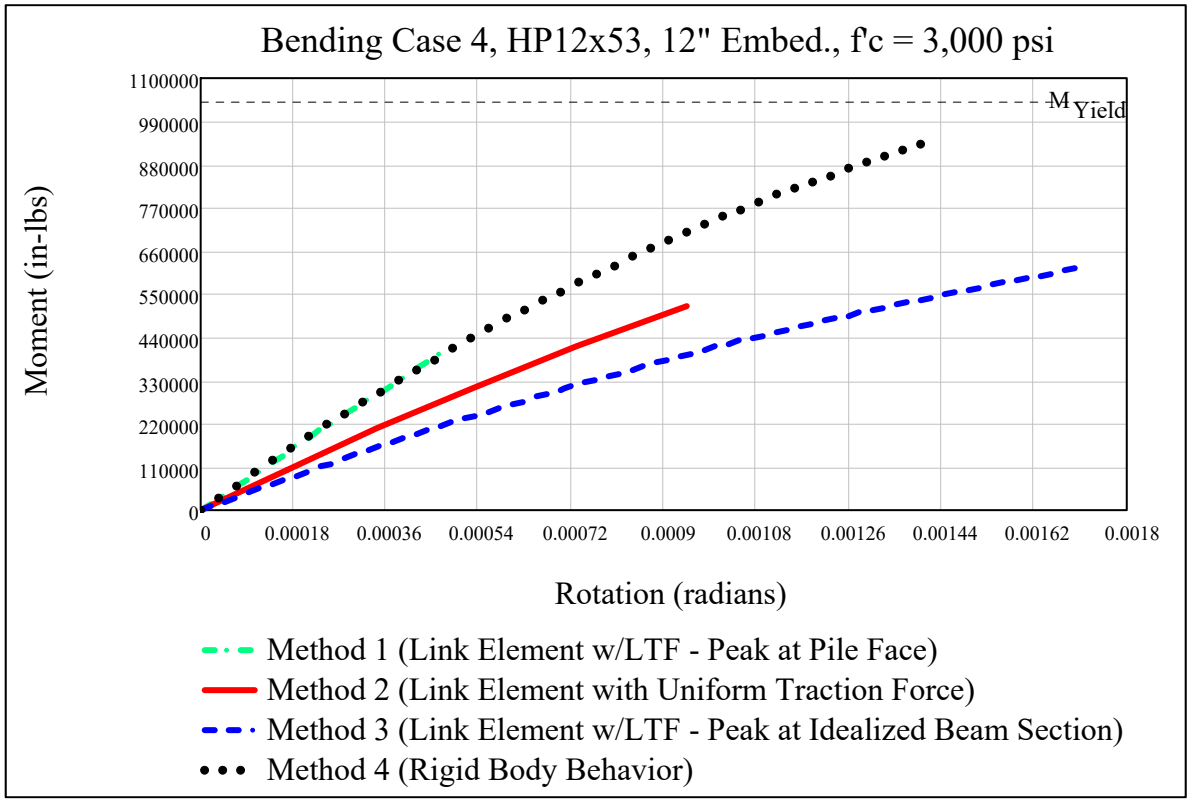
Bending Case 4, HP12x53, 12" Embed., f'c = 3,000 psi
Moment (in-lbs)
1100000
990000
880000
770000
660000
550000
440000
330000
220000
110000
0
M Yield
0
0.00018
0.00036
0.00054
0.00072
0.0009
0.00108
0.00126
0.00144
0.00162
0.0018
Rotation (radians)
Method 1 (Link Element w/LTF - Peak at Pile Face)
Method 2 (Link Element with Uniform Traction Force)
Method 3 (Link Element w/LTF - Peak at Idealized Beam Section)
Method 4 (Rigid Body Behavior)

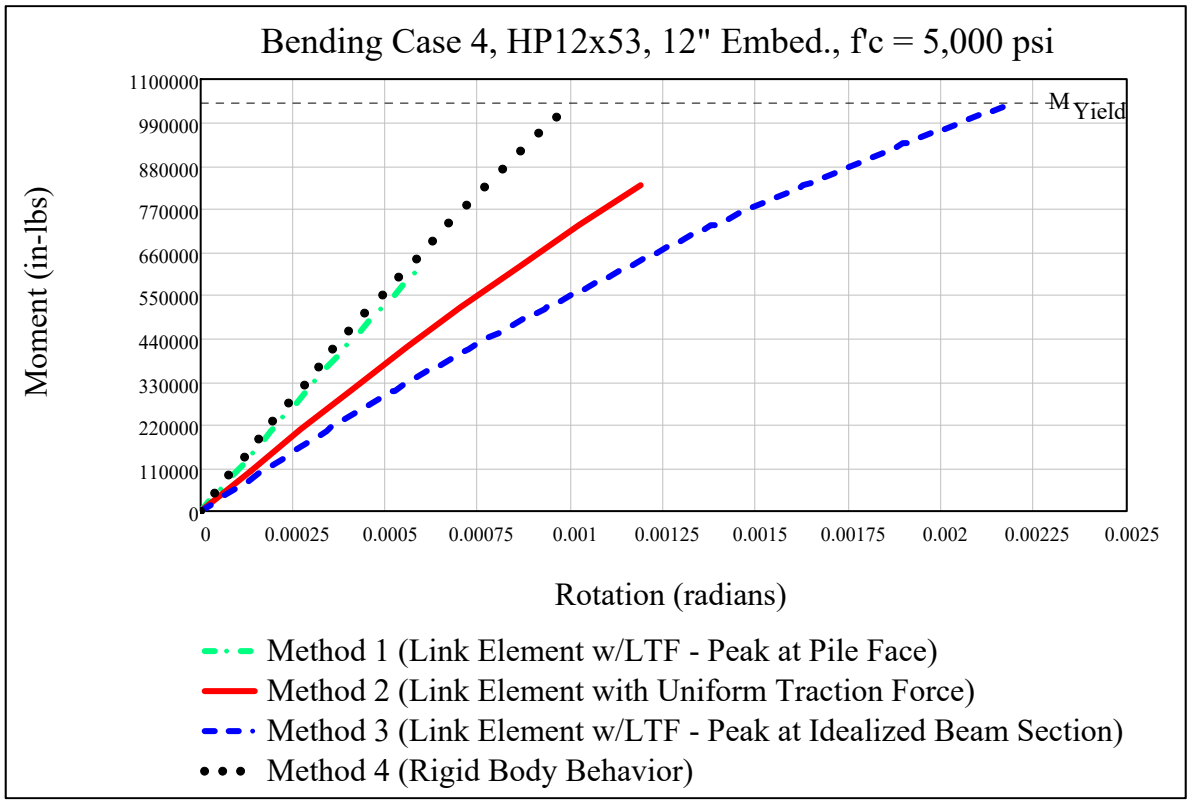
Bending Case 4, HP12x53, 12" Embed., f'c = 5,000 psi
Moment (in-lbs)
1100000
990000
880000
770000
660000
550000
440000
330000
220000
110000
0
M Yield
0
0.00025
0.0005
0.00075
0.001
0.00125
0.0015
0.00175
0.002
0.00225
0.0025
Rotation (radians)
Method 1 (Link Element w/LTF - Peak at Pile Face)
Method 2 (Link Element with Uniform Traction Force)
Method 3 (Link Element w/LTF - Peak at Idealized Beam Section)
Method 4 (Rigid Body Behavior)

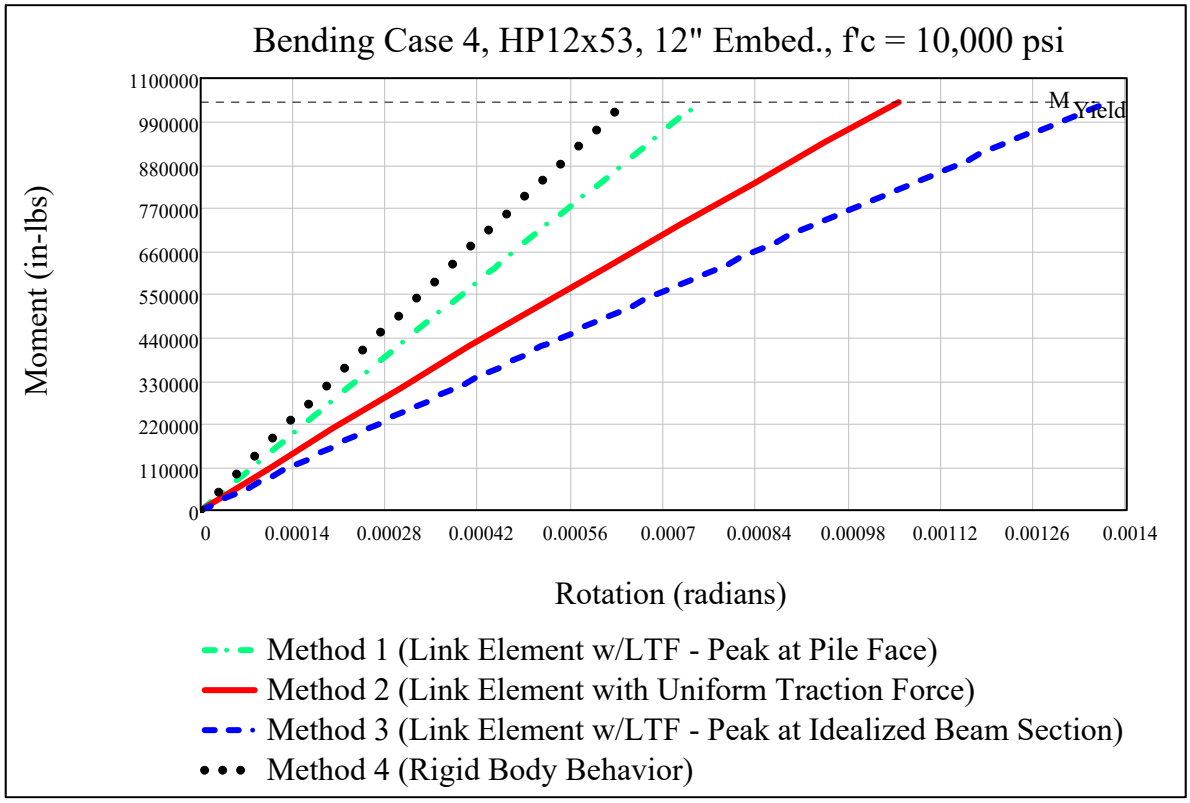
Bending Case 4, HP12x53, 12" Embed., f'c = 10,000 psi
Moment (in-lbs)
1100000
990000
880000
770000
660000
550000
440000
330000
220000
110000
0
M Yield
0
0.00014
0.00028
0.00042
0.00056
0.0007
0.00084
0.00098
0.00112
0.00126
0.0014
Rotation (radians)
Method 1 (Link Element w/LTF - Peak at Pile Face)
Method 2 (Link Element with Uniform Traction Force)
Method 3 (Link Element w/LTF - Peak at Idealized Beam Section)
Method 4 (Rigid Body Behavior)

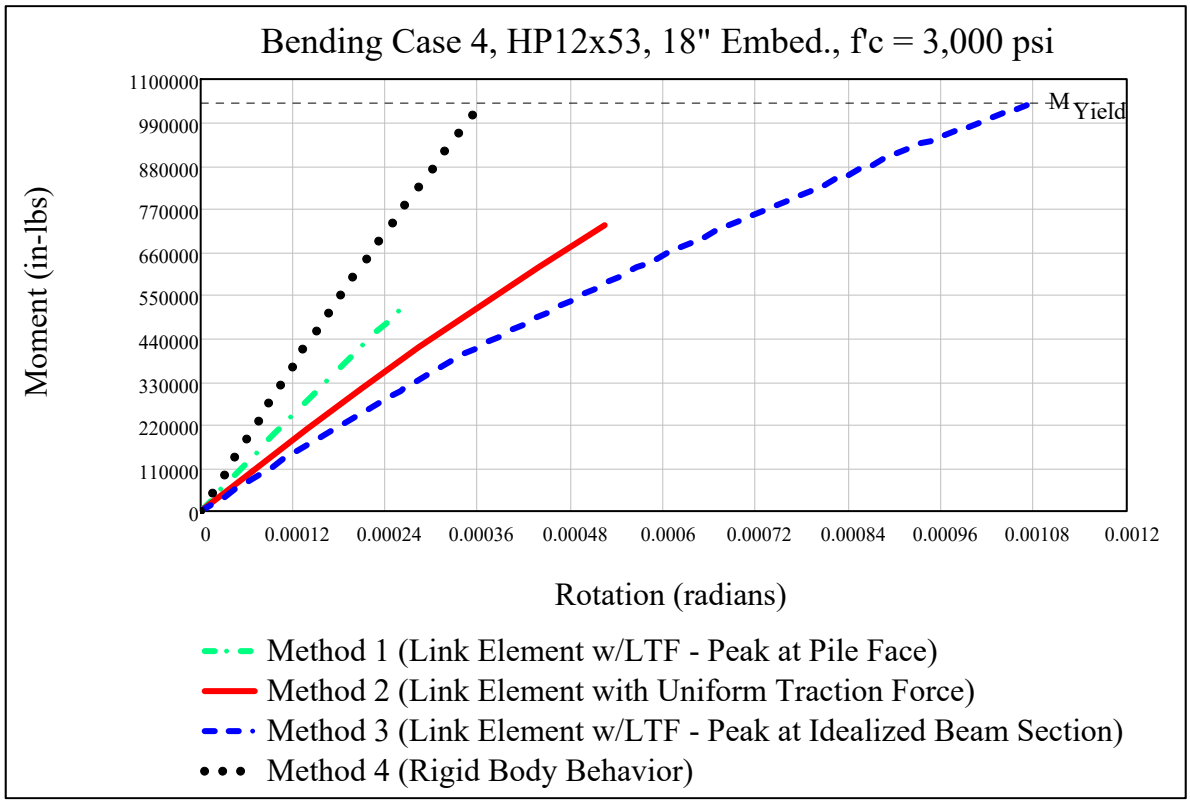
Bending Case 4, HP12x53, 18" Embed., f'c = 3,000 psi
Moment (in-lbs)
1100000
990000
880000
770000
660000
550000
440000
330000
220000
110000
0
M Yield
0
0.00012
0.00024
0.00036
0.00048
0.0006
0.00072
0.00084
0.00096
0.00108
0.0012
Rotation (radians)
Method 1 (Link Element w/LTF - Peak at Pile Face)
Method 2 (Link Element with Uniform Traction Force)
Method 3 (Link Element w/LTF - Peak at Idealized Beam Section)
Method 4 (Rigid Body Behavior)

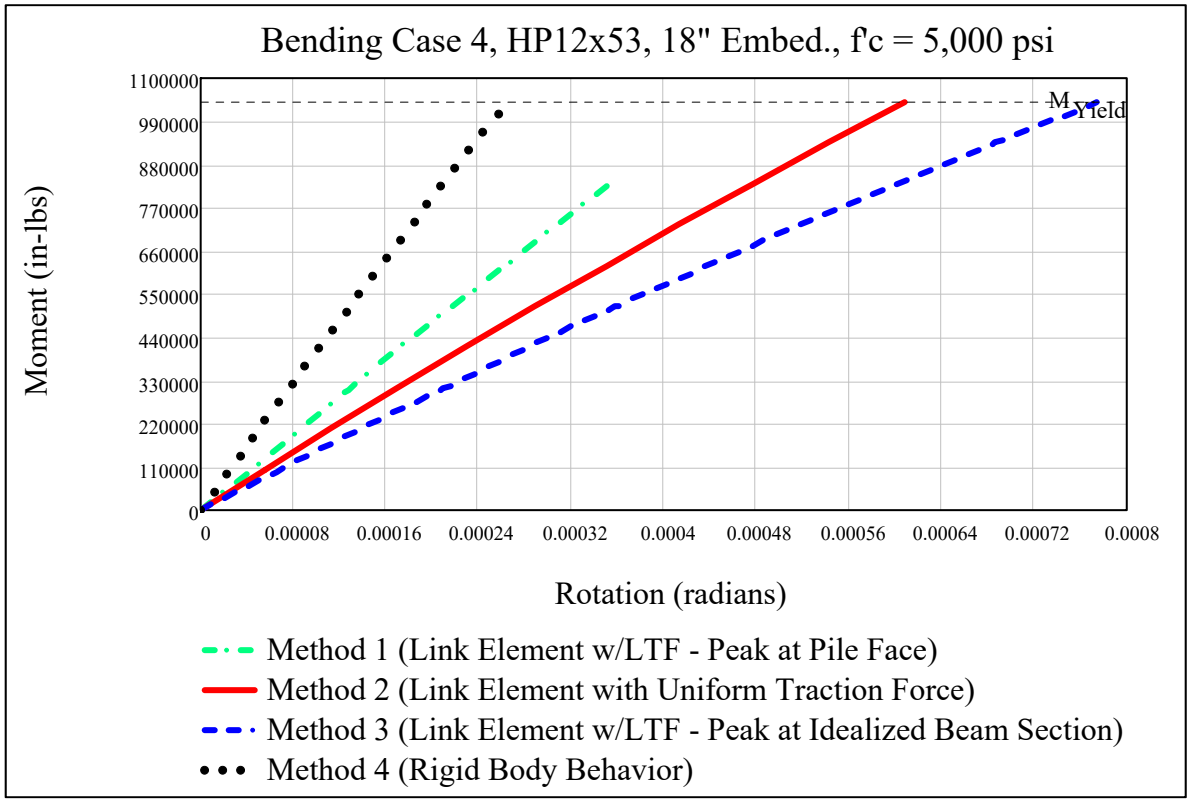
Bending Case 4, HP12x53, 18" Embed., f'c = 5,000 psi
Moment (in-lbs)
1100000
990000
880000
770000
660000
550000
440000
330000
220000
110000
0
M Yield
0
0.00008
0.00016
0.00024
0.00032
0.0004
0.00048
0.00056
0.00064
0.00072
0.0008
Rotation (radians)
Method 1 (Link Element w/LTF - Peak at Pile Face)
Method 2 (Link Element with Uniform Traction Force)
Method 3 (Link Element w/LTF - Peak at Idealized Beam Section)
Method 4 (Rigid Body Behavior)

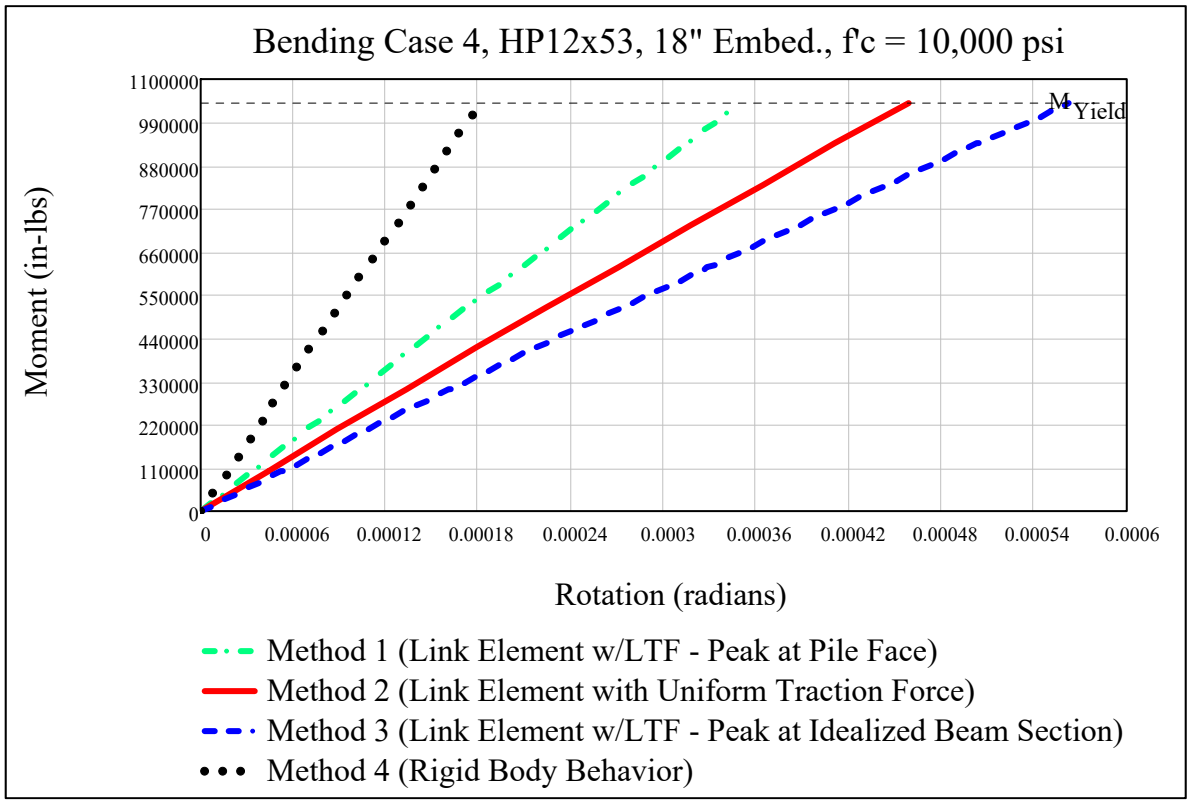
Bending Case 4, HP12x53, 18" Embed., f'c = 10,000 psi
Moment (in-lbs)
1100000
990000
880000
770000
660000
550000
440000
330000
220000
110000
0
M Yield
0
0.00006
0.00012
0.00018
0.00024
0.0003
0.00036
0.00042
0.00048
0.00054
0.0006
Rotation (radians)
Method 1 (Link Element w/LTF - Peak at Pile Face)
Method 2 (Link Element with Uniform Traction Force)
Method 3 (Link Element w/LTF - Peak at Idealized Beam Section)
Method 4 (Rigid Body Behavior)

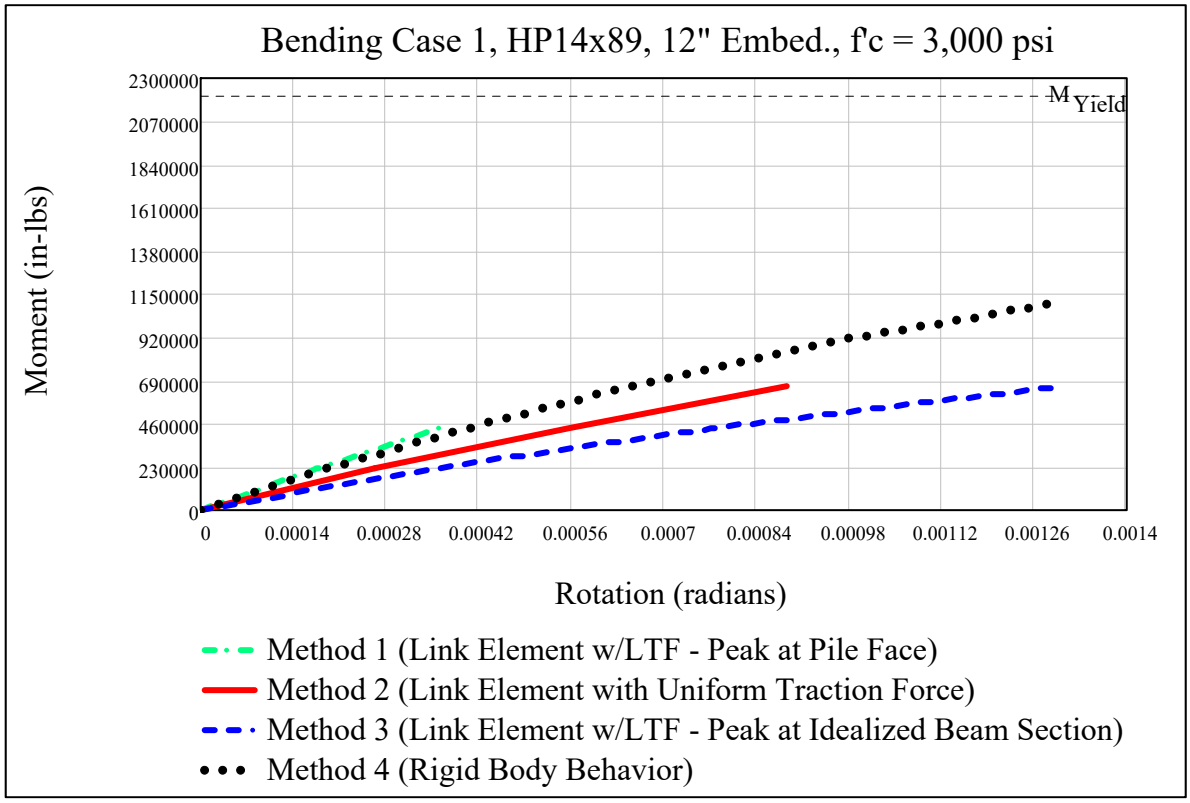
Bending Case 1, HP14x89, 12" Embed., f'c = 3,000 psi
Moment (in-lbs)
2300000
2070000
1840000
1610000
1380000
1150000
920000
690000
460000
230000
0
M Yield
0
0.00014
0.00028
0.00042
0.00056
0.0007
0.00084
0.00098
0.00112
0.00126
0.0014
Rotation (radians)
Method 1 (Link Element w/LTF - Peak at Pile Face)
Method 2 (Link Element with Uniform Traction Force)
Method 3 (Link Element w/LTF - Peak at Idealized Beam Section)
Method 4 (Rigid Body Behavior)

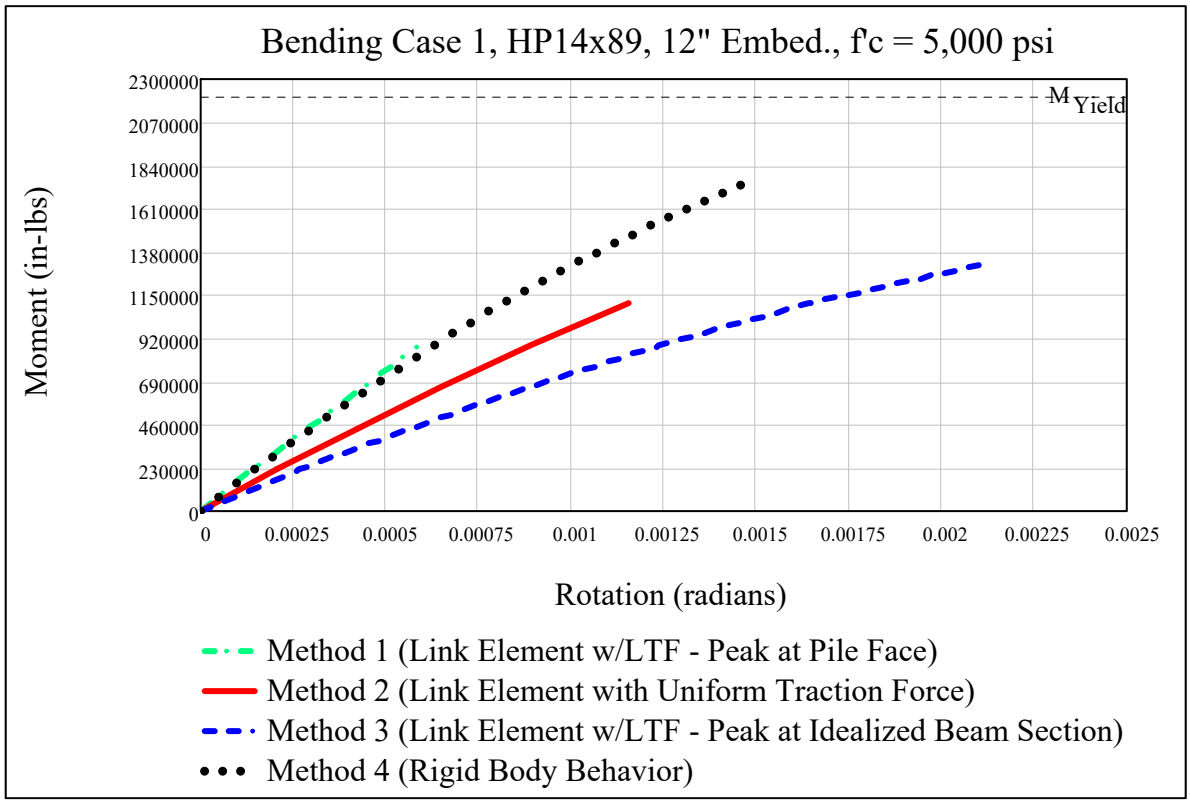
Bending Case 1, HP14x89, 12" Embed., f'c = 5,000 psi
Moment (in-lbs)
2300000
2070000
1840000
1610000
1380000
1150000
920000
690000
460000
230000
0
M Yield
0
0.00025
0.0005
0.00075
0.001
0.00125
0.0015
0.00175
0.002
0.00225
0.0025
Rotation (radians)
Method 1 (Link Element w/LTF - Peak at Pile Face)
Method 2 (Link Element with Uniform Traction Force)
Method 3 (Link Element w/LTF - Peak at Idealized Beam Section)
Method 4 (Rigid Body Behavior)

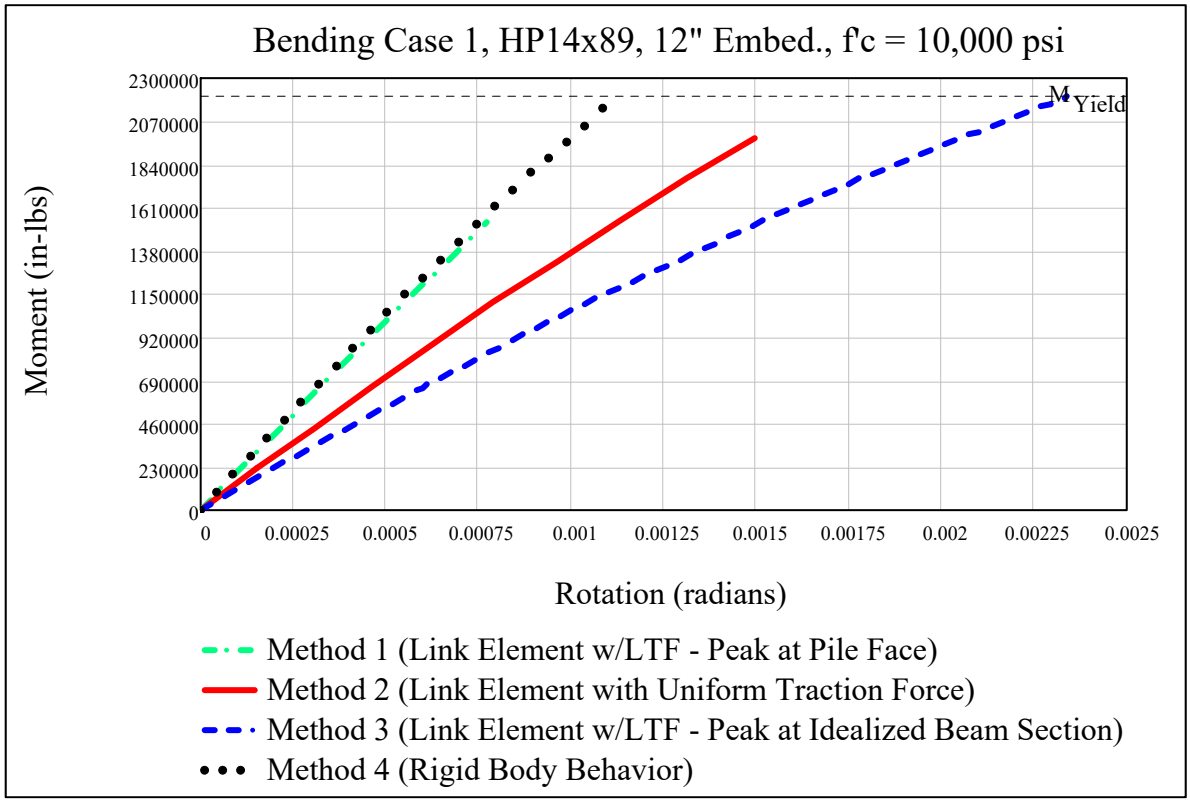
Bending Case 1, HP14x89, 12" Embed., f'c = 10,000 psi
Moment (in-lbs)
2300000
2070000
1840000
1610000
1380000
1150000
920000
690000
460000
230000
0
M Yield
0
0.00025
0.0005
0.00075
0.001
0.00125
0.0015
0.00175
0.002
0.00225
0.0025
Rotation (radians)
Method 1 (Link Element w/LTF - Peak at Pile Face)
Method 2 (Link Element with Uniform Traction Force)
Method 3 (Link Element w/LTF - Peak at Idealized Beam Section)
Method 4 (Rigid Body Behavior)

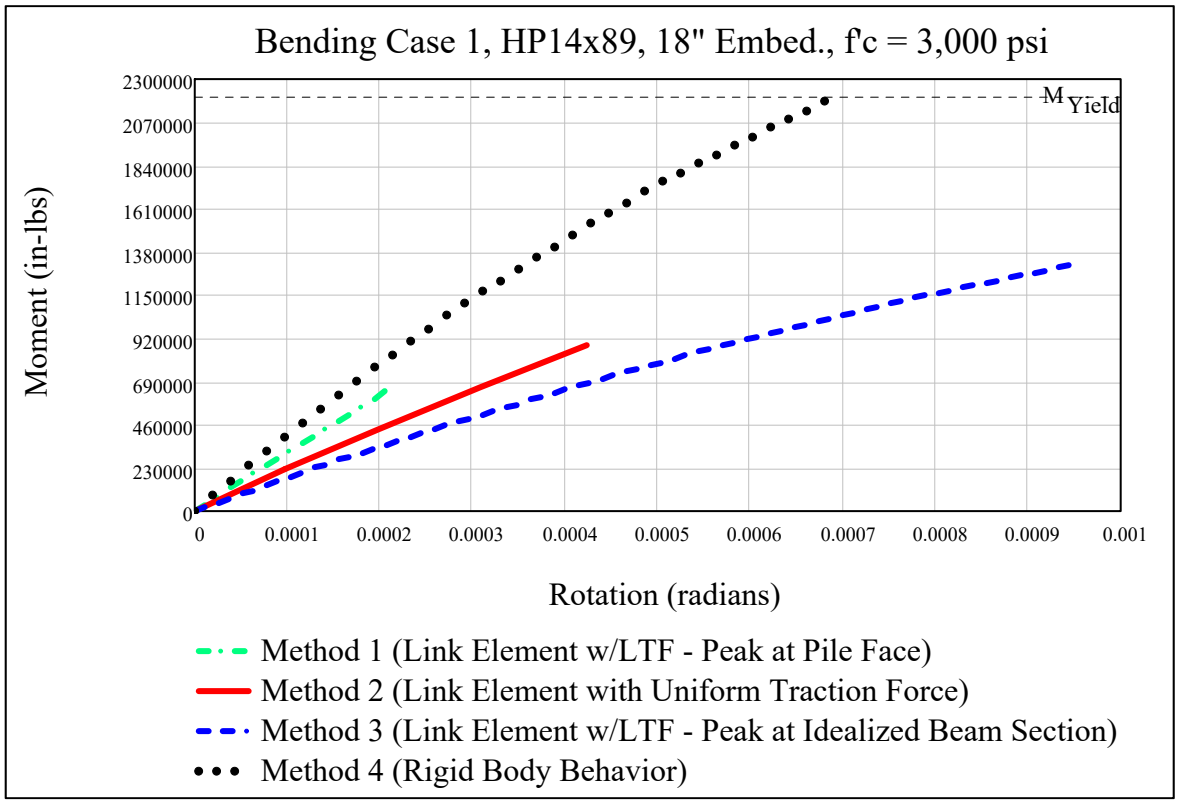
Bending Case 1, HP14x89, 18" Embed., f'c = 3,000 psi
Moment (in-lbs)
2300000
2070000
1840000
1610000
1380000
1150000
920000
690000
460000
230000
0
M Yield
0
0.0001
0.0002
0.0003
0.0004
0.0005
0.0006
0.0007
0.0008
0.0009
0.001
Rotation (radians)
Method 1 (Link Element w/LTF - Peak at Pile Face)
Method 2 (Link Element with Uniform Traction Force)
Method 3 (Link Element w/LTF - Peak at Idealized Beam Section)
Method 4 (Rigid Body Behavior)

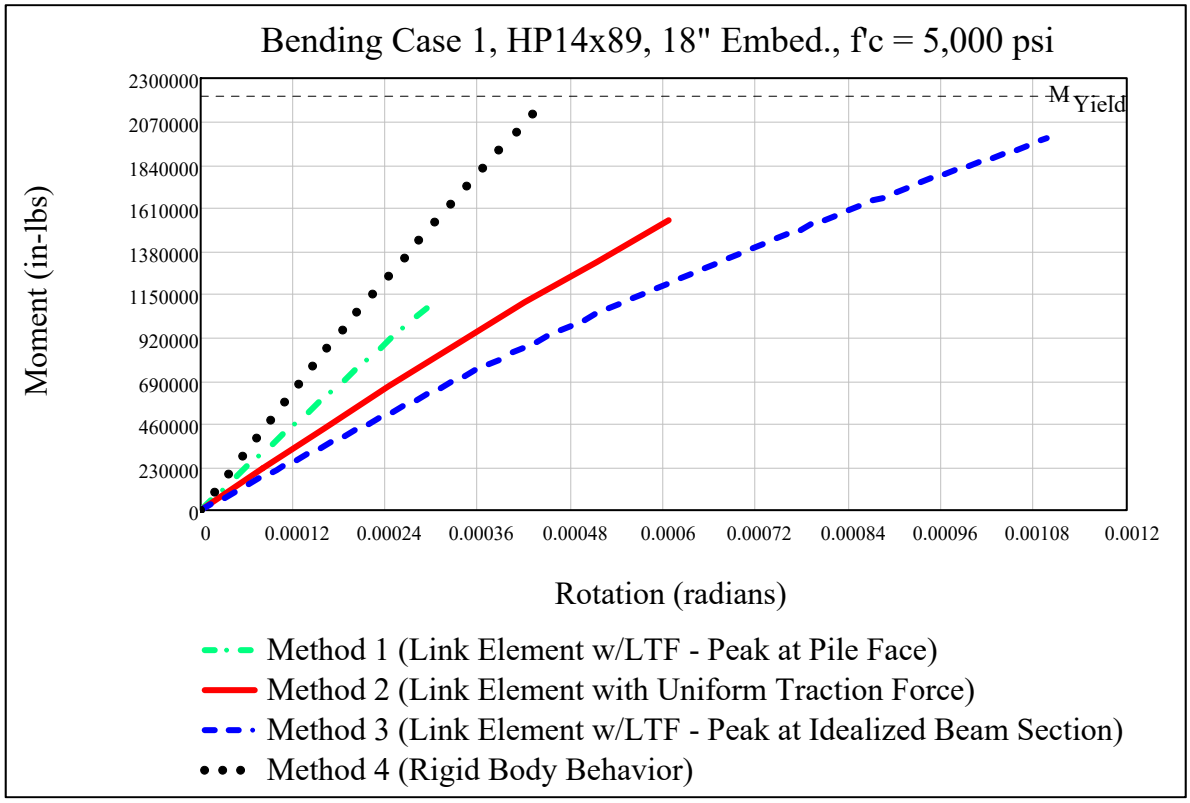
Bending Case 1, HP14x89, 18" Embed., f'c = 5,000 psi
Moment (in-lbs)
2300000
2070000
1840000
1610000
1380000
1150000
920000
690000
460000
230000
0
M Yield
0
0.00012
0.00024
0.00036
0.00048
0.0006
0.00072
0.00084
0.00096
0.00108
0.0012
Rotation (radians)
Method 1 (Link Element w/LTF - Peak at Pile Face)
Method 2 (Link Element with Uniform Traction Force)
Method 3 (Link Element w/LTF - Peak at Idealized Beam Section)
Method 4 (Rigid Body Behavior)

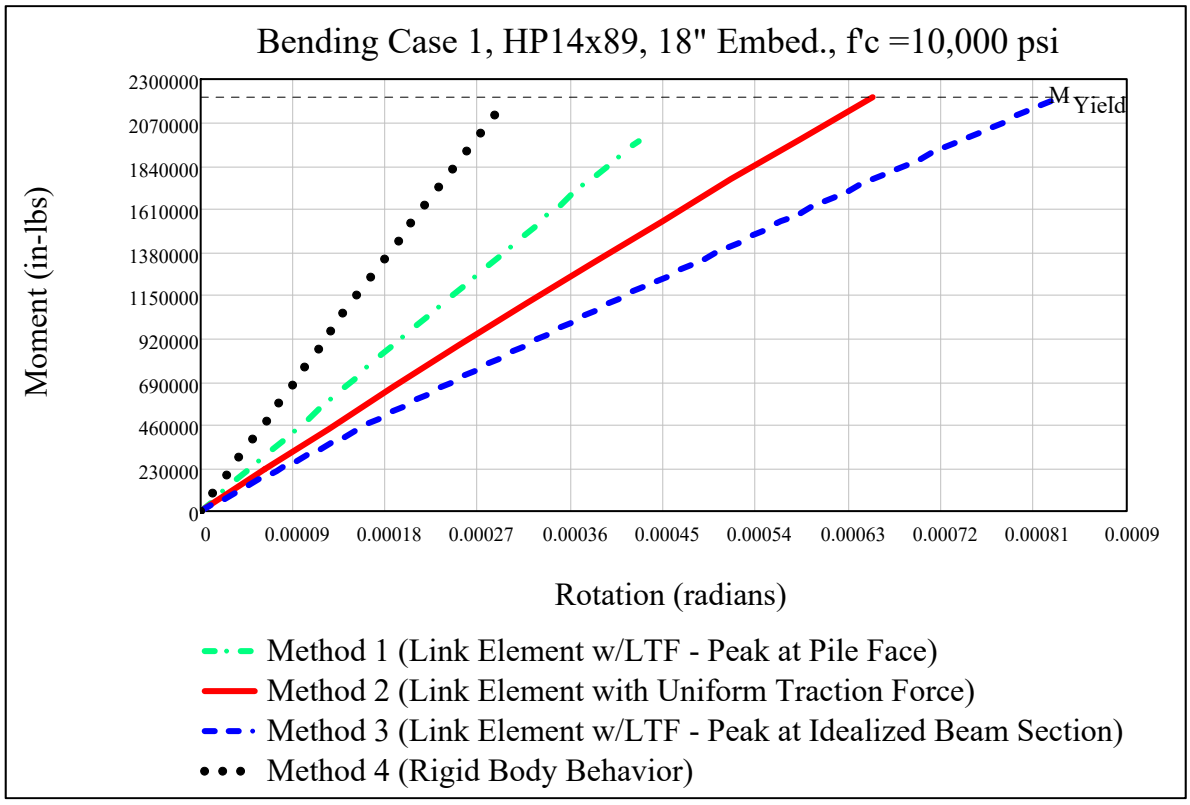
Bending Case 1, HP14x89, 18" Embed., f'c =10,000 psi
Moment (in-lbs)
2300000
2070000
1840000
1610000
1380000
1150000
920000
690000
460000
230000
0
M Yield
0
0.00009
0.00018
0.00027
0.00036
0.00045
0.00054
0.00063
0.00072
0.00081
0.0009
Rotation (radians)
Method 1 (Link Element w/LTF - Peak at Pile Face)
Method 2 (Link Element with Uniform Traction Force)
Method 3 (Link Element w/LTF - Peak at Idealized Beam Section)
Method 4 (Rigid Body Behavior)

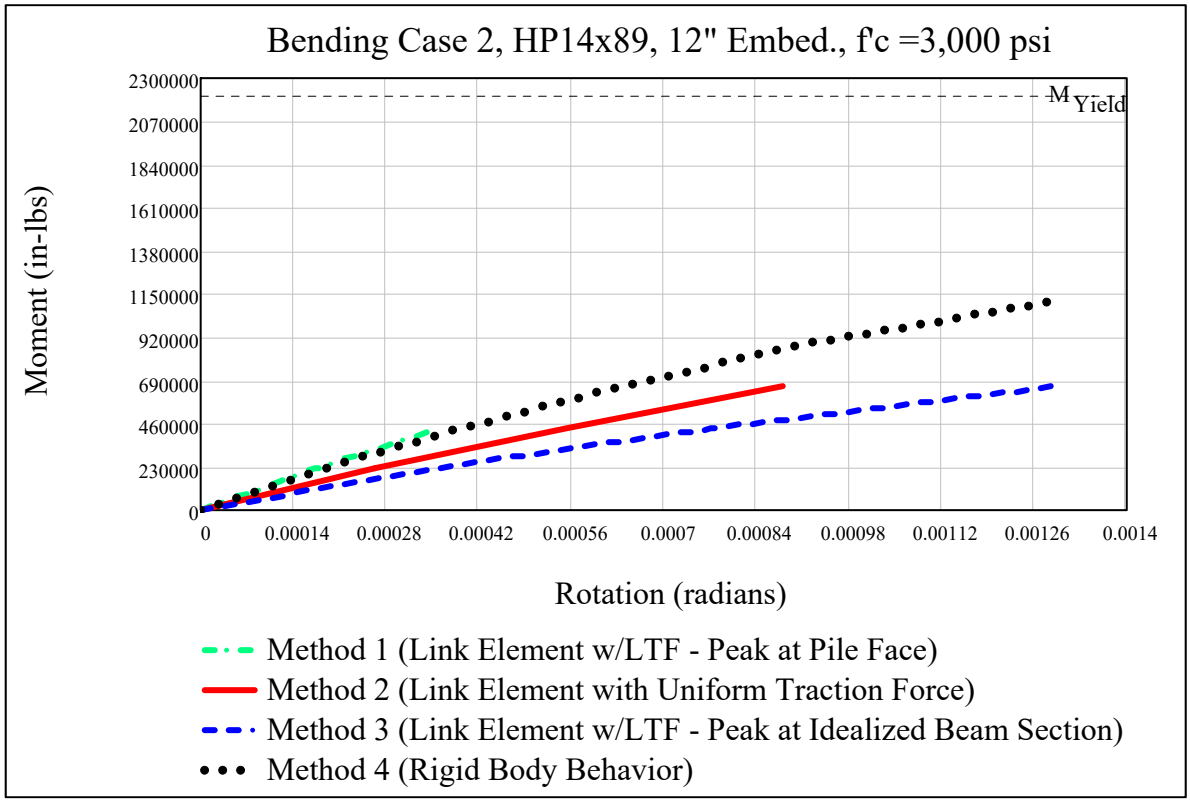
Bending Case 2, HP14x89, 12" Embed., f'c =3,000 psi
Moment (in-lbs)
2300000
2070000
1840000
1610000
1380000
1150000
920000
690000
460000
230000
0
M Yield
0
0.00014
0.00028
0.00042
0.00056
0.0007
0.00084
0.00098
0.00112
0.00126
0.0014
Rotation (radians)
Method 1 (Link Element w/LTF - Peak at Pile Face)
Method 2 (Link Element with Uniform Traction Force)
Method 3 (Link Element w/LTF - Peak at Idealized Beam Section)
Method 4 (Rigid Body Behavior)

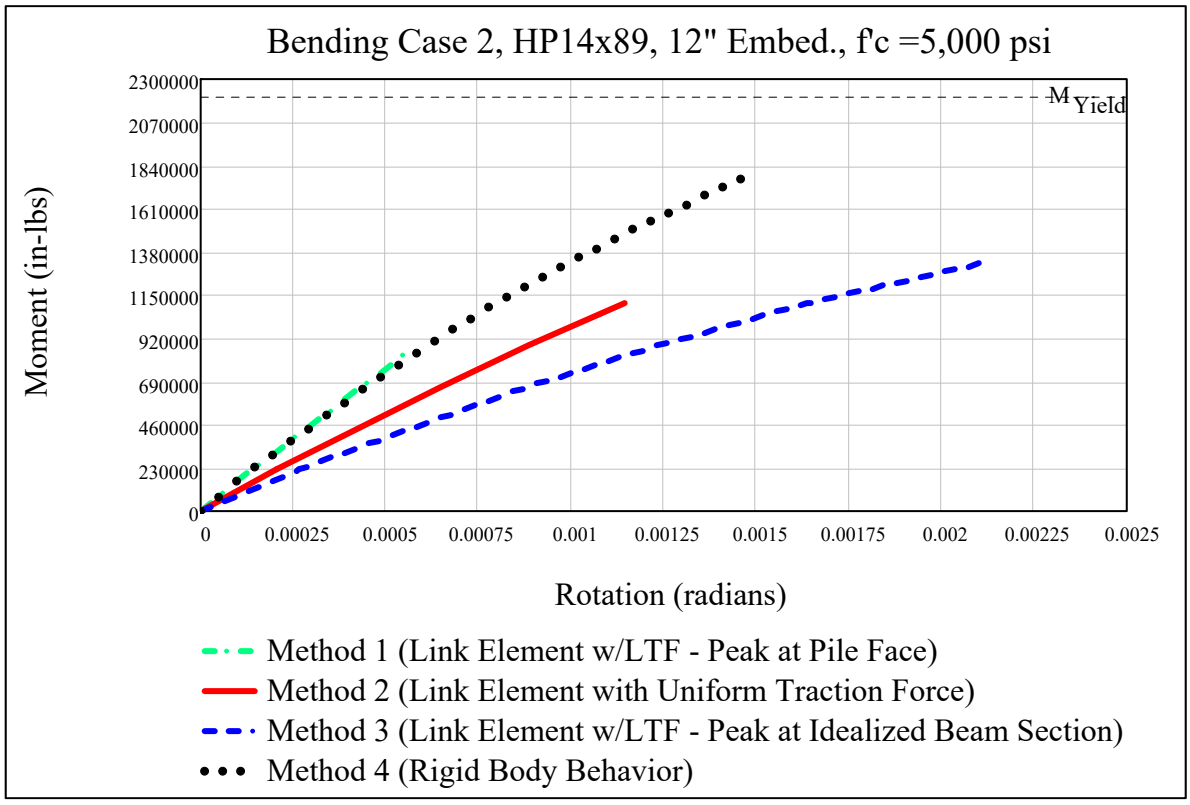
Bending Case 2, HP14x89, 12" Embed., f'c =5,000 psi
Moment (in-lbs)
2300000
2070000
1840000
1610000
1380000
1150000
920000
690000
460000
230000
0
M Yield
0
0.00025
0.0005
0.00075
0.001
0.00125
0.0015
0.00175
0.002
0.00225
0.0025
Rotation (radians)
Method 1 (Link Element w/LTF - Peak at Pile Face)
Method 2 (Link Element with Uniform Traction Force)
Method 3 (Link Element w/LTF - Peak at Idealized Beam Section)
Method 4 (Rigid Body Behavior)

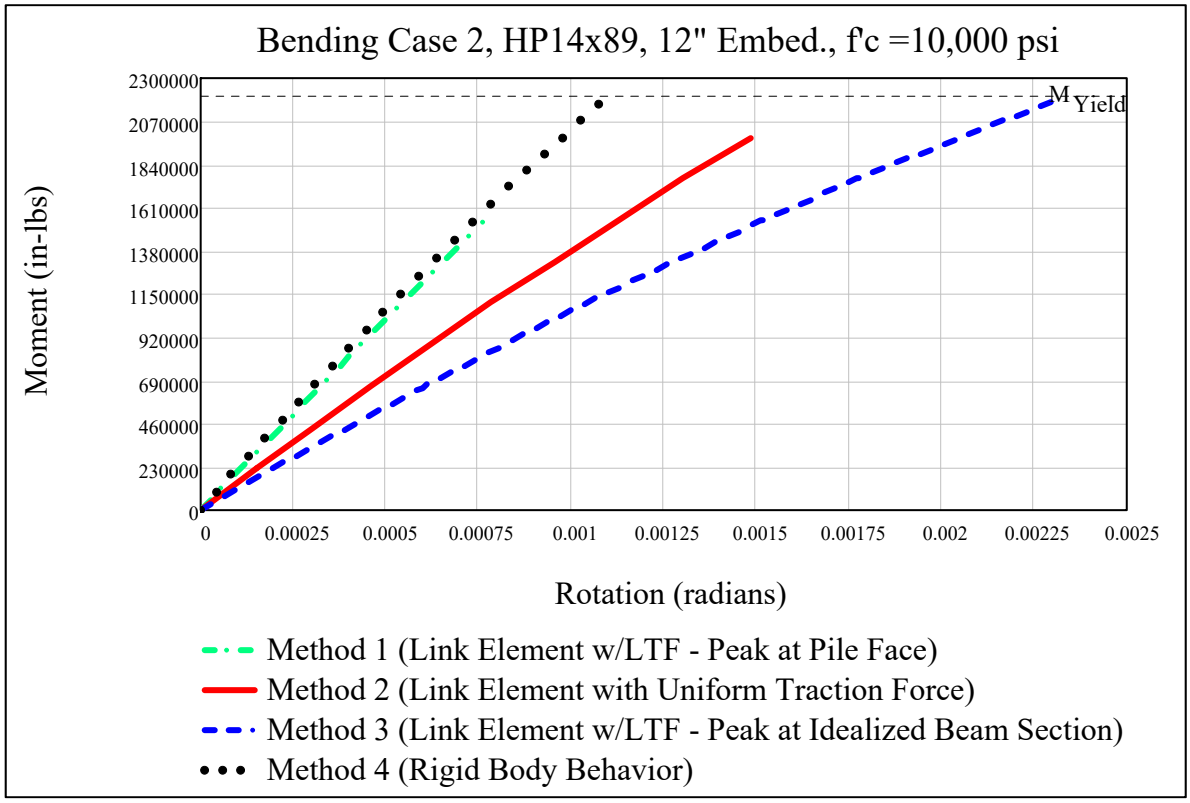
Bending Case 2, HP14x89, 12" Embed., f'c =10,000 psi
Moment (in-lbs)
2300000
2070000
1840000
1610000
1380000
1150000
920000
690000
460000
230000
0
M Yield
0
0.00025
0.0005
0.00075
0.001
0.00125
0.0015
0.00175
0.002
0.00225
0.0025
Rotation (radians)
Method 1 (Link Element w/LTF - Peak at Pile Face)
Method 2 (Link Element with Uniform Traction Force)
Method 3 (Link Element w/LTF - Peak at Idealized Beam Section)
Method 4 (Rigid Body Behavior)

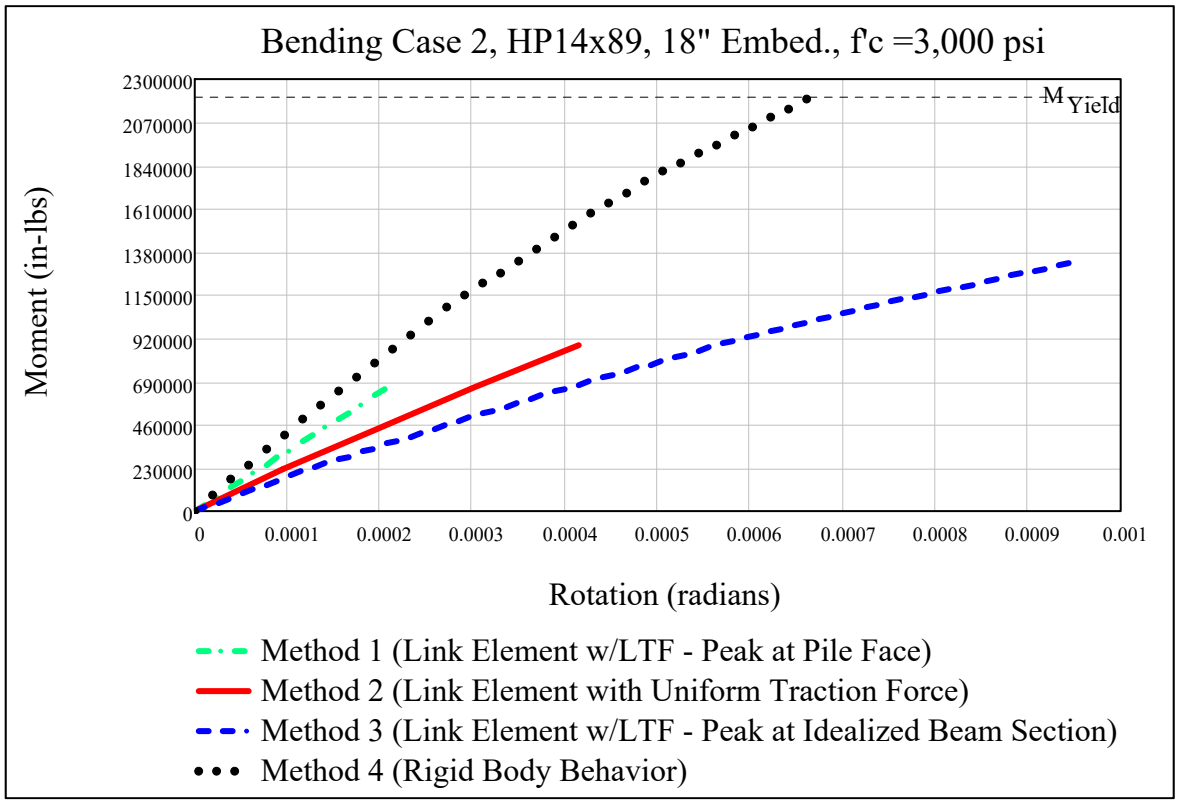
Bending Case 2, HP14x89, 18" Embed., f'c =3,000 psi
Moment (in-lbs)
2300000
2070000
1840000
1610000
1380000
1150000
920000
690000
460000
230000
0
M Yield
0
0.0001
0.0002
0.0003
0.0004
0.0005
0.0006
0.0007
0.0008
0.0009
0.001
Rotation (radians)
Method 1 (Link Element w/LTF - Peak at Pile Face)
Method 2 (Link Element with Uniform Traction Force)
Method 3 (Link Element w/LTF - Peak at Idealized Beam Section)
Method 4 (Rigid Body Behavior)

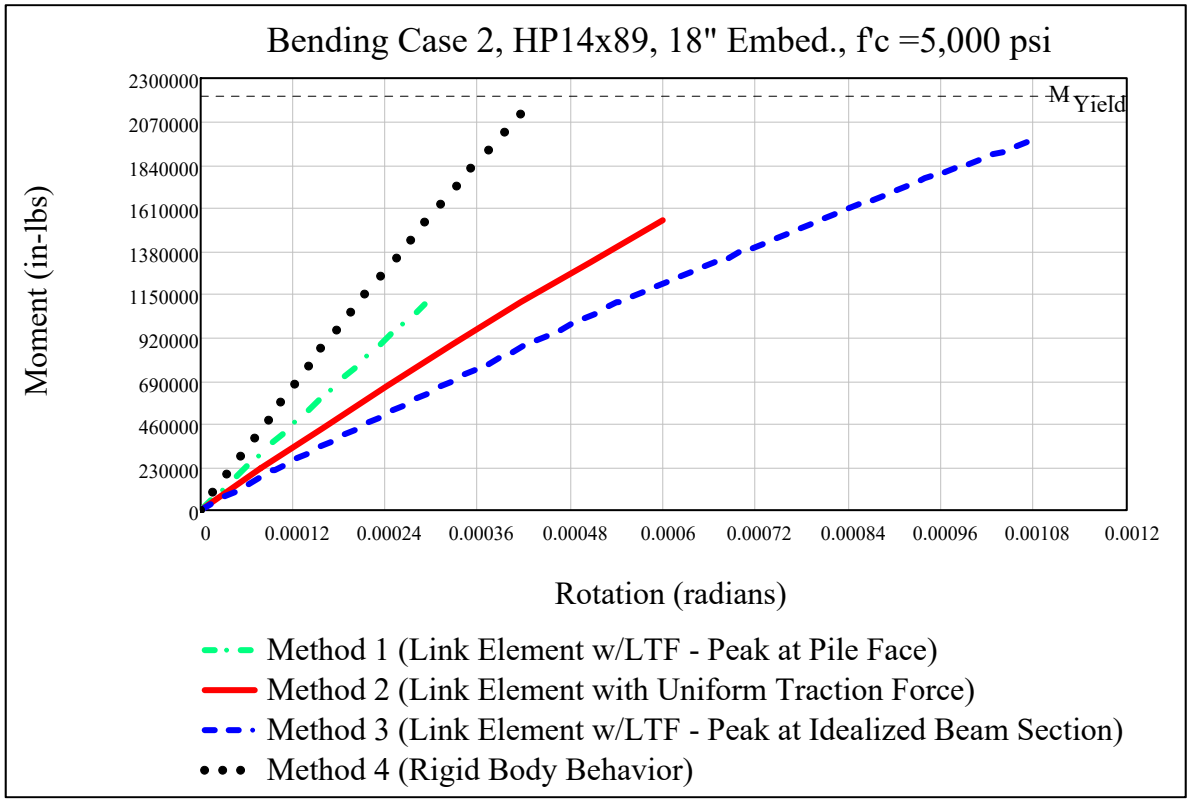
Bending Case 2, HP14x89, 18" Embed., f'c =5,000 psi
Moment (in-lbs)
2300000
2070000
1840000
1610000
1380000
1150000
920000
690000
460000
230000
0
M Yield
0
0.00012
0.00024
0.00036
0.00048
0.0006
0.00072
0.00084
0.00096
0.00108
0.0012
Rotation (radians)
Method 1 (Link Element w/LTF - Peak at Pile Face)
Method 2 (Link Element with Uniform Traction Force)
Method 3 (Link Element w/LTF - Peak at Idealized Beam Section)
Method 4 (Rigid Body Behavior)

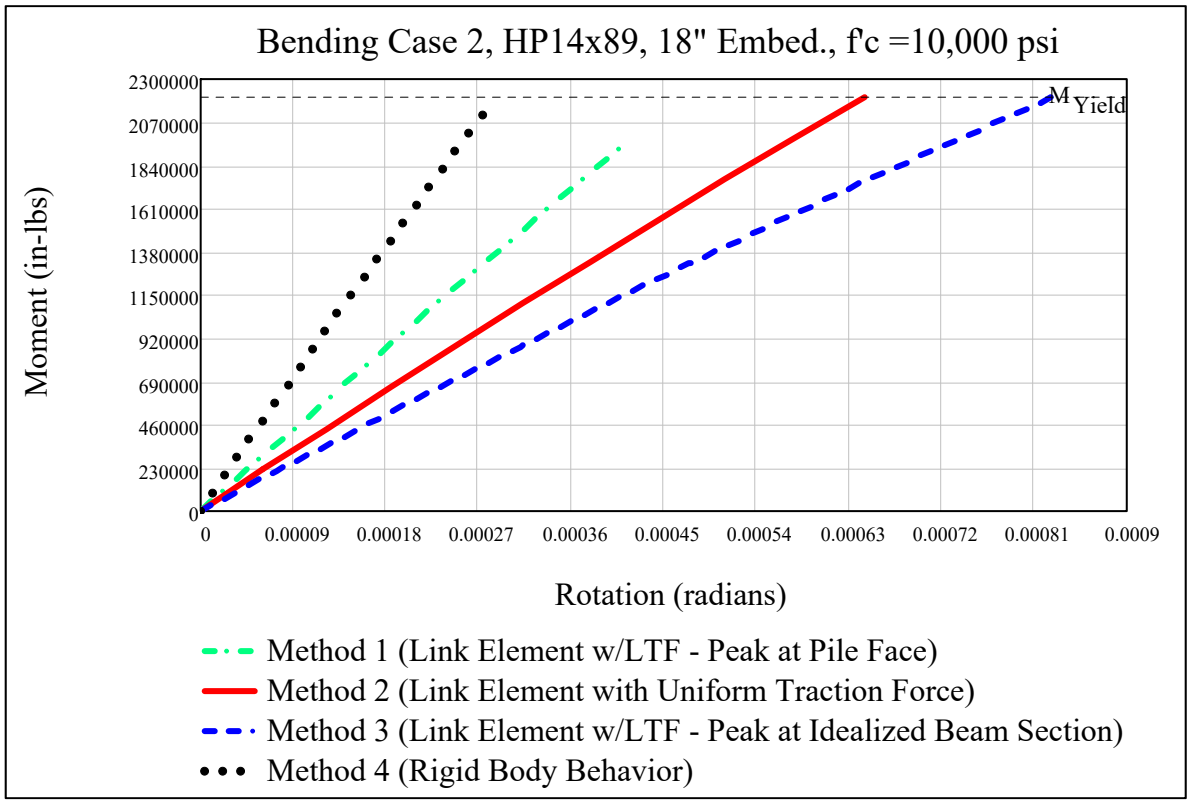
Bending Case 2, HP14x89, 18" Embed., f'c =10,000 psi
Moment (in-lbs)
2300000
2070000
1840000
1610000
1380000
1150000
920000
690000
460000
230000
0
M Yield
0
0.00009
0.00018
0.00027
0.00036
0.00045
0.00054
0.00063
0.00072
0.00081
0.0009
Rotation (radians)
Method 1 (Link Element w/LTF - Peak at Pile Face)
Method 2 (Link Element with Uniform Traction Force)
Method 3 (Link Element w/LTF - Peak at Idealized Beam Section)
Method 4 (Rigid Body Behavior)

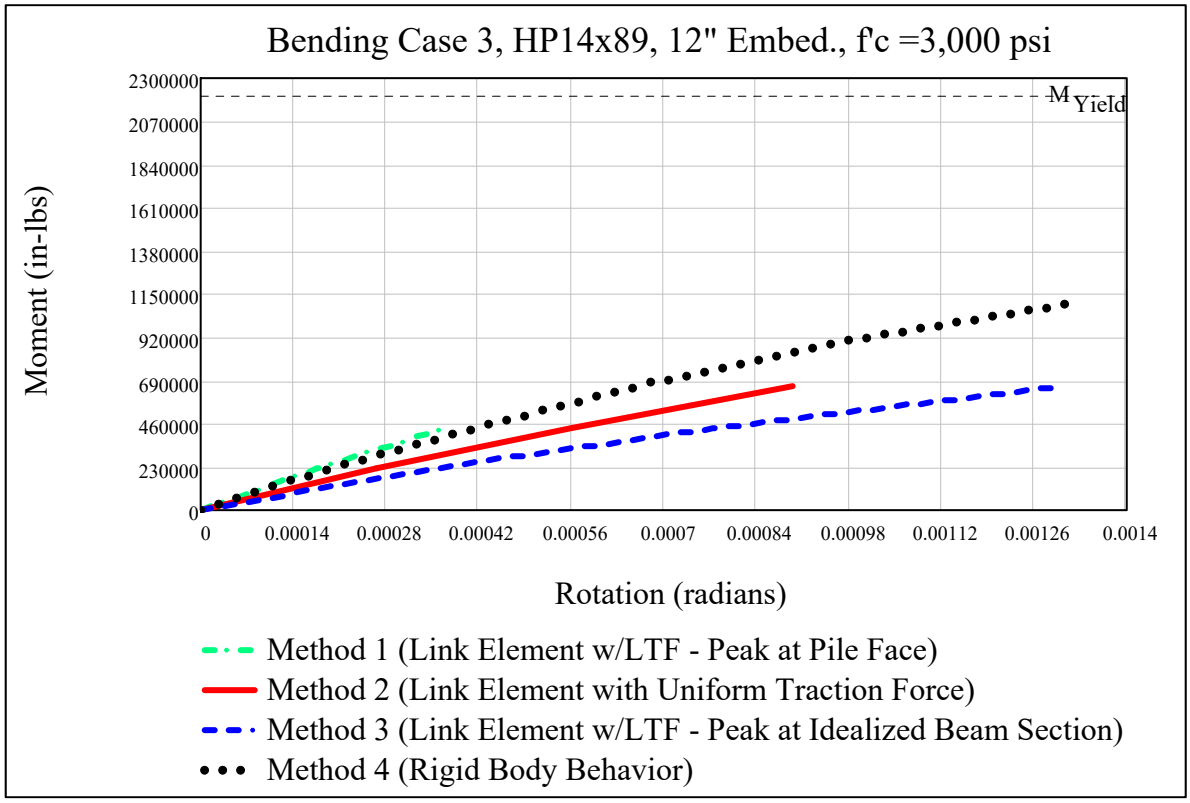
Bending Case 3, HP14x89, 12" Embed., f'c =3,000 psi
Moment (in-lbs)
2300000
2070000
1840000
1610000
1380000
1150000
920000
690000
460000
230000
0
M Yield
0
0.00014
0.00028
0.00042
0.00056
0.0007
0.00084
0.00098
0.00112
0.00126
0.0014
Rotation (radians)
Method 1 (Link Element w/LTF - Peak at Pile Face)
Method 2 (Link Element with Uniform Traction Force)
Method 3 (Link Element w/LTF - Peak at Idealized Beam Section)
Method 4 (Rigid Body Behavior)

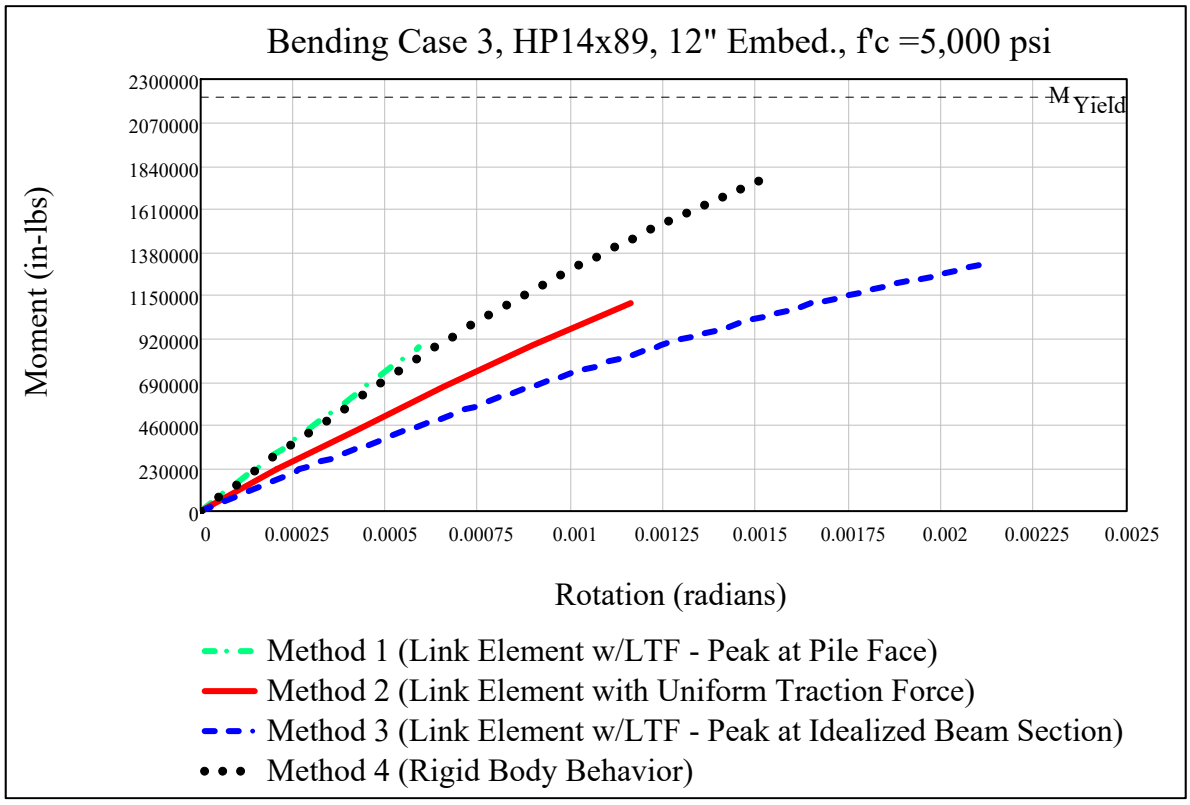
Bending Case 3, HP14x89, 12" Embed., f'c =5,000 psi
Moment (in-lbs)
2300000
2070000
1840000
1610000
1380000
1150000
920000
690000
460000
230000
0
M Yield
0
0.00025
0.0005
0.00075
0.001
0.00125
0.0015
0.00175
0.002
0.00225
0.0025
Rotation (radians)
Method 1 (Link Element w/LTF - Peak at Pile Face)
Method 2 (Link Element with Uniform Traction Force)
Method 3 (Link Element w/LTF - Peak at Idealized Beam Section)
Method 4 (Rigid Body Behavior)

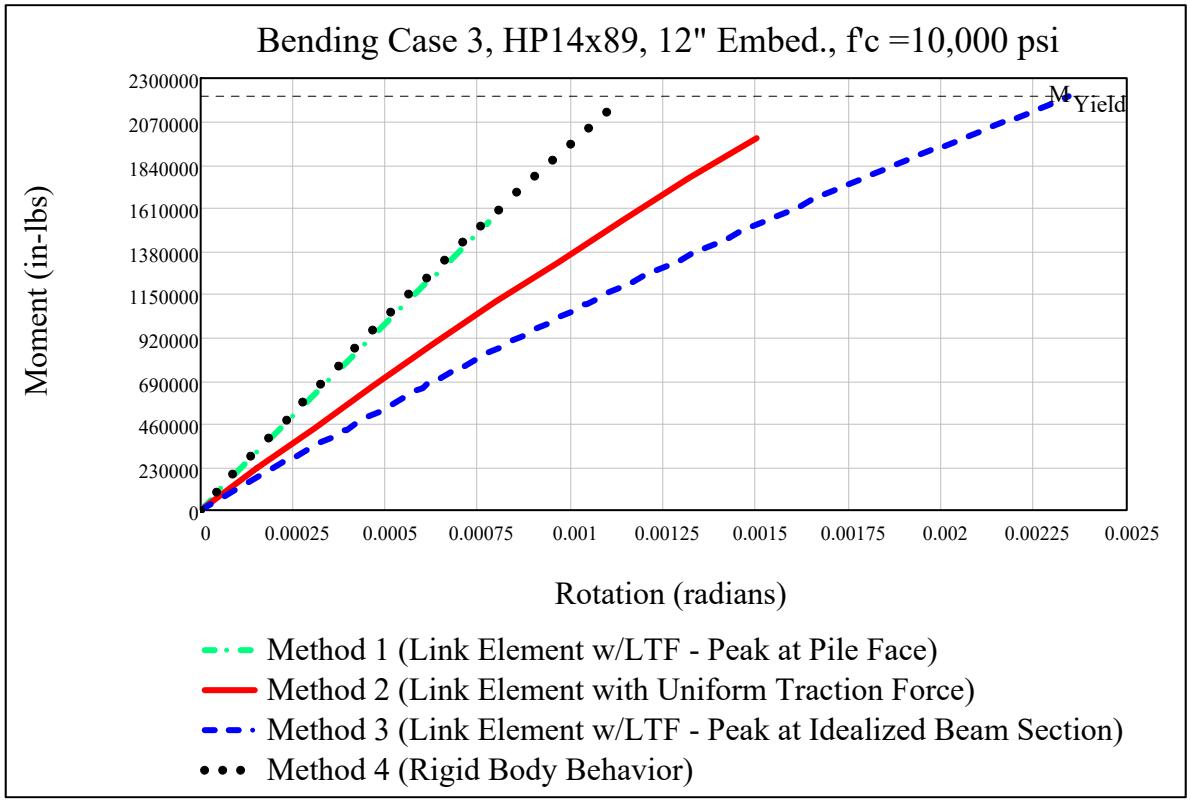
Bending Case 3, HP14x89, 12" Embed., f'c =10,000 psi
Moment (in-lbs)
2300000
2070000
1840000
1610000
1380000
1150000
920000
690000
460000
230000
0
M Yield
0
0.00025
0.0005
0.00075
0.001
0.00125
0.0015
0.00175
0.002
0.00225
0.0025
Rotation (radians)
Method 1 (Link Element w/LTF - Peak at Pile Face)
Method 2 (Link Element with Uniform Traction Force)
Method 3 (Link Element w/LTF - Peak at Idealized Beam Section)
Method 4 (Rigid Body Behavior)

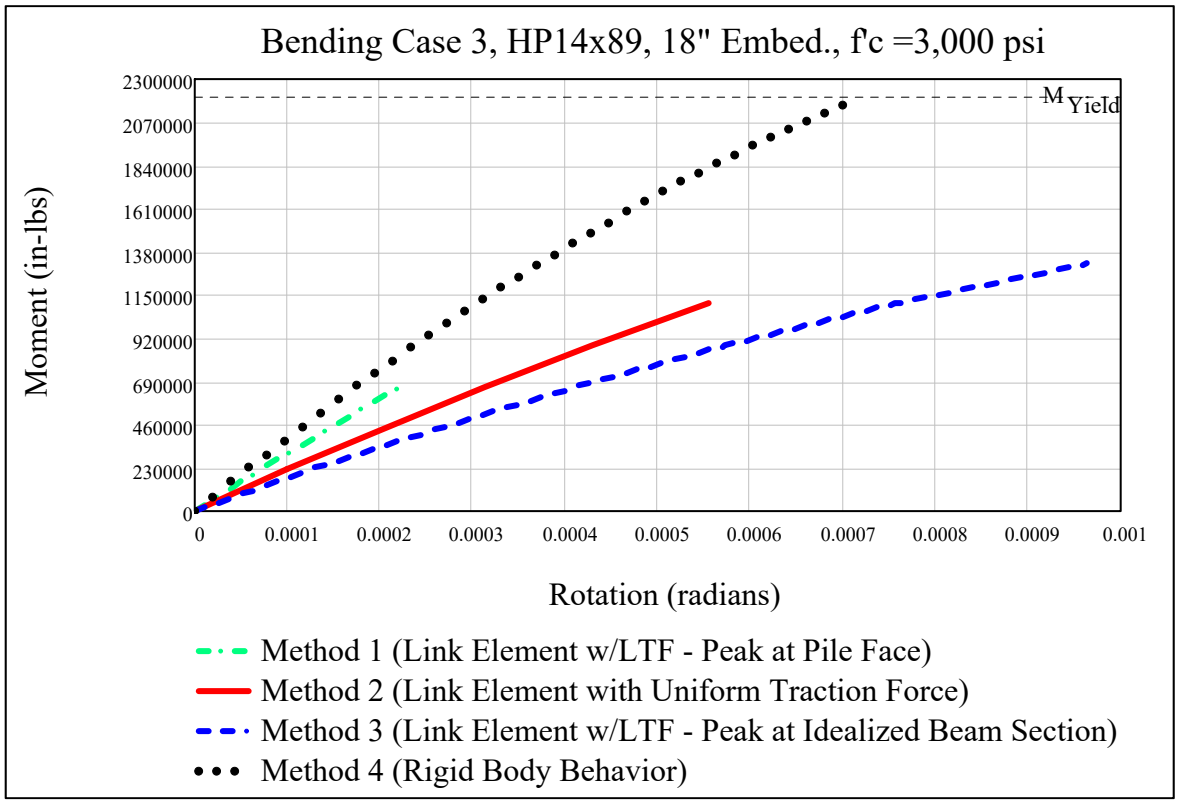
Bending Case 3, HP14x89, 18" Embed., f'c =3,000 psi
Moment (in-lbs)
2300000
2070000
1840000
1610000
1380000
1150000
920000
690000
460000
230000
0
M Yield
0
0.0001
0.0002
0.0003
0.0004
0.0005
0.0006
0.0007
0.0008
0.0009
0.001
Rotation (radians)
Method 1 (Link Element w/LTF - Peak at Pile Face)
Method 2 (Link Element with Uniform Traction Force)
Method 3 (Link Element w/LTF - Peak at Idealized Beam Section)
Method 4 (Rigid Body Behavior)

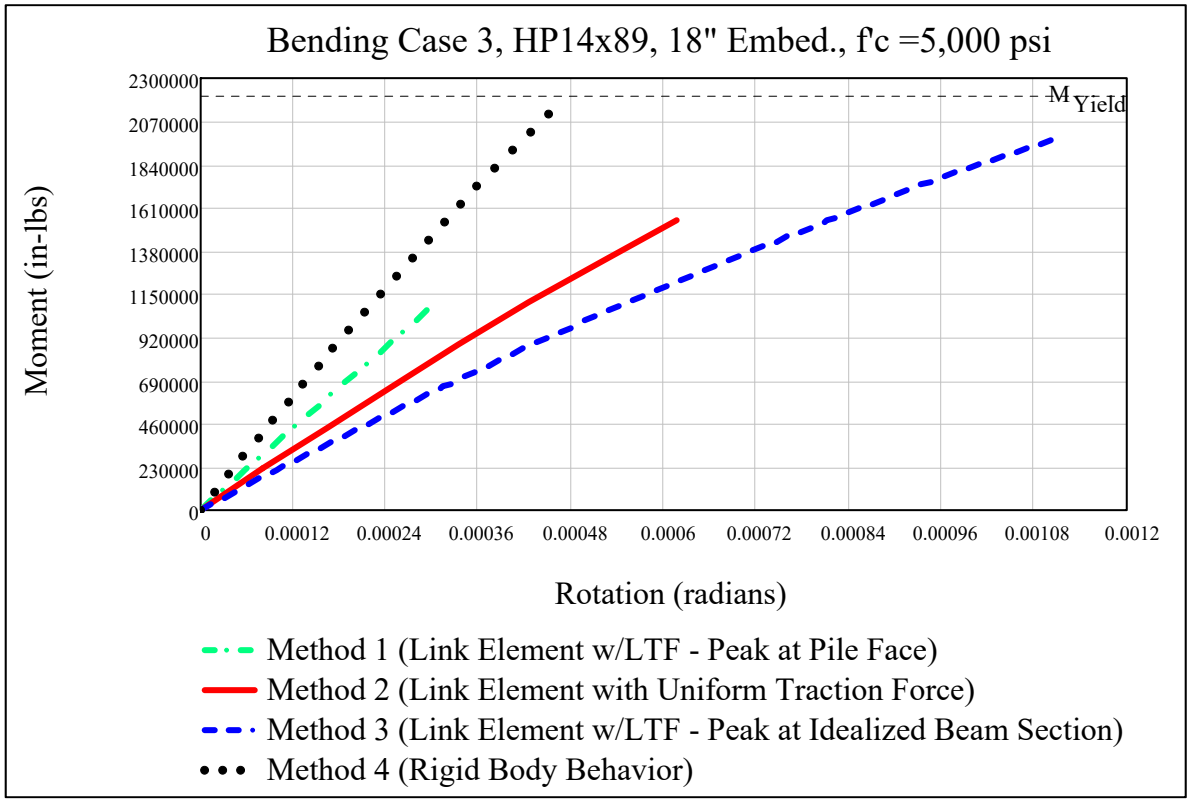
Bending Case 3, HP14x89, 18" Embed., f'c =5,000 psi
Moment (in-lbs)
2300000
2070000
1840000
1610000
1380000
1150000
920000
690000
460000
230000
0
M Yield
0
0.00012
0.00024
0.00036
0.00048
0.0006
0.00072
0.00084
0.00096
0.00108
0.0012
Rotation (radians)
Method 1 (Link Element w/LTF - Peak at Pile Face)
Method 2 (Link Element with Uniform Traction Force)
Method 3 (Link Element w/LTF - Peak at Idealized Beam Section)
Method 4 (Rigid Body Behavior)

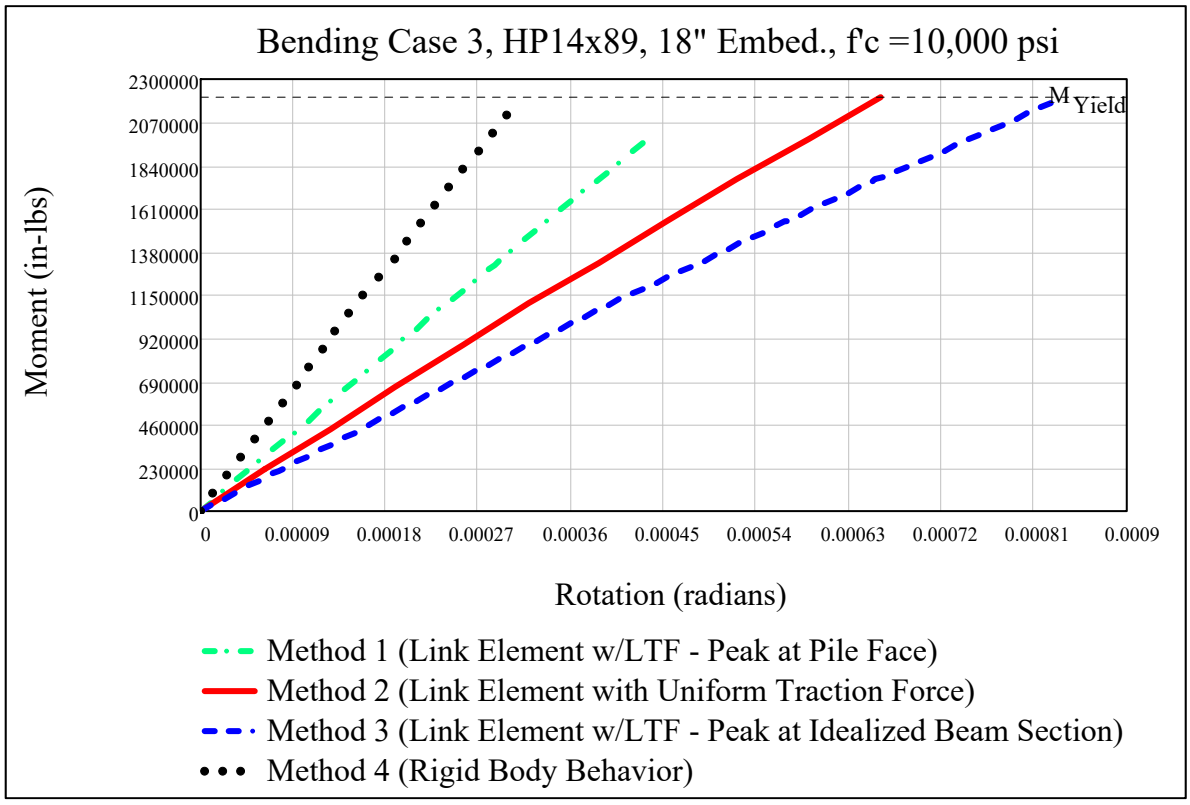
Bending Case 3, HP14x89, 18" Embed., f'c =10,000 psi
Moment (in-lbs)
2300000
2070000
1840000
1610000
1380000
1150000
920000
690000
460000
230000
0
M Yield
0
0.00009
0.00018
0.00027
0.00036
0.00045
0.00054
0.00063
0.00072
0.00081
0.0009
Rotation (radians)
Method 1 (Link Element w/LTF - Peak at Pile Face)
Method 2 (Link Element with Uniform Traction Force)
Method 3 (Link Element w/LTF - Peak at Idealized Beam Section)
Method 4 (Rigid Body Behavior)

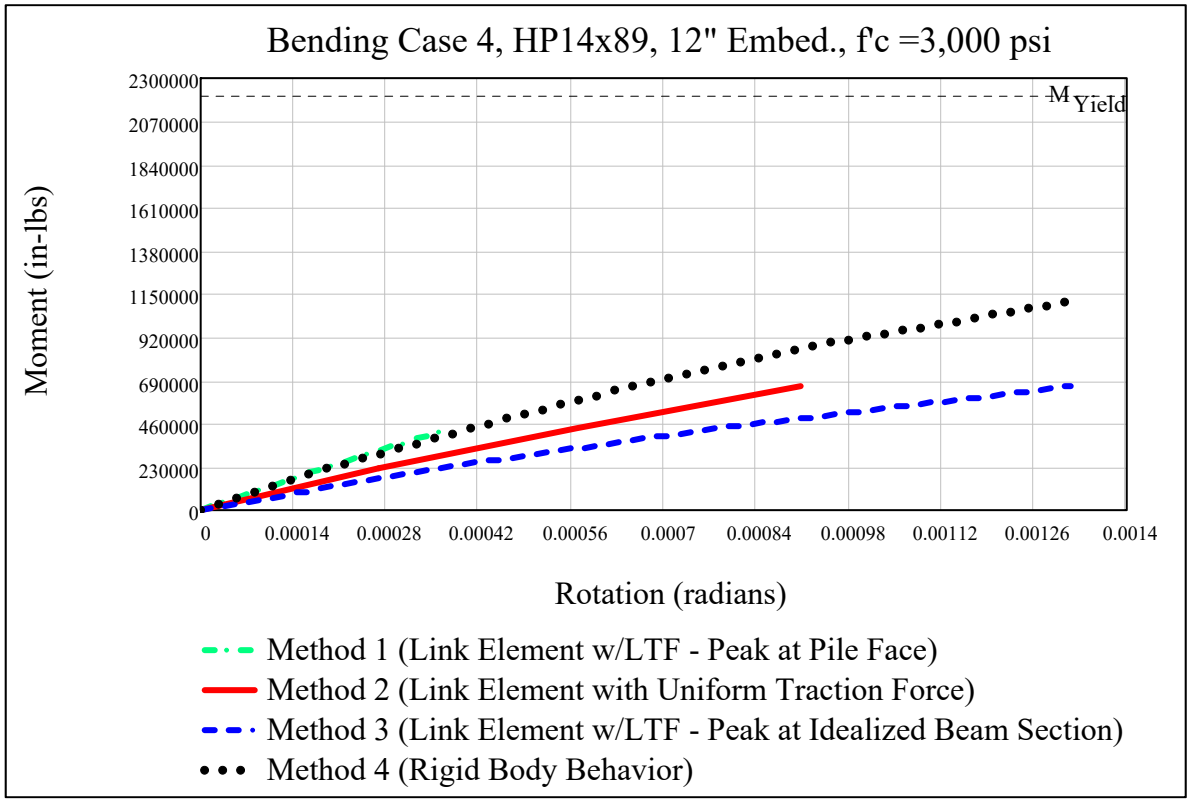
Bending Case 4, HP14x89, 12" Embed., f'c =3,000 psi
Moment (in-lbs)
2300000
2070000
1840000
1610000
1380000
1150000
920000
690000
460000
230000
0
M Yield
0
0.00014
0.00028
0.00042
0.00056
0.0007
0.00084
0.00098
0.00112
0.00126
0.0014
Rotation (radians)
Method 1 (Link Element w/LTF - Peak at Pile Face)
Method 2 (Link Element with Uniform Traction Force)
Method 3 (Link Element w/LTF - Peak at Idealized Beam Section)
Method 4 (Rigid Body Behavior)

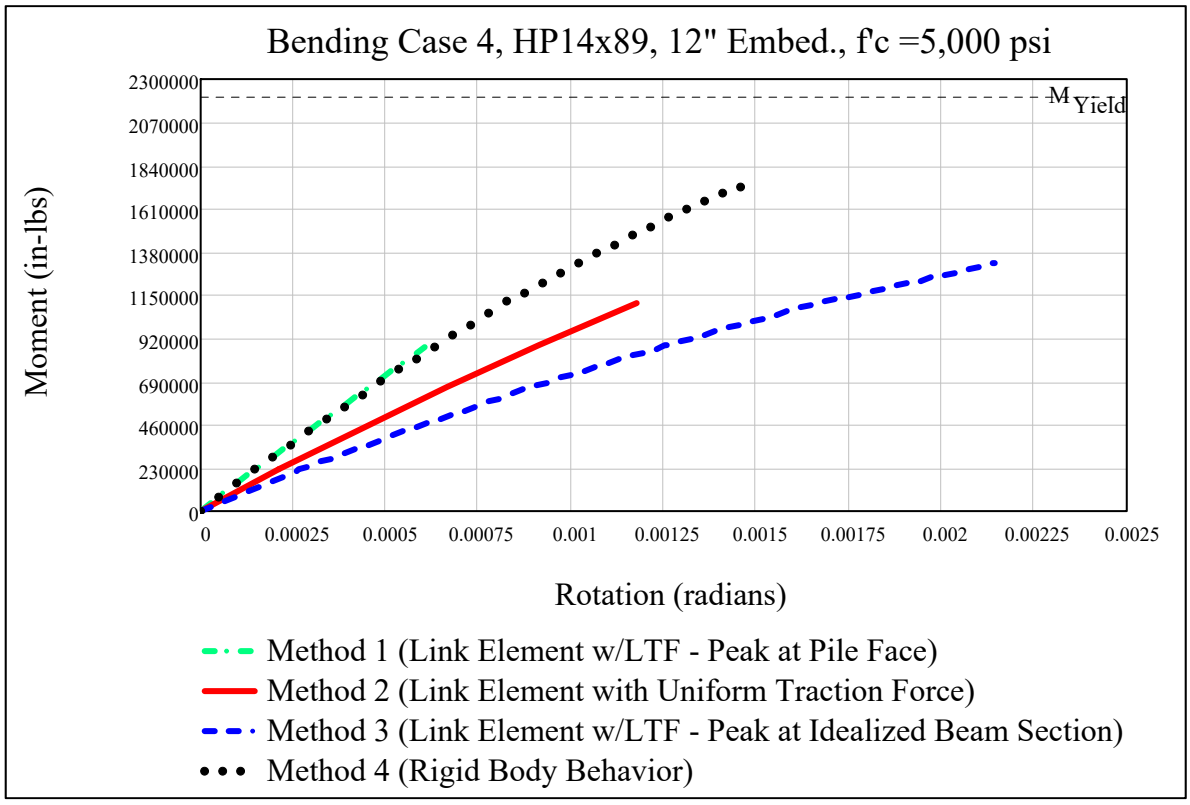
Bending Case 4, HP14x89, 12" Embed., f'c =5,000 psi
Moment (in-lbs)
2300000
2070000
1840000
1610000
1380000
1150000
920000
690000
460000
230000
0
M Yield
0
0.00025
0.0005
0.00075
0.001
0.00125
0.0015
0.00175
0.002
0.00225
0.0025
Rotation (radians)
Method 1 (Link Element w/LTF - Peak at Pile Face)
Method 2 (Link Element with Uniform Traction Force)
Method 3 (Link Element w/LTF - Peak at Idealized Beam Section)
Method 4 (Rigid Body Behavior)

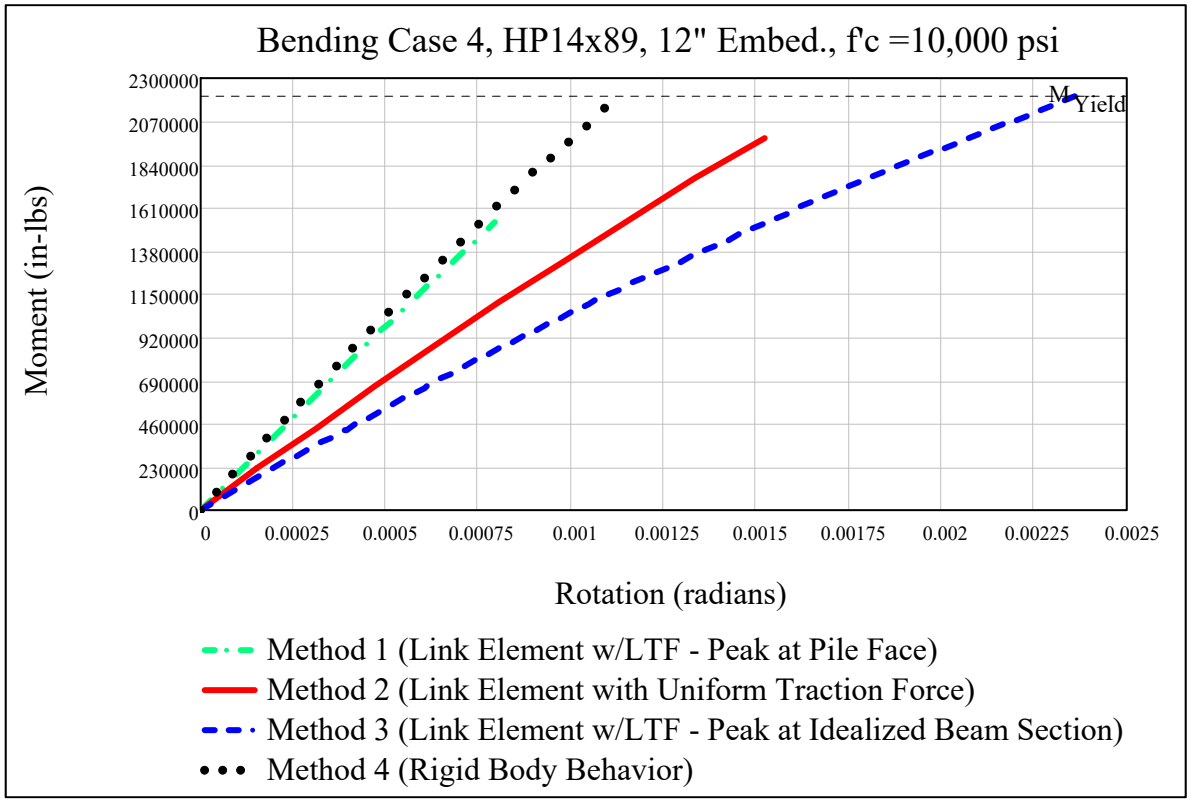
Bending Case 4, HP14x89, 12" Embed., f'c =10,000 psi
Moment (in-lbs)
2300000
2070000
1840000
1610000
1380000
1150000
920000
690000
460000
230000
0
M Yield
0
0.00025
0.0005
0.00075
0.001
0.00125
0.0015
0.00175
0.002
0.00225
0.0025
Rotation (radians)
Method 1 (Link Element w/LTF - Peak at Pile Face)
Method 2 (Link Element with Uniform Traction Force)
Method 3 (Link Element w/LTF - Peak at Idealized Beam Section)
Method 4 (Rigid Body Behavior)

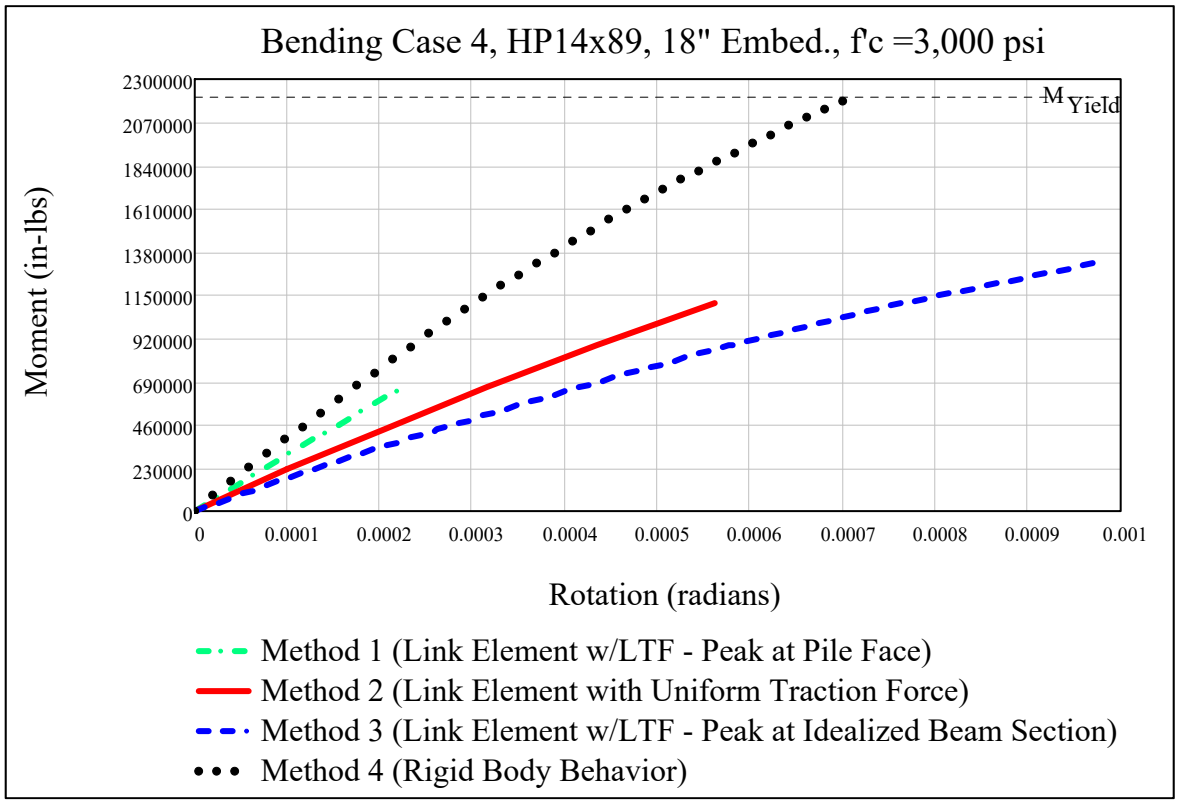
Bending Case 4, HP14x89, 18" Embed., f'c =3,000 psi
Moment (in-lbs)
2300000
2070000
1840000
1610000
1380000
1150000
920000
690000
460000
230000
0
M Yield
0
0.0001
0.0002
0.0003
0.0004
0.0005
0.0006
0.0007
0.0008
0.0009
0.001
Rotation (radians)
Method 1 (Link Element w/LTF - Peak at Pile Face)
Method 2 (Link Element with Uniform Traction Force)
Method 3 (Link Element w/LTF - Peak at Idealized Beam Section)
Method 4 (Rigid Body Behavior)

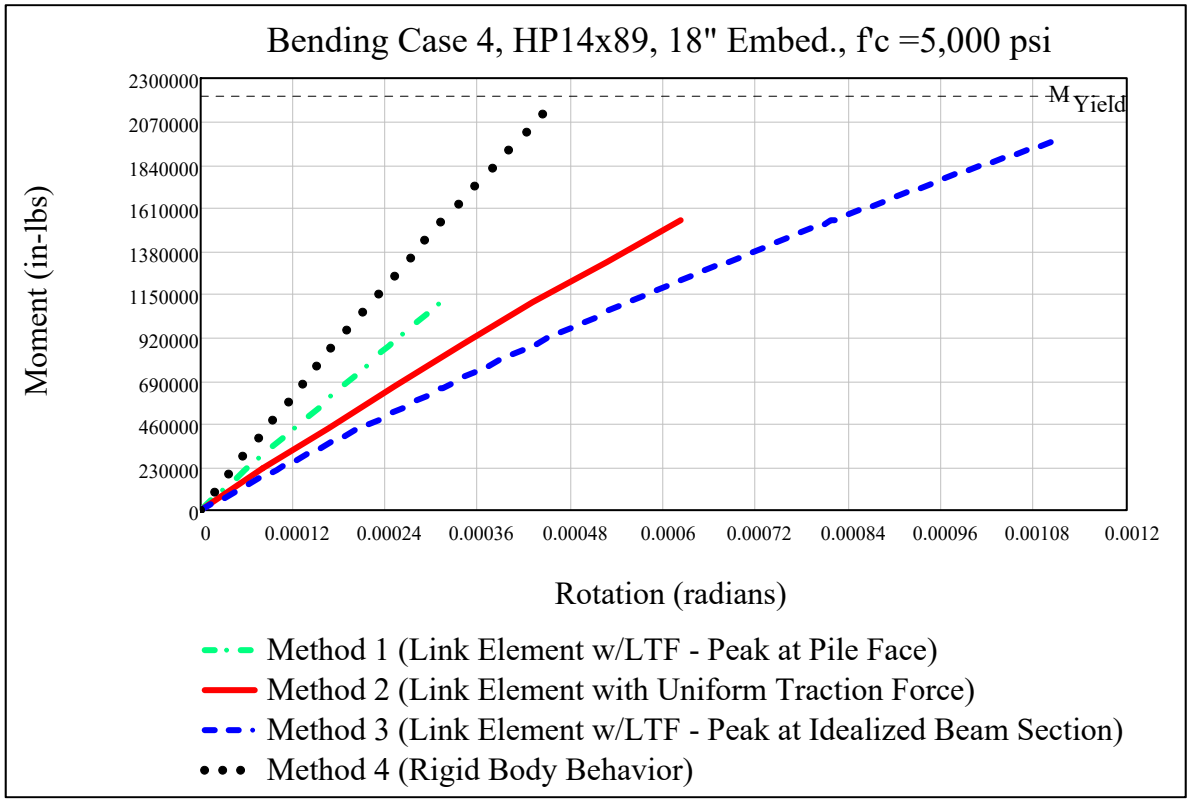
Bending Case 4, HP14x89, 18" Embed., f'c =5,000 psi
Moment (in-lbs)
2300000
2070000
1840000
1610000
1380000
1150000
920000
690000
460000
230000
0
M Yield
0
0.00012
0.00024
0.00036
0.00048
0.0006
0.00072
0.00084
0.00096
0.00108
0.0012
Rotation (radians)
Method 1 (Link Element w/LTF - Peak at Pile Face)
Method 2 (Link Element with Uniform Traction Force)
Method 3 (Link Element w/LTF - Peak at Idealized Beam Section)
Method 4 (Rigid Body Behavior)

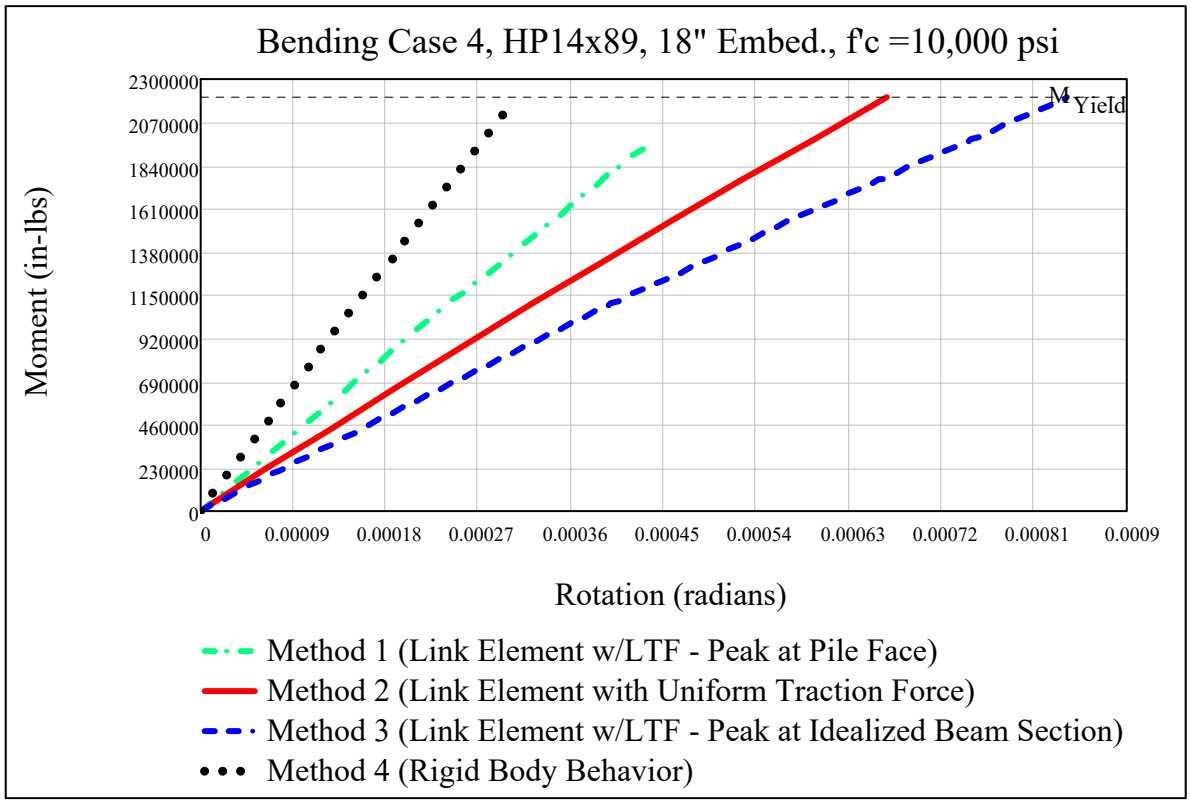
Bending Case 4, HP14x89, 18" Embed., f'c =10,000 psi
Moment (in-lbs)
2300000
2070000
1840000
1610000
1380000
1150000
920000
690000
460000
230000
0
M Yield
0
0.00009
0.00018
0.00027
0.00036
0.00045
0.00054
0.00063
0.00072
0.00081
0.0009
Rotation (radians)
Method 1 (Link Element w/LTF - Peak at Pile Face)
Method 2 (Link Element with Uniform Traction Force)
Method 3 (Link Element w/LTF - Peak at Idealized Beam Section)
Method 4 (Rigid Body Behavior)

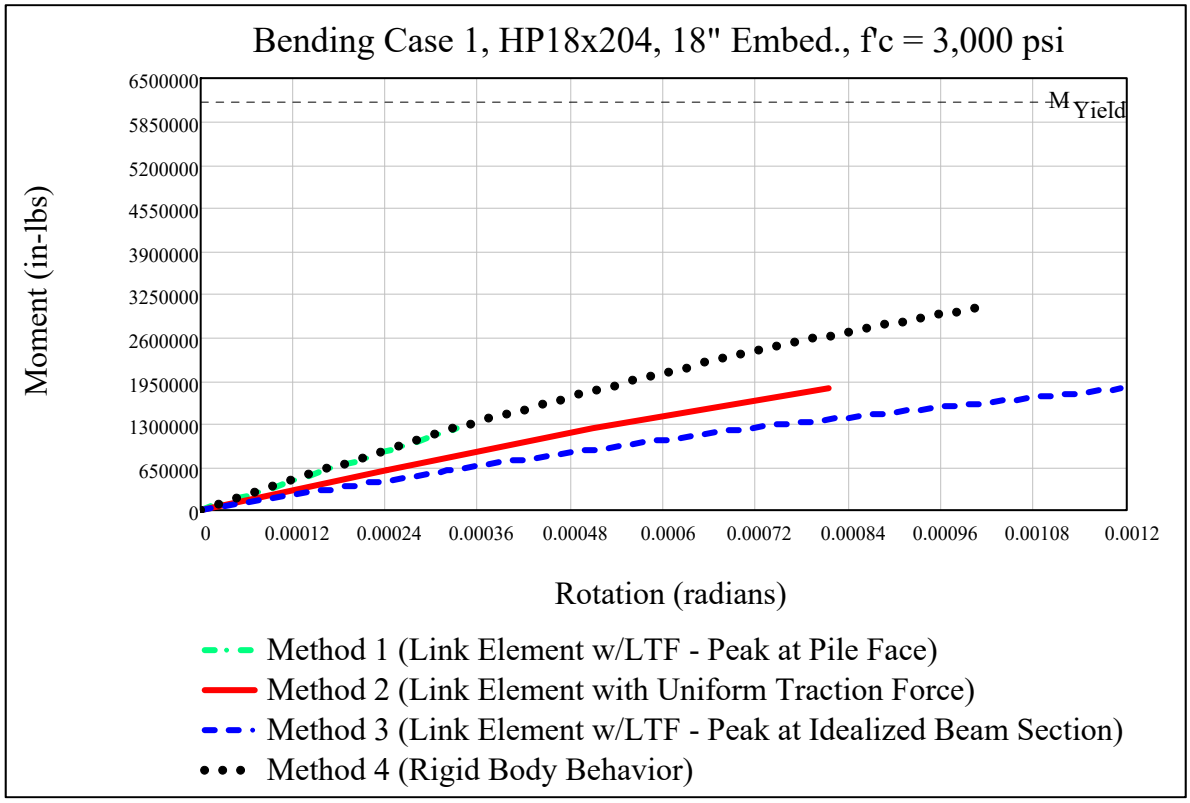
Bending Case 1, HP18x204, 18" Embed., f'c = 3,000 psi
Moment (in-lbs)
6500000
5850000
5200000
4550000
3900000
3250000
2600000
1950000
1300000
650000
0
M Yield
0
0.00012
0.00024
0.00036
0.00048
0.0006
0.00072
0.00084
0.00096
0.00108
0.0012
Rotation (radians)
Method 1 (Link Element w/LTF - Peak at Pile Face)
Method 2 (Link Element with Uniform Traction Force)
Method 3 (Link Element w/LTF - Peak at Idealized Beam Section)
Method 4 (Rigid Body Behavior)

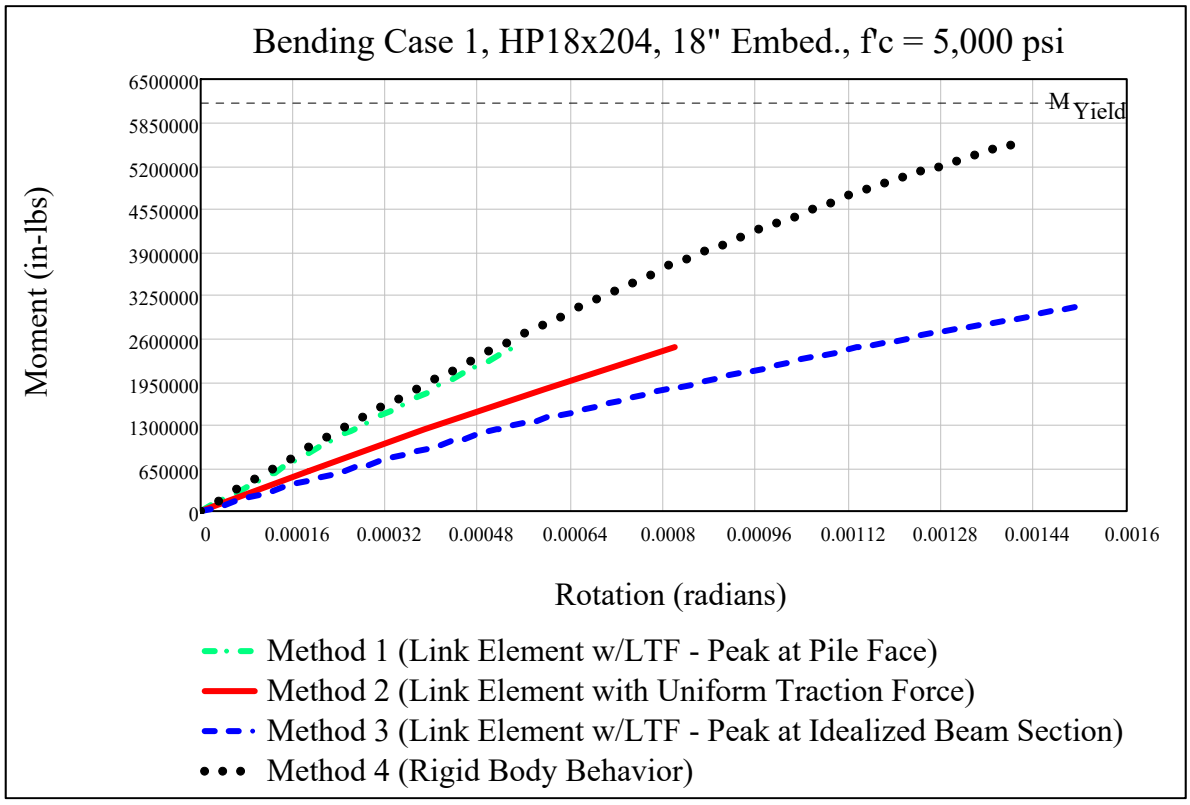
Bending Case 1, HP18x204, 18" Embed., f'c = 5,000 psi
Moment (in-lbs)
6500000
5850000
5200000
4550000
3900000
3250000
2600000
1950000
1300000
650000
0
M Yield
0
0.00016
0.00032
0.00048
0.00064
0.0008
0.00096
0.00112
0.00128
0.00144
0.0016
Rotation (radians)
Method 1 (Link Element w/LTF - Peak at Pile Face)
Method 2 (Link Element with Uniform Traction Force)
Method 3 (Link Element w/LTF - Peak at Idealized Beam Section)
Method 4 (Rigid Body Behavior)

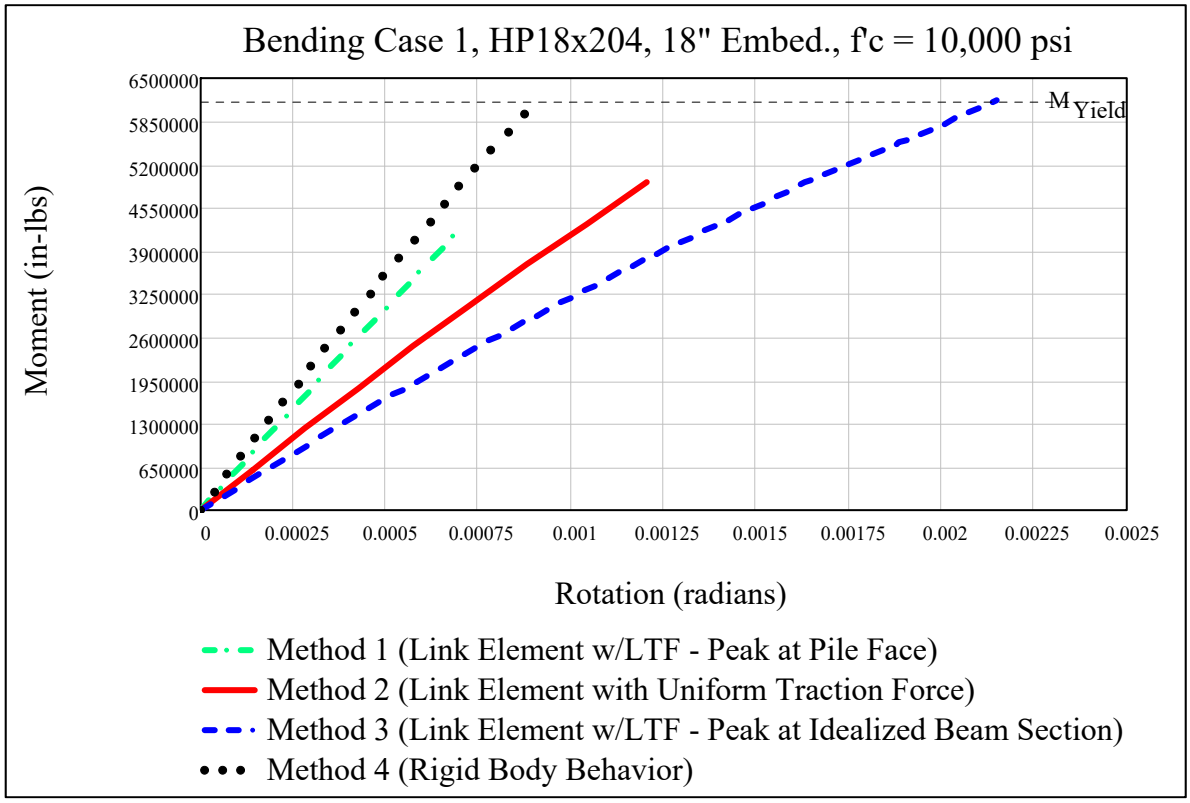
Bending Case 1, HP18x204, 18" Embed., f'c = 10,000 psi
Moment (in-lbs)
6500000
5850000
5200000
4550000
3900000
3250000
2600000
1950000
1300000
650000
0
M Yield
0
0.00025
0.0005
0.00075
0.001
0.00125
0.0015
0.00175
0.002
0.00225
0.0025
Rotation (radians)
Method 1 (Link Element w/LTF - Peak at Pile Face)
Method 2 (Link Element with Uniform Traction Force)
Method 3 (Link Element w/LTF - Peak at Idealized Beam Section)
Method 4 (Rigid Body Behavior)

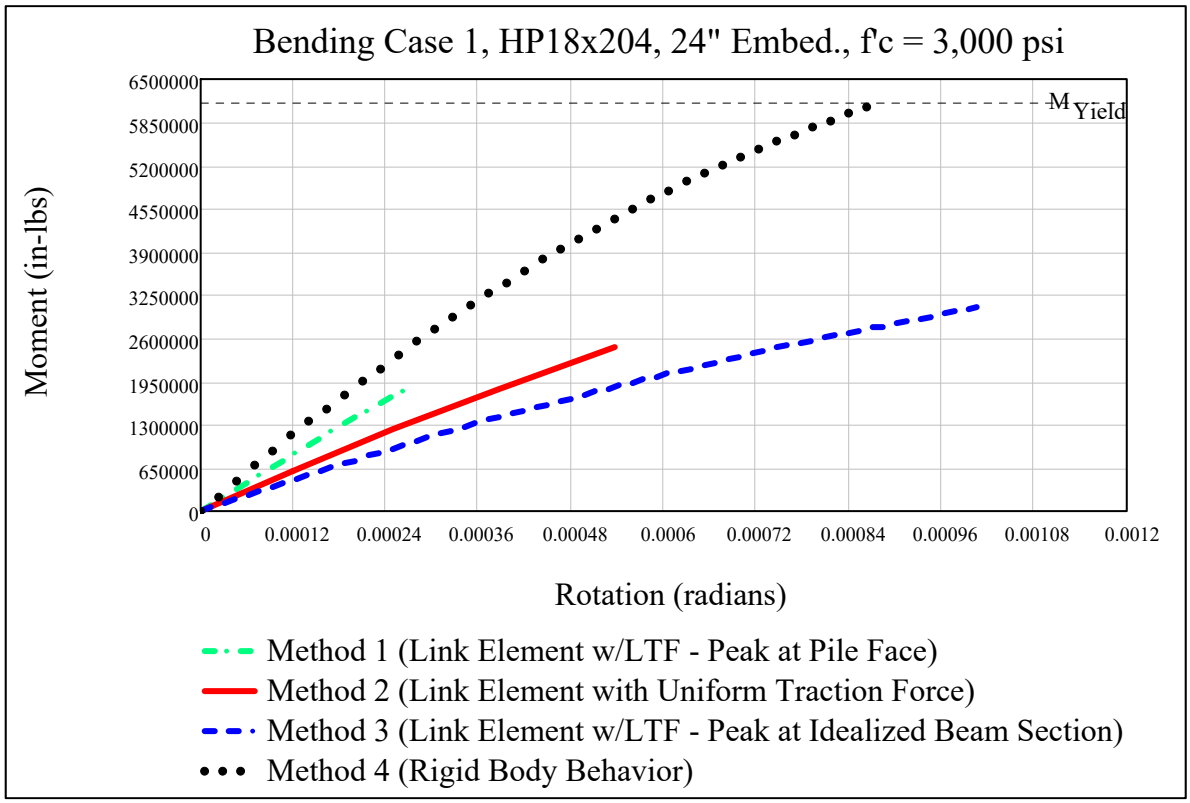
Bending Case 1, HP18x204, 24" Embed., f'c = 3,000 psi
Moment (in-lbs)
6500000
5850000
5200000
4550000
3900000
3250000
2600000
1950000
1300000
650000
0
M Yield
0
0.00012
0.00024
0.00036
0.00048
0.0006
0.00072
0.00084
0.00096
0.00108
0.0012
Rotation (radians)
Method 1 (Link Element w/LTF - Peak at Pile Face)
Method 2 (Link Element with Uniform Traction Force)
Method 3 (Link Element w/LTF - Peak at Idealized Beam Section)
Method 4 (Rigid Body Behavior)

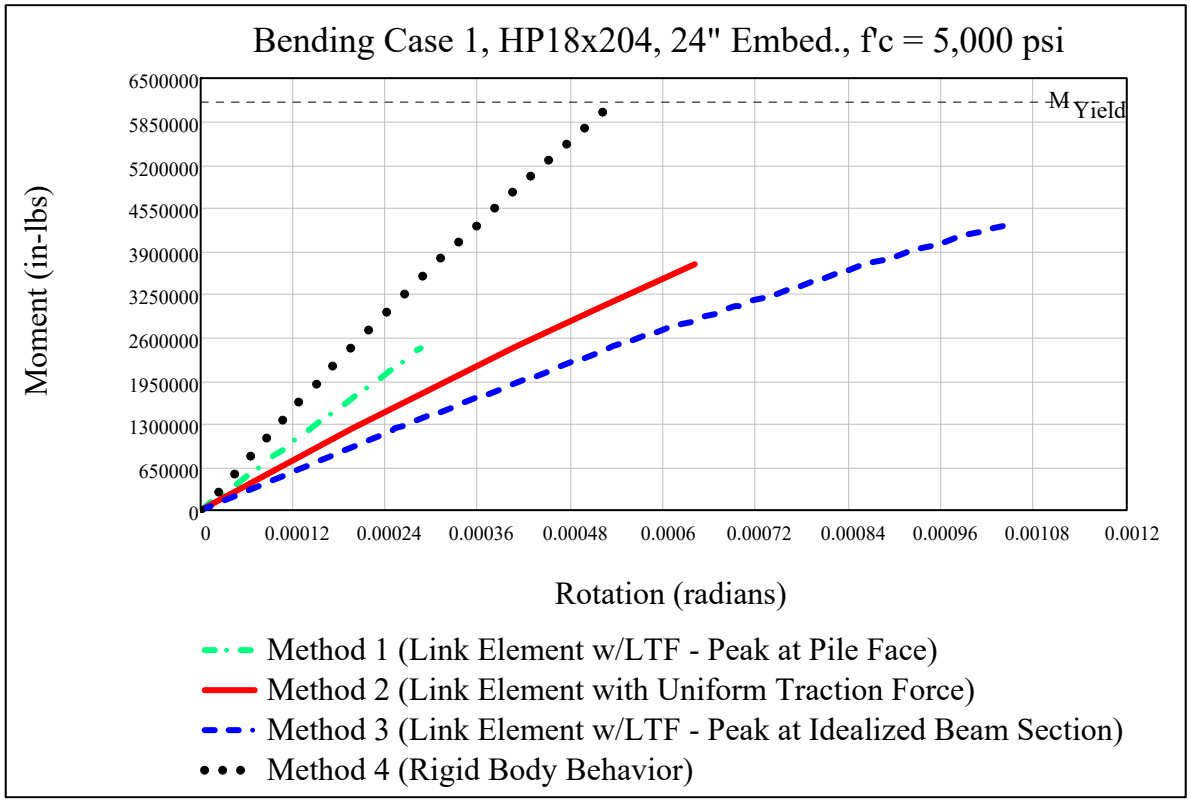
Bending Case 1, HP18x204, 24" Embed., f'c = 5,000 psi
Moment (in-lbs)
6500000
5850000
5200000
4550000
3900000
3250000
2600000
1950000
1300000
650000
0
M Yield
0
0.00012
0.00024
0.00036
0.00048
0.0006
0.00072
0.00084
0.00096
0.00108
0.0012
Rotation (radians)
Method 1 (Link Element w/LTF - Peak at Pile Face)
Method 2 (Link Element with Uniform Traction Force)
Method 3 (Link Element w/LTF - Peak at Idealized Beam Section)
Method 4 (Rigid Body Behavior)

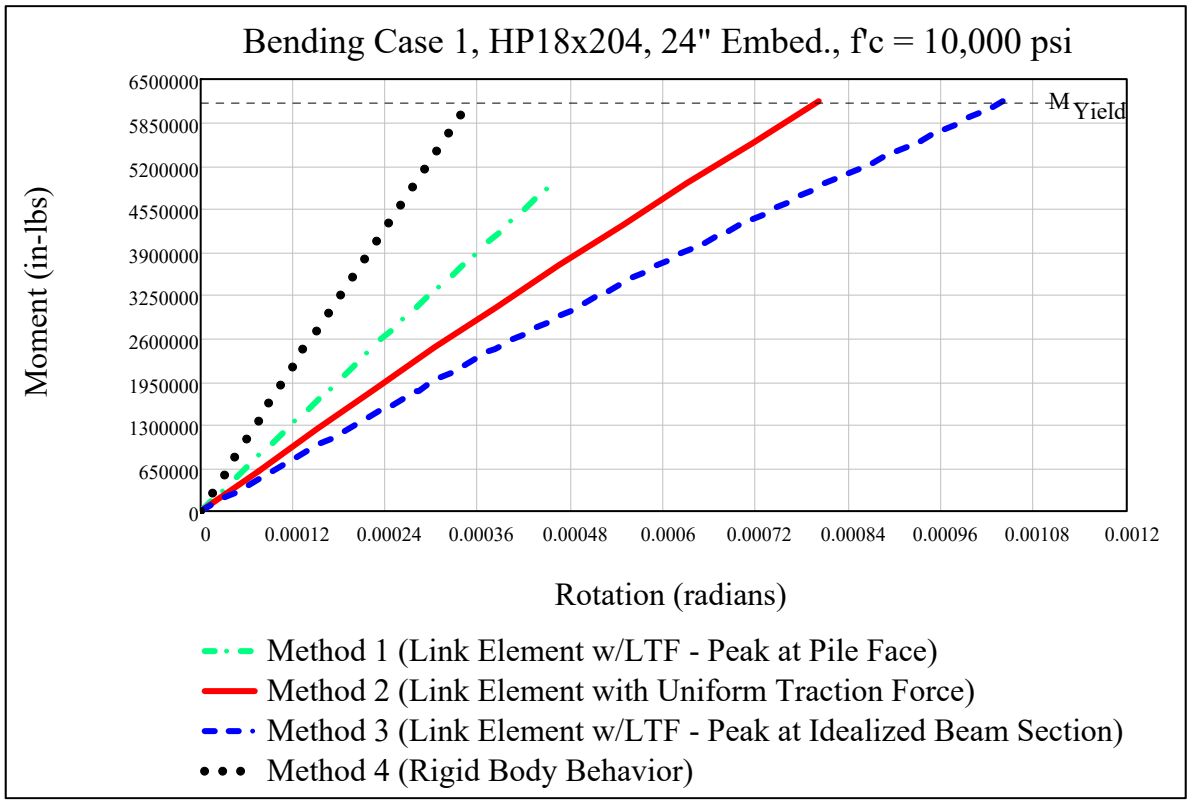
Bending Case 1, HP18x204, 24" Embed., f'c = 10,000 psi
Moment (in-lbs)
6500000
5850000
5200000
4550000
3900000
3250000
2600000
1950000
1300000
650000
0
M Yield
0
0.00012
0.00024
0.00036
0.00048
0.0006
0.00072
0.00084
0.00096
0.00108
0.0012
Rotation (radians)
Method 1 (Link Element w/LTF - Peak at Pile Face)
Method 2 (Link Element with Uniform Traction Force)
Method 3 (Link Element w/LTF - Peak at Idealized Beam Section)
Method 4 (Rigid Body Behavior)

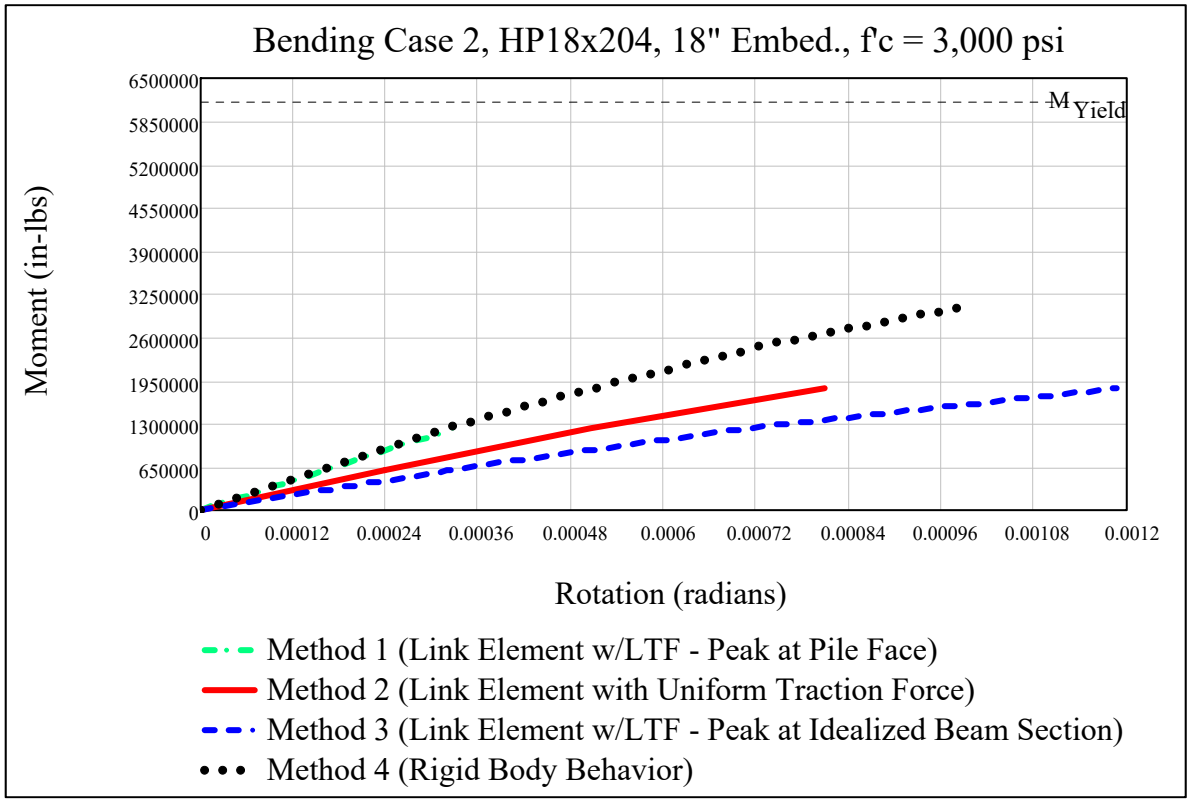
Bending Case 2, HP18x204, 18" Embed., f'c = 3,000 psi
Moment (in-lbs)
6500000
5850000
5200000
4550000
3900000
3250000
2600000
1950000
1300000
650000
0
M Yield
0
0.00012
0.00024
0.00036
0.00048
0.0006
0.00072
0.00084
0.00096
0.00108
0.0012
Rotation (radians)
Method 1 (Link Element w/LTF - Peak at Pile Face)
Method 2 (Link Element with Uniform Traction Force)
Method 3 (Link Element w/LTF - Peak at Idealized Beam Section)
Method 4 (Rigid Body Behavior)

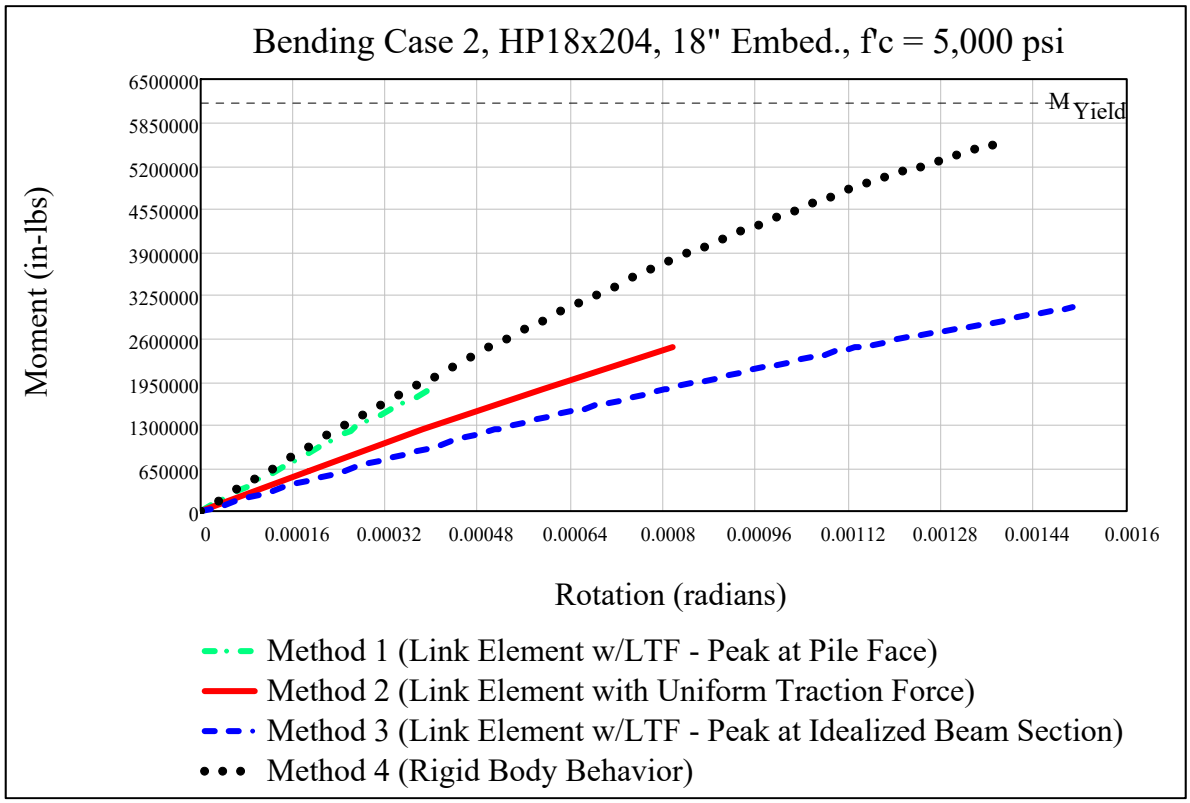
Bending Case 2, HP18x204, 18" Embed., f'c = 5,000 psi
Moment (in-lbs)
6500000
5850000
5200000
4550000
3900000
3250000
2600000
1950000
1300000
650000
0
M Yield
0
0.00016
0.00032
0.00048
0.00064
0.0008
0.00096
0.00112
0.00128
0.00144
0.0016
Rotation (radians)
Method 1 (Link Element w/LTF - Peak at Pile Face)
Method 2 (Link Element with Uniform Traction Force)
Method 3 (Link Element w/LTF - Peak at Idealized Beam Section)
Method 4 (Rigid Body Behavior)

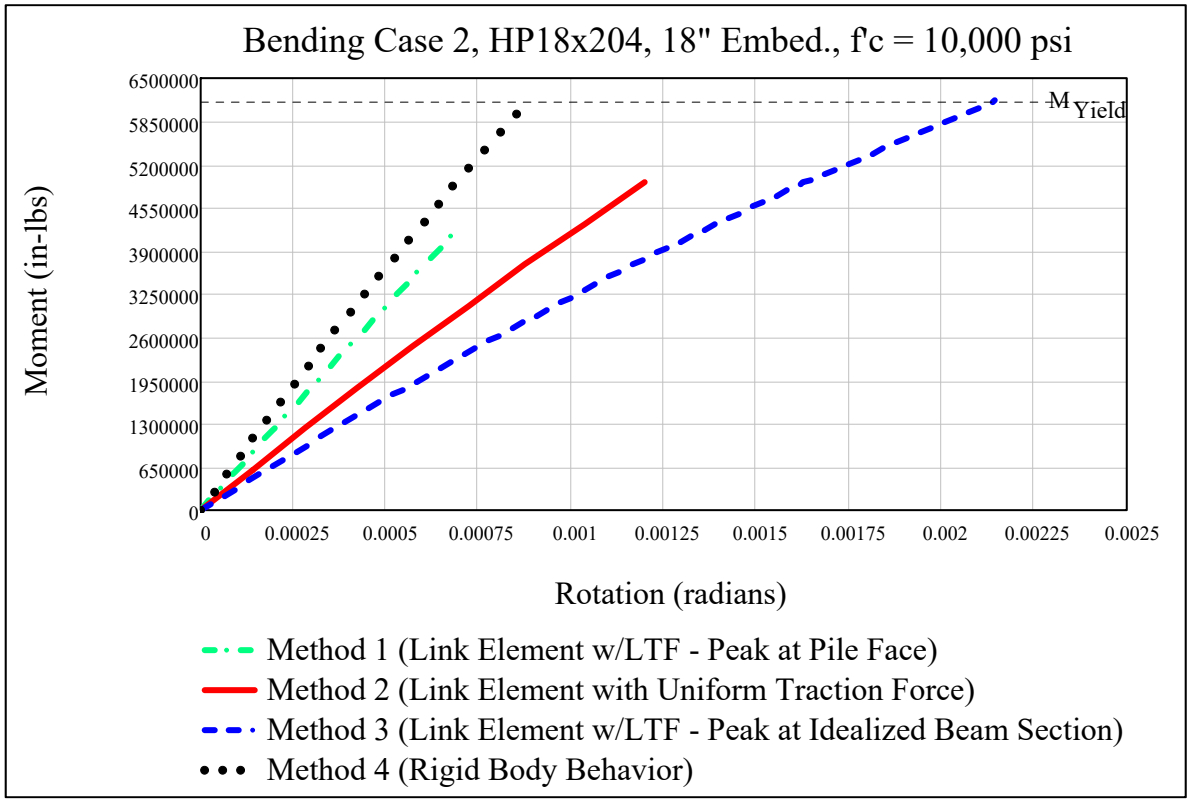
Bending Case 2, HP18x204, 18" Embed., f'c = 10,000 psi
Moment (in-lbs)
6500000
5850000
5200000
4550000
3900000
3250000
2600000
1950000
1300000
650000
0
M Yield
0
0.00025
0.0005
0.00075
0.001
0.00125
0.0015
0.00175
0.002
0.00225
0.0025
Rotation (radians)
Method 1 (Link Element w/LTF - Peak at Pile Face)
Method 2 (Link Element with Uniform Traction Force)
Method 3 (Link Element w/LTF - Peak at Idealized Beam Section)
Method 4 (Rigid Body Behavior)

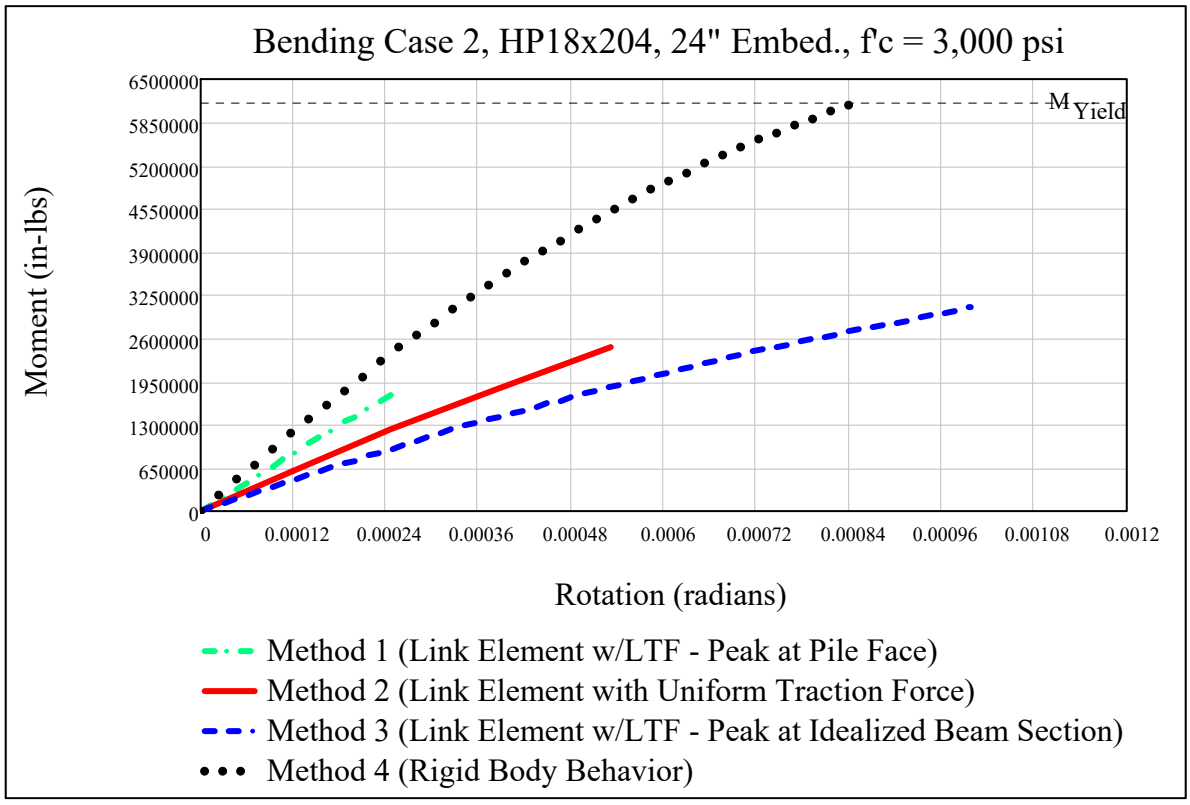
Bending Case 2, HP18x204, 24" Embed., f'c = 3,000 psi
Moment (in-lbs)
6500000
5850000
5200000
4550000
3900000
3250000
2600000
1950000
1300000
650000
0
M Yield
0
0.00012
0.00024
0.00036
0.00048
0.0006
0.00072
0.00084
0.00096
0.00108
0.0012
Rotation (radians)
Method 1 (Link Element w/LTF - Peak at Pile Face)
Method 2 (Link Element with Uniform Traction Force)
Method 3 (Link Element w/LTF - Peak at Idealized Beam Section)
Method 4 (Rigid Body Behavior)

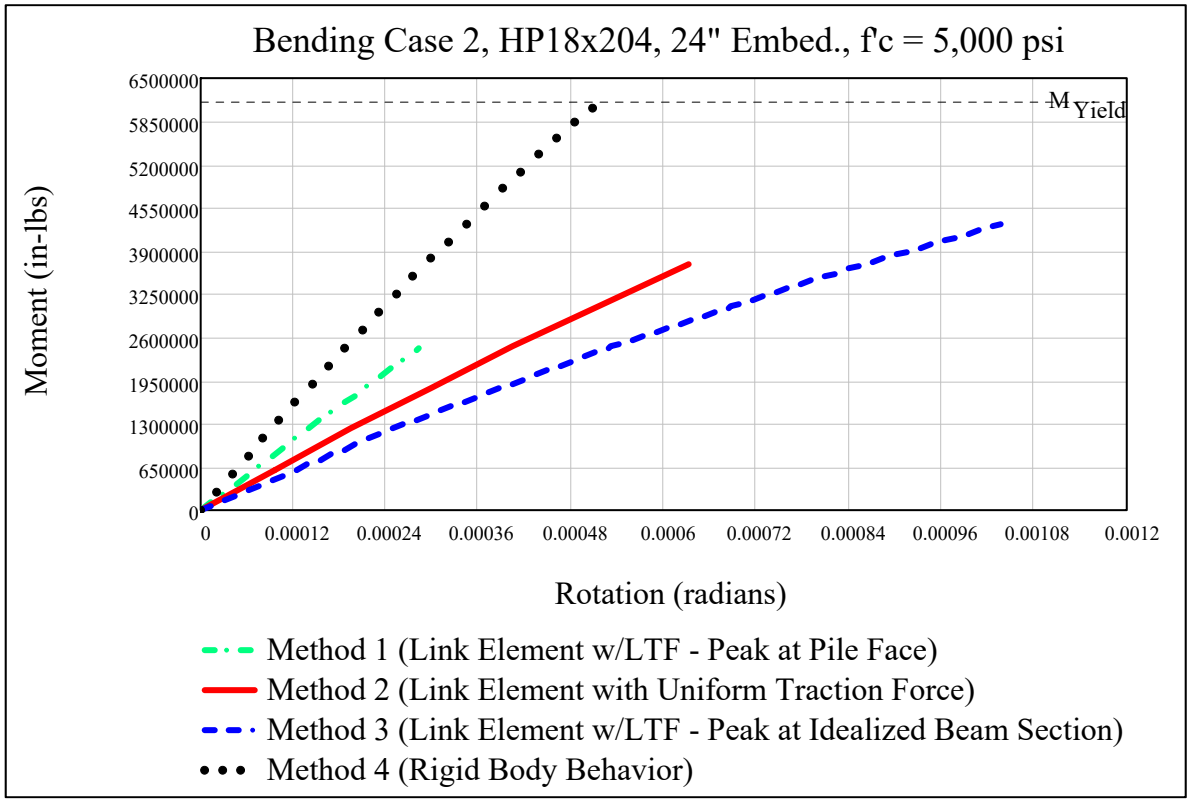
Bending Case 2, HP18x204, 24" Embed., f'c = 5,000 psi
Moment (in-lbs)
6500000
5850000
5200000
4550000
3900000
3250000
2600000
1950000
1300000
650000
0
M Yield
0
0.00012
0.00024
0.00036
0.00048
0.0006
0.00072
0.00084
0.00096
0.00108
0.0012
Rotation (radians)
Method 1 (Link Element w/LTF - Peak at Pile Face)
Method 2 (Link Element with Uniform Traction Force)
Method 3 (Link Element w/LTF - Peak at Idealized Beam Section)
Method 4 (Rigid Body Behavior)

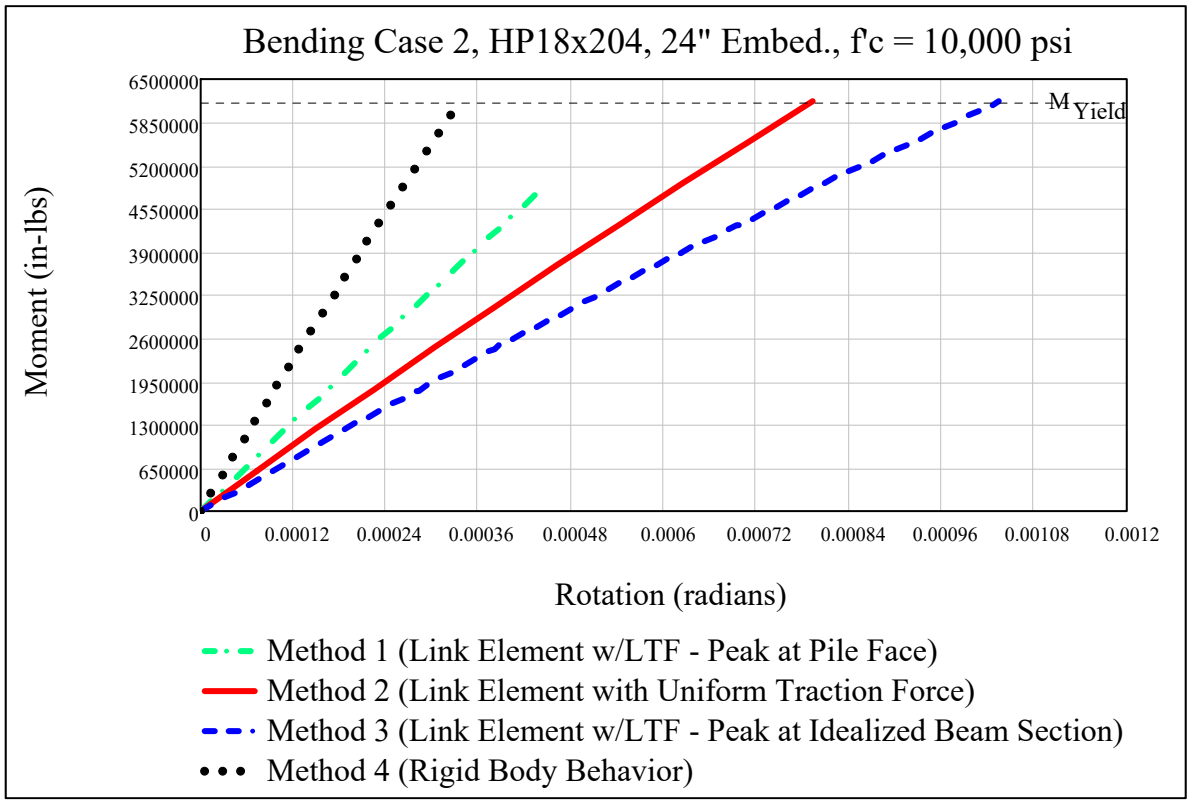
Bending Case 2, HP18x204, 24" Embed., f'c = 10,000 psi
Moment (in-lbs)
6500000
5850000
5200000
4550000
3900000
3250000
2600000
1950000
1300000
650000
0
M Yield
0
0.00012
0.00024
0.00036
0.00048
0.0006
0.00072
0.00084
0.00096
0.00108
0.0012
Rotation (radians)
Method 1 (Link Element w/LTF - Peak at Pile Face)
Method 2 (Link Element with Uniform Traction Force)
Method 3 (Link Element w/LTF - Peak at Idealized Beam Section)
Method 4 (Rigid Body Behavior)

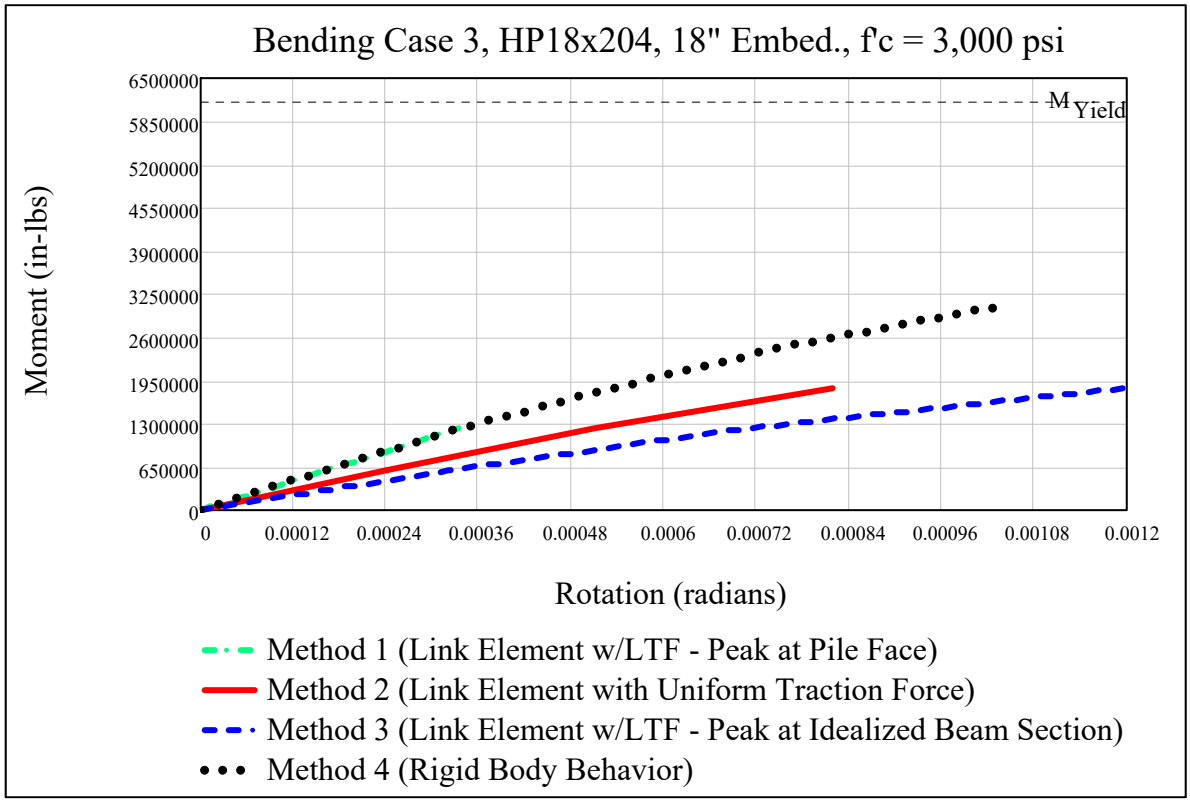
Bending Case 3, HP18x204, 18" Embed., f'c = 3,000 psi
Moment (in-lbs)
6500000
5850000
5200000
4550000
3900000
3250000
2600000
1950000
1300000
650000
0
M Yield
0
0.00012
0.00024
0.00036
0.00048
0.0006
0.00072
0.00084
0.00096
0.00108
0.0012
Rotation (radians)
Method 1 (Link Element w/LTF - Peak at Pile Face)
Method 2 (Link Element with Uniform Traction Force)
Method 3 (Link Element w/LTF - Peak at Idealized Beam Section)
Method 4 (Rigid Body Behavior)

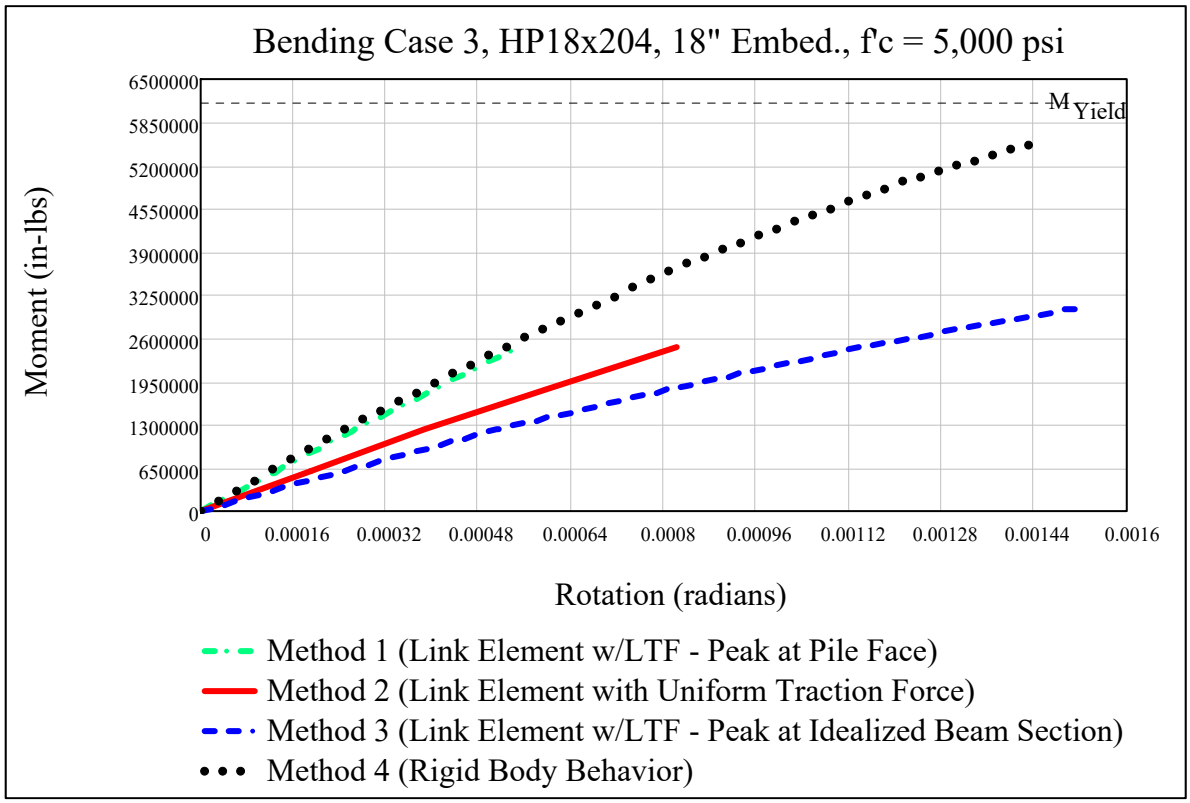
Bending Case 3, HP18x204, 18" Embed., f'c = 5,000 psi
Moment (in-lbs)
6500000
5850000
5200000
4550000
3900000
3250000
2600000
1950000
1300000
650000
0
M Yield
0
0.00016
0.00032
0.00048
0.00064
0.0008
0.00096
0.00112
0.00128
0.00144
0.0016
Rotation (radians)
Method 1 (Link Element w/LTF - Peak at Pile Face)
Method 2 (Link Element with Uniform Traction Force)
Method 3 (Link Element w/LTF - Peak at Idealized Beam Section)
Method 4 (Rigid Body Behavior)

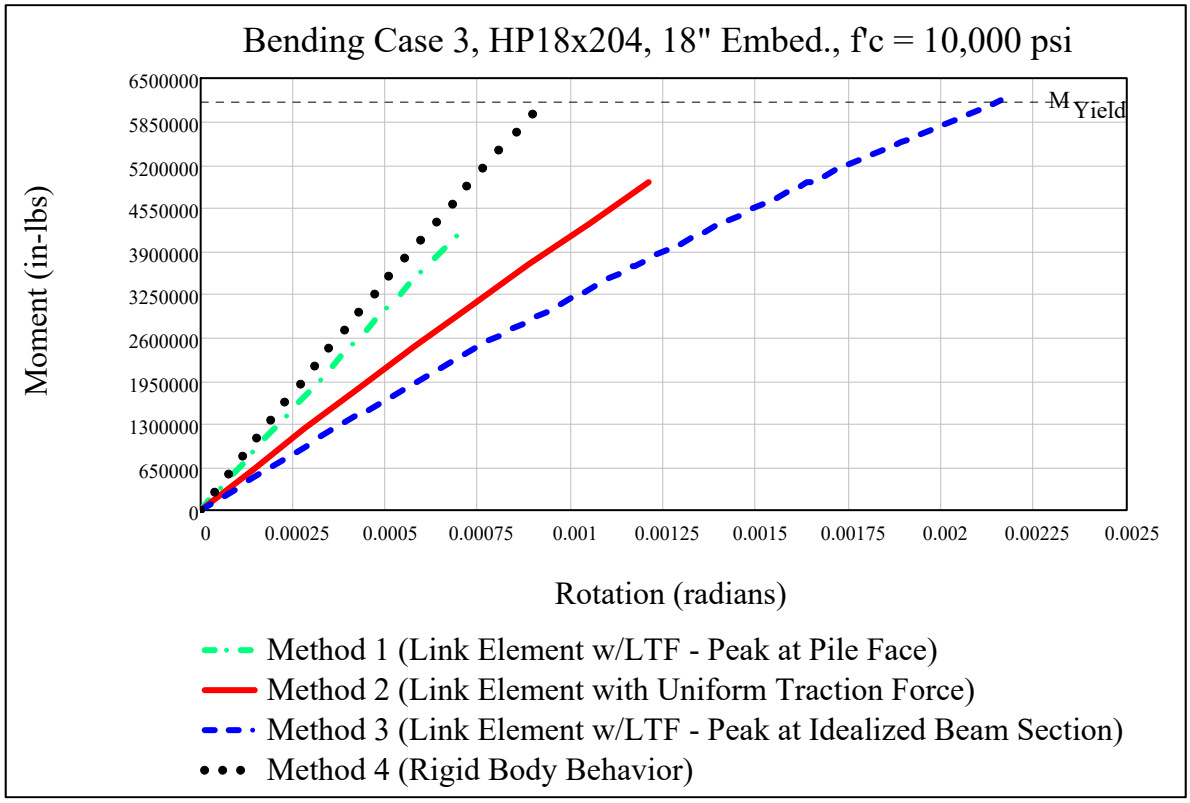
Bending Case 3, HP18x204, 18" Embed., f'c = 10,000 psi
Moment (in-lbs)
6500000
5850000
5200000
4550000
3900000
3250000
2600000
1950000
1300000
650000
0
M Yield
0
0.00025
0.0005
0.00075
0.001
0.00125
0.0015
0.00175
0.002
0.00225
0.0025
Rotation (radians)
Method 1 (Link Element w/LTF - Peak at Pile Face)
Method 2 (Link Element with Uniform Traction Force)
Method 3 (Link Element w/LTF - Peak at Idealized Beam Section)
Method 4 (Rigid Body Behavior)

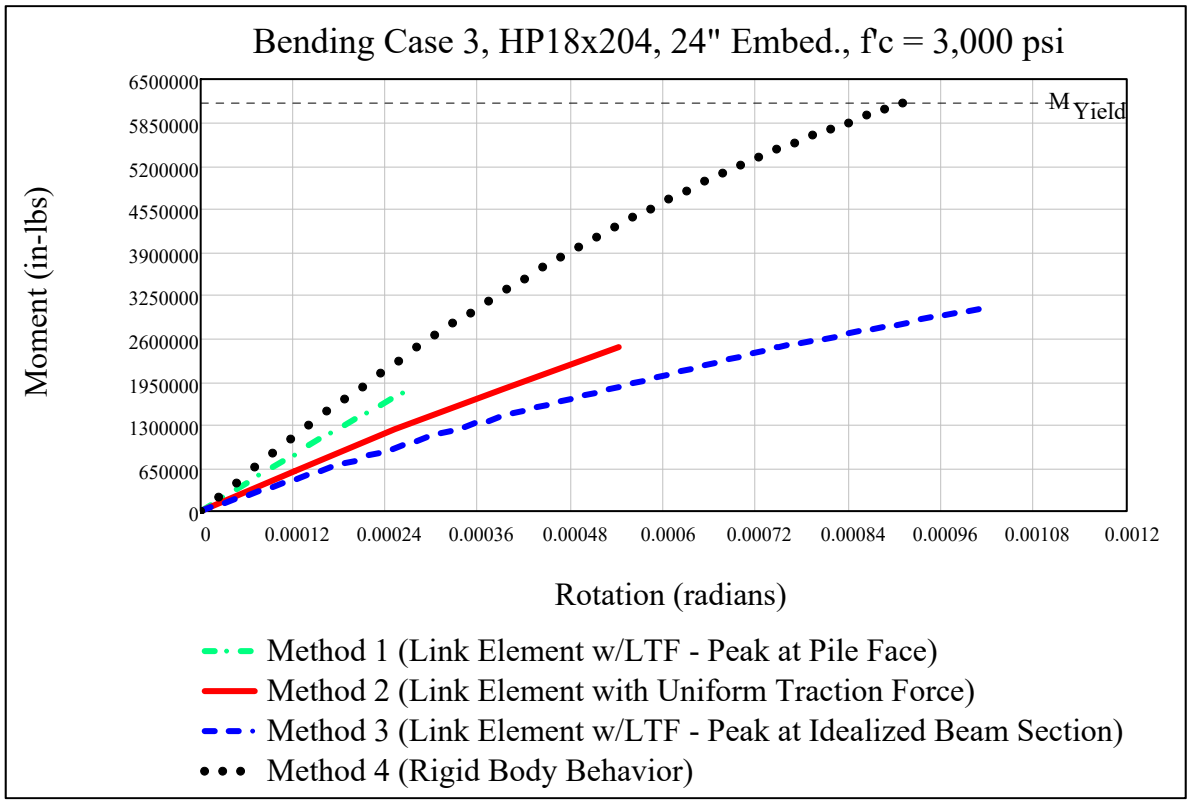
Bending Case 3, HP18x204, 24" Embed., f'c = 3,000 psi
Moment (in-lbs)
6500000
5850000
5200000
4550000
3900000
3250000
2600000
1950000
1300000
650000
0
M Yield
0
0.00012
0.00024
0.00036
0.00048
0.0006
0.00072
0.00084
0.00096
0.00108
0.0012
Rotation (radians)
Method 1 (Link Element w/LTF - Peak at Pile Face)
Method 2 (Link Element with Uniform Traction Force)
Method 3 (Link Element w/LTF - Peak at Idealized Beam Section)
Method 4 (Rigid Body Behavior)

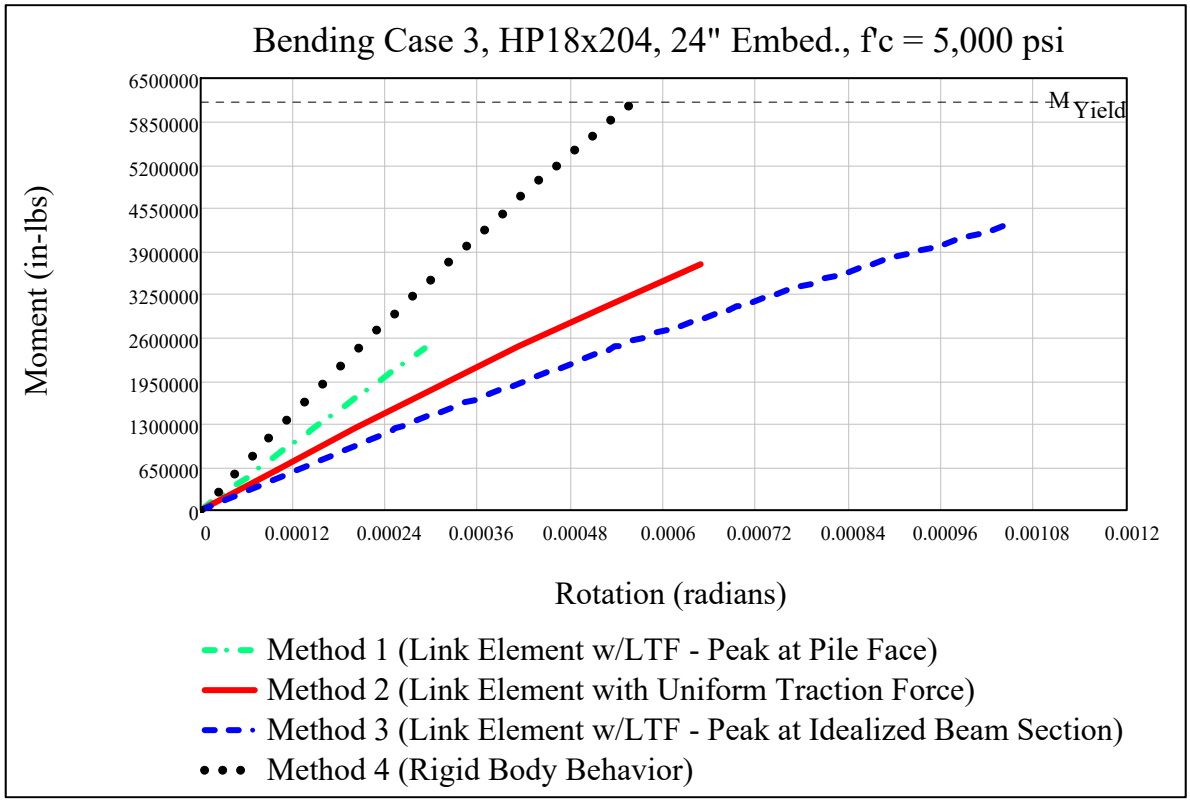
Bending Case 3, HP18x204, 24" Embed., f'c = 5,000 psi
Moment (in-lbs)
6500000
5850000
5200000
4550000
3900000
3250000
2600000
1950000
1300000
650000
0
M Yield
0
0.00012
0.00024
0.00036
0.00048
0.0006
0.00072
0.00084
0.00096
0.00108
0.0012
Rotation (radians)
Method 1 (Link Element w/LTF - Peak at Pile Face)
Method 2 (Link Element with Uniform Traction Force)
Method 3 (Link Element w/LTF - Peak at Idealized Beam Section)
Method 4 (Rigid Body Behavior)

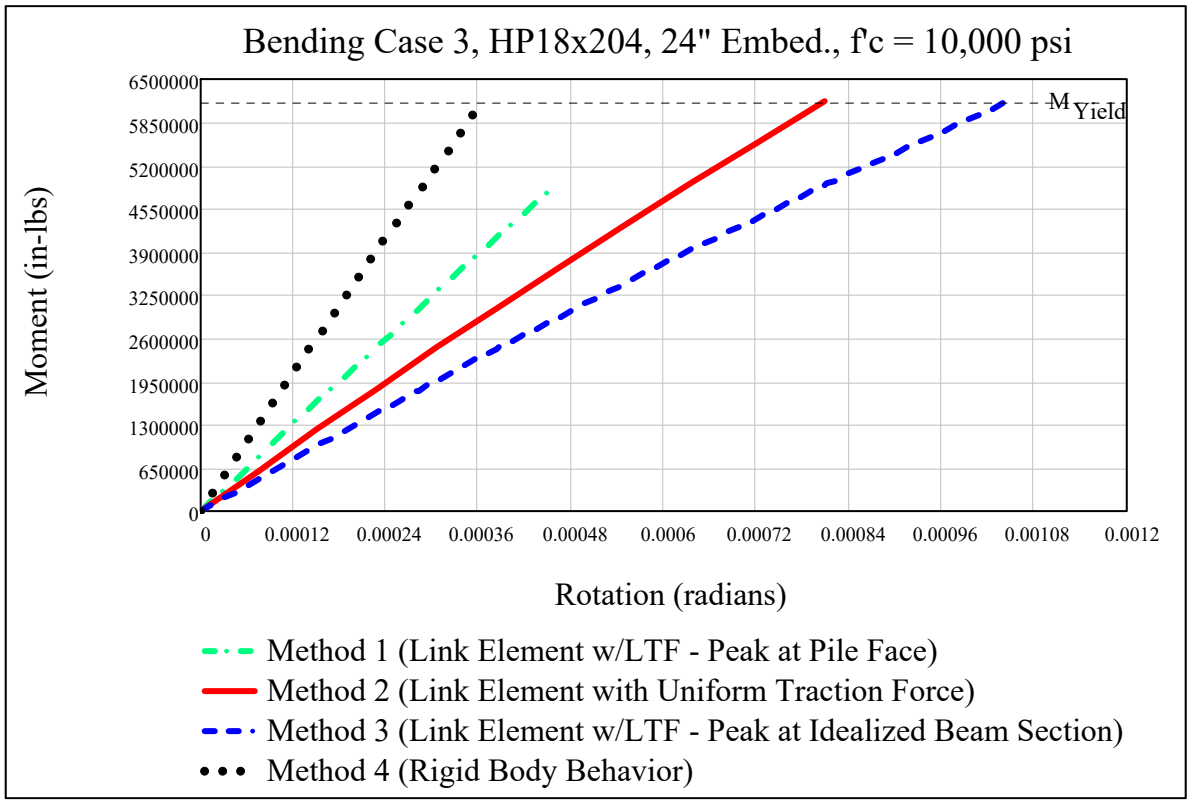
Bending Case 3, HP18x204, 24" Embed., f'c = 10,000 psi
Moment (in-lbs)
6500000
5850000
5200000
4550000
3900000
3250000
2600000
1950000
1300000
650000
0
M Yield
0
0.00012
0.00024
0.00036
0.00048
0.0006
0.00072
0.00084
0.00096
0.00108
0.0012
Rotation (radians)
Method 1 (Link Element w/LTF - Peak at Pile Face)
Method 2 (Link Element with Uniform Traction Force)
Method 3 (Link Element w/LTF - Peak at Idealized Beam Section)
Method 4 (Rigid Body Behavior)

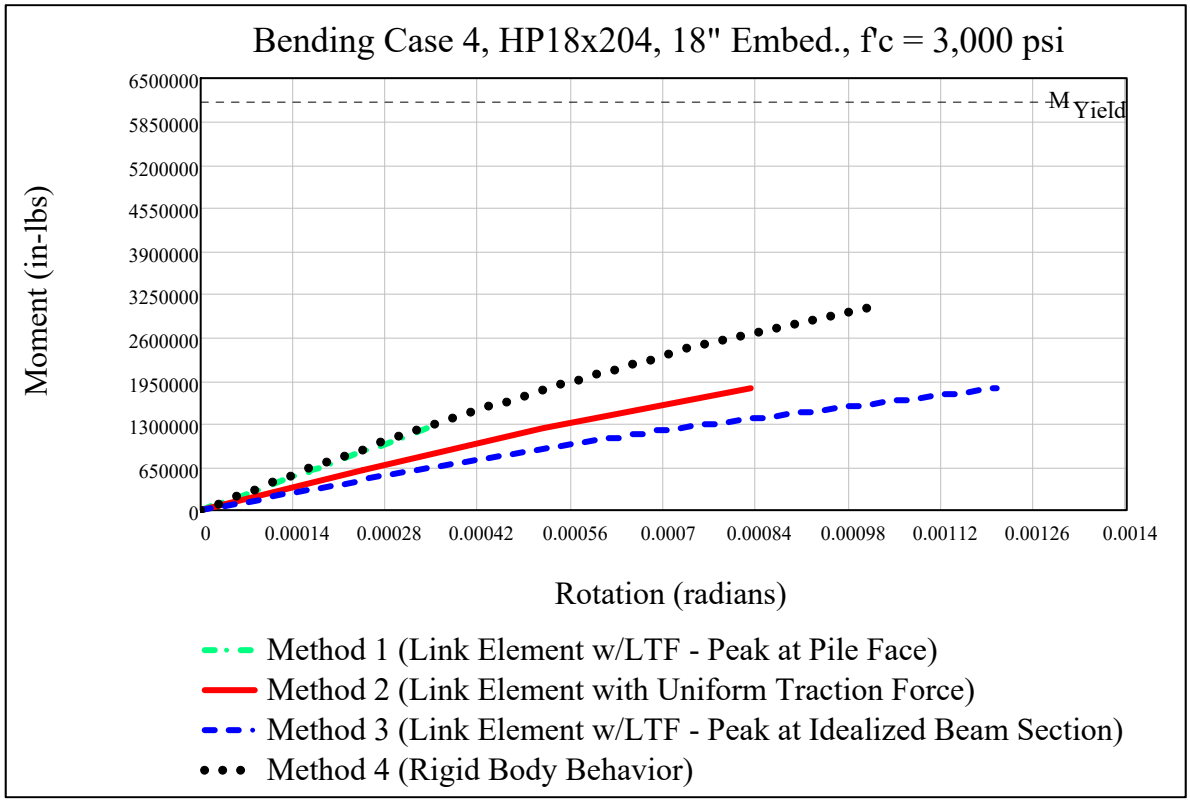
Bending Case 4, HP18x204, 18" Embed., f'c = 3,000 psi
Moment (in-lbs)
6500000
5850000
5200000
4550000
3900000
3250000
2600000
1950000
1300000
650000
0
M Yield
0
0.00014
0.00028
0.00042
0.00056
0.0007
0.00084
0.00098
0.00112
0.00126
0.0014
Rotation (radians)
Method 1 (Link Element w/LTF - Peak at Pile Face)
Method 2 (Link Element with Uniform Traction Force)
Method 3 (Link Element w/LTF - Peak at Idealized Beam Section)
Method 4 (Rigid Body Behavior)

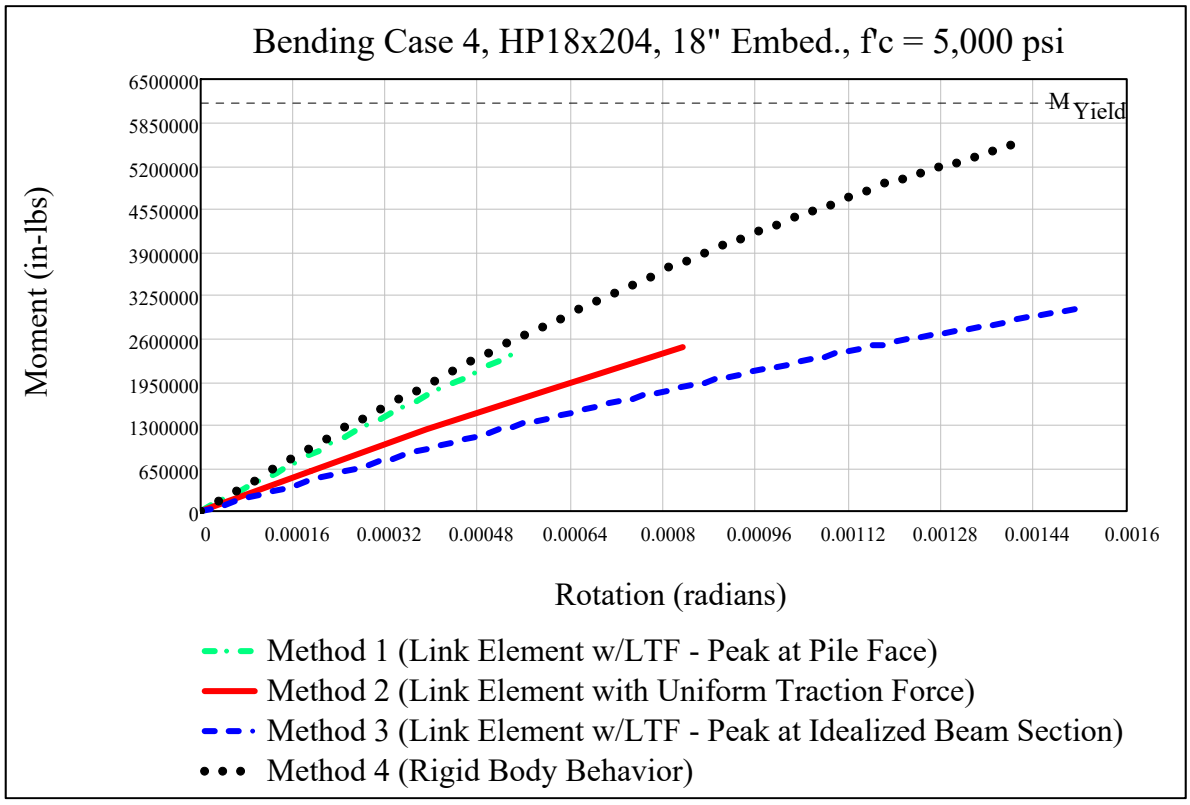
Bending Case 4, HP18x204, 18" Embed., f'c = 5,000 psi
Moment (in-lbs)
6500000
5850000
5200000
4550000
3900000
3250000
2600000
1950000
1300000
650000
0
M Yield
0
0.00016
0.00032
0.00048
0.00064
0.0008
0.00096
0.00112
0.00128
0.00144
0.0016
Rotation (radians)
Method 1 (Link Element w/LTF - Peak at Pile Face)
Method 2 (Link Element with Uniform Traction Force)
Method 3 (Link Element w/LTF - Peak at Idealized Beam Section)
Method 4 (Rigid Body Behavior)

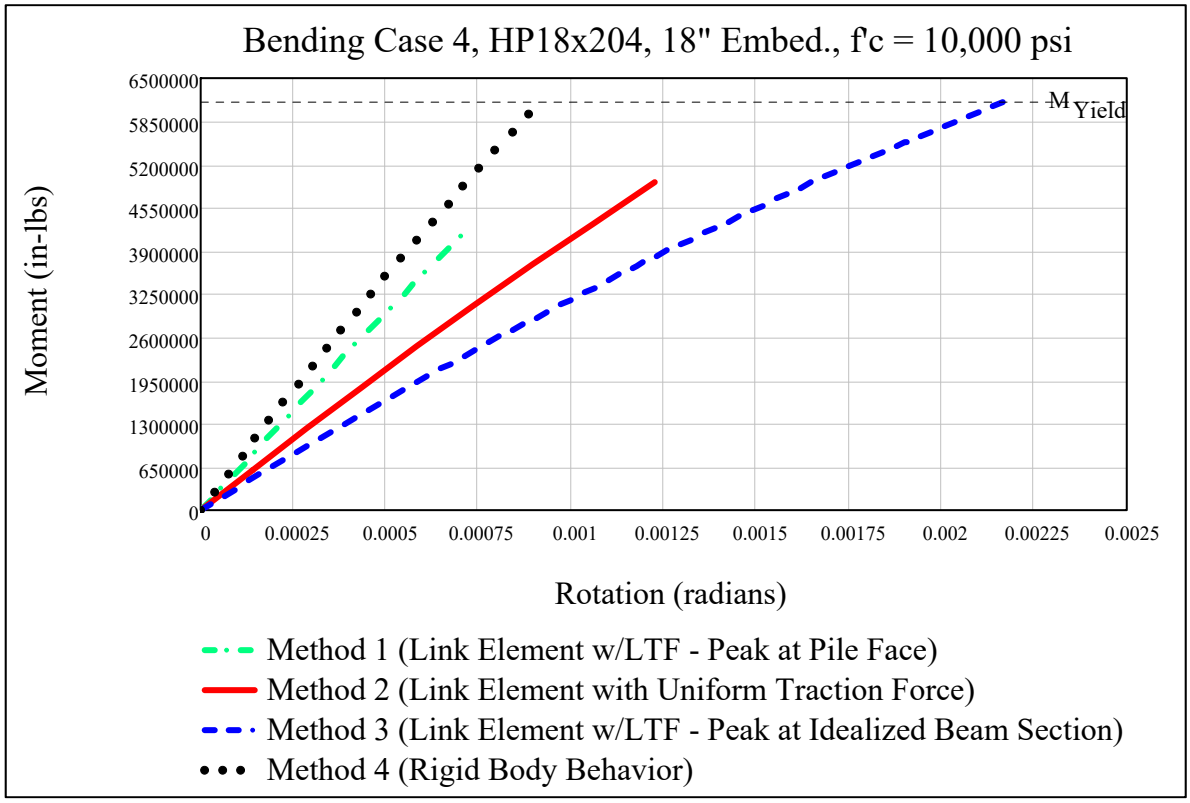
Bending Case 4, HP18x204, 18" Embed., f'c = 10,000 psi
Moment (in-lbs)
6500000
5850000
5200000
4550000
3900000
3250000
2600000
1950000
1300000
650000
0
M Yield
0
0.00025
0.0005
0.00075
0.001
0.00125
0.0015
0.00175
0.002
0.00225
0.0025
Rotation (radians)
Method 1 (Link Element w/LTF - Peak at Pile Face)
Method 2 (Link Element with Uniform Traction Force)
Method 3 (Link Element w/LTF - Peak at Idealized Beam Section)
Method 4 (Rigid Body Behavior)

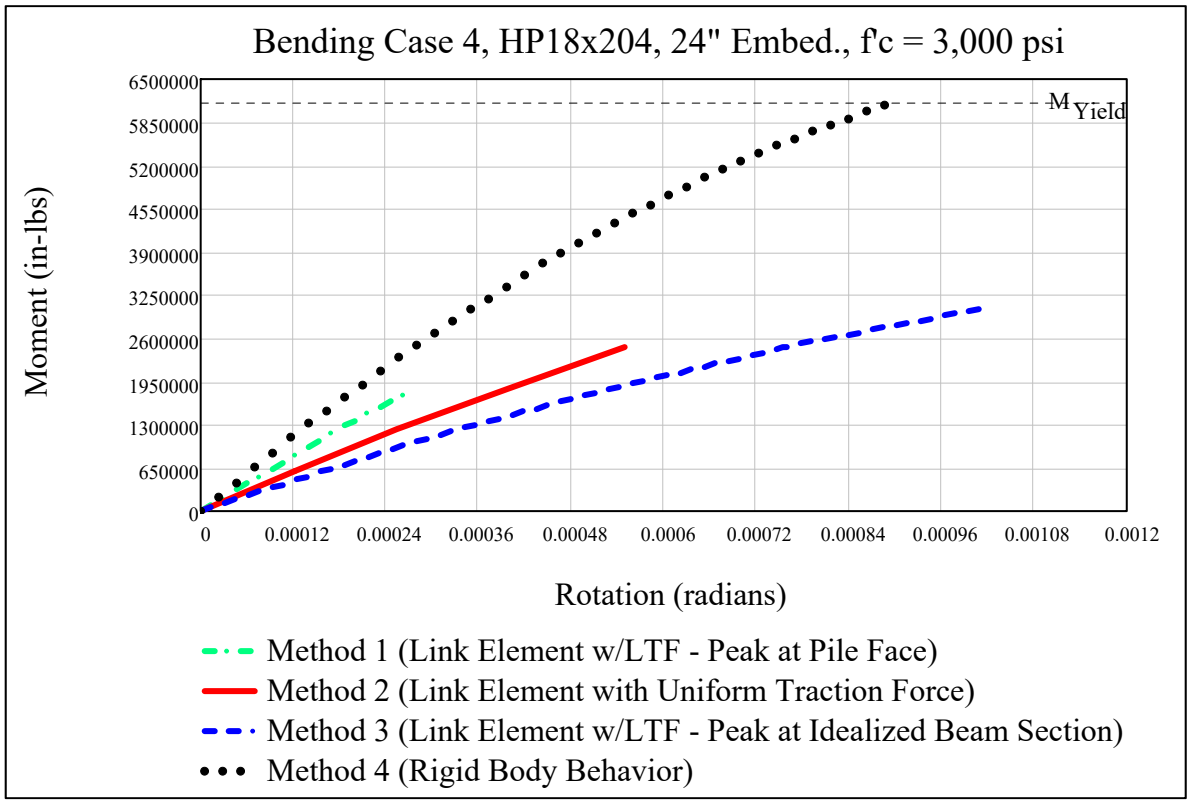
Bending Case 4, HP18x204, 24" Embed., f'c = 3,000 psi
Moment (in-lbs)
6500000
5850000
5200000
4550000
3900000
3250000
2600000
1950000
1300000
650000
0
M Yield
0
0.00012
0.00024
0.00036
0.00048
0.0006
0.00072
0.00084
0.00096
0.00108
0.0012
Rotation (radians)
Method 1 (Link Element w/LTF - Peak at Pile Face)
Method 2 (Link Element with Uniform Traction Force)
Method 3 (Link Element w/LTF - Peak at Idealized Beam Section)
Method 4 (Rigid Body Behavior)

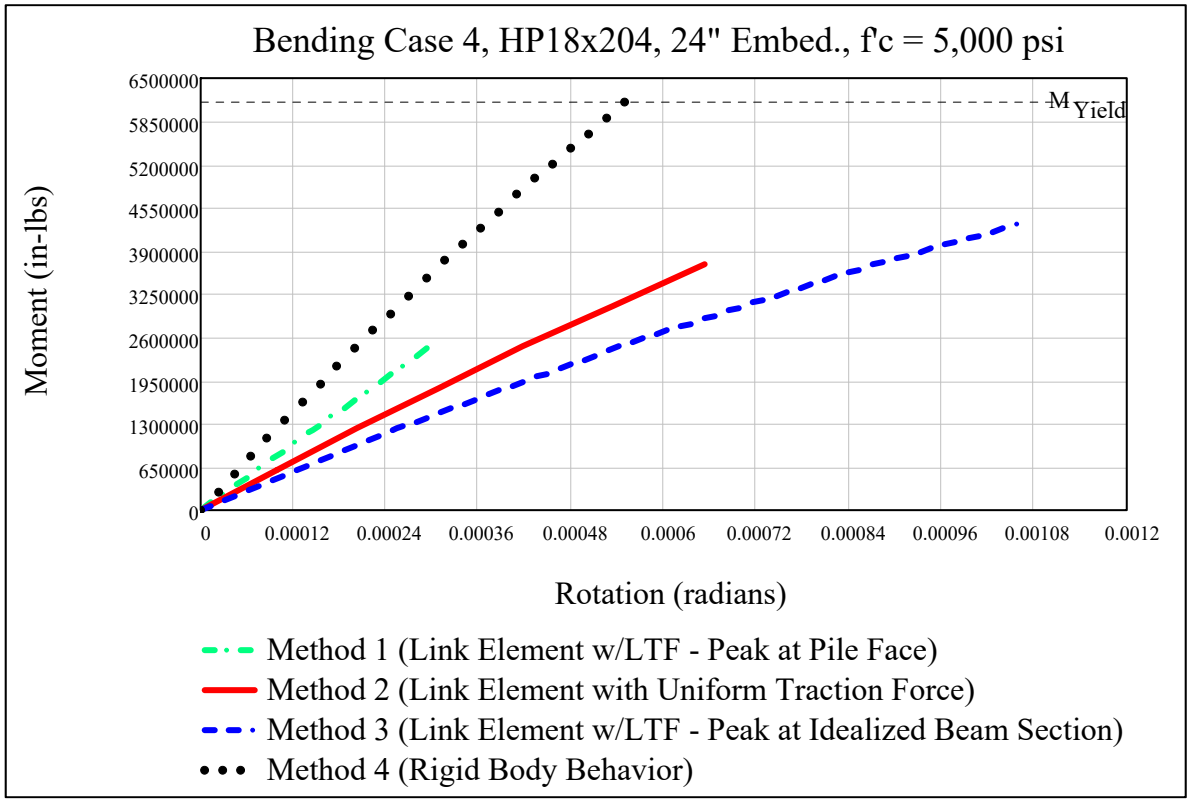
Bending Case 4, HP18x204, 24" Embed., f'c = 5,000 psi
Moment (in-lbs)
6500000
5850000
5200000
4550000
3900000
3250000
2600000
1950000
1300000
650000
0
M Yield
0
0.00012
0.00024
0.00036
0.00048
0.0006
0.00072
0.00084
0.00096
0.00108
0.0012
Rotation (radians)
Method 1 (Link Element w/LTF - Peak at Pile Face)
Method 2 (Link Element with Uniform Traction Force)
Method 3 (Link Element w/LTF - Peak at Idealized Beam Section)
Method 4 (Rigid Body Behavior)

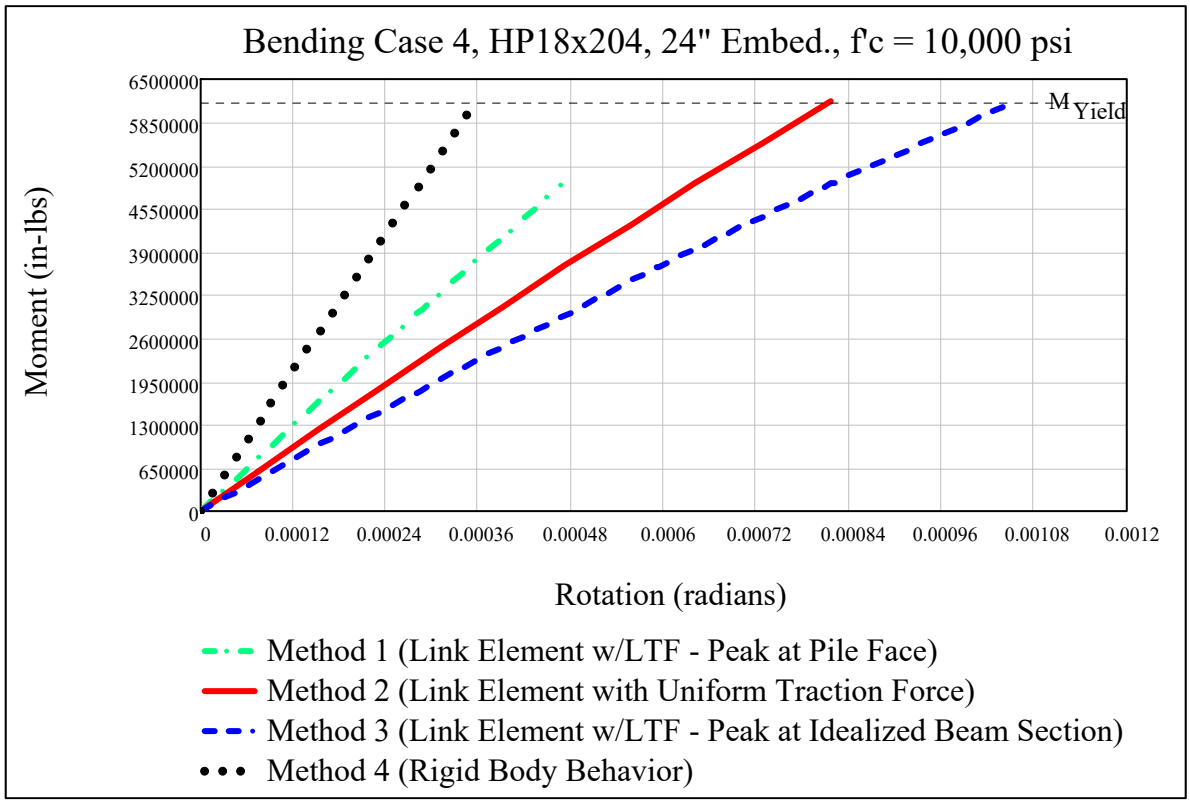
Bending Case 4, HP18x204, 24" Embed., f'c = 10,000 psi
Moment (in-lbs)
6500000
5850000
5200000
4550000
3900000
3250000
2600000
1950000
1300000
650000
0
M Yield
0
0.00012
0.00024
0.00036
0.00048
0.0006
0.00072
0.00084
0.00096
0.00108
0.0012
Rotation (radians)
Method 1 (Link Element w/LTF - Peak at Pile Face)
Method 2 (Link Element with Uniform Traction Force)
Method 3 (Link Element w/LTF - Peak at Idealized Beam Section)
Method 4 (Rigid Body Behavior)

Theoretical Moment-Rotation Curve for Embedded Steel Piles

ORIGIN := 1

Steel Data (pounds, inches):

$E_s := 29000000$ $f_y := 36000$ $f_{su} := 58000$

$E_{sh} := 1160000$ $\varepsilon_{sh} := 0.008$ $\varepsilon_{su} := 0.12$

G := 11000000

$$P := \frac{E_{sh}\cdot(\varepsilon_{su} - \varepsilon_{sh})}{(f_{su} - f_y)} = 5.91$$

$$f_{sLinear}(\varepsilon_s) := \begin{cases} E_s\cdot\varepsilon_s & \text{if } \varepsilon_s \le \frac{f_y}{E_s} \\ f_y & \text{if } \varepsilon_s > \frac{f_y}{E_s} \end{cases}$$

$$f_s(\varepsilon_s) := \left| \begin{array}{l} \text{"Steel stress-strain curve equation, assumed to be symmetric about origin."} \\ \text{"From "Stress-Block Parameters for Unconfined and Confined Concrete Based on a Unified Stress-Strain Model" by Karthik and Mander, 2011."} \\ \dfrac{E_s\cdot\varepsilon_s}{\left[1 + \left(\left|\dfrac{E_s\cdot\varepsilon_s}{f_y}\right|\right)^{20}\right]^{0.05}} + (f_{su} - f_y)\cdot\left[1 - \dfrac{(|\varepsilon_{su} - \varepsilon_s|)^P}{\left[(|\varepsilon_{su} - \varepsilon_{sh}|)^{20\cdot P} + (|\varepsilon_{su} - \varepsilon_s|)^{20\cdot P}\right]^{0.05}}\right] \end{array} \right.$$

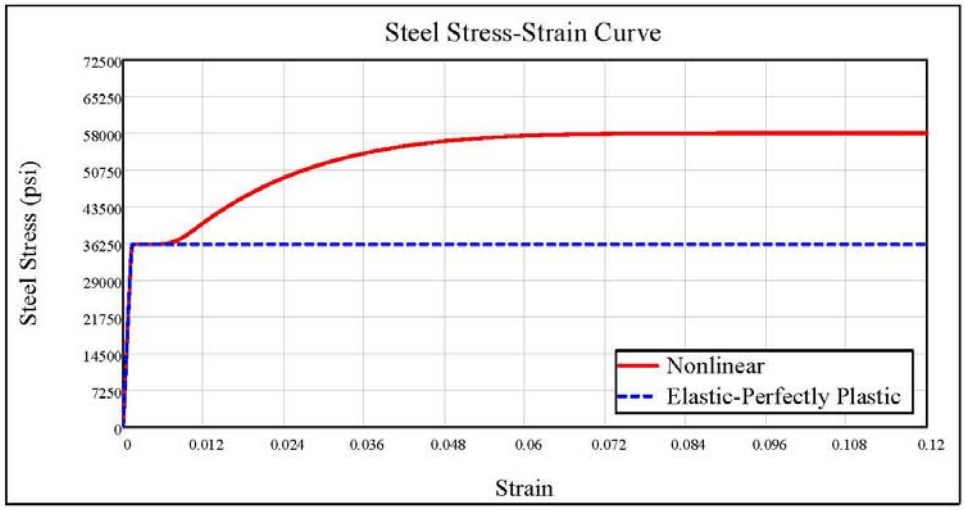

Moment Capacity of Pile Bent About Weak Axis (pounds, inches):

$b_f :=$	"Pile Flange Width" 10.1	$t_{fw} :=$	"Flange and Web Thickness" 0.420	d :=	"Depth of Pile" 9.70	NoFbrsPile :=	"Any Number" 50

FbrLocPile :=

"Calculates fiber locations over one-half of the symmetric cross-section."

for $i \in 1 .. NoFbrsPile$

"Fiber Locations Above Web Face"

$$y_i \leftarrow \frac{b_f}{2} - \left(\frac{\frac{b_f}{2} - \frac{t_{fw}}{2}}{NoFbrsPile - 1} \right) \cdot (i - 1) \quad \text{if } i < NoFbrsPile$$

"Fiber Location at Web Face"

$$y_i \leftarrow \frac{t_{fw}}{2} \quad \text{if } i = NoFbrsPile$$

y

StrainPile :=	"Bottom fiber strain vector."
	"Increase NoPnts to refine the pile moment-rotation curve."
	$NoPnts \leftarrow 500$
	for $i \in 1 .. NoPnts$
	$\varepsilon_i \leftarrow \left(\frac{i - 1}{NoPnts - 1} \right) \cdot \varepsilon_{su}$
	ε

TribAreaPile :=

"Calculates tributary area (in2) for each fiber."

for $i \in 1 .. NoFbrsPile$

"Tributary area for fiber at flange tips."

$$ta_i \leftarrow \left(\frac{1}{2} \right) \cdot \left(\frac{\frac{b_f}{2} - \frac{t_{fw}}{2}}{NoFbrsPile - 1} \right) \cdot (t_{fw}) \cdot (2) \quad \text{if } i = 1$$

"Tributary area for fibers between tips and web face."

$$ta_i \leftarrow \left(\frac{\frac{b_f}{2} - \frac{t_{fw}}{2}}{NoFbrsPile - 1} \right) \cdot (t_{fw}) \cdot (2) \quad \text{if } 1 < i < NoFbrsPile$$

"Tributary area for fiber at web face."

$$ta_i \leftarrow \left(\frac{1}{2} \right) \cdot \left(\frac{\frac{b_f}{2} - \frac{t_{fw}}{2}}{NoFbrsPile - 1} \right) \cdot (t_{fw}) \cdot (2) + \left(\frac{t_{fw}}{4} \right) \cdot d \quad \text{if } i = NoFbrsPile$$

ta

PileMomentNL :=

"Pile moment (in-lbs) corresponding to each bottom fiber strain."

"Strain at each fiber is calculated using the assumption that plane sections remain plane."

for $i \in 1 .. \text{rows}(\text{StrainPile})$

$j \leftarrow 1 .. \text{rows}(\text{FbrLocPile})$

$$m_i \leftarrow 2 \cdot \sum_j \left[f_s\left(\text{StrainPile}_i \cdot \frac{\text{FbrLocPile}_j}{\frac{b_f}{2}} \right) \cdot \left(\text{TribAreaPile}_j\right) \cdot \left(\text{FbrLocPile}_j\right) \right]$$

m

Moment Curves (pounds, inches):

Note: The elastic section modulus, Sy and plastic section modulus, Zy shown below were taken from the AISC Steel Construction Manual, 14th ed.

$I_y := 71.7$ $S_y := 14.2$ $Z_y := 21.8$ $A_{xs} := 12.4$

$$\text{StrainPileLinear} := \begin{pmatrix} 0 \\ \frac{f_y}{E_s} \\ \varepsilon_{su} \end{pmatrix} = \begin{pmatrix} 0.00000 \\ 0.00124 \\ 0.12000 \end{pmatrix} \qquad \text{PileMomLinear} := \begin{pmatrix} 0 \\ S_y \cdot f_y \\ Z_y \cdot f_y \end{pmatrix} = \begin{pmatrix} 0 \\ 511200 \\ 784800 \end{pmatrix}$$

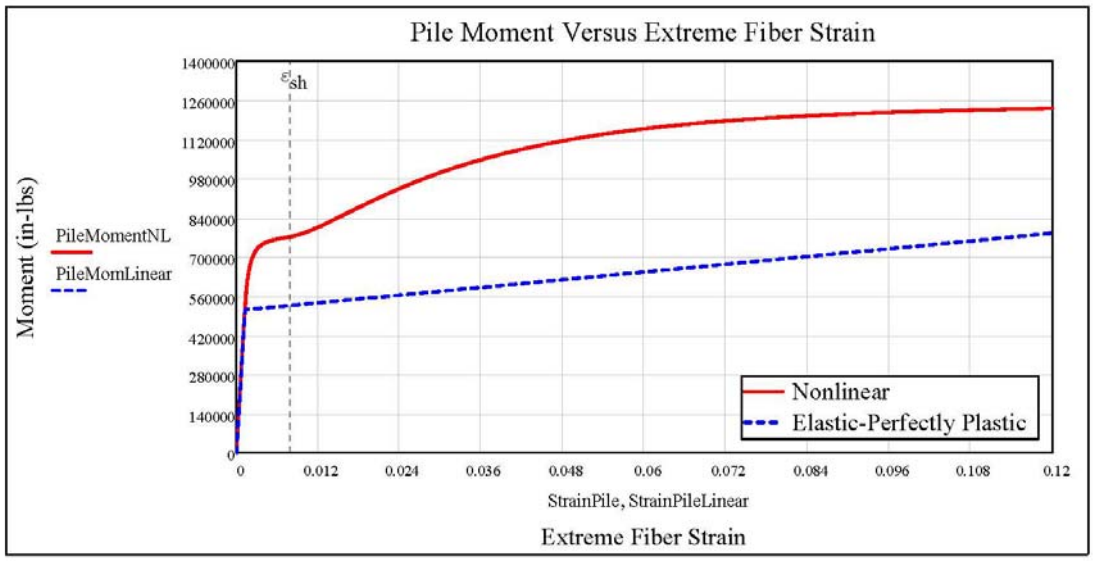

Shape Factor Determined from Nonlinear Model (Just Prior to Onset of Strain Hardening):

$$\text{YieldStrain} := \frac{f_y}{E_s} = 0.0012414$$

$$j := 1 .. \text{rows}(\text{FbrLocPile})$$

$$M_{Yield} := 2 \cdot \sum_j \left[f_s \left(\frac{f_y}{E_s} \cdot \frac{\text{FbrLocPile}_j}{\frac{b_f}{2}} \right) \cdot \left(\text{TribAreaPile}_j \right) \cdot \left(\text{FbrLocPile}_j \right) \right] = 512122$$

$$M_{Plastic} := 2 \cdot \sum_j \left[f_s \left(\varepsilon_{sh} \cdot \frac{\text{FbrLocPile}_j}{\frac{b_f}{2}} \right) \cdot \left(\text{TribAreaPile}_j \right) \cdot \left(\text{FbrLocPile}_j \right) \right] = 772761$$

$$\text{ShapeFactorNL}_{\text{NoStrainHardening}} := \frac{M_{Plastic}}{M_{Yield}} = 1.509$$

Shape Factor Determined from Nonlinear Model (At Ultimate Strain as defined in 2011 paper by Karthik and Mander):

$$M_{PlasticwithSH} := 2 \cdot \sum_j \left[f_s \left(\varepsilon_{su} \cdot \frac{\text{FbrLocPile}_j}{\frac{b_f}{2}} \right) \cdot \left(\text{TribAreaPile}_j \right) \cdot \left(\text{FbrLocPile}_j \right) \right] = 1231008$$

$$\text{ShapeFactorNL}_{\text{withStrainHardening}} := \frac{M_{PlasticwithSH}}{M_{Yield}} = 2.404$$

Concrete Data (pounds, inches):

$f_{co} := 3000$ $\quad f_{c1} := 1740$ $\quad f_{sp} := 0$

$\varepsilon_{co} := 0.0015 + \frac{f_{co}}{10000000}$ $\quad \varepsilon_{c1} := 0.0036$ $\quad \varepsilon_{sp} := \left[0.012 - (0.0000007) f_{co}\right]$

$f_{ct} := (7.5)\cdot\sqrt{f_{co}}$ $\quad \varepsilon_{ct} := (0.1)\cdot\varepsilon_{co}$ $\quad E_c := 60000\cdot\sqrt{f_{co}}$ $\quad n_c := \frac{E_c\cdot\varepsilon_{co}}{f_{co}}$ $\quad n_t := \frac{E_c\cdot\varepsilon_{ct}}{f_{ct}}$

$f_c(\varepsilon_c) :=$ "Concrete stress-strain curve equation."

"From "Stress-Block Parameters for Unconfined and Confined Concrete Based on a Unified Stress-Strain Model" by Karthik and Mander, 2011."

$f_c \leftarrow -f_{ct}\cdot\left[1 - \left(\left|1 + \frac{\varepsilon_c}{\varepsilon_{ct}}\right|\right)^{n_t}\right]$ if $\frac{\varepsilon_c}{\varepsilon_{ct}} < 0$

$f_c \leftarrow f_{co}\cdot\left[1 - \left(\left|1 - \frac{\varepsilon_c}{\varepsilon_{co}}\right|\right)^{n_c}\right]$ if $0 \le \frac{\varepsilon_c}{\varepsilon_{co}} < 1$

$f_c \leftarrow f_{co} - \left(\frac{f_{co} - f_{c1}}{\frac{\varepsilon_{c1}}{\varepsilon_{co}} - 1}\right)\cdot\left(\frac{\varepsilon_c}{\varepsilon_{co}} - 1\right)$ if $1 \le \frac{\varepsilon_c}{\varepsilon_{co}} < \frac{\varepsilon_{c1}}{\varepsilon_{co}}$

$f_c \leftarrow f_{c1}\cdot\left(\frac{\frac{\varepsilon_c}{\varepsilon_{co}} - \frac{\varepsilon_{sp}}{\varepsilon_{co}}}{\frac{\varepsilon_{c1}}{\varepsilon_{co}} - \frac{\varepsilon_{sp}}{\varepsilon_{co}}}\right)$ if $\frac{\varepsilon_{c1}}{\varepsilon_{co}} \le \frac{\varepsilon_c}{\varepsilon_{co}} < \frac{\varepsilon_{sp}}{\varepsilon_{co}}$

f_c

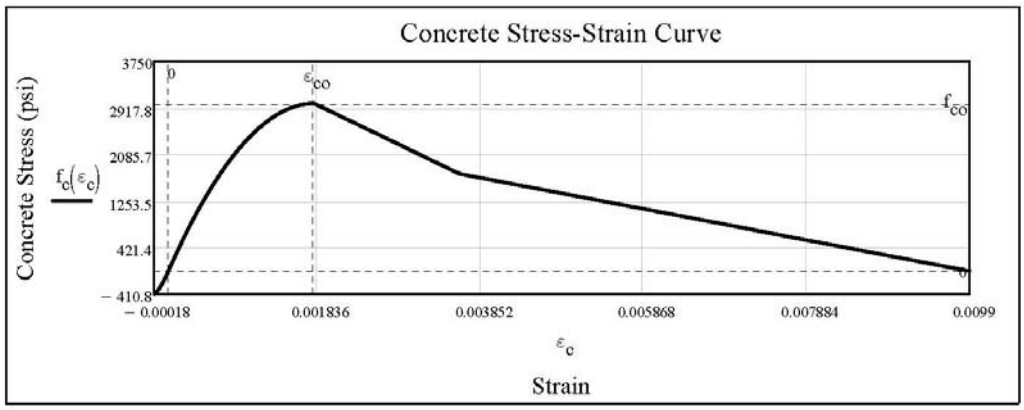

Moment Capacity of Unreinforced Concrete Beam (pounds, inches):

h :=	"Height of section." 36	b :=	"Width of section." 36	p_e :=	"Pile embeddment depth." 12

NoFbrsCap :=	"Use an odd number of fibers to create an equal number of elements above and below top of pile." 51

FbrLocCap :=

"This routine calculates fiber locations measured from bottom face in inches."

"An equal number of fibers are created above and below the top of pile."

for $i \in 1..NoFbrsCap$

"Fiber locations from bottom face to top of pile."

$$y_i \leftarrow \left[\frac{p_e}{0.5\cdot(NoFbrsCap - 1)}\right]\cdot(i - 1) \quad \text{if } i < \frac{NoFbrsCap}{2}$$

"Fiber locations above top of pile."

$$y_i \leftarrow h - \left[\frac{h - p_e}{0.5\cdot(NoFbrsCap - 1)}\right]\cdot(NoFbrsCap - i) \quad \text{if } i \geq \frac{NoFbrsCap}{2}$$

y

StrainCap :=

"This routine calculates the strain vector used in the calculation of the nonlinear cap moments below. Each entry in this vector"

"is a tension strain existing in the extreme fiber of the cross-section. A unique cap moment corresponds to each of these strains"

"and together these two values provide a unique point on the moment-strain curve below."

"Increase the NoPnts value (below) to refine the cap moment versus extreme fiber strain curve."

$NoPnts \leftarrow 21$

for $i \in 1..NoPnts$

$$\varepsilon_i \leftarrow \left(\frac{i - 1}{NoPnts - 1}\right)\cdot\varepsilon_{ct}$$

ε

TribAreaCap :=

"This routine calculates the tributary area (in2) for each fiber in the cap cross-section."

for $i \in 1 .. NoFbrsCap$

"Tributary area for fiber at bottom of cap"

$$ta_1 \leftarrow \left[\frac{1}{2}\cdot\left[\frac{P_e}{0.5(NoFbrsCap - 1)}\right]\cdot b\right] \quad \text{if } i = 1$$

"Tributary area for fibers below top of pile"

$$ta_1 \leftarrow \left[\left[\frac{P_e}{0.5(NoFbrsCap - 1)}\right]\cdot b\right] \quad \text{if } 1 < i < \frac{NoFbrsCap + 1}{2}$$

"Tributary area for fiber at top of pile"

$$ta_1 \leftarrow \left[\left[\frac{h}{(NoFbrsCap - 1)}\right]\cdot b\right] \quad \text{if } i = \frac{NoFbrsCap + 1}{2}$$

"Tributary area for fibers above top of pile"

$$ta_1 \leftarrow \left[\left[\frac{h - P_e}{0.5(NoFbrsCap - 1)}\right]\cdot b\right] \quad \text{if } \frac{NoFbrsCap + 1}{2} < i < NoFbrsCap$$

"Tributary area for fiber at top of cap"

$$ta_1 \leftarrow \left[\frac{1}{2}\cdot\left[\frac{h - P_e}{0.5(NoFbrsCap - 1)}\right]\cdot b\right] \quad \text{if } i = NoFbrsCap$$

ta

YbarCap :=

"This routine calculates the neutral axis in the cap corresponding to each extreme fiber tension strain in the above."

"StrainCap routine. The neutral axis location is measured in inches from the bottom face (or tension side) of the cap."

for $i \in 1 .. rows(StrainCap)$

$$ybarcap_i \leftarrow \frac{h}{2}$$

$Fnet \leftarrow 1$

while $|Fnet| \geq 0.001$

$j \leftarrow 1 .. rows(FbrLocCap)$

"Fnet is the sum of the normal forces acting on the cap cross-section."

$$Fnet \leftarrow \sum_j \left(f_c\left(StrainCap_i \cdot \frac{FbrLocCap_j - ybarcap_i}{ybarcap_i}\right)\cdot TribAreaCap_j\right)$$

"Fgross is the sum of the absolute values of the normal forces acting on the cross-section."

$$Fgross \leftarrow \sum_j \left(\left|f_c\left(StrainCap_i \cdot \frac{FbrLocCap_j - ybarcap_i}{ybarcap_i}\right)\right|\cdot TribAreaCap_j\right)$$

$$temp \leftarrow \left(\frac{h}{2}\right) \quad \text{if } StrainCap_i = 0$$

"Fnet and Fgross are used in the temp variable below to adjust the neutral axis"

"location for each subsequent iteration."

$$temp \leftarrow \left(ybarcap_i + \frac{Fnet}{Fgross}\right) \quad \text{if } StrainCap_i > 0$$

$$ybarcap_i \leftarrow temp$$

ybarcap

CapMomNL :=
"Unreinforced cap moment (in-lbs) corresponding to each bottom fiber strain in the above StrainCap routine."
"Strain at each fiber is calculated using the assumption that plane sections remain plane."
for $i \in 1 .. \text{rows}(\text{YbarCap})$
  $j \leftarrow 1 .. \text{rows}(\text{FbrLocCap})$
  $m_i \leftarrow \sum_j \left[f_c\left(\text{StrainCap}_i \cdot \frac{\text{FbrLocCap}_j - \text{YbarCap}_i}{\text{YbarCap}_i} \right) \cdot \left(\text{TribAreaCap}_j\right) \cdot \left(\text{FbrLocCap}_j - \text{YbarCap}_i\right) \right]$
m

Data for Approximate Cap Moment Curve Using Linear and Symmetrical Stress Strain Relationship (pounds, inches):

$$\text{StrainCapLinear} := \begin{pmatrix} 0 \\ \varepsilon_{ct} \end{pmatrix}$$

$$\text{CapMomLinear} := \left[\begin{pmatrix} 0 \\ \left(\frac{b \cdot h^2}{6}\right) \cdot f_{ct} \end{pmatrix} \right] = \begin{pmatrix} 0 \\ 3194318 \end{pmatrix}$$

$$\text{CapMomNL}_{\text{rows}(\text{YbarCap})} = 3860213$$

CapCapacityRatio :=
"A comparison of the unreinforced cap flexural capacities determined by the nonlinear model and the assumed linear,"
"symmetrical stress strain relationship. This ratio appears to approach 1.21 (for f'c = 3000) as NoFbrsCap increases."
$$\frac{\text{CapMomNL}_{\text{rows}(\text{YbarCap})}}{\text{CapMomLinear}_2}$$

CapCapacityRatio = 1.2085

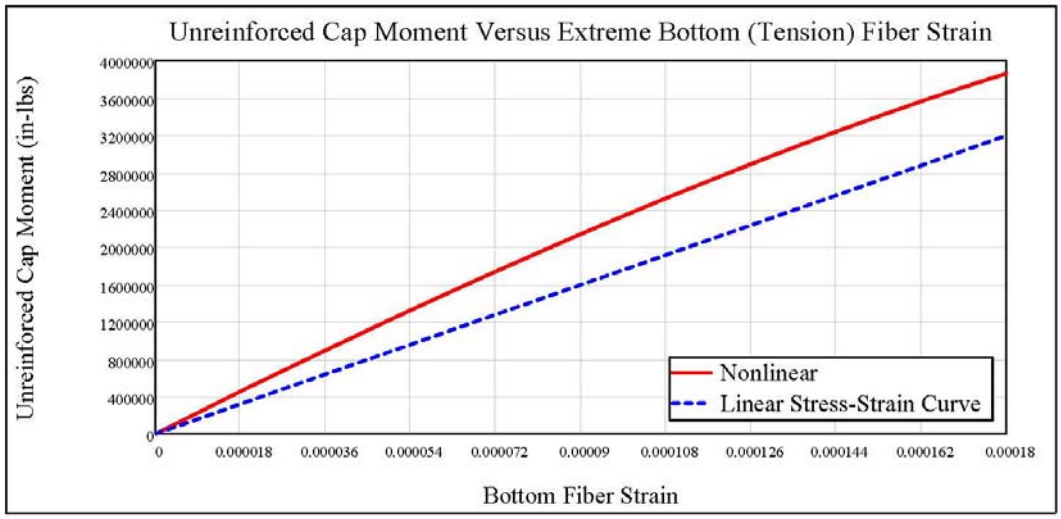

Stiffness Matrix for Elements without Shear Deformations (radians, pounds, inches):

$$NoPileElements := \frac{NoFbrsCap - 1}{2} = 25.00$$

$$DOFS := 2 \cdot (NoPileElements) + 2 = 52.00$$

$$L_{PE} := \left| \begin{array}{l} \text{"Typical length of pile elements."} \\ \dfrac{p_e}{0.5(NoFbrsCap - 1)} \end{array} \right.$$

$$L_{PE} = 0.4800$$

$$k_{ElementNoShear} := \begin{bmatrix} \frac{12 \cdot E_s \cdot I_y}{(L_{PE})^3} & \frac{6 \cdot E_s \cdot I_y}{(L_{PE})^2} & -\left[\frac{12 \cdot E_s \cdot I_y}{(L_{PE})^3}\right] & \frac{6 \cdot E_s \cdot I_y}{(L_{PE})^2} \\ \frac{6 \cdot E_s \cdot I_y}{(L_{PE})^2} & \frac{4 \cdot E_s \cdot I_y}{L_{PE}} & -\left[\frac{6 \cdot E_s \cdot I_y}{(L_{PE})^2}\right] & \frac{2 \cdot E_s \cdot I_y}{L_{PE}} \\ -\left[\frac{12 \cdot E_s \cdot I_y}{(L_{PE})^3}\right] & -\left[\frac{6 \cdot E_s \cdot I_y}{(L_{PE})^2}\right] & \frac{12 \cdot E_s \cdot I_y}{(L_{PE})^3} & -\left[\frac{6 \cdot E_s \cdot I_y}{(L_{PE})^2}\right] \\ \frac{6 \cdot E_s \cdot I_y}{(L_{PE})^2} & \frac{2 \cdot E_s \cdot I_y}{L_{PE}} & -\left[\frac{6 \cdot E_s \cdot I_y}{(L_{PE})^2}\right] & \frac{4 \cdot E_s \cdot I_y}{L_{PE}} \end{bmatrix}$$

Stiffness Matrix for Elements with Shear Deformations (radians, pounds, inches):

$A_v :=$ "Area used for weak-axis shear deformations in pile."

"The shape factor accounts for the nonuniform distribution of shear stresses within the cross-section."

"The 1.2 value is taken from page 538 in "Matrix Analysis of Structures," by Aslam Kassimali"

$V_{ShapeFactor} \leftarrow 1.2$

$$\frac{2 \cdot b_f \cdot t_{fw}}{V_{ShapeFactor}}$$

$$d_{ReducedShear} := \begin{pmatrix} \frac{L_{PE}^3}{3E_s \cdot I_y} + \frac{L_{PE}}{G \cdot A_v} & \frac{L_{PE}^2}{2 \cdot E_s \cdot I_y} \\ \frac{L_{PE}^2}{2 \cdot E_s \cdot I_y} & \frac{L_{PE}}{E_s \cdot I_y} \end{pmatrix} \qquad k_{ReducedShear} := d_{ReducedShear}^{-1} \qquad a := \begin{pmatrix} -1 & -L_{PE} & 1 & 0 \\ 0 & -1 & 0 & 1 \end{pmatrix}$$

$$k_{ElementWithShear} := a^T \cdot k_{ReducedShear} \cdot a$$

Check of Stiffness Matrix for Elements with Shear Deformations (radians, pounds, inches):

Note: The matrix formulation below is taken from page 540 in "Matrix Analysis of Structures," by Aslam Kassimali. This formulation is used as a check on the stiffness matrix calculated above.

$\beta_s :=$ "This dimensionless parameter is defined in the above text as the shear deformation constant."

$$\frac{\left(12 \cdot E_s \cdot I_y \cdot 1.2\right)}{G \cdot \left(2 \cdot b_f \cdot t_{fw}\right) \cdot L_{PE}^2}$$

$$k_{Check} := \frac{E_s \cdot I_y}{L_{PE}^3 \left(1 + \beta_s\right)} \cdot \begin{bmatrix} 12 & 6 \cdot L_{PE} & -12 & 6 \cdot L_{PE} \\ 6 \cdot L_{PE} & L_{PE}^2 \left(4 + \beta_s\right) & -6 \cdot L_{PE} & L_{PE}^2 \left(2 - \beta_s\right) \\ -12 & -6 \cdot L_{PE} & 12 & -6 \cdot L_{PE} \\ 6 \cdot L_{PE} & L_{PE}^2 \left(2 - \beta_s\right) & -6 \cdot L_{PE} & L_{PE}^2 \left(4 + \beta_s\right) \end{bmatrix}$$

$$k_{ElementWithShear} - k_{Check} = \begin{pmatrix} 0.0000000 & 0.0000000 & 0.0000000 & 0.0000000 \\ 0.0000000 & 0.0000000 & -0.0000000 & -0.0000010 \\ 0.0000000 & -0.0000000 & 0.0000000 & -0.0000000 \\ 0.0000000 & -0.0000010 & -0.0000000 & 0.0000000 \end{pmatrix}$$

Global Stiffness Matrix for Embedded Pile Structure (radians, pounds, inches):

$K_{GlobalElementsOnly} :=$

"This routine assembles the global stiffness matrix for the pile-to-cap structural model."

"To ignore shear deformations, set ShearDeformations to 0."

"To include shear deformations, set ShearDeformations to 1."

$ShearDeformations \leftarrow 1$

$K_{GEO} \leftarrow matrix(DOFS, DOFS, f(i,j) \leftarrow 0)$

"In the loops below, h is an indexing variable that locates the k11 entry from each element stiffness matrix"

"within the global stiffness matrix. The h+i-1 and h+j-1 values locate each element stiffness coefficient within"

"the global stiffness matrix."

for $h \in 1, 3 .. (DOFS - 3)$

  for $i \in 1 .. 4$

    for $j \in 1 .. 4$

      $k_{Element_{i,j}} \leftarrow k_{ElementNoShear_{i,j}}$ if $ShearDeformations = 0$

      $k_{Element_{i,j}} \leftarrow k_{ElementWithShear_{i,j}}$ if $ShearDeformations = 1$

      $K_{GEO_{h+i-1,h+j-1}} \leftarrow K_{GEO_{h+i-1,h+j-1}} + k_{Element_{i,j}}$

K_{GEO}

$L_{pst} :=$

"Pile bearing stress transfer length."

"Lpst is the distance along the length of the beam from the pile face to the point where the localized"

"pile bearing stresses are assumed to be equal to the idealized beam bending stresses."

$\frac{1}{2} \cdot (b - d)$

$K_{GlobalSpringsOnly} :=$ "This routine calculates the translational resistance of the concrete at each node as a simplified linear spring (AEc/Lpst)."

"These spring constants provide the initial support conditions used in the first iteration for each of the nonlinear analyses below."

$K_{GSO} \leftarrow matrix(DOFS, DOFS, f(i,j) \leftarrow 0)$

for $h \in 1, 3 .. (DOFS - 1)$

$$K_{GSO_{h,h}} \leftarrow \frac{d \cdot \frac{(L_{PE})}{2} \cdot E_c}{L_{pst}} \quad \text{if } h = 1$$

$$K_{GSO_{h,h}} \leftarrow \frac{d \cdot L_{PE} \cdot E_c}{L_{pst}} \quad \text{if } h > 1$$

$$K_{GSO_{h,h}} \leftarrow \frac{d \cdot \left(\frac{L_{PE}}{2}\right) \cdot E_c}{L_{pst}} \quad \text{if } h = DOFS - 1$$

K_{GSO}

$K_{GlobalSpringsTransOnly} :=$ "This routine extracts the translations spring values from the global stiffness matrix."

for $h \in 1 .. \frac{DOFS}{2}$

$K_{GSTO_h} \leftarrow K_{GlobalSpringsOnly_{2 \cdot h-1, 2 \cdot h-1}}$

K_{GSTO}

$K_{GlobalComplete} :=$ "This equation provides the final assembly of the complete global stiffness matrix."

$K_{GlobalElementsOnly} + K_{GlobalSpringsOnly}$

NoPileForceEvaluationPoints :=	"This input provides the number of evaluation points used to establish the moment-rotation curve for a" "given pile-to-cap connection scenario (bending case, pile section, concrete strength and embedment depth)." 11

$F_{Pile} :=$

"This routine creates the array of externally applied pile forces acting at the base of the cap for each pile force evaluation point."

"The shear in the pile at the base of the cap is based on a 20 foot tall, 4 pile bent with a rigid cap. The pile is assumed to be"

"fixed connected at the top and bottom. The portal method (assuming equal shear at each pile) is used to calculate the shear that"

"corresponds to the moment under consideration."

$F_{EAP} \leftarrow \text{matrix}(DOFS, NoPileForceEvaluationPoints, f(i,j) \leftarrow 0)$

"The value VBaseCapMax (below) must be a positive value."

$V_{BaseCapMin} \leftarrow 0$

$V_{BaseCapMax} \leftarrow \frac{4 \cdot (M_{Yield})}{(10) \cdot (12)}$

"The value MBaseCapMax (below) must be a negative value."

$M_{BaseCapMin} \leftarrow 0$

$M_{BaseCapMax} \leftarrow -M_{Yield}$

for $j \in 1 .. NoPileForceEvaluationPoints$

$F_{EAP_{1,j}} \leftarrow (V_{BaseCapMax} - V_{BaseCapMin}) \cdot \left(\frac{j-1}{NoPileForceEvaluationPoints - 1}\right)$

$F_{EAP_{2,j}} \leftarrow (M_{BaseCapMax} - M_{BaseCapMin}) \cdot \left(\frac{j-1}{NoPileForceEvaluationPoints - 1}\right)$

F_{EAP}

$\Delta_{Global} :=$

"The translational displacements of the pile-to-cap connection are provided in the odd numbered rows of this matrix. Row 1 is the"

"translational DOF at the bottom face of the cap. The last odd numbered row (next to last row) is the translational DOF at the top-of-pile."

$(K_{GlobalComplete})^{-1} \cdot (F_{Pile})$

$\Delta_{GlobalTransOnly} :=$

"This routine extracts the translational displacements from the full global displacemnet vector."

for $i \in 1 .. \frac{DOFS}{2}$

for $j \in 1 .. NoPileForceEvaluationPoints$

$Delta_{1,j} \leftarrow \Delta_{Global_{2 \cdot i - 1, j}}$

Delta

$P_{PileFace} :=$ "This routine calculates the global reaction (spring force) at the pile face for each translational DOF. The results are approximations"
"based on the simplified first order analysis using the above assumptions for the supporting springs (AEc/Lpst)."
"Each row in the resulting matrix represents an individual, translational DOF. Each column represents the translational nodal reactions"
"corresponding to one loading condition from the FPile matrix."

for $i \in 1 .. \frac{DOFS}{2}$

  for $j \in 1 .. NoPileForceEvaluationPoints$

    $R_{i,j} \leftarrow K_{GlobalSpringsTransOnly_i} \cdot \Delta_{GlobalTransOnly_{i,j}}$

R

$M_{Beam} :=$

"This routine calculates the cap moments that exist in the vicinity of the pile-to-cap connection. These are the moments that, in practice,"

"would be determined by an idealized structural analysis giving no consideration to the localized behavior near the pile-to-cap connection.

"Set the CapBendingScenario variable (below with description) to 1, 2 3 or 4 to evaluate the pile support condition desired."

"CapBendingScenario = 1 consists of equal cap moments placed on each side of the pile."

"CapBendingScenario = 2 consists of a cap moment placed on the left side only."

"CapBendingScenario = 3 consists of a cap moment placed on the right side only."

"CapBendingScenario = 4 sets the cap moment equal to zero on both sides of the pile."

$\text{CapBendingScenario} \leftarrow 1$

"Span length (inches) of beams on the left and right sides of the pile."

$\text{Span} \leftarrow 96$

"End moments of right and left spans are assumed to be equal. Moments are assumed to vary linearly along length of beam."

for $j \in 1..\text{cols}(F_{Pile})$

"MCapTotal: Term 1 is due to the applied shear at the bearing. Term 2 is resisting pile moment."

$M_{CapTotal} \leftarrow \left(F_{Pile_{1,j}}\right) \cdot h - F_{Pile_{2,j}}$

"MLeft is the moment at right end of left span."

$M_{Left} \leftarrow \left(\frac{1}{2}\right) \cdot M_{CapTotal} \quad \text{if CapBendingScenario} = 1$

$M_{Left} \leftarrow M_{CapTotal} \quad \text{if CapBendingScenario} = 2$

$M_{Left} \leftarrow 0 \quad \text{if CapBendingScenario} = 3 \vee \text{CapBendingScenario} = 4$

"M1j is the beam moment at the pile face."

$$M_{1,j} \leftarrow M_{Left} \cdot \frac{\frac{\text{Span}}{2} - \frac{b_f}{2}}{\frac{\text{Span}}{2}}$$

"M2j is the beam moment at Lpst from left pile face."

$$M_{2,j} \leftarrow M_{Left} \cdot \frac{\frac{\text{Span}}{2} - \frac{b_f}{2} - L_{pst}}{\frac{\text{Span}}{2}}$$

"MRight is the moment at left end of right span."

$M_{Right} \leftarrow M_{CapTotal} - M_{Left} \quad \text{if CapBendingScenario} = 1$

$M_{Right} \leftarrow 0 \quad \text{if CapBendingScenario} = 2 \vee \text{CapBendingScenario} = 4$

$M_{Right} \leftarrow M_{CapTotal} \quad \text{if CapBendingScenario} = 3$

"M3j is the beam moment at right pile face."

$$M_{3,j} \leftarrow M_{Right} \cdot \frac{\frac{\text{Span}}{2} - \frac{b_f}{2}}{\frac{\text{Span}}{2}}$$

"M4j is the beam moment at Lpst from right pile face."

$$M_{4,j} \leftarrow M_{Right} \cdot \frac{\frac{\text{Span}}{2} - \frac{b_f}{2} - L_{pst}}{\frac{\text{Span}}{2}}$$

M

PSTBStrains :=

"PSTB is the abbreviation for the Pile Stress Transfer Block region within the cap and in the vicinity of the pile-to-cap connection."
"This region defines the volume through which the localized connection behavior is transformed into idealized beam behavior."
"This routine calculates the idealized strains in the cap due to bending. On both the left and right sides of the pile, the strains in the"
"extreme tension fiber are calculated for a section at the pile face and for a section at a distance Lpst from the pile face where the"
"localized pile bearing strains are assumed to be equal to the idealized strains in the cap due to bending."

for $i \in 1 .. \text{rows}(M_{Beam})$

  for $j \in 1 .. \text{NoPileForceEvaluationPoints}$

    $\varepsilon_{i,1} \leftarrow 0$

    for $k \in 1 .. \text{rows}(\text{CapMomNL}) - 1$

      $\varepsilon_{i,j} \leftarrow \text{StrainCap}_k + \frac{\text{StrainCap}_{k+1} - \text{StrainCap}_k}{\text{CapMomNL}_{k+1} - \text{CapMomNL}_k} \cdot \left(M_{Beam_{i,j}} - \text{CapMomNL}_k\right)$ if $\text{CapMomNL}_k \le M_{Beam_{i,j}}$

ε

PSTBYbarCap :=

"This routine calulates the neutral axis location in the cap for all moments in the MBeam matrix. The neutral axis is measured"
"in inches from the face where the extreme tension fiber exists (top of cap for moments on left, bottom of cap for moments on right)."

for $i \in 1 .. \text{rows}(\text{PSTBStrains})$

  for $j \in 1 .. \text{NoPileForceEvaluationPoints}$

    $\text{ybarcap}_{i,j} \leftarrow \frac{h}{2}$

    $\text{Fnet} \leftarrow 1$

    while $|\text{Fnet}| \ge 0.001$

      $k \leftarrow 1 .. \text{rows}(\text{FbrLocCap})$

      $\text{Fnet} \leftarrow \sum_k \left(f_c\left(\text{PSTBStrains}_{i,j} \cdot \frac{\text{FbrLocCap}_k - \text{ybarcap}_{i,j}}{\text{ybarcap}_{i,j}} \right) \cdot \text{TribAreaCap}_k \right)$

      $\text{Fgross} \leftarrow \sum_k \left(\left| f_c\left(\text{PSTBStrains}_{i,j} \cdot \frac{\text{FbrLocCap}_k - \text{ybarcap}_{i,j}}{\text{ybarcap}_{i,j}} \right) \right| \cdot \text{TribAreaCap}_k \right)$

      $\text{temp} \leftarrow \left(\frac{h}{2}\right)$ if $\text{PSTBStrains}_{i,j} = 0$

      $\text{temp} \leftarrow \left(\text{ybarcap}_{i,j} + \frac{\text{Fnet}}{\text{Fgross}}\right)$ if $\text{PSTBStrains}_{i,j} > 0$

      $\text{ybarcap}_{i,j} \leftarrow \text{temp}$

      return "Tension Strain Exceeded. Increase Cap Section." if $\text{PSTBStrains}_{i,j} > \varepsilon_{ct}$

ybarcap

$$\text{PSTBCapMomNL} := \left| \begin{array}{l} \text{"This routine calculates the moment (in-lbs) in the unreinforced cap corresponding to each extreme fiber tension strain."} \\ \text{for } i \in 1..\text{rows(PSTBYbarCap)} \\ \quad \text{for } j \in 1..\text{NoPileForceEvaluationPoints} \\ \quad\quad k \leftarrow 1..\text{rows(FbrLocCap)} \\ \quad\quad \text{YBC} \leftarrow \text{PSTBYbarCap}_{i,j} \\ \quad\quad m_{i,j} \leftarrow \sum_k \left[f_c\left(\text{PSTBStrains}_{i,j} \cdot \frac{\text{FbrLocCap}_k - \text{YBC}}{\text{YBC}} \right) \cdot \left(\text{TribAreaCap}_k\right) \cdot \left(\text{FbrLocCap}_k - \text{YBC}\right) \right] \\ m \end{array} \right.$$

$$\text{Check}_{\text{CapMomNL}} := \left| \begin{array}{l} \text{"This routine provides a check on the accuracy of the calculated nonlinear cap moments."} \\ M_{\text{Beam}} - \text{PSTBCapMomNL} \end{array} \right.$$

$$\text{Check}_{\text{CapMomNL}} = \begin{pmatrix} 0.0 & -258.1 & -370.9 & -337.7 & -157.7 & -142.1 & -338.3 & -381.4 & -270.6 & -5.2 & -272.8 \\ 0.0 & -194.5 & -319.1 & -373.7 & -357.9 & -271.6 & -114.4 & -101.6 & -269.0 & -363.0 & -383.2 \\ 0.0 & -258.1 & -370.9 & -337.7 & -157.7 & -142.1 & -338.3 & -381.4 & -270.6 & -5.2 & -272.8 \\ 0.0 & -194.5 & -319.1 & -373.7 & -357.9 & -271.6 & -114.4 & -101.6 & -269.0 & -363.0 & -383.2 \end{pmatrix}$$

$$\min\left(\text{Check}_{\text{CapMomNL}}\right) = -383.2$$

$$\max\left(\text{Check}_{\text{CapMomNL}}\right) = 0.0$$

$$\text{TribArea}_{\text{PSTB}} := \left| \begin{array}{l} \text{"This routine calculates the tributary area (in2) for each fiber along the bearing face of the embedded pile."} \\ \text{"These tributary areas are also used in the evaluation of the rigid body behavior scenario of the pile-to-cap connection."} \\ \text{for } i \in 1..\left(\frac{\text{NoFbrsCap} + 1}{2}\right) \\ \quad \text{"Tributary area for fiber at bottom of cap and top of pile."} \\ \quad ta_i \leftarrow \left[\frac{1}{2} \cdot \left[\frac{P_e}{0.5(\text{NoFbrsCap} - 1)} \right] \cdot d \right] \text{ if } i = 1 \vee i = \frac{\text{NoFbrsCap} + 1}{2} \\ \quad \text{"Tributary area for fibers between bottom of cap and top of pile."} \\ \quad ta_i \leftarrow \left[\left[\frac{P_e}{0.5(\text{NoFbrsCap} - 1)} \right] \cdot d \right] \text{ if } 1 < i < \frac{\text{NoFbrsCap} + 1}{2} \\ ta \end{array} \right.$$

$P_{CapFbrLeft} :=$

"This routine calculates the idealized force at each cap fiber located at or below the top of pile"

"due to MBeam at a distance Lpst from the left face of the pile."

for $i \in 1 .. \frac{DOFS}{2}$

for $j \in 1 .. cols(PSTBStrains)$

"The resulting fiber forces at Lpst are in compression for Cap Bending Scenarios 1 and 2 and zero for Scenarios 3 and 4."

"The negative sign indicates direction with respect to the global DOFs. For the assumed loading conditions, these forces will"

"generally inhibit pile translation and rotation by reducing the nodal displacements that occur as the connection couple forces"

"develop near the bottom face of the cap (below the center of rotation of the embedded portion of the pile)."

$$P_{Left_{i,j}} \leftarrow -f_c\left[\left(PSTBStrains_{2,j}\right)\cdot\frac{h - PSTBYbarCap_{2,j} - FbrLocCap_i}{PSTBYbarCap_{2,j}}\right]\cdot\left(TribArea_{PSTB_i}\right)$$

P_{Left}

$P_{CapFbrRight} :=$

"This routine calculates the idealized force at each cap fiber located at or below the top of pile"

"due to MBeam at a distance Lpst from the right face of the pile."

for $i \in 1 .. \frac{DOFS}{2}$

for $j \in 1 .. cols(PSTBStrains)$

"The resulting fiber forces at Lpst are in tension for Cap Bending Scenarios 1 and 3 and zero for Scenarios 2 and 4."

"The negative sign indicates direction with respect to the global DOFs. For the assumed loading conditions, these forces will"

"generally promote pile translation and rotation by increasing the nodal displacements that occur as the connection couple"

"forces develop near the top of the pile (above the center of rotation of the embedded portion of the pile)."

$$P_{Right_{i,j}} \leftarrow f_c\left[\left(PSTBStrains_{4,j}\right)\cdot\frac{FbrLocCap_i - PSTBYbarCap_{4,j}}{PSTBYbarCap_{4,j}}\right]\cdot\left(TribArea_{PSTB_i}\right)$$

P_{Right}

$NLA_{Method1} :=$

"This routine performs an iterative, nonlinear structural analysis of a steel pile embedded in an unreinforced concrete beam."

"1-D link elements with full length, linear tranction forces (peak at the pile face) model the 3-D connection behavior through'

"the PSTB."

"Refer to the MBeam routine above for the Cap Bending Scenario being considered."

for $j \in 1 .. NoPileForceEvaluationPoints$

$Count_{1,j} \leftarrow 0$

$Q_{LinkTotal} \leftarrow matrix(DOFS, 1, f(i,j) \leftarrow 0)$

$Q_{LinkPileFace} \leftarrow matrix(DOFS, 1, f(i,j) \leftarrow 0)$

$ReactionError \leftarrow 1$

while $ReactionError \geq 0.1$

$\Delta_{Global}^{\langle j \rangle} \leftarrow \left(K_{GlobalComplete}^{-1}\right) \cdot \left(F_{Pile}^{\langle j \rangle} + Q_{LinkPileFace}\right)$

$P_{PileFace} \leftarrow K_{GlobalSpringsOnly} \cdot \Delta_{Global}^{\langle j \rangle} - Q_{LinkPileFace}$

for $i \in 1 .. \frac{DOFS}{2}$

$Reaction_{AtIdealizedBeam_{i,j}} \leftarrow -P_{PileFace_{2 \cdot i-1}} - Q_{LinkTotal_{2 \cdot i-1}}$

$ReactionError_{i,j} \leftarrow Reaction_{AtIdealizedBeam_{i,j}} + P_{CapFbrLeft_{i,j}}$ if $P_{PileFace_{2 \cdot i-1}} \geq 0$

$ReactionError_{i,j} \leftarrow Reaction_{AtIdealizedBeam_{i,j}} - P_{CapFbrRight_{i,j}}$ if $P_{PileFace_{2 \cdot i-1}} < 0$

$Q_{LinkTotalNew_{i,j}} \leftarrow Q_{LinkTotal_{2 \cdot i-1}} + ReactionError_{i,j}$

$Q_{LinkPileFaceNew_{i,j}} \leftarrow Q_{LinkPileFace_{2 \cdot i-1}} + \left(\frac{2}{3}\right) \cdot ReactionError_{i,j}$

$\sigma_{PileFace_{i,j}} \leftarrow \frac{\left|P_{PileFace_{2 \cdot i-1}}\right|}{TribArea_{PSTB_i}}$

$P_{Midpoint_{i,j}} \leftarrow \left|P_{PileFace_{2 \cdot i-1}} + \frac{3}{4} \cdot Q_{LinkTotalNew_{i,j}}\right|$

$\sigma_{Midpoint_{i,j}} \leftarrow \frac{P_{Midpoint_{i,j}}}{TribArea_{PSTB_i}}$

$\varepsilon_{Midpoint_{i,j}} \leftarrow \varepsilon_{co} \cdot \left[1 - \left(\left|1 - \frac{\sigma_{Midpoint_{i,j}}}{f_{co}}\right|\right)^{\left(\frac{1}{n_c}\right)}\right]$

$E_{MidpointTangent_{i,j}} \leftarrow \frac{f_{co} \cdot n_c}{\varepsilon_{co}} \cdot \left(\left|1 - \frac{\varepsilon_{Midpoint_{i,j}}}{\varepsilon_{co}}\right|\right)^{\left(n_c - 1\right)}$

$k_{SpringMidpoint_{i,j}} \leftarrow \frac{\left(TribArea_{PSTB_i}\right) \cdot \left(E_{MidpointTangent_{i,j}}\right)}{L_{pst}}$

$REMin \leftarrow \left|min(ReactionError)\right|$

$REMax \leftarrow max(ReactionError)$

$REMin \leftarrow |\min(ReactionError)|$

$REMax \leftarrow \max(ReactionError)$

$ReactionError \leftarrow \max(REMin, REMax)$

$Q_{LinkTotal} \leftarrow \text{matrix}(DOFS, 1, f(i,j) \leftarrow 0)$

$Q_{LinkPileFace} \leftarrow \text{matrix}(DOFS, 1, f(i,j) \leftarrow 0)$

$K_{GlobalSpringsOnly} \leftarrow \text{matrix}(DOFS, DOFS, f(i,j) \leftarrow 0)$

for $i \in 1..\frac{DOFS}{2}$

$Q_{LinkTotal_{2\cdot i-1}} \leftarrow Q_{LinkTotalNew_{i,j}}$

$Q_{LinkPileFace_{2\cdot i-1}} \leftarrow Q_{LinkPileFaceNew_{i,j}}$

$K_{GlobalSpringsOnly_{2\cdot i-1,\,2\cdot i-1}} \leftarrow k_{SpringMidpoint_{i,j}}$

$K_{GlobalComplete} \leftarrow K_{GlobalElementsOnly} + K_{GlobalSpringsOnly}$

$m \leftarrow 1..\frac{DOFS}{2}$

$SumMoments_{1,j} \leftarrow \sum_{m}\left[\left(P_{PileFace_{2\cdot m-1}}\right)\cdot(m-1)\cdot\left(L_{PE}\right)\right] - F_{Pile_{2,j}}$

$SumShears_{1,j} \leftarrow \sum_{m}\left(P_{PileFace_{2\cdot m-1}}\right) - F_{Pile_{1,j}}$

$\sigma_{PileFaceMax_{1,j}} \leftarrow \max\left(\sigma_{PileFace}\right)$

$Count_{1,j} \leftarrow Count_{1,j} + 1$

return "Iteration Limit Exceeded" if $Count_{1,j} > 1000$

break if $\sigma_{PileFaceMax_{1,j}} > f_{co}$

$CombinedResults \leftarrow \text{stack}\left(Count, \sigma_{PileFaceMax}, SumMoments, SumShears, \Delta_{Global}\right)$

$NLA_{Method2} :=$

"This routine performs an iterative, nonlinear structural analysis of a steel pile embedded in an unreinforced concrete beam."

"1-D link elements with full length, uniform tranction forces model the 3-D connection behavior through the PSTB."

"Refer to the MBeam routine above for the Cap Bending Scenario being considered."

for $j \in 1..NoPileForceEvaluationPoints$

$Count_{1,j} \leftarrow 0$

$Q_{LinkTotal} \leftarrow matrix(DOFS, 1, f(i,j) \leftarrow 0)$

$Q_{LinkPileFace} \leftarrow matrix(DOFS, 1, f(i,j) \leftarrow 0)$

$ReactionError \leftarrow 1$

while $ReactionError \geq 0.1$

$\Delta_{Global}^{\langle j \rangle} \leftarrow \left(K_{GlobalComplete}^{-1}\right) \cdot \left(F_{Pile}^{\langle j \rangle} + Q_{LinkPileFace}\right)$

$P_{PileFace} \leftarrow K_{GlobalSpringsOnly} \cdot \Delta_{Global}^{\langle j \rangle} - Q_{LinkPileFace}$

for $i \in 1.. \frac{DOFS}{2}$

$Reaction_{AtIdealizedBeam_{i,j}} \leftarrow -P_{PileFace_{2 \cdot i-1}} - Q_{LinkTotal_{2 \cdot i-1}}$

$ReactionError_{i,j} \leftarrow Reaction_{AtIdealizedBeam_{i,j}} + P_{CapFbrLeft_{i,j}} \text{ if } P_{PileFace_{2 \cdot i-1}} \geq 0$

$ReactionError_{i,j} \leftarrow Reaction_{AtIdealizedBeam_{i,j}} - P_{CapFbrRight_{i,j}} \text{ if } P_{PileFace_{2 \cdot i-1}} < 0$

$Q_{LinkTotalNew_{i,j}} \leftarrow Q_{LinkTotal_{2 \cdot i-1}} + ReactionError_{i,j}$

$Q_{LinkPileFaceNew_{i,j}} \leftarrow Q_{LinkPileFace_{2 \cdot i-1}} + \left(\frac{1}{2}\right) \cdot ReactionError_{i,j}$

$\sigma_{PileFace_{i,j}} \leftarrow \frac{\left|P_{PileFace_{2 \cdot i-1}}\right|}{TribArea_{PSTB_i}}$

$P_{Midpoint_{i,j}} \leftarrow \left|P_{PileFace_{2 \cdot i-1}} + \frac{1}{2} \cdot Q_{LinkTotalNew_{i,j}}\right|$

$\sigma_{Midpoint_{i,j}} \leftarrow \frac{P_{Midpoint_{i,j}}}{TribArea_{PSTB_i}}$

$\varepsilon_{Midpoint_{i,j}} \leftarrow \varepsilon_{co} \cdot \left[1 - \left(\left|1 - \frac{\sigma_{Midpoint_{i,j}}}{f_{co}}\right|\right)^{\left(\frac{1}{n_c}\right)}\right]$

$E_{MidpointTangent_{i,j}} \leftarrow \frac{f_{co} \cdot n_c}{\varepsilon_{co}} \cdot \left(\left|1 - \frac{\varepsilon_{Midpoint_{i,j}}}{\varepsilon_{co}}\right|\right)^{\left(n_c - 1\right)}$

$k_{SpringMidpoint_{i,j}} \leftarrow \frac{\left(TribArea_{PSTB_i}\right) \cdot \left(E_{MidpointTangent_{i,j}}\right)}{L_{pst}}$

$REMin \leftarrow \left|min(ReactionError)\right|$

$REMax \leftarrow max(ReactionError)$

$$\text{REMin} \leftarrow \left|\min(\text{ReactionError})\right|$$

$$\text{REMax} \leftarrow \max(\text{ReactionError})$$

$$\text{ReactionError} \leftarrow \max(\text{REMin}, \text{REMax})$$

$$Q_{\text{LinkTotal}} \leftarrow \text{matrix}(\text{DOFS}, 1, f(i,j) \leftarrow 0)$$

$$Q_{\text{LinkPileFace}} \leftarrow \text{matrix}(\text{DOFS}, 1, f(i,j) \leftarrow 0)$$

$$K_{\text{GlobalSpringsOnly}} \leftarrow \text{matrix}(\text{DOFS}, \text{DOFS}, f(i,j) \leftarrow 0)$$

for $i \in 1..\frac{\text{DOFS}}{2}$

$$Q_{\text{LinkTotal}_{2\cdot i-1}} \leftarrow Q_{\text{LinkTotalNew}_{i,j}}$$

$$Q_{\text{LinkPileFace}_{2\cdot i-1}} \leftarrow Q_{\text{LinkPileFaceNew}_{i,j}}$$

$$K_{\text{GlobalSpringsOnly}_{2\cdot i-1,\,2\cdot i-1}} \leftarrow k_{\text{SpringMidpoint}_{i,j}}$$

$$K_{\text{GlobalComplete}} \leftarrow K_{\text{GlobalElementsOnly}} + K_{\text{GlobalSpringsOnly}}$$

$$m \leftarrow 1..\frac{\text{DOFS}}{2}$$

$$\text{SumMoments}_{1,j} \leftarrow \sum_m \left[\left(P_{\text{PileFace}_{2\cdot m-1}}\right)\cdot(m-1)\cdot\left(L_{PE}\right)\right] - F_{\text{Pile}_{2,j}}$$

$$\text{SumShears}_{1,j} \leftarrow \sum_m \left(P_{\text{PileFace}_{2\cdot m-1}}\right) - F_{\text{Pile}_{1,j}}$$

$$\sigma_{\text{PileFaceMax}_{1,j}} \leftarrow \max\left(\sigma_{\text{PileFace}}\right)$$

$$\text{Count}_{1,j} \leftarrow \text{Count}_{1,j} + 1$$

return "Iteration Limit Exceeded" if $\text{Count}_{1,j} > 1000$

break if $\sigma_{\text{PileFaceMax}_{1,j}} > f_{co}$

$$\text{CombinedResults} \leftarrow \text{stack}\left(\text{Count}, \sigma_{\text{PileFaceMax}}, \text{SumMoments}, \text{SumShears}, \Delta_{\text{Global}}\right)$$

$NLA_{Method3}$:=

"This routine performs an iterative, nonlinear structural analysis of a steel pile embedded in an unreinforced concrete beam."

"1-D link elements with full length, linear tranction forces (peak at the idealized beam section) model the 3-D connection behavior "through the PSTB."

"Refer to the MBeam routine above for the Cap Bending Scenario being considered."

for $j \in 1..\ NoPileForceEvaluationPoints$

$Count_{1,j} \leftarrow 0$

$Q_{LinkTotal} \leftarrow matrix(DOFS, 1, f(i,j) \leftarrow 0)$

$Q_{LinkPileFace} \leftarrow matrix(DOFS, 1, f(i,j) \leftarrow 0)$

$ReactionError \leftarrow 1$

while $ReactionError \geq 0.1$

$\Delta_{Global}^{\langle j \rangle} \leftarrow \left(K_{GlobalComplete}^{-1}\right) \cdot \left(F_{Pile}^{\langle j \rangle} + Q_{LinkPileFace}\right)$

$P_{PileFace} \leftarrow K_{GlobalSpringsOnly} \cdot \Delta_{Global}^{\langle j \rangle} - Q_{LinkPileFace}$

for $i \in 1..\ \frac{DOFS}{2}$

$Reaction_{AtIdealizedBeam_{i,j}} \leftarrow -P_{PileFace_{2 \cdot i-1}} - Q_{LinkTotal_{2 \cdot i-1}}$

$ReactionError_{i,j} \leftarrow Reaction_{AtIdealizedBeam_{i,j}} + P_{CapFbrLeft_{i,j}}$ if $P_{PileFace_{2 \cdot i-1}} \geq 0$

$ReactionError_{i,j} \leftarrow Reaction_{AtIdealizedBeam_{i,j}} - P_{CapFbrRight_{i,j}}$ if $P_{PileFace_{2 \cdot i-1}} < 0$

$Q_{LinkTotalNew_{i,j}} \leftarrow Q_{LinkTotal_{2 \cdot i-1}} + ReactionError_{i,j}$

$Q_{LinkPileFaceNew_{i,j}} \leftarrow Q_{LinkPileFace_{2 \cdot i-1}} + \left(\frac{1}{3}\right) \cdot ReactionError_{i,j}$

$\sigma_{PileFace_{i,j}} \leftarrow \frac{\left|P_{PileFace_{2 \cdot i-1}}\right|}{TribArea_{PSTB_i}}$

$P_{Midpoint_{i,j}} \leftarrow \left|P_{PileFace_{2 \cdot i-1}} + \frac{1}{4} \cdot Q_{LinkTotalNew_{i,j}}\right|$

$\sigma_{Midpoint_{i,j}} \leftarrow \frac{P_{Midpoint_{i,j}}}{TribArea_{PSTB_i}}$

$\varepsilon_{Midpoint_{i,j}} \leftarrow \varepsilon_{co} \cdot \left[1 - \left(\left|1 - \frac{\sigma_{Midpoint_{i,j}}}{f_{co}}\right|\right)^{\left(\frac{1}{n_c}\right)}\right]$

$E_{MidpointTangent_{i,j}} \leftarrow \frac{f_{co} \cdot n_c}{\varepsilon_{co}} \cdot \left(\left|1 - \frac{\varepsilon_{Midpoint_{i,j}}}{\varepsilon_{co}}\right|\right)^{\left(n_c - 1\right)}$

$k_{SpringMidpoint_{i,j}} \leftarrow \frac{\left(TribArea_{PSTB_i}\right) \cdot \left(E_{MidpointTangent_{i,j}}\right)}{L_{pst}}$

$REMin \leftarrow \left|min(ReactionError)\right|$

$REMax \leftarrow max(ReactionError)$

$REMin \leftarrow \left|\min(ReactionError)\right|$

$REMax \leftarrow \max(ReactionError)$

$ReactionError \leftarrow \max(REMin, REMax)$

$Q_{LinkTotal} \leftarrow \text{matrix}(DOFS, 1, f(i,j) \leftarrow 0)$

$Q_{LinkPileFace} \leftarrow \text{matrix}(DOFS, 1, f(i,j) \leftarrow 0)$

$K_{GlobalSpringsOnly} \leftarrow \text{matrix}(DOFS, DOFS, f(i,j) \leftarrow 0)$

for $i \in 1..\frac{DOFS}{2}$

$Q_{LinkTotal_{2\cdot i-1}} \leftarrow Q_{LinkTotalNew_{i,j}}$

$Q_{LinkPileFace_{2\cdot i-1}} \leftarrow Q_{LinkPileFaceNew_{i,j}}$

$K_{GlobalSpringsOnly_{2\cdot i-1,\,2\cdot i-1}} \leftarrow k_{SpringMidpoint_{i,j}}$

$K_{GlobalComplete} \leftarrow K_{GlobalElementsOnly} + K_{GlobalSpringsOnly}$

$m \leftarrow 1..\frac{DOFS}{2}$

$SumMoments_{1,j} \leftarrow \sum_m \left[\left(P_{PileFace_{2\cdot m-1}}\right)\cdot(m-1)\cdot\left(L_{PE}\right)\right] - F_{Pile_{2,j}}$

$SumShears_{1,j} \leftarrow \sum_m \left(P_{PileFace_{2\cdot m-1}}\right) - F_{Pile_{1,j}}$

$\sigma_{PileFaceMax_{1,j}} \leftarrow \max\left(\sigma_{PileFace}\right)$

$Count_{1,j} \leftarrow Count_{1,j} + 1$

return "Iteration Limit Exceeded" if $Count_{1,j} > 1000$

break if $\sigma_{PileFaceMax_{1,j}} > f_{co}$

$CombinedResults \leftarrow \text{stack}\left(Count, \sigma_{PileFaceMax}, SumMoments, SumShears, \Delta_{Global}\right)$

$$\Theta M1 := \begin{array}{l} \text{ResultsColumn} \leftarrow \text{cols}\left(\text{NLA}_{\text{Method1}}\right) \text{ if } \left(\text{NLA}_{\text{Method1}}\right)_{2,\,\text{cols}\left(\text{NLA}_{\text{Method1}}\right)} \le f_{co} \\ \text{ResultsColumn} \leftarrow \text{cols}\left(\text{NLA}_{\text{Method1}}\right) - 1 \text{ if } \left(\text{NLA}_{\text{Method1}}\right)_{2,\,\text{cols}\left(\text{NLA}_{\text{Method1}}\right)} > f_{co} \\ \text{for } j \in 1 .. \text{ResultsColumn} \\ \quad \Theta_{\text{Appx}_j} \leftarrow \text{atan}\left[\dfrac{\left[\left(\text{NLA}_{\text{Method1}}\right)_{5,j} - \left(\text{NLA}_{\text{Method1}}\right)_{\text{DOFS}+3,j}\right]}{p_e}\right] \\ \Theta_{\text{Appx}} \end{array}$$

$$\Theta M1 = \begin{pmatrix} 0.000000 \\ 0.000075 \\ 0.000151 \\ 0.000228 \\ 0.000307 \\ 0.000387 \\ 0.000468 \\ 0.000551 \end{pmatrix}$$

$$M1 := \begin{array}{l} \text{ResultsColumn} \leftarrow \text{cols}\left(\text{NLA}_{\text{Method1}}\right) \text{ if } \left(\text{NLA}_{\text{Method1}}\right)_{2,\,\text{cols}\left(\text{NLA}_{\text{Method1}}\right)} \le f_{co} \\ \text{ResultsColumn} \leftarrow \text{cols}\left(\text{NLA}_{\text{Method1}}\right) - 1 \text{ if } \left(\text{NLA}_{\text{Method1}}\right)_{2,\,\text{cols}\left(\text{NLA}_{\text{Method1}}\right)} > f_{co} \\ \left(-\text{submatrix}\left(F_{\text{Pile}}, 2, 2, 1, \text{ResultsColumn}\right)\right)^{T} \end{array}$$

$$M1 = \begin{pmatrix} 0 \\ 51212 \\ 102424 \\ 153637 \\ 204849 \\ 256061 \\ 307273 \\ 358486 \end{pmatrix}$$

$$YBar_{M1} := \begin{array}{l} \text{ResultsColumn} \leftarrow \text{cols}\left(\text{NLA}_{\text{Method1}}\right) \text{ if } \left(\text{NLA}_{\text{Method1}}\right)_{2,\,\text{cols}\left(\text{NLA}_{\text{Method1}}\right)} \le f_{co} \\ \text{ResultsColumn} \leftarrow \text{cols}\left(\text{NLA}_{\text{Method1}}\right) - 1 \text{ if } \left(\text{NLA}_{\text{Method1}}\right)_{2,\,\text{cols}\left(\text{NLA}_{\text{Method1}}\right)} > f_{co} \\ \text{YBarM1} \leftarrow \dfrac{p_e \cdot \left[\left(\text{NLA}_{\text{Method1}}\right)_{5,\,\text{ResultsColumn}}\right]}{\left(\text{NLA}_{\text{Method1}}\right)_{5,\,\text{ResultsColumn}} - \left(\text{NLA}_{\text{Method1}}\right)_{\text{DOFS}+3,\,\text{ResultsColumn}}} \end{array}$$

$$\Theta M2 := \left| \begin{array}{l} \text{ResultsColumn} \leftarrow \text{cols}\left(\text{NLA}_{\text{Method2}}\right) \text{ if } \left(\text{NLA}_{\text{Method2}}\right)_{2,\,\text{cols}\left(\text{NLA}_{\text{Method2}}\right)} \le f_{co} \\ \text{ResultsColumn} \leftarrow \text{cols}\left(\text{NLA}_{\text{Method2}}\right) - 1 \text{ if } \left(\text{NLA}_{\text{Method2}}\right)_{2,\,\text{cols}\left(\text{NLA}_{\text{Method2}}\right)} > f_{co} \\ \text{for } j \in 1 .. \text{ResultsColumn} \\ \quad \Theta_{\text{Appx}_j} \leftarrow \text{atan}\left[\dfrac{\left[\left(\text{NLA}_{\text{Method2}}\right)_{5,j} - \left(\text{NLA}_{\text{Method2}}\right)_{\text{DOFS+3},j}\right]}{p_e}\right] \\ \Theta_{\text{Appx}} \end{array} \right.$$

$$\Theta M2 = \begin{pmatrix} 0.000000 \\ 0.000106 \\ 0.000216 \\ 0.000329 \\ 0.000447 \\ 0.000570 \\ 0.000697 \\ 0.000830 \\ 0.000968 \end{pmatrix}$$

$$M2 := \left| \begin{array}{l} \text{ResultsColumn} \leftarrow \text{cols}\left(\text{NLA}_{\text{Method2}}\right) \text{ if } \left(\text{NLA}_{\text{Method2}}\right)_{2,\,\text{cols}\left(\text{NLA}_{\text{Method2}}\right)} \le f_{co} \\ \text{ResultsColumn} \leftarrow \text{cols}\left(\text{NLA}_{\text{Method2}}\right) - 1 \text{ if } \left(\text{NLA}_{\text{Method2}}\right)_{2,\,\text{cols}\left(\text{NLA}_{\text{Method2}}\right)} > f_{co} \\ \left(-\text{submatrix}\left(F_{\text{Pile}}, 2, 2, 1, \text{ResultsColumn}\right)\right)^{T} \end{array} \right.$$

$$M2 = \begin{pmatrix} 0 \\ 51212 \\ 102424 \\ 153637 \\ 204849 \\ 256061 \\ 307273 \\ 358486 \\ 409698 \end{pmatrix}$$

$$YBar_{M2} := \left| \begin{array}{l} \text{ResultsColumn} \leftarrow \text{cols}\left(\text{NLA}_{\text{Method2}}\right) \text{ if } \left(\text{NLA}_{\text{Method2}}\right)_{2,\,\text{cols}\left(\text{NLA}_{\text{Method2}}\right)} \le f_{co} \\ \text{ResultsColumn} \leftarrow \text{cols}\left(\text{NLA}_{\text{Method2}}\right) - 1 \text{ if } \left(\text{NLA}_{\text{Method2}}\right)_{2,\,\text{cols}\left(\text{NLA}_{\text{Method2}}\right)} > f_{co} \\ \text{YBarM1} \leftarrow \dfrac{p_e \cdot \left[\left(\text{NLA}_{\text{Method2}}\right)_{5,\,\text{ResultsColumn}}\right]}{\left(\text{NLA}_{\text{Method2}}\right)_{5,\,\text{ResultsColumn}} - \left(\text{NLA}_{\text{Method2}}\right)_{\text{DOFS+3},\,\text{ResultsColumn}}} \end{array} \right.$$

$$\Theta M3 := \begin{array}{l} \text{ResultsColumn} \leftarrow \text{cols}\left(\text{NLA}_{\text{Method3}}\right) \text{ if } \left(\text{NLA}_{\text{Method3}}\right)_{2,\,\text{cols}\left(\text{NLA}_{\text{Method3}}\right)} \le f_{co} \\ \text{ResultsColumn} \leftarrow \text{cols}\left(\text{NLA}_{\text{Method3}}\right) - 1 \text{ if } \left(\text{NLA}_{\text{Method3}}\right)_{2,\,\text{cols}\left(\text{NLA}_{\text{Method3}}\right)} > f_{co} \\ \text{for } j \in 1 .. \text{ResultsColumn} \\ \quad \Theta_{\text{Appx}_j} \leftarrow \text{atan}\left[\dfrac{\left[\left(\text{NLA}_{\text{Method3}}\right)_{5,j} - \left(\text{NLA}_{\text{Method3}}\right)_{\text{DOFS+3},j}\right]}{p_e}\right] \\ \Theta_{\text{Appx}} \end{array}$$

$$\Theta M3 = \begin{pmatrix} 0.000000 \\ 0.000138 \\ 0.000283 \\ 0.000436 \\ 0.000598 \\ 0.000771 \\ 0.000956 \\ 0.001155 \\ 0.001370 \\ 0.001604 \\ 0.001861 \end{pmatrix}$$

$$M3 := \begin{array}{l} \text{ResultsColumn} \leftarrow \text{cols}\left(\text{NLA}_{\text{Method3}}\right) \text{ if } \left(\text{NLA}_{\text{Method3}}\right)_{2,\,\text{cols}\left(\text{NLA}_{\text{Method3}}\right)} \le f_{co} \\ \text{ResultsColumn} \leftarrow \text{cols}\left(\text{NLA}_{\text{Method3}}\right) - 1 \text{ if } \left(\text{NLA}_{\text{Method3}}\right)_{2,\,\text{cols}\left(\text{NLA}_{\text{Method3}}\right)} > f_{co} \\ \left(-\text{submatrix}\left(F_{\text{Pile}}, 2, 2, 1, \text{ResultsColumn}\right)\right)^{T} \end{array}$$

$$M3 = \begin{pmatrix} 0 \\ 51212 \\ 102424 \\ 153637 \\ 204849 \\ 256061 \\ 307273 \\ 358486 \\ 409698 \\ 460910 \\ 512122 \end{pmatrix}$$

$$YBar_{M3} := \begin{array}{l} \text{ResultsColumn} \leftarrow \text{cols}\left(\text{NLA}_{\text{Method3}}\right) \text{ if } \left(\text{NLA}_{\text{Method3}}\right)_{2,\,\text{cols}\left(\text{NLA}_{\text{Method3}}\right)} \le f_{co} \\ \text{ResultsColumn} \leftarrow \text{cols}\left(\text{NLA}_{\text{Method3}}\right) - 1 \text{ if } \left(\text{NLA}_{\text{Method3}}\right)_{2,\,\text{cols}\left(\text{NLA}_{\text{Method3}}\right)} > f_{co} \\ \text{YBarM1} \leftarrow \dfrac{p_e \cdot \left[\left(\text{NLA}_{\text{Method3}}\right)_{5,\,\text{ResultsColumn}}\right]}{\left(\text{NLA}_{\text{Method3}}\right)_{5,\,\text{ResultsColumn}} - \left(\text{NLA}_{\text{Method3}}\right)_{\text{DOFS+3},\,\text{ResultsColumn}}} \end{array}$$

$h_{RB} :=$ "The height of the rigid body (hRB) is equal to the pile e

$h_{RB} \leftarrow p_e$

Analysis$_{RB}$:=

"This routine evaluates the range of possible extreme fiber strains corresponding to a set of assumed neutral axis locations"
"to determine the equilibrium position of the rigid body (embedded pile segment) for each set of applied loads in the FPile matrix."
"A matrix with dimensions NAPrecision X StrainPrecision is created for each set of applied loads inthe FPile matrix. The entries in"
"each of these matrices are the residual values (errors) resulting from the summation of horizontal forces (VEQ) and moments (MEQ)"
"due to the applied loads, the assumed neutral axis and the assumed bottom fiber strain. The minimum value, typically near zero, for"
"each of these matrices represents the equilibrium postion. The bottom fiber strian corresponding to the equilibrium position is used"
"to calculate the corresponding top of pile strain and ultimately the rigid body rotation in subsequent calculations."
"NARange defines the range of potential neutral axis locations evaluated in this routine. The range begins at the centroid of the"
"rigid body (embedded pile segment) and increases from there so that the neutral axis is at or just above the centroid."

$NA_{Range} \leftarrow (0.15)\cdot h_{RB}$

"NAPrecision controls the number of equally spaced evaluation points within NARange. Use an odd number to create an evaluation"
"point at the centroid of the rigid body."

$NA_{Precision} \leftarrow 501$

"StrainPrecision controls the number of strain evaluation points between zero and the maximum compressive strain,εco."

$Strain_{Precision} \leftarrow 1500$

$$n_c \leftarrow \frac{E_c \cdot \varepsilon_{co}}{f_{co}}$$

"The range variable h cycles this routine through the FPile matrix to determine the neutral axis and bottom fiber strain for each load set."

for $h \in 1..NoPileForceEvaluationPoints$

$V \leftarrow F_{Pile_{1,h}}$

$M \leftarrow F_{Pile_{2,h}}$

for $i \in 1..NA_{Precision}$

$$Y_{RB} \leftarrow \frac{h_{RB}}{2} + \left(\frac{NA_{Range}}{NA_{Precision} - 1}\right)\cdot(i-1)$$

for $j \in 1..Strain_{Precision}$

"εbfj is the fiber strian at the bottom of the rigid body (bottom face of cap) for a given evaluation point."

$$\varepsilon_{bf} \leftarrow \left(\frac{\varepsilon_{co}}{Strain_{Precision} - 1}\right)\cdot(j-1)$$

if $\varepsilon_{bf} > 0$

$$V_{Upper} \leftarrow f_{co}\cdot d\cdot\left[h_{RB} - Y_{RB} + \frac{\varepsilon_{co}\cdot Y_{RB}\cdot\left[\left|1 - \frac{\varepsilon_{bf}\cdot(h_{RB} - Y_{RB})}{\varepsilon_{co}\cdot Y_{RB}}\right|\right]^{n_c+1}}{\varepsilon_{bf}\cdot(n_c+1)} - \frac{\varepsilon_{co}\cdot Y_{RB}}{\varepsilon_{bf}\cdot(n_c+1)}\right]$$

$$V_{Lower} \leftarrow f_{co}\cdot d\cdot\left[Y_{RB} + \frac{\varepsilon_{co}\cdot Y_{RB}\cdot\left(\left|1 - \frac{\varepsilon_{bf}}{\varepsilon_{co}}\right|\right)^{n_c+1}}{\varepsilon_{bf}\cdot(n_c+1)} - \frac{\varepsilon_{co}\cdot Y_{RB}}{\varepsilon_{bf}\cdot(n_c+1)}\right]$$

$$M_{UpperPart1} \leftarrow \frac{\left(h_{RB} - Y_{RB}\right)^2}{2} + \frac{\left(h_{RB} - Y_{RB}\right)\cdot\varepsilon_{co}\cdot Y_{RB}\cdot\left[\left|1 - \frac{\varepsilon_{bf}\cdot\left(h_{RB} - Y_{RB}\right)}{\varepsilon_{co}\cdot Y_{RB}}\right|\right]^{n_c+1}}{\varepsilon_{bf}\cdot\left(n_c + 1\right)}$$

$$M_{UpperPart2} \leftarrow \frac{\varepsilon_{co}^{\ 2}\cdot Y_{RB}^{\ 2}\cdot\left[\left|1 - \frac{\varepsilon_{bf}\cdot\left(h_{RB} - Y_{RB}\right)}{\varepsilon_{co}\cdot Y_{RB}}\right|\right]^{n_c+2}}{\varepsilon_{bf}^{\ 2}\cdot\left(n_c + 1\right)\cdot\left(n_c + 2\right)} - \frac{\varepsilon_{co}^{\ 2}\cdot Y_{RB}^{\ 2}}{\varepsilon_{bf}^{\ 2}\cdot\left(n_c + 1\right)\cdot\left(n_c + 2\right)}$$

$$M_{Upper} \leftarrow f_{co}\cdot d\cdot\left(M_{UpperPart1} + M_{UpperPart2}\right)$$

$$M_{LowerPart1} \leftarrow \frac{Y_{RB}^{\ 2}}{2} + \frac{\varepsilon_{co}\cdot Y_{RB}^{\ 2}\cdot\left(\left|1 - \frac{\varepsilon_{bf}}{\varepsilon_{co}}\right|\right)^{n_c+1}}{\varepsilon_{bf}\cdot\left(n_c + 1\right)}$$

$$M_{LowerPart2} \leftarrow \frac{\varepsilon_{co}^{\ 2}\cdot Y_{RB}^{\ 2}\cdot\left(\left|1 - \frac{\varepsilon_{bf}}{\varepsilon_{co}}\right|\right)^{n_c+2}}{\varepsilon_{bf}^{\ 2}\cdot\left(n_c + 1\right)\cdot\left(n_c + 2\right)} - \frac{\varepsilon_{co}^{\ 2}\cdot Y_{RB}^{\ 2}}{\varepsilon_{bf}^{\ 2}\cdot\left(n_c + 1\right)\cdot\left(n_c + 2\right)}$$

$$M_{Lower} \leftarrow f_{co}\cdot d\cdot\left(M_{LowerPart1} + M_{LowerPart2}\right)$$

$$VEQ \leftarrow \left|F_{Pile_{1,h}} + V_{Upper} - V_{Lower}\right|$$

$$MEQ \leftarrow \left|F_{Pile_{2,h}} - \frac{F_{Pile_{1,h}}}{\frac{h_{RB}}{2}} + M_{Upper} + M_{Lower}\right|$$

$$EQ_{Total_{i,j}} \leftarrow 0 \quad \text{if } \varepsilon_{bf} = 0$$

$$EQ_{Total_{i,j}} \leftarrow \max(VEQ, MEQ) \quad \text{if } \varepsilon_{bf} > 0$$

$$EQ_{Reduced} \leftarrow \text{submatrix}\left(EQ_{Total}, 1, NA_{Precision}, 2, Strain_{Precision}\right)$$

$$EQ_{Minimum_h} \leftarrow \min\left(EQ_{Reduced}\right)$$

$$EQ_{Indices} \leftarrow \text{match}\left(EQ_{Minimum_h}, EQ_{Reduced}\right)$$

$$EQ_{IndicesExtracted} \leftarrow EQ_{Indices_1}$$

$$Row_h \leftarrow EQ_{IndicesExtracted_{1,1}}$$

$$Column_h \leftarrow EQ_{IndicesExtracted_{2,1}}$$

$$\text{Column}_h \leftarrow EQ_{\text{IndicesExtracted}_{2,1}}$$

$$Y_{RB} \leftarrow \frac{h_{RB}}{2} + \left(\frac{NA_{Range}}{NA_{Precision} - 1}\right)\cdot(\text{Row} - 1)$$

$$\varepsilon_{bf} \leftarrow \left(\frac{\varepsilon_{co}}{\text{Strain}_{Precision} - 1}\right)\cdot(\text{Column})$$

$$\sigma_{bf_h} \leftarrow f_{co}\cdot\left[1 - \left(\left|1 - \frac{\varepsilon_{bf_h}}{\varepsilon_{co}}\right|\right)^{n_c}\right]$$

break if $\sigma_{bf_h} = f_{co}$

$$\text{ResultsRaw1} \leftarrow \text{augment}\left(\text{Row}, \text{Column}, Y_{RB}, \varepsilon_{bf}, \sigma_{bf}, EQ_{Minimum}\right)$$

$$\text{ResultsRaw2} \leftarrow \text{submatrix}(\text{ResultsRaw1}, 2, h, 1, 6)$$

$$\text{ResultsTopRow} \leftarrow \left("NA" \quad "NA" \quad \frac{h_{RB}}{2} \quad 0 \quad 0 \quad 0\right)$$

"Columns left to right are row of min value, column of min value, neutral axis, bottom fiber strain, bottom fiber stress, residual (error)."

$$\text{Results} \leftarrow \text{stack}(\text{ResultsTopRow}, \text{ResultsRaw2})$$

$$\text{Analysis}_{RB} = \begin{pmatrix} \text{"NA"} & \text{"NA"} & 6.00000000 & 0.00000000 & 0.00000000 & 0.00000000 \\ 117.00000000 & 60.00000000 & 6.41760000 & 0.00007205 & 232.16722841 & 62.91675968 \\ 108.00000000 & 121.00000000 & 6.38520000 & 0.00014530 & 458.75136624 & 207.80062716 \\ 114.00000000 & 185.00000000 & 6.40680000 & 0.00022215 & 686.22104211 & 29.35903049 \\ 117.00000000 & 251.00000000 & 6.41760000 & 0.00030140 & 909.78279399 & 101.56518272 \\ 117.00000000 & 319.00000000 & 6.41760000 & 0.00038306 & 1128.40269292 & 74.38283617 \\ 118.00000000 & 390.00000000 & 6.42120000 & 0.00046831 & 1343.95756995 & 155.48853681 \\ 116.00000000 & 463.00000000 & 6.41400000 & 0.00055597 & 1552.02265443 & 158.13967070 \\ 117.00000000 & 540.00000000 & 6.41760000 & 0.00064843 & 1756.55869284 & 172.65517765 \\ 118.00000000 & 621.00000000 & 6.42120000 & 0.00074570 & 1955.14072759 & 192.18442609 \\ 120.00000000 & 707.00000000 & 6.42840000 & 0.00084897 & 2147.32884068 & 87.65452461 \end{pmatrix}$$

$$\text{MaxFC}_{RB} := \begin{cases} RR \leftarrow \text{rows}\left(\text{Analysis}_{RB}\right) \text{ if } \left(\text{Analysis}_{RB}\right)_{\text{rows}\left(\text{Analysis}_{RB}\right),5} < f_{co} \\ RR \leftarrow \text{rows}\left(\text{Analysis}_{RB}\right) - 1 \text{ if } \left(\text{Analysis}_{RB}\right)_{\text{rows}\left(\text{Analysis}_{RB}\right),5} \geq f_{co} \vee \left(\text{Analysis}_{RB}\right)_{\text{rows}\left(\text{Analysis}_{RB}\right),3} = \dfrac{h_{RB}}{2} \\ \text{Analysis}_{RB_{RR,5}} \end{cases}$$

$$\text{YBar}_{RB} := \begin{cases} \text{ResultsRow} \leftarrow \text{rows}\left(\text{Analysis}_{RB}\right) \text{ if } \left(\text{Analysis}_{RB}\right)_{\text{rows}\left(\text{Analysis}_{RB}\right),5} < f_{co} \\ \text{ResultsRow} \leftarrow \text{rows}\left(\text{Analysis}_{RB}\right) - 1 \text{ if } \left(\text{Analysis}_{RB}\right)_{\text{rows}\left(\text{Analysis}_{RB}\right),5} \geq f_{co} \vee \left(\text{Analysis}_{RB}\right)_{\text{rows}\left(\text{Analysis}_{RB}\right),3} = \dfrac{h_{RB}}{2} \\ \text{Analysis}_{RB_{\text{ResultsRow},3}} \end{cases}$$

$\text{YBar}_{RB} = 6.43$

$\text{YLocationCheck}_{RB} :=$ "This routine checks to make sure that all neutral axis locations are within the assumed range."

$\text{YMax}_{RB} \leftarrow \max\left(\text{Analysis}_{RB}^{\langle 3 \rangle}\right)$

$\text{NALimit}_{RB} \leftarrow (0.15)\left(h_{RB}\right) + \dfrac{h_{RB}}{2}$

"OK" if $\text{YMax}_{RB} \leq \text{NALimit}_{RB}$

"NG" if $\text{YMax}_{RB} > \text{NALimit}_{RB}$

$\text{YLocationCheck}_{RB} = \text{"OK"}$

$\Theta RB :=$ "This routine calulates the rotation of the pile-to-cap connection by assuming rigid body behavior of the embedded portion of the pile."

"The translation of the pile at both the bottom face of the cap and at the top of the pile is based on a strain density calculation using the"

"difference between the idealized beam strains and the localized strains due to rigid body behavior that are assumed to provide the"

"resisting couple."

$ResultsRow \leftarrow rows(Analysis_{RB})$ if $(Analysis_{RB})_{rows(Analysis_{RB}),5} < f_{co}$

$ResultsRow \leftarrow rows(Analysis_{RB}) - 1$ if $(Analysis_{RB})_{rows(Analysis_{RB}),5} \geq f_{co} \vee (Analysis_{RB})_{rows(Analysis_{RB}),3} = \frac{h_{RB}}{2}$

for $i \in 1..ResultsRow$

$\varepsilon_{bf} \leftarrow Analysis_{RB_{i,4}}$

$\varepsilon_{tp} \leftarrow \varepsilon_{bf} \cdot \left(\frac{h_{RB}}{Analysis_{RB_{i,3}}} - 1 \right)$

if $i = 1$

$A_{BottomFace_1} \leftarrow 0$

$A_{TopOfPile_1} \leftarrow 0$

if $i > 1$

$A_{BottomFace_i} \leftarrow \frac{1}{2} \cdot (L_{pst}) \cdot \left[\varepsilon_{bf} - PSTBStrains_{1,i} \cdot \left(\frac{h}{PSTBYbarCap_{1,i}} - 1 \right) \right]$

$A_{TopOfPile_i} \leftarrow \frac{1}{2} \cdot (L_{pst}) \cdot \left[\varepsilon_{tp} + PSTBStrains_{3,i} \cdot \left(1 - \frac{p_e}{PSTBYbarCap_{3,i}} \right) \right]$

$\Theta_{RB_i} \leftarrow atan\left(\frac{A_{BottomFace_i} + A_{TopOfPile_i}}{h_{RB}} \right)$

Θ_{RB}

$$\Theta RB = \begin{pmatrix} 0.000000 \\ 0.000073 \\ 0.000148 \\ 0.000226 \\ 0.000306 \\ 0.000389 \\ 0.000475 \\ 0.000565 \\ 0.000659 \\ 0.000757 \\ 0.000861 \end{pmatrix}$$

$$MRB := \begin{cases} ResultsRow \leftarrow rows\left(Analysis_{RB}\right) \text{ if } \left(Analysis_{RB}\right)_{rows\left(Analysis_{RB}\right),5} < f_{co} \\ ResultsRow \leftarrow rows\left(Analysis_{RB}\right) - 1 \text{ if } \left(Analysis_{RB}\right)_{rows\left(Analysis_{RB}\right),5} \geq f_{co} \vee \left(Analysis_{RB}\right)_{rows\left(Analysis_{RB}\right),3} = \frac{h_{RB}}{2} \\ \left(-submatrix\left(F_{Pile}, 2, 2, 1, ResultsRow\right)\right)^{T} \end{cases}$$

$$MRB = \begin{pmatrix} 0.00 \\ 51212.24 \\ 102424.48 \\ 153636.73 \\ 204848.97 \\ 256061.21 \\ 307273.45 \\ 358485.69 \\ 409697.94 \\ 460910.18 \\ 512122.42 \end{pmatrix}$$

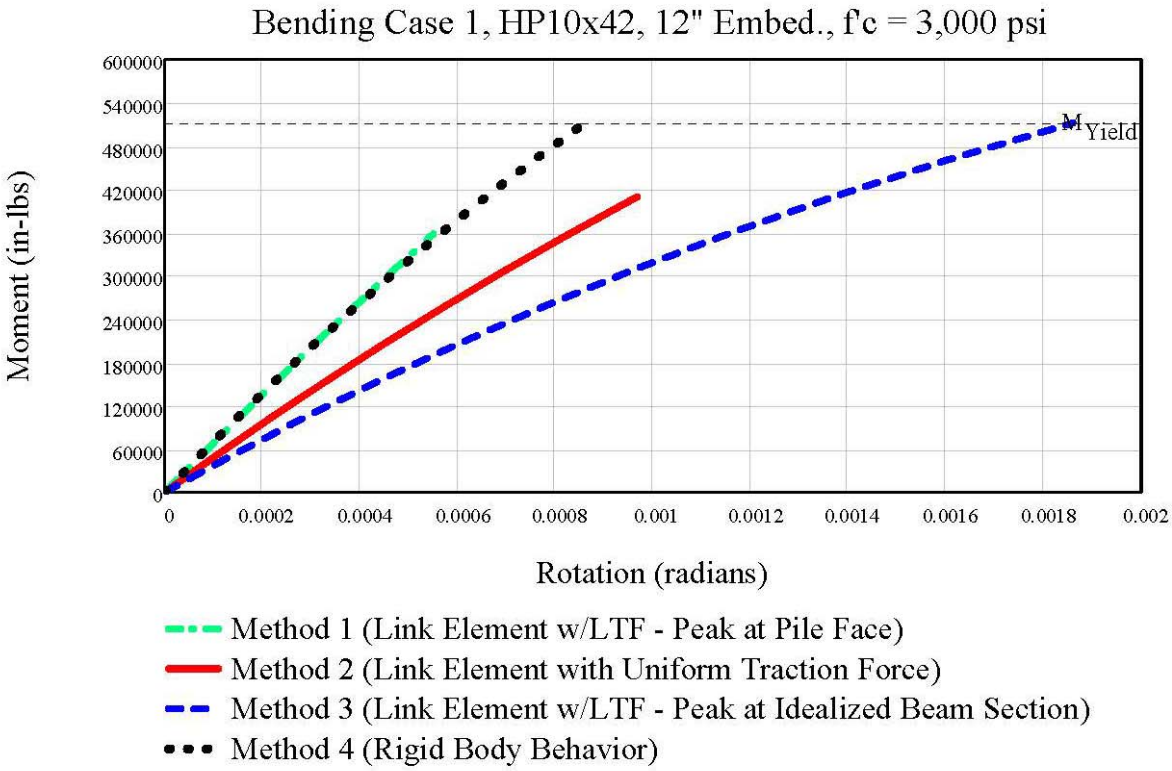
Bending Case 1, HP10x42, 12" Embed., f'c = 3,000 psi
Moment (in-lbs)
600000
540000
480000
420000
360000
300000
240000
180000
120000
60000
0
0
0.0002
0.0004
0.0006
0.0008
0.001
0.0012
0.0014
0.0016
0.0018
0.002
M Yield
Rotation (radians)
Method 1 (Link Element w/LTF - Peak at Pile Face)
Method 2 (Link Element with Uniform Traction Force)
Method 3 (Link Element w/LTF - Peak at Idealized Beam Section)
Method 4 (Rigid Body Behavior)

$\text{Capacity}_{RB} :=$

"This routine calculates the capacity of the embedded pile connection to resist an applied moment (no shear). This analysis is based"
"on strain compatibility and treating the embedded pile segment as a rigid body. Note that this routine could have been performed"
"without a search for the nuetral axis; however, the inclusion of this comlex step provides an additional check on the correctness of the"
"AnalysisRB routine above. NARange defines the range of potential neutral axis locations evaluated in this routine. This range is"
"centered on the centroid of the rigid body (embedded pile segment)."

$NA_{Range} \leftarrow (0.10) \cdot h_{RB}$

$n_c \leftarrow \frac{E_c \cdot \varepsilon_{co}}{f_{co}}$

"εbf is set equal to εco to calculate the capacity of the connection subject to an applied moment only."

$\varepsilon_{bf} \leftarrow \varepsilon_{co}$

"NAPrecision controls the number of equally spaced evaluation points within NARange. Use an odd number to create an evaluation"
"point at the centroid of the rigid body."

$NA_{Precision} \leftarrow 101$

for $i \in 1 .. NA_{Precision}$

$Y_{RB} \leftarrow \frac{h_{RB}}{2} + \left(\frac{NA_{Range}}{NA_{Precision} - 1} \right) \cdot (i - 1)$

$M_{UpperPart1} \leftarrow \frac{(h_{RB} - Y_{RB})^2}{2} + \frac{(h_{RB} - Y_{RB}) \cdot \varepsilon_{co} \cdot Y_{RB} \cdot \left[\left| 1 - \frac{\varepsilon_{bf} \cdot (h_{RB} - Y_{RB})}{\varepsilon_{co} \cdot Y_{RB}} \right| \right]^{n_c+1}}{\varepsilon_{bf} \cdot (n_c + 1)}$

$M_{UpperPart2} \leftarrow \frac{\varepsilon_{co}^2 \cdot Y_{RB}^2 \cdot \left[\left| 1 - \frac{\varepsilon_{bf} \cdot (h_{RB} - Y_{RB})}{\varepsilon_{co} \cdot Y_{RB}} \right| \right]^{n_c+2}}{\varepsilon_{bf}^2 \cdot (n_c + 1) \cdot (n_c + 2)} - \frac{\varepsilon_{co}^2 \cdot Y_{RB}^2}{\varepsilon_{bf}^2 \cdot (n_c + 1) \cdot (n_c + 2)}$

$M_{Upper} \leftarrow f_{co} \cdot d \cdot (M_{UpperPart1} + M_{UpperPart2})$

$M_{LowerPart1} \leftarrow \frac{Y_{RB}^2}{2} + \frac{\varepsilon_{co} \cdot Y_{RB}^2 \cdot \left(\left| 1 - \frac{\varepsilon_{bf}}{\varepsilon_{co}} \right| \right)^{n_c+1}}{\varepsilon_{bf} \cdot (n_c + 1)}$

$M_{LowerPart2} \leftarrow \frac{\varepsilon_{co}^2 \cdot Y_{RB}^2 \cdot \left(\left| 1 - \frac{\varepsilon_{bf}}{\varepsilon_{co}} \right| \right)^{n_c+2}}{\varepsilon_{bf}^2 \cdot (n_c + 1) \cdot (n_c + 2)} - \frac{\varepsilon_{co}^2 \cdot Y_{RB}^2}{\varepsilon_{bf}^2 \cdot (n_c + 1) \cdot (n_c + 2)}$

$M_{Lower} \leftarrow f_{co} \cdot d \cdot (M_{LowerPart1} + M_{LowerPart2})$

$MEQ_i \leftarrow |M_{Upper} - M_{Lower}|$

$MomentCapacity \leftarrow M_{Upper} + M_{Lower}$

MEQ

$MEQ_{Minimum} \leftarrow \min(MEQ)$

$MEQ_{Indices} \leftarrow \text{match}(MEQ_{Minimum}, MEQ)$

$Row \leftarrow MEQ_{Indices_1}$

$Y_{RB} \leftarrow \frac{h_{RB}}{2} + \left(\frac{NA_{Range}}{NA_{Precision} - 1} \right) \cdot (Row - 1)$

"The result columns from left to right are row of minimum value, neutral axis, bottom fiber strain, residual, moment capacity (in-lbs)."

$Results \leftarrow \text{augment}(Row, Y_{RB}, \varepsilon_{bf}, MEQ_{Minimum}, MomentCapacity)$

Start Pile Bent Design

Generate Trial Bent Geometry

In General:

- All piles should be vertical.
- The strong-axis for each pile shall exist within and be parallel to the plane of the bent so that lateral, in-plane bent displacements cause weak-axis bending in the pile section. Section axes are defined in Section 6.
- Provide one pile for each girder line.
- Locate each girder line over the centroid of its supporting pile.
- Determine the supporting soil surface elevation for Service and Strength Limit States.
- Determine the supporting soil surface elevation for Extreme Event Limit States.

Determine Boundary Conditions

- Each pile bent shall be modeled as a space frame.
- In-plane bent displacements (sidesway/drift) are assumed unrestrained, but are limited to the condition when the joint centered on the bent forms a closed wedge. See attached Figure 2 for the recommended drift limit calculation and its derivation.
- Out-of-plane bent displacements are assumed to be unrestrained, but are limited to the width of the largest of the three open deck joints on either of the two supported spans.
- Use pinned support at pile tip for piles bearing on rock. For piles not bearing on rock, replace vertical component of pinned support with an appropriate soil spring to relate pile axial load to displacement.
- Calculate lateral soil springs to model horizontal soil-structure interaction. The horizontal subgrade modulus can be used to determine linear spring values for structures exhibiting small displacements below the ground surface. The project geotechnical engineer should verify that the use of linear soil springs is appropriate for the structure considered. Linear springs should be replaced with force-displacement curves if nonlinear soil behavior is to be modeled.
- Saturated soil will often be present and should be accounted for in the model used to represent soil-structure interaction.
- Note that specialized programs such as Group or FB-MultiPier are available if a more rigorous treatment of the above considerations is deemed necessary.

1

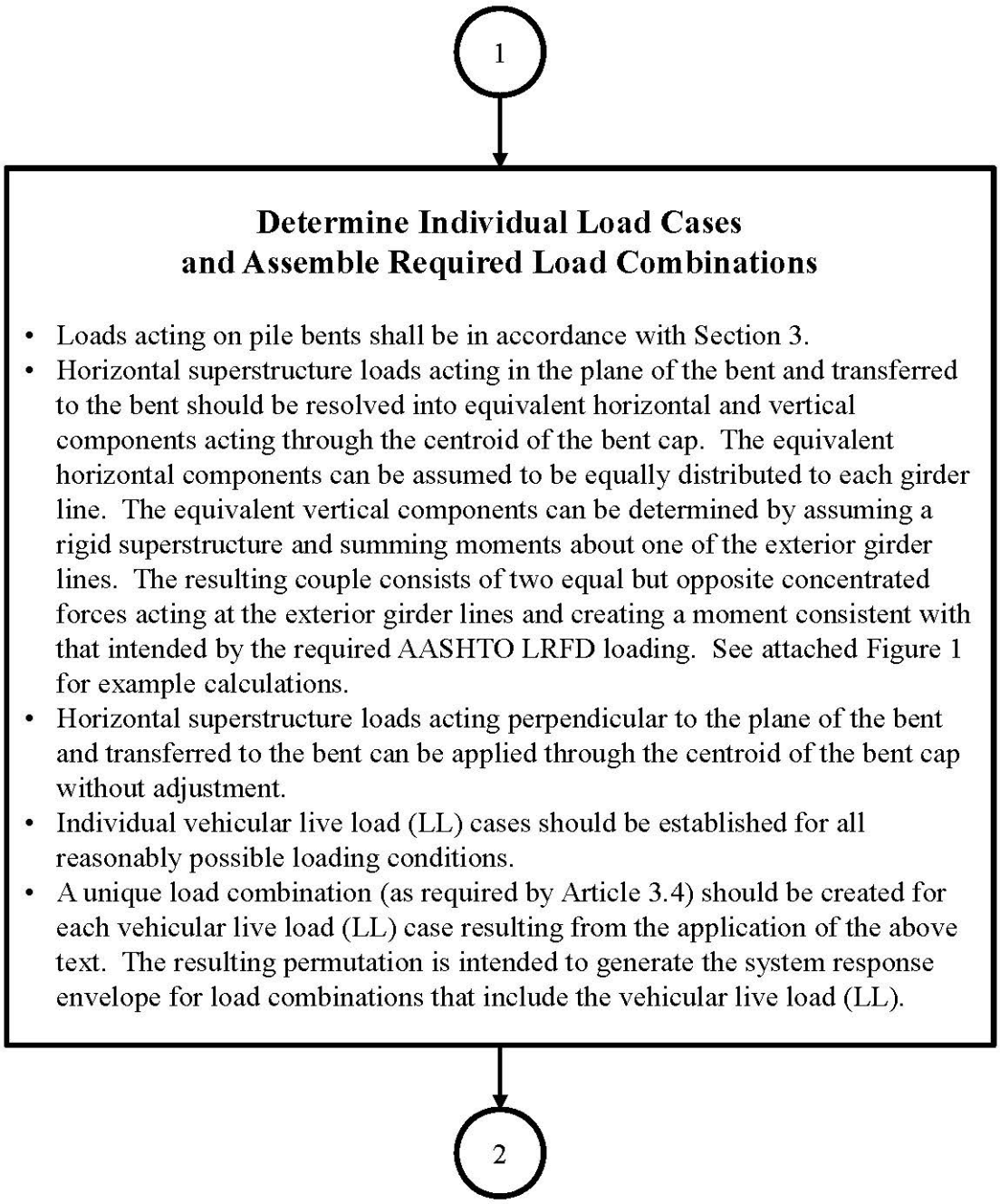
1
Determine Individual Load Cases
and Assemble Required Load Combinations
• Loads acting on pile bents shall be in accordance with Section 3.
• Horizontal superstructure loads acting in the plane of the bent and transferred to the bent should be resolved into equivalent horizontal and vertical components acting through the centroid of the bent cap. The equivalent horizontal components can be assumed to be equally distributed to each girder line. The equivalent vertical components can be determined by assuming a rigid superstructure and summing moments about one of the exterior girder lines. The resulting couple consists of two equal but opposite concentrated forces acting at the exterior girder lines and creating a moment consistent with that intended by the required AASHTO LRFD loading. See attached Figure 1 for example calculations.
• Horizontal superstructure loads acting perpendicular to the plane of the bent and transferred to the bent can be applied through the centroid of the bent cap without adjustment.
• Individual vehicular live load (LL) cases should be established for all reasonably possible loading conditions.
• A unique load combination (as required by Article 3.4) should be created for each vehicular live load (LL) case resulting from the application of the above text. The resulting permutation is intended to generate the system response envelope for load combinations that include the vehicular live load (LL).
2

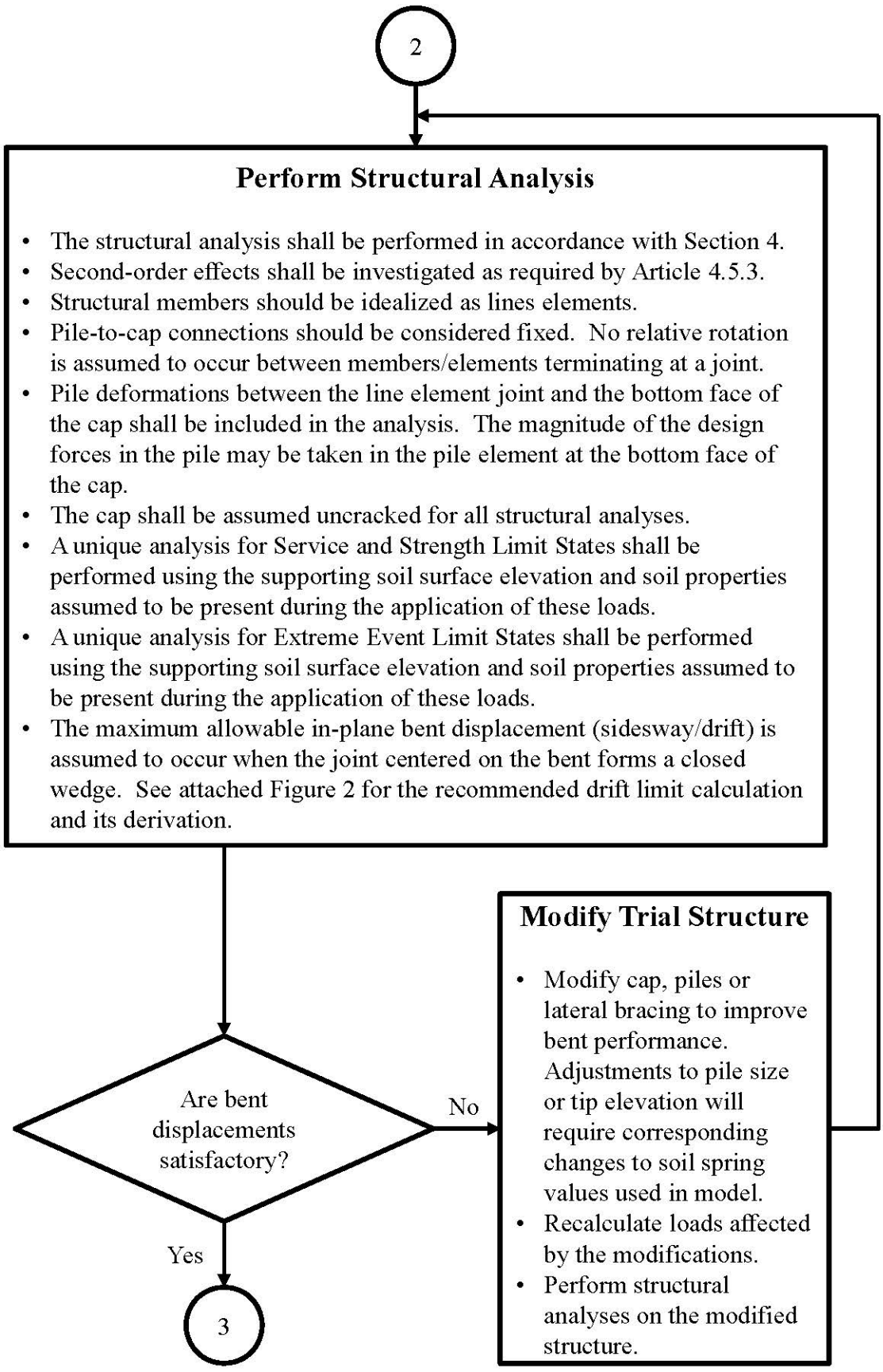
2
Perform Structural Analysis
• The structural analysis shall be performed in accordance with Section 4.
• Second-order effects shall be investigated as required by Article 4.5.3.
• Structural members should be idealized as lines elements.
• Pile-to-cap connections should be considered fixed. No relative rotation is assumed to occur between members/elements terminating at a joint.
• Pile deformations between the line element joint and the bottom face of the cap shall be included in the analysis. The magnitude of the design forces in the pile may be taken in the pile element at the bottom face of the cap.
• The cap shall be assumed uncracked for all structural analyses.
• A unique analysis for Service and Strength Limit States shall be performed using the supporting soil surface elevation and soil properties assumed to be present during the application of these loads.
• A unique analysis for Extreme Event Limit States shall be performed using the supporting soil surface elevation and soil properties assumed to be present during the application of these loads.
• The maximum allowable in-plane bent displacement (sidesway/drift) is assumed to occur when the joint centered on the bent forms a closed wedge. See attached Figure 2 for the recommended drift limit calculation and its derivation.
Are bent displacements satisfactory?
No
Yes
Modify Trial Structure
• Modify cap, piles or lateral bracing to improve bent performance. Adjustments to pile size or tip elevation will require corresponding changes to soil spring values used in model.
• Recalculate loads affected by the modifications.
• Perform structural analyses on the modified structure.
3

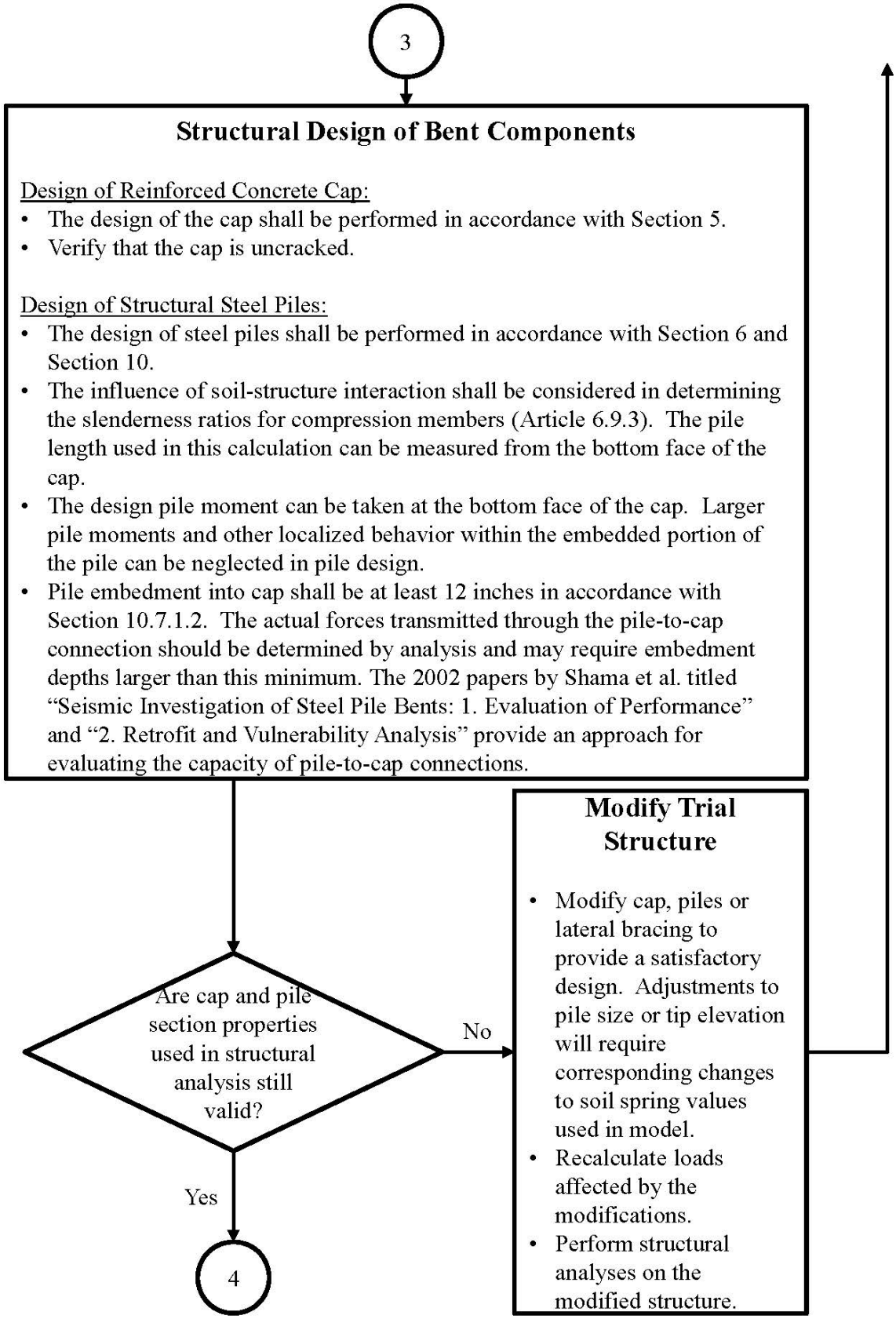
3
Structural Design of Bent Components
Design of Reinforced Concrete Cap:
• The design of the cap shall be performed in accordance with Section 5.
• Verify that the cap is uncracked.
Design of Structural Steel Piles:
• The design of steel piles shall be performed in accordance with Section 6 and Section 10.
• The influence of soil-structure interaction shall be considered in determining the slenderness ratios for compression members (Article 6.9.3). The pile length used in this calculation can be measured from the bottom face of the cap.
• The design pile moment can be taken at the bottom face of the cap. Larger pile moments and other localized behavior within the embedded portion of the pile can be neglected in pile design.
• Pile embedment into cap shall be at least 12 inches in accordance with Section 10.7.1.2. The actual forces transmitted through the pile-to-cap connection should be determined by analysis and may require embedment depths larger than this minimum. The 2002 papers by Shama et al. titled "Seismic Investigation of Steel Pile Bents: 1. Evaluation of Performance" and "2. Retrofit and Vulnerability Analysis" provide an approach for evaluating the capacity of pile-to-cap connections.
Are cap and pile section properties used in structural analysis still valid?
No
Yes
Modify Trial Structure
• Modify cap, piles or lateral bracing to provide a satisfactory design. Adjustments to pile size or tip elevation will require corresponding changes to soil spring values used in model.
• Recalculate loads affected by the modifications.
• Perform structural analyses on the modified structure.
4

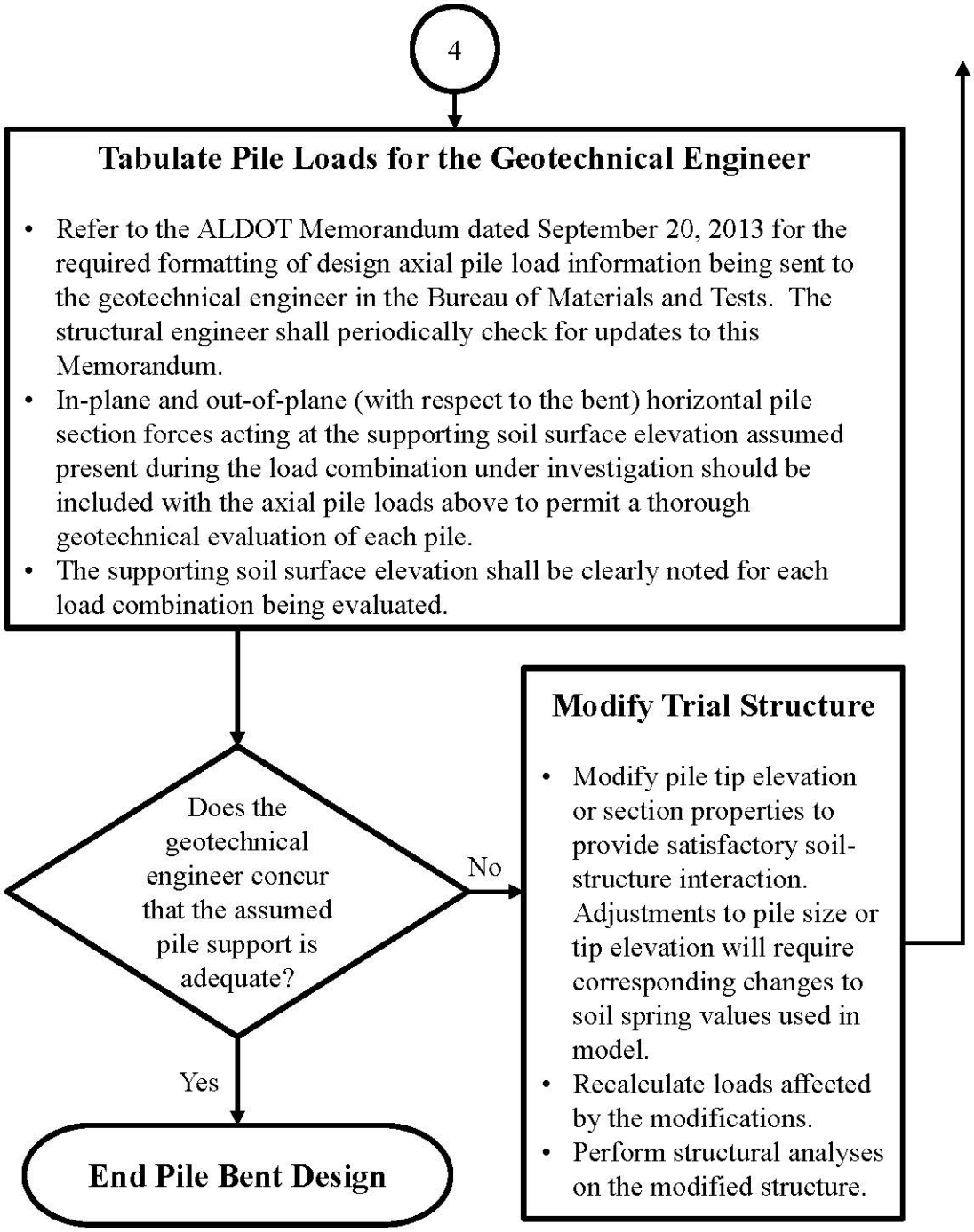

General Notes:

- This flowchart is only intended to provide modeling and analysis guidance for pile bents.
- All Section and Article references are to the AASHTO LRFD Bridge Design Specifications, Seventh Edition, 2014
- Competent application of the referenced Sections and Articles is the responsibility of the engineers in the ALDOT Bridge Bureau.

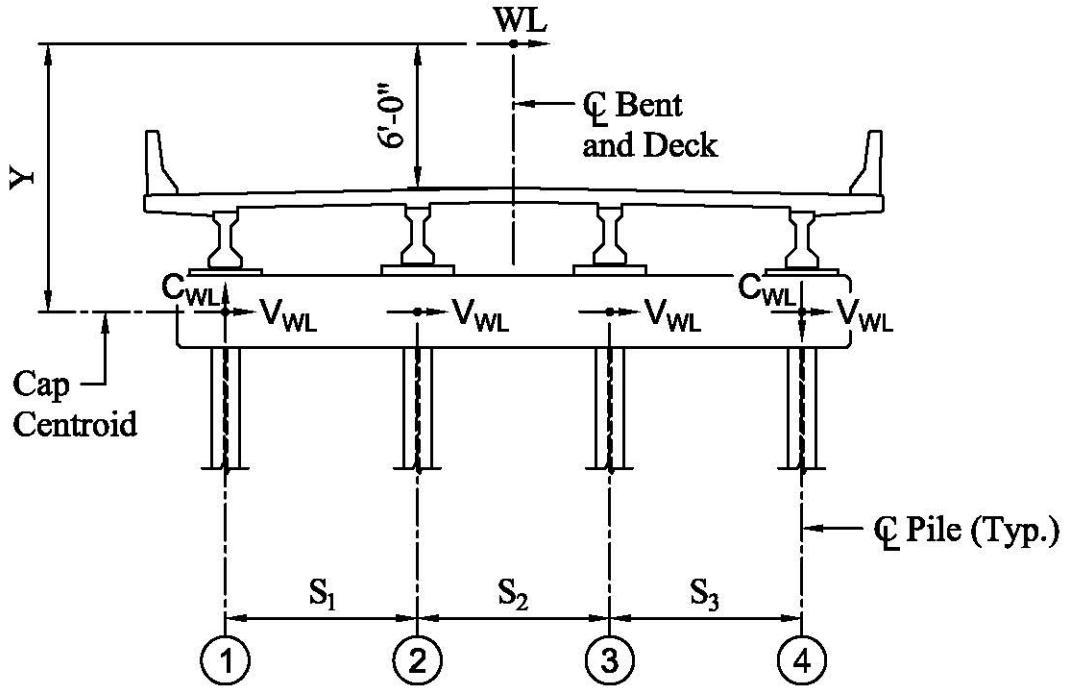

Shear from in-plane WL at each pile:

V_{WL} = (WL)/(No. of Piles)

Couple forces from in-plane WL at exterior piles:

$\Sigma M_{Pile1} = 0$:

$-(WL)(Y)+(C_{WL})(S_1+S_2+S_3) = 0$

$C_{WL} = (WL)(Y)/(S_1+S_2+S_3)$

EXAMPLE CALCULATIONS FOR RESOLVING HORIZONTALLY APPLIED FORCES INTO EQUIVALENT FORCES ACTING ON BENT

FIGURE 1

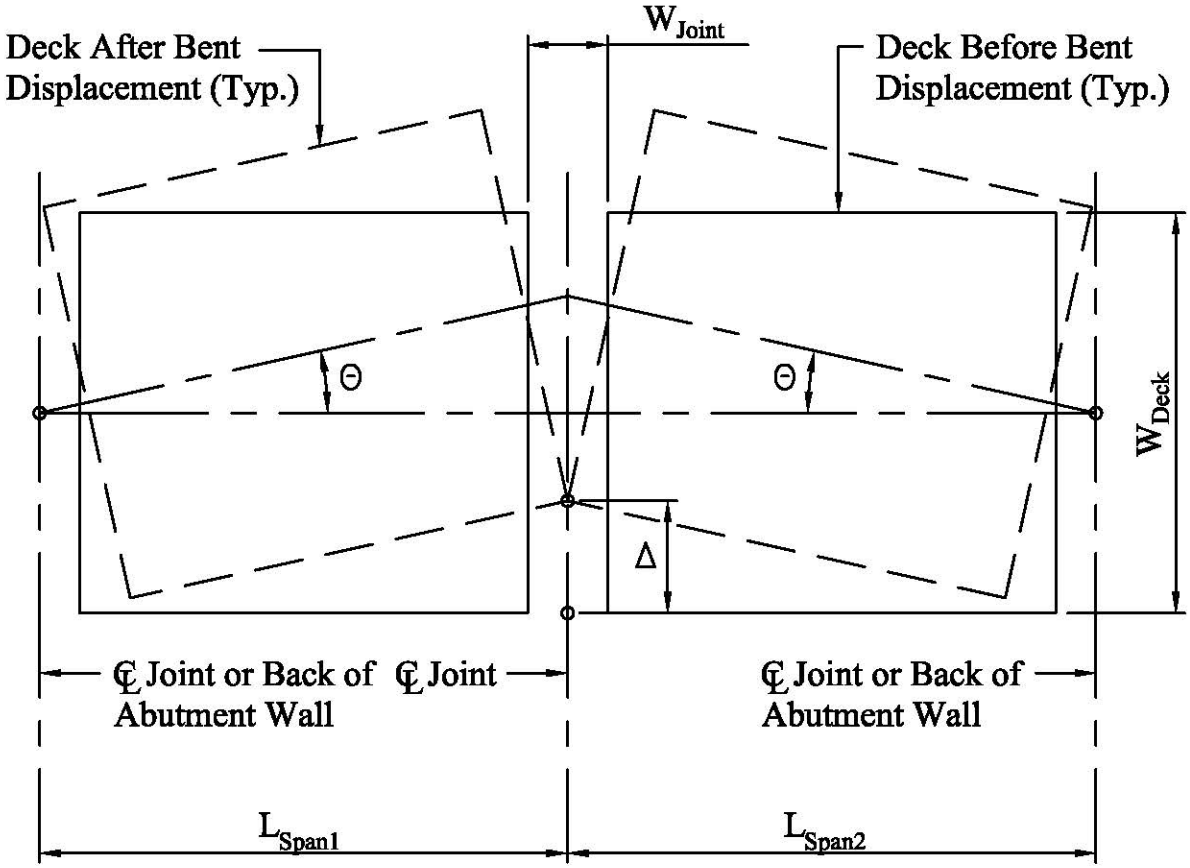

Approximate rotation required to close deck joint:

$\Theta = S/R = (W_{Joint}/2)/(W_{Deck}/2) = W_{Joint}/W_{Deck}$

Approximate bent drift limit corresponding to rotation:

$\Delta = R\Theta = (L_{Min})(W_{Joint})/W_{Deck}$

Where L_{Min} is the shorter of L_{Span1} and L_{Span2}.

Note: Adjacent bents/abutments are assumed stationary in above calculations. Any unit of length may be used, but the chosen unit must be applied consistently to all variables. Mixing units (e.g., inches and feet) is not permissible.

DERIVATION OF BENT DRIFT LIMIT EQUATION

FIGURE 2

ALABAMA DEPARTMENT OF TRANSPORTATION
Bridge Bureau, 1409 Coliseum Boulevard, Montgomery, Alabama 36110
Phone: (334) 242-6001 FAX: (334) 353-6502
Internet: http://www.dot.state.al.us

Robert Bentley
Governor

John R. Cooper
Transportation Director

MEMORANDUM

Date: September 20, 2013

To: Bridge Design Section Supervisors

From: John F. Black, P.E.
Bridge Engineer

Re: LRFD Design Axial Loads

To insure consistency in the information the Bridge Bureau sends to the Materials and Tests Bureau in the process of designing foundations using LRFD, please instruct designers under your supervision to furnish design axial loads using the following format.

Location	No. of Piles/Shafts	LRFD Axial Load (tons) Service I	Strength I	Ext. Event II	Elevation @ Load 'P'	Pile/Shaft Size
Abut. 1	12	30	45	N/A	533'	HP12x53
Bent 2	2	400	600	440	518'	4' diam.

Note: For the purpose of ASD design calculations, LRFD Service I shall be used.

JFB:jnw